CONTAMINANT FATE AND TRANSPORT ANALYSIS IN SOIL-PLANT SYSTEMS

A Thesis
Presented to
The Academic Faculty

By

Recep Kaya Goktas

In Partial Fulfillment
Of the Requirements for the Degree
Doctor of Philosophy in Environmental Engineering

Georgia Institute of Technology

May 2011

CONTAMINANT FATE AND TRANSPORT ANALYSIS IN SOIL-PLANT SYSTEMS

Approved by:

Dr. Mustafa M. Aral, Advisor
School of Civil and Environmental Engineering
Georgia Institute of Technology

Dr. Marc Stieglitz
School of Civil and Environmental Engineering
Georgia Institute of Technology

Dr. Jiabao Guan
School of Civil and Environmental Engineering
Georgia Institute of Technology

Dr. Turgay Uzer
School of Physics
Georgia Institute of Technology

Dr. Wonyong Jang
School of Civil and Environmental Engineering
Georgia Institute of Technology

Date Approved: December 17, 2010

Aileme

ACKNOWLEDGEMENTS

I would like to express my deepest gratitude to my advisor Dr. Mustafa M. Aral for his guidance, patience, understanding and support all throughout the study.

I would like to send my sincere appreciation to Dr. Jiabao Guan and Dr. Wonyong Jang, who have been extremely helpful throughout the study as the members of the MESL group, as well as the members of the Ph.D. committee.

I would also like to thank to the Ph.D. committee members Dr. Marc Stieglitz and Dr. Turgay Uzer for their very valuable comments and enlightening suggestions.

I gratefully acknowledge the financial support from the Turkish Higher Education Council and Kocaeli University.

I would like to send my special thanks to the past and present MESL members Dr. Elcin Kentel, Dr. Jinjun Wang, Dr. Sinem Gokgoz Kilic, Dr. Kijin Nam, Dr. Scott Rogers, Mr. Ilker T. Telci, Ms. Radhika Dhingra, Mr. Andi Zhang, Mr. Biao Chang, and Mr. Will Morgan for their professional support and friendship.

I would also like to send my regards and love to my dear friends Ulas Tezel, Burcak Kaynak, Ayten Memmedova Telci, Deniz Telci, Akash Dixit, Kaya Demir, Bahar

Ulukan, Zohre Kurt, Tjames Scott, and Ronda Patino, who have made my life in the U.S. much more meaningful than it could otherwise have been.

The words fall short to express my gratitude to my family – my mother Cemile, my father Kadir, and my sister Demet – who have always been there with their endless love and support.

TABLE OF CONTENTS

LIST OF TABLES

LIST OF FIGURES

SUMMARY

An integrated view to the environmental contamination has to take into account the biotic entities as well as the abiotic environmental media such as water, air and soil. Plants are among the most important components of such biota. They influence and are influenced by the contamination in the atmosphere and in the soil. Plant contaminant uptake has critical implications from a human health perspective since plants are at the beginning of an exposure route via food intake by animals and humans. The other factor that needs to be understood is the effect of plant contaminant uptake on the overall contaminant migration pattern at a site. The main objective of this study is to develop a modeling methodology that facilitates incorporating the plant pathway into environmental contamination models recognizing the fact that plants are dynamic entities that regulate their life cycle according to natural and anthropogenic environmental conditions.

A modeling framework that incorporates the plant pathway into an integrated water flow and contaminant transport model in terrestrial systems is developed. The modeling framework is aimed to provide a tool to analyze the plant pathway of exposure to contaminants. The model developed using this framework describes the temporal and spatial variation of the contaminant concentration within the plant as it is interacting with the soil and the atmosphere.

The first part of the study focuses on the integration of the dynamics of water and contaminant distribution and plant related processes within the vadose zone. A soil-plant

system model is developed by coupling soil-water flow, contaminant transport, plant life-cycle, and plant pathway models. The outcome unifies single media continuous models with multimedia compartmental models in a flexible framework. The coupling of the models was established at multiple interfaces and at different levels of solution steps (i.e. model development phase vs. numerical solution phase). Two main components were identified when developing the overall coupling scheme: (i) coupling the unsaturated zone soil-water flow and the plant life-cycle models; and, (ii) coupling the vadose zone contaminant transport and the plant pathway models.

In the second part of the study, the soil-plant system model is extended to cover large spatial areas by describing the environmental system as a collection of soil-plant systems connected through overland flow and transport processes on the ground surface and through lateral interactions in the subsurface. An overland flow model is integrated with the previously coupled model of unsaturated zone soil-water flow and plant life-cycle by solving the flow model equations simultaneously within a single global matrix structure. An overland / subsurface interaction algorithm is developed to handle the ground surface conditions. The simultaneous solution, single-matrix approach is also adopted when integrating the overland transport model with the previously coupled models of vadose zone transport and plant pathway.

The model developed is applied to various environmental contamination scenarios where the effect of the presence of plants on the contaminant migration within environmental systems is investigated.

CHAPTER 1

INTRODUCTION

1.1 Environmental Modeling and Plants

Exposure to environmental contaminants occurs through multiple pathways since the environmental contamination is a multi-media problem (Aral 2010). Each of the environmental media (e.g. surface waters, subsurface waters, atmosphere, soil) can become an exposure pathway even when they do not contain the contamination source. Thus, an integrated view to environmental contamination by considering its multi-media nature is necessary when developing models to analyze the fate and transport of contaminants within the environment.

In addition to the abiotic environmental media such as water, air and soil, the biotic entities that are a part of the environmental system have to be considered for improved modeling of environmental contamination. The biota in ecological systems represents an additional medium that transfers and transforms the contaminants, and also, they may become an additional exposure pathway for humans.

Plants are among the most important members of such biota. They influence and are influenced by the contamination in the atmosphere and in the soil since they lie at the intersection of these mediums. They have the potential to be used as field biomonitors (Powell 1997) as they may become a depository for the contaminants originally present

in the soil and / or in the atmosphere due to their continuous interaction with these two media. On the other hand, plant contaminant uptake has critical implications from a human health perspective since plants lie at the bottom of the food chain. Thus, they are at the beginning of an exposure route via food intake by animals and humans (Currado and Harrad 2001). In this exposure process, the other factor that needs to be understood is the effect of plant contaminant uptake on the overall contaminant migration pattern at a site. Thus there is a need to develop reliable models of plant root uptake and plant contamination in order to improve soil and atmospheric contamination models as well as to better understand and predict the exposure of humans to contaminants through food intake. However, the plant contaminant uptake modeling is impeded by the extreme complexity of the dependence of this process on the life-cycle of the plant within the analysis period. The main objective of this study is to develop a modeling methodology that facilitates incorporating the plant pathway into environmental contamination models recognizing the fact that plants are dynamic entities that regulate their life cycle according to natural and anthropogenic environmental conditions.

1.2 Environmental Modeling Approach Adopted in this Study

Modeling implies creating a simplified representation of the system of concern. This simplification is guided by the objectives of the modeling activity. The information that is aimed to be obtained from the model dictates the selection of the processes that are going to be included in the model.

Environmental contamination modeling, in accordance with its objectives, has benefited from the conceptualization of the environment as a collection of separate multiple domains such as water, atmosphere, and soil. By imposing such boundaries to the model, certain contaminant fate and transport processes were able to be identified as critical; and subsequently, they were able to be described using relatively simple mathematical forms that are applicable throughout the domain. This approach has led to a better comprehension, understanding, and tackling of the contamination problem. However, there is a deceiving aspect in this approach since it gives the impression of a separation within the environment.

The term “single media continuous models” can be used to describe the models that are developed specifically for a single environmental medium. These models give detailed description of the contaminant fate and transport in that environmental domain of concern. However, in these models, the interactions of the model domain with the neighboring environmental media have to be represented by relatively simplified boundary condition formulations. The attempts to integrate the model with another single media model that is developed for the neighboring environmental medium usually face various incompatibility problems as a result of trying to establish communication between independently developed environmental models through artificial interfaces.

On the other hand, “multimedia compartmental modeling” is a complementary approach to single media continuous modeling although it still treats the environment as a collection of separate domains. Multimedia environmental models focus on the

intermedia transfer processes by treating the different environmental media as separate compartments that are interacting with each other (Mackay 2001; Ramaswami et al. 2005). In these models, the outcome is the description of the contaminant distribution within the model domain which covers multiple environmental media. However, the intramedia heterogeneity and complexity have to be neglected in this approach since complete mixing and homogeneity is assumed for each compartment. In order to represent intramedia heterogeneity, the environmental media of concern may be divided into multiple compartments. However, the applicability of this methodology is questionable under certain conditions (Warren et al. 2009).

It is obvious that the above mentioned two complementary approaches to environmental modeling would face difficulties when it is attempted to extend their capabilities to cover each other's problem domains.

In the context of this study, integrated environmental modeling refers to the contamination modeling approach that adopts a holistic view of the environment. The premise is that contaminants are transformed and transported throughout the environment obeying the physical laws but disregarding any of the boundaries between different environmental media that are a result of the abstractions created as a part of the modeling process.

There is a significant advantage in using the wealth of scientific knowledge that produced the established models focusing on individual environmental media and environmental

pathways. The challenge is then to be able to combine these individual models in a framework that allows seamless information flow between its components. One of the goals of this study is to develop such a framework.

The soil-plant system as an environmental modeling domain provides a unique challenge where single media continuous models or multimedia compartmental models are inadequate to resolve when implemented separately. Plants and soil represent two separate environmental media that are in close interaction with each other. However, this interaction is very much affected by the spatial heterogeneities within the soil as the soil characteristics, root density, contaminant concentration, and water content are variable throughout the soil depth. Adding to the complexity is the effect of plants on the hydrological processes occurring within the system which in turn affect the contaminant fate and transport processes. Moreover, all the hydrological and transport processes within the system are in close interaction with the plant's dynamic life-cycle.

1.3 Scope of the Study

The objective of this study is to develop a modeling framework that incorporates the plant pathway into an integrated water flow and contaminant transport model in terrestrial systems. The modeling framework is aimed to provide a flexible tool to analyze the plant pathway of exposure to contaminants. The temporal and spatial variation of the pollutant concentration within the plant as it is interacting with the soil and the atmosphere are the desired outcomes to be produced by the model. The scope is limited with the immediate

terrestrial environment of the plants, including the upper soil and the land surface but excluding the groundwater below the water table and the surface water bodies. The atmosphere is treated as a part of the external environment that is in contact with the modeling domain.

The goal is to unify single media continuous models with multimedia compartmental models in a flexible framework. The modeling approach adopted recognizes the plants as dynamic biologic systems that regulate their life-cycle in interaction with the existing conditions in the ambient environment which significantly influence the dynamics of the overall complex system.

1.4 Thesis Organization

The first part of the study focuses on the integration of the dynamics of water and contaminant distribution and plant related processes within the vadose zone. A soil-plant system model is developed by coupling soil moisture distribution, contaminant transport, plant life-cycle and plant pathway models. In the second part of the study, the soil-plant system model is extended to cover large spatial areas by describing the environmental system as a collection of soil-plant systems connected through overland flow and transport processes on the ground surface and through lateral interactions in the subsurface. The model developed is applied to various environmental contamination scenarios where the effect of the presence of plants on the contaminant migration within environmental systems is investigated.

The thesis is organized as to provide the background before explaining the developed integration methods and their applications. Chapters 2, 3 and 4 serve for this purpose. The main concepts and the literature on the available modeling approaches for the processes relevant to the terrestrial system that is being studied are summarized in Chapter 2. Chapter 3 is devoted to the plant models used in the study. The plant pathway and the plant life-cycle model components are described. Chapter 4 presents flow and transport models together with the governing equations and their numerical solutions.

Throughout Chapters 5, 6 and 7, the concepts and the models described in the previous chapters are synthesized and integrated. Chapter 5 focuses on the soil-plant system which is the key component of the overall study as it is treated as the basic modeling unit. In this chapter, vadose zone flow and transport processes are dynamically integrated with the plant pathway processes. Chapter 6 and 7 extends the soil-plant system model so that larger spatial areas can be covered. Chapter 6 deals with the hydrological processes whereas Chapter 7 incorporates the contaminant fate and transport processes.

Finally, Chapter 8 concludes the thesis by summarizing the overall modeling methodology, highlighting significant aspects of the study and listing the further improvement possibilities as informed by this research study.

CHAPTER 2

BACKGROUND AND LITERATURE REVIEW

2.1 Multimedia Compartmental Models

Multimedia compartmental models are used in tracking the contaminant distribution among multiple environmental media which are represented as compartments. The attention is given to the mass transfer processes between interacting compartments whereas each compartment is assumed to be completely mixed. The mass transfer processes that describe the interaction between the compartments may be treated as equilibrium or dynamic processes depending on the nature of the process, the contaminant, the compartment, or the overall model. The nonequilibrium mass transfer processes can be grouped into two main categories: advective transfer processes and diffusive transfer processes.

Advective transfer processes occur as contaminants move between different media due to bulk media transfers (Ramaswami et al. 2005). Transfer of contaminants from the atmosphere to the soil through wet or dry deposition and the uptake of contaminants by the plants from the soil through root water uptake are examples of advective transfer processes between different environmental media. The advective flux between two different media can be represented as:

$$J_{adv,a-b} = k_{adv,a-b} C_a \tag{2.1}$$

where $J_{adv,a\text{-}b}$ is the advective flux [M L^{-2} T^{-1}] from medium *a* to medium *b*, $k_{adv,a\text{-}b}$ is the mass transfer rate coefficient [L T^{-1}] through advection from medium *a* to medium *b* (which is usually the bulk media transfer rate over the interface between the two interacting media), and C_a is the contaminant concentration [M L^{-3}] in medium *a*.

The diffusive mass transfer in a single medium is proportional to the concentration gradient according to the Fick's law (Ramaswami et al. 2005). The diffusive flux between two different environmental media, on the other hand, is usually expressed using the two film theory which makes use of the Fick's law and the equilibrium partitioning relationships between the respective media (Ramaswami et al. 2005):

$$J_{dif,a-b} = -k_{dif,a-b}\left(C_a - C_b K_{ab}\right) \tag{2.2}$$

where $J_{dif,a\text{-}b}$ is the diffusive mass flux [M L^{-2} T^{-1}] from medium *a* to medium *b*, $k_{dif,a\text{-}b}$ is the diffusive mass transfer rate coefficient [L T^{-1}] from medium *a* to medium *b*, C_b is the contaminant concentration [M L^{-3}] in medium *b*. K_{ab} is the equilibrium partition coefficient [L^3 L^{-3}] of the contaminant between medium *a* and medium *b*:

$$K_{ab} = \frac{C_{a,eq}}{C_{b,eq}} \tag{2.3}$$

where $C_{a,eq}$ is the equilibrium concentration of the contaminant in medium *a* (in units of mass of contaminant per unit volume of *a*) and $C_{b,eq}$ is the equilibrium concentration of the contaminant in medium *b* (in units of mass of contaminant per unit volume of *b*). The equilibrium partition coefficients form the basis of equilibrium type multimedia compartmental models, which ignore the kinetics of mass transfer. The dynamic multimedia models, on the other hand, employ them in the diffusive flux representations derived from the two-film theory as shown in Equation (2.2). Diffusive exchange of the contaminants between the plant leaves and the atmosphere and the volatilization of the contaminants from the soil to the atmosphere are some examples of diffusive intermedia mass transfer processes that are related to the subject of this study.

Equation (2.2) can be rewritten to put it into a more convenient form to use in multimedia compartmental models:

$$J_{dif,a-b} = -k_{dif,a-b}C_a + k_{dif,b-a}C_b \tag{2.4}$$

$k_{dif,b\text{-}a}$ is the mass transfer rate coefficient [L T^{-1}] from medium *b* to medium *a*:

$$k_{dif,b-a} = k_{dif,a-b}K_{ab} \tag{2.5}$$

After the mass transfer process descriptions are completed, a mass balance equation is developed for each compartment within the system boundaries. The end product is a set of ordinary differential equations (ODEs) that is solved simultaneously to obtain the time

evolution of contaminant concentration in each compartment of the system. As an example, the set of ODEs for the two-compartment system that describes the advectrive and diffusive mass transfers between medium *a* and medium *b* as developed above can be represented as:

$$\frac{d\left(V_a C_a\right)}{dt} = -\left(k_{adv,a-b} A_{ab} + k_{dif,a-b} A_{ab}\right) C_a + \left(k_{adv,b-a} A_{ab} + k_{dif,b-a} A_{ab}\right) C_b + m_a \qquad (2.6a)$$

$$\frac{d\left(V_b C_b\right)}{dt} = -\left(k_{adv,b-a} A_{ab} + k_{dif,b-a} A_{ab}\right) C_b + \left(k_{adv,a-b} A_{ab} + k_{dif,a-b} A_{ab}\right) C_a + m_b \qquad (2.6b)$$

where V_a and V_b are compartment volumes [L^3] of medium *a* and medium *b*, respectively; $k_{adv,b\text{-}a}$ is the advective mass transfer rate coefficient [$L\ T^{-1}$] from medium *b* to medium *a*, A_{ab} is the interfacial area [L^2] between compartments *a* and *b*, m_a and m_b are the source input rates [$M\ T^{-1}$] into compartments *a* and *b*, respectively. The mass balance equations given in Equation (2.6) neglect reactive processes within the environmental pathway. For non-conservative contaminants, the reactive processes are added to the mass balance equations after identifying the mass transfer rate coefficients due to the reactive processes.

Following the same principles, a multimedia compartmental model can be developed for as many compartments as desired. The resultant ODE system will be in the same format as in Equation (2.6) with the number of equations equal to the number of compartments. The critical part in developing a multimedia compartmental model is identifying the proper mass transfer rate coefficient values. Ramaswami et al. (2005) and Mackay (2001)

provide detailed review of the methods for the construction of multimedia compartmental models and for the determination of mass transfer rate coefficients.

It is desirable to use relationships that are based on fundamental chemical properties such as molecular diffusion coefficients, molecular weight, and partition coefficients between standard mediums (e.g. air-water, octanol-water) in order to decrease the input parameter requirements, and to increase the range of contaminants that can be modeled. This approach makes multimedia compartmental models very suitable for environmental screening of chemicals for risk assessment (Mackay et al. 2003). Examples of studies that have used multimedia compartmental models to compare the environmental risk associated with different chemicals can be found in Bennet et al. (2002), MacLeod and Mackay (2004), Hollander et al. (2006) and Gokgoz-Kilic and Aral (2008).

The spatial resolution can be incorporated to the multimedia models by dividing the environmental media into multiple compartments that are in interaction with each other. Using this methodology, many multimedia models have been developed to analyze contaminant fate at regional (Coulibaly et al. 2004a; Coulibaly et al. 2004b; Hollander et al. 2006; Li et al. 2006b; Luo and Yang 2004; Luo et al. 2007; Luo and Yang 2007; Macleod et al. 2005; MacLeod et al. 2002; MacLeod et al. 2001; Pennington et al. 2005; Prevedouros et al. 2004; Sweetman et al. 2002; Tao et al. 2003; Wania et al. 2006; Woodfine et al. 2002; Woodfine et al. 2001; Zhang et al. 2003) and even at global (Toose et al. 2004; Wei et al. 2008) scales.

2.2 Single Media Continuous Models

In the context of this study, the term “single media continuous models” is used to refer generally to the type of models that describe the physical processes that govern the fate and transport of contaminants within a single environmental media, such as surface waters, air or soil. The outcome from this type of models is the temporal and spatial distribution of the contaminant within the specific media. The transport processes are grouped into three categories: advection, dispersion and reaction. Accounting for all these processes and also the contamination source, the application of the conservation of mass principles within a control volume produces the partial differential equation (PDE) expression given in Equation (2.7) (Aral 2010):

$$\frac{\partial C}{\partial t}+\underbrace{\frac{\partial\left(Cu_x\right)}{\partial x}+\frac{\partial\left(Cu_y\right)}{\partial y}+\frac{\partial\left(Cu_z\right)}{\partial z}}_{advrection}=\underbrace{\frac{\partial}{\partial x}\left(D_{Hx}\frac{\partial C}{\partial x}\right)+\frac{\partial}{\partial y}\left(D_{Hy}\frac{\partial C}{\partial y}\right)+\frac{\partial}{\partial z}\left(D_{Hz}\frac{\partial C}{\partial z}\right)}_{dispersion} \\ +\underbrace{\sum_{w=1}^{N}S_w\delta\left(x_w,y_w,z_w\right)}_{source}+\underbrace{R_{reaction}}_{reaction} \tag{2.7}$$

where, C is the concentration of the contaminant [M L^{-3}]; t is time [T], x, y and z are the spatial dimensions [L]; u_x, u_y and u_z are the fluid velocities [L T^{-1}] in x, y and z directions, respectively; D_{Hx}, D_{Hy} and D_{Hz} are the dispersion coefficients [L^2 T^{-1}] in x, y and z directions, respectively; S_w is the source input rate at location (x_w, y_w, z_w), $\delta(x_w, y_w, z_w)$ is the Dirac-delta function which has a value of 1 at the point (x_w, y_w, z_w) and zero elsewhere (Gunduz and Aral 2005a). The term $R_{reaction}$ represents all the reaction processes within

the modeling domain. The mathematical description of the reaction processes depend on the modeling assumptions as well as the contaminant characteristics and also, the nature of the environmental medium.

Equation (2.7) is written in the general three-dimensional form. In practice, the number of the spatial dimensions of the specific problem can be reduced to two or one depending on the nature of the modeling domain. And for the steady state solutions, the accumulation term (the first term on the left hand side of Equation (2.7)) is set equal to zero.

The advection process describes the transport of the contaminant due to bulk fluid flow so it requires the knowledge of the fluid velocities. Thus, the prerequisite to solve the transport equation is the solution of a hydrodynamic model of the system. The dispersion term in Equation (2.7) describes the combined effect of the diffusion and dispersion processes. While diffusion is due to the random movements of the contaminant particles, dispersion is due to small scale turbulences in fluid flow (in water and air) or due to mechanical mixing (in groundwater) (Ramaswami et al. 2005).

The solution of the transport equation given in Equation (2.7) requires the assignment of the proper boundary conditions. The boundary conditions are represented as specified concentrations or specified fluxes at the modeling domain boundaries. Due to the inherent complexity of the environmental systems, the transport equation has to be solved using numerical techniques in most of the applications.

Equation (2.7) is the governing equation in the models that describe the environmental fate and transport of contaminants in any environmental media. The differences between the models applied to different environmental media manifest themselves in the expression of the reaction terms and the dispersion coefficients.

2.3 Plant Pathway Modeling

In the context of this study, the term “plant pathway modeling” refers to the development of models that describe the soil-plant and soil-atmosphere mass transfer processes and also the contaminant fate within the plant. Plant pathway models are important tools for describing the contaminant-environment interactions and assessing the environmental and human health risk associated with this important exposure pathway. Other than environmental risk assessment, the plant pathway models are used in the areas of pesticide design, ecotoxicology, environmental biotechnology and plant physiology (Trapp 2004). So, studying the plant pathway models is a multidisciplinary effort.

The plant pathway models can be grouped as regression models, equilibrium / steady-state models, and dynamic models. Collins and Fryer (2003) present a comparison study of plant pathway models of different types. The regression models are based on equations that relate one or more chemical properties to a bioconcentration factor within the plant using experimental results (e.g. Calamari et al. 1987; Topp et al. 1986; Travis and Arms 1988). Regression based models may have predictive power within their (usually narrow) application range but they do not provide any insight into the actual

processes that make up the plant pathway (Trapp 2004). The equilibrium / steady-state models assume that the contaminant concentrations within the plant are in equilibrium with the surrounding environment and do not change with time (e.g. Chiou et al. 2001; Muller et al. 1994; Trapp and Matthies 1995). The equilibrium / steady-state group of models are simpler than dynamic models and have less input parameter requirements. They may give sufficient results when applied to conditions of chronic contaminant exposure (Collins and Fryer 2003). However, a dynamical model is required when the contaminant concentrations in the environment is variable and when the plant growth and other dynamical environmental factors are significant during the simulation period (Collins and Fryer 2003; Undeman et al. 2009). Dynamical models provide the contaminant concentration variation within the plant with respect to time. They take into account the plant growth and contaminant metabolism within the plant as well as the variation in the various intermedia fluxes between the plant and its environment. Thus, they require more input parameters and are structurally more complex compared to the other group of models. This study focuses on dynamical models and the rest of the text in this section is devoted to the discussion of dynamical plant pathway models.

The modeling of plants as an environmental media and a pathway for contaminant transport has been the focus of multimedia environmental modeling research for several decades. Trapp and McFarlane (1995) provided an overview of plant physiology as well as plant pathway modeling principles together with several examples of developed models. Cousins and Mackay (2001) have discussed the inclusion of plant models into multimedia models after assessing the importance of the plant pathway. More recently,

Trapp (2004) reviewed the theory of plant pathway models differentiating between the models for neutral chemicals and ionic chemicals. Models for ionic chemicals are still in development while the models for neutral chemicals are fairly established (Trapp 2004). Examples of dynamic plant pathway models are given in Paterson et al. (1994), Trapp (1995; 2002), Burken and Schnoor (1996), Hung and Mackay (1997), Cousins and Mackay (2000), Juraske et al. (2009), and Undeman (2009).

A recent review of the plant uptake processes of non-ionic organic chemicals is given by Collins et al. (2006). The plant's interaction with its environment is analyzed in two main categories: (i) plant-atmosphere interactions; and, (ii) plant-soil interactions.

Contaminant transfer between the plant and the atmosphere occurs through diffusive transfers through the leaves and also through the atmospheric deposition processes. Atmospheric deposition may introduce contaminants onto plant surfaces through wet and dry deposition of atmospheric particles. The precipitation may also contain contaminants in the dissolved phase. A detailed analysis of atmosphere-leaves interaction has been provided by Riederer (1995).

Plant-soil interactions occur through the plant roots. The soil-to-plant pathway can be described by diffusive transfers between the plant roots and the soil together with the transport of contaminants through the transpiration stream to the upper plant parts (Collins et al. 2006).

The developed models for plant contaminant uptake are variable in their complexity and this complexity mainly stems from the number of compartments used to represent the plant. Simpler models choose to model the plant as a single compartment representing the above ground plant parts (e.g. Cousins and Mackay 2001; Severinsen and Jager 1998; Trapp and Matthies 1995) while more complex models represent different plant organs (such as roots, leaves, fruits) as separate compartments in interaction with each other (e.g. Batiha et al. 2009; Trapp 1995; Trapp 2007; Undeman et al. 2009).

On the other hand, in most of the multimedia models that have incorporated the plants, the soil in interaction with the plant is modeled as a single compartment (e.g. Batiha et al. 2009; Cousins and Mackay 2000; Hung and Mackay 1997). Although Trapp's model (2007) includes two separate soil compartments, each one is only interacting with its corresponding root compartment, and the contaminant migration and the spatial variability of contaminant concentrations within the soil is not considered.

2.4 Plant Growth Modeling

The plant growth is a critical process in assessing the level of contamination within the plant (Undeman et al. 2009). The plant models use the information of plant biomass and volume in determining the contaminant concentration within the plant, which is critical in calculating the diffusive mass transfer processes between the plant and its environment and also in calculating various loss processes. However, plant growth is usually neglected

(e.g. Cousins and Mackay 2001) or represented using growth rate coefficients (e.g. Hung and Mackay 1997; Trapp 2007) while developing the plant models.

Plant growth is also very closely related with the overall water balance of the terrestrial system. The evapotranspiration process is governed by the presence of plants and varies according to the growth stage of the plants. Besides the plant cover on the ground surface, the root distribution within the upper soil also affects the soil moisture distribution as the root availability and the density determines the spatial and temporal distribution of root water uptake.

The leaf area index (*LAI*) is a key parameter of plant growth. It is defined as the ratio of the one-sided surface area of the plant leaves to the ground surface area. *LAI* and the plant biomass for a certain species of plants are related as *LAI* determines the solar radiation that can be absorbed by the plants as an energy source to produce biomass (Dwyer and Stewart 1986). On the other hand, *LAI* is closely related with the evapotranspiration as increased leaf area increases transpiration but decreases evaporation as more of the ground surface is covered (Mailhol et al. 1997).

The minimum outputs required from a plant growth model which would be a part of the water flow and contaminant transport model in a soil-plant system are *LAI*, plant biomass and volume, root depth, and root distribution.

This study is mainly interested in the crop plants since the focus is on the analysis of the plant pathway as an exposure route via food intake. Therefore, the rest of the discussion is mainly concerned with the crop models.

The crop models have been developed and used by agricultural scientists as a tool for assessing the crop yield and its water and nutrient requirements. The simplest models make use of empirical functions to predict the development of *LAI* and biomass. For example, Cox and Joliff (1986) use polynomial functions of time to predict the growth and yield of sunflower and soybean. However, the empirical models that don't use physically meaningful parameters are of little use out of a narrow application range. Relatively more sophisticated crop models incorporate parameters of physical significance to increase the reliability and the predictive power of the model output. The accumulated value of daily temperature values, the amount of intercepted light, and the efficiency of the specific crop in turning the intercepted light into biomass are common parameters that are related with the crop growth in many crop models (e.g. Chapman et al. 1993; Dwyer and Stewart 1986; Mailhol and Merot 2008; Mailhol et al. 1997; Pengelly et al. 1999; Setiyono et al. 2008; Stewart and Dwyer 1994; Villalobos et al. 1996; Wohling and Schmitz 2007; Zhang and Brandle 1996). These types of models can be put into the descriptive models category and are usually robust and good for predictive purposes (van Ittersum et al. 2003). The explanatory models category, on the other hand, includes comprehensive models that are highly mechanistic and that give detailed explanation of crop growth based on fundamental physiological processes (e.g. photosynthesis). Examples of such comprehensive models can be found in Stockle et al.

(2003; 1994), Brisson et al. (1998), Fournier and Andrieu (1998; 1999), Abrahamsen and Hansen (2000), Hansen (2002), Drouet and Pages (2003), van Ittersum et al. (2003), Asaeda et al. (2008), Di Vittorio et al. (2010), and Smith et al. (2010).

The crop models have to incorporate various environmental factors such as temperature, radiation, and the availability of water, nitrogen, phosphorus and salt since the crop growth is closely related with these factors. In most of the descriptive models, this is done by defining a function which describes the severity of stress experienced by the crop due to the relevant environmental factors. For example, Mailhol et al. (1997), Wu et al. (1999), Wohling and Schmitz (2007), Mailhol and Merot (2008), and Luo et al. (2008) incorporate a water stress index to describe the impeded growth under water scarcity.

Much attention has been given to the interaction between the soil-water dynamics and crops as a part of the analysis of irrigation requirements. In this interaction, the function of the roots is critical, thus the root growth is an important part of crop models. Root growth models commonly follow a simplified approach focusing on the function of the roots in the water and nutrient uptake processes. For example, Wohling and Schmitz (2007) model root growth as a linear function of time, whereas Fasinmirin et al. (2008) use a sigmoidal function. Setiyono et al. (2008) model rooting depth via a logistic function of crop's development stage. Li et al. (1999) use estimations using a linear relationship between the rooting depth and daily accumulated temperature. The root distribution within the soil is also commonly represented by various functional forms dependent on root depth such as uniform (Feddes et al. 1978), linear (Prasad 1988), or

exponential (Li et al. 1999; Novak 1987) functions. This simplified approach for representing root length and distribution by focusing on the root function proved to be useful in studies that focus on soil hydrology and crop yield although they have the limitation of not being able to represent root growth response in certain environments (such as unfavorable soil conditions and presence of significant spatial heterogeneity in water and nutrient availability in soil). The detailed root models that are interested in the root structure itself have also been proposed. These models generally represent single-plant systems and their applicability is restricted due to extensive data requirements. Wang and Smith (2004) provide a review on root growth modeling summarizing the approaches used as well as describing various models.

2.5 Hydrological Processes in Soil-Plant Systems

2.5.1 Hydrological Process Models

The hydrological processes in soil-plant systems can be analyzed in two broad categories. The first category involves the major water flow processes within the soil and above the ground surface. The second category involves various water transfer processes affecting the major flow processes as the atmosphere and the plants interfere with the soil hydrology. These are precipitation, interception, infiltration, evapotranspiration, and root water uptake.

Soil-water flow in soil-plant systems generally occurs within the vadose zone near the ground surface where soil grains and water and air phases co-exist. It should be noted that in some systems (e.g. paddy fields), the root zone may extend below the water table into the saturated soil. The models of soil-water flow in soil-plant systems may be divided into bucket type models and dynamic models (Yadav et al. 2009b). The bucket type models are based on a water budget over one or more soil reservoirs (e.g. Mailhol and Merot 2008; Mailhol et al. 1997). These models neglect the spatial heterogeneity of soil moisture distribution. The dynamic models are based on the solution of the Richards' equation which is developed by the combination of the Darcy's law and the continuity equation (Richards 1931). Examples of the application of Richards' equation to model soil-water flow in soil-plant systems can be found in Wohling and Schmitz (2007), van Dam et al. (2008) and Yadav et al. (2009a). The dynamic models provide the temporal and spatial distribution of soil moisture. The infiltration and evaporation processes are also implicitly calculated as a part of the ground surface boundary condition.

The other major flow process is the water flow above the ground surface. Overland flow and runoff terms are interchangeably used for this flow pathway. The hydrological researchers have been interested in overland flow models for analyzing flooding events. The two-dimensional Saint-Venant equations or various simplifications of these equations are used to describe shallow water flow over the ground surface. Hunter et al. (2007) provide an overview of the flood models and the simplifications used in these modeling studies. The zero-inertia (diffusive wave) approximation to the two-dimensional Saint Venant equations represents an optimum point between the simpler

approximations and the full equations in describing the slow, shallow water flow although it may have inaccuracies at the local scale. The zero-inertia approximation has been successfully applied to describe shallow water flow in many studies such as Xanthopoulos and Koutitas (1976), Hromadka and Yen (1986), DiGiammarco et al. (1996), Feng and Molz (1997), Dutta et al. (2000), and Jain and Singh (2005).

The irrigation modeling in agricultural systems also deals with the overland flow process. However, in irrigation system design a more practical approach that uses rule-of-thumbs and empirical decision-making have generally been adopted (Brouwer et al. 1988). Nevertheless, the value of modeling in irrigation system design is acknowledged as it leads to more efficient use of water (Maheshwari and McMahon 1993a). Maheshwari and McMahon (1993b) divides the irrigation modeling approaches into the categories of empirical, semi-empirical, and analytical. The empirical models are basically regression equations developed using field data. The semi-empirical models combine field data with theoretical principals such as volume balance to describe certain phases of irrigation flow development. The analytical models use Saint-Venant equations or a simplification of them. The flows in surface irrigation are shallow (<150 mm) and the flow velocity is slow (0.02 to 0.04 m/s) (Maheshwari 1992) making them suitable for applying the zero-inertia approximation to the Saint-Venant equations. However, the accuracy of the results obtained from the analytical models depends on the accurate representation of the infiltration process and the surface roughness (Clemmens 2009). The determination of the right surface roughness is especially difficult in cropped fields since it is affected by the presence of plants and their growth stage (Maheshwari 1992; Strelkoff et al. 2009).

The second category of hydrological processes in soil-plant systems involve atmosphere and plant related water transfer processes. Among these, precipitation is the transfer of water from the atmosphere to the soil. In the context of this study, it is incorporated to the developed models as a temporally and spatially variable source input term. The irrigation input is incorporated similarly to the precipitation term. The difference in the description of the irrigation and precipitation terms is in their susceptibility to interception by the plant cover. Certain forms of irrigation (e.g. sprinkler irrigation) may be assumed to be equivalent to precipitation when modeling their interception by the plant cover whereas other forms of irrigation (e.g border irrigation) may be assumed to be exempt from interception by the plant cover.

The interception of the precipitation by the plant cover is important since it determines the amount of water input to the ground surface. It also interferes with the evapotranspiration process as the intercepted water subsequently evaporates back to the atmosphere. Sophisticated models of rainfall interception by plants have been developed since it is critical in obtaining an accurate water balance for a catchment. van Dijk and Bruijnzeel (2001a) provide a discussion of the widely used Gash model and the revisions and improvements proposed to that model. Simpler models of interception have also been developed. For example, Ajayi et al. (2008), in their surface runoff model that has been applied to a basin in West Africa, assume that the fraction of the rainfall that is being intercepted by the plants and thus not reaching the soil surface is equal to the fraction of

the land covered with vegetation. On the other hand, Panday and Huyakorn (2004) calculate a water balance over the interception storage volume which is related to *LAI*.

Infiltration is the process of water transfer between the overland flow and soil-water flow domains. It is dependent on the water availability on the ground surface and in the immediate subsurface and also on the soil characteristics near the surface. Although the soil-water flow models that solve the Richards' equation implicitly models the infiltration process, empirical and semi-empirical equations have been extensively used to account for infiltration when soil-water flow is not modeled. The use of empirical functions to determine infiltration is especially common in surface irrigation modeling. The Kostiakov function and its modifications are the most commonly used infiltration functions in irrigation modeling (Furman et al. 2006). Strelkoff et al. (2009) discuss the shortcomings of empirical infiltration functions. They suggest the use of the Green and Ampt (1911) equation, which represents an approximation to the Richards' equation, as a "midway in complexity" between the Richards' equation and purely empirical infiltration equations.

Another important hydrological process in soil-plant systems is evapotranspiration. Evapotranspiration is the combination of two processes: water lost from the soil surface by evaporation and water lost through the plant leaves by transpiration (Allen et al. 1998). The water loss occurs through the vaporization of the water and its subsequent removal from the vaporization surface. Thus, the climatic factors that supply the energy for the vaporization process (i.e. solar radiation and air temperature) and that drive the

vapor removal process (i.e. air humidity and wind speed) are the key parameters that determine the potential evapotranspiration rate (Allen et al. 1998). The actual evapotranspiration rate on the other hand would be dependent on the availability of water at the soil and plant surfaces and also on the ability of soil to conduct water to its surface layers and to the plant roots. Allen et al. (1998) and Farahani et al. (2007) provide reviews of the factors that affect the evapotranspiration rate and the methods used in its measurement and prediction. When the evapotranspiration process is seen from the irrigation design perspective or from the perspective of the large scale studies that are interested in water transfer between land and atmosphere, it is not necessary to split it into its evaporation and transpiration components. This is not the case for the studies that are interested in soil-water dynamics. However, differentiating between the evaporation and transpiration components of evapotranspiration (whether it is determined by measurements or by modeling) is a difficult problem (Lauenroth and Bradford 2006). An example of a detailed model is presented by Lagos et al. (2009) where surface energy balances and the resistances to energy fluxes by the plant and soil surfaces are determined to partition the evapotranspiration into transpiration and evaporation. On the other hand, many soil-water models that consider the plant effects have handled this problem by splitting the evapotranspiration to soil evaporation and plant transpiration based on the fraction of the soil surface covered by vegetation (e.g. Allen and Pereira 2009; Hansen 2002; Kroes et al. 2008; Mailhol et al. 1997; Simunek et al. 2008; Stockle et al. 1994; Wohling and Schmitz 2007). The potential values for evaporation and transpiration rates reflect the atmospheric demand for these processes for the specific site. The actual rates observed may be lower than the potential rates due to limitations in the water availability.

The way the dynamic soil-water models take into account the reduced evaporation due to dry conditions is through a special handling of the ground surface boundary conditions (Simunek et al. 2008; van Dam and Feddes 2000). The actual transpiration rate on the other hand is determined through the modeling of the root water uptake process (Braud et al. 2005).

First attempts to model root water uptake approached the problem at the microscopic scale and assumed radial flow into a single root driven by the water potential difference between the soil-root interface and the surrounding soil (Green et al. 2006). However, at larger temporal and spatial scales this microscopic approach was of little use because of the practical limitations of upscaling the single-root models to a whole root system and also because of the steady-state assumptions used in the solution of microscopic models (Hopmans and Bristow 2002). Therefore, later studies adopted a macroscopic approach where the root water uptake term is incorporated to the soil-water flow model as a sink term (Feddes et al. 2001). The temporally and spatially variable sink term in the macroscopic models is determined using one of the two approaches (i) Type I (bottom-up) (ii) Type II (top-down) (Hopmans and Bristow 2002; Yadav et al. 2009b). In the bottom-up approach (Type I), the microscopic models are adopted to determine water uptake rates at different soil layers. Example applications of this approach can be found in Nimah and Hanks (1973), Feddes et al. (1974), and Personne et al. (2003). Although Type I models provide a physical description of the soil-root system, they require often unavailable plant related data (such as the root's water potential and conductivity) (Feddes et al. 2001; Yadav et al. 2009b). In the top-down (Type II) approach, empirical

functions are used to distribute the potential transpiration within the root zone based on the water availability within the soil (Green et al. 2006; Yadav et al. 2009b). The data required by Type II models is easier to obtain and it is the most common approach adopted in root water uptake simulations (e.g. Feddes et al. 1976; Molz and Remson 1970; Perrochet 1987; Yadav et al. 2009b). Further details on root water uptake models can be found in the reviews of Feddes et al. (2001), Hopmans and Bristow (2002), and Green et al. (2006). Besides the empirical functions that relate the root water uptake rate to the soil moisture availability, root distribution and root growth functions (see Section 2.4) are also incorporated to the Type II models to better represent the spatial and temporal variations in the root water uptake rate (Li et al. 1999; Li et al. 2006a; Ojha et al. 2009; Yadav and Mathur 2008)). Recent studies also incorporate water stress compensation functions that describe the increased water uptake in the wetter parts of the root zone when the plant starts to experience water stress (Braud et al. 2005; Lai and Katul 2000; Li et al. 2001; Li et al. 2006a; Simunek and Hopmans 2009; Yadav et al. 2009a).

2.5.2 Coupling the Hydrological Process Models

The coupling of the hydrological process models of the soil-plant system can be analyzed in two categories: (i) the coupling of the soil-water flow models with the models of interception, infiltration, evaporation, transpiration, and root water uptake; and, (ii) the coupling of the soil-water flow models with overland flow models.

The coupling of the soil-water flow models with the models of minor but important hydrological pathways of interception, infiltration, evaporation, transpiration, and root water uptake has been discussed in the previous section (section 2.5.1) while reviewing the corresponding models. In a soil-water flow model that is based on the Richards' equation, the coupling with the interception, infiltration and evaporation models are established through the special treatment of the ground surface boundary. On the other hand, the transpiration and root water uptake processes are incorporated as a sink term to the governing flow equation. The early studies that have established this methodology are Nimah and Hanks (1973), Feddes et al. (1974), and Belmans et al. (1983). Examples of more recent studies can be found in Braud et al. (1995), Joshi et al. (1995), Varado et al. (2006) and Yadav et al. (2009b).

The incorporation of the plant life-cycle into the analysis of the soil-plant system hydrology requires coupling the hydrology models with the models of *LAI* and root development. The integration of the root development processes to the soil-water flow models has been accomplished by incorporating the functional description of root growth and distribution to the root water uptake models (e.g. Li et al. 1999; Li et al. 2006a; Ojha et al. 2009; Yadav and Mathur 2008). Schymanski et al.'s (2008) study in which an optimality based description of root dynamics with an emphasis on plant adaptability to the environment is used represents an interesting divergence to this common approach. On the other hand, incorporating the *LAI* development requires the integration of soil-water flow models with plant growth models. Since the plant growth is closely related with soil hydrology, detailed crop growth models include the integrated solution of the

soil-water flow equation as well (Abrahamsen and Hansen 2000; Hansen 2002; Jara and Stockle 1999; Stöckle et al. 2003; Stockle et al. 1994; Wohling and Schmitz 2007; Wu et al. 1999). Some hydrological models are also integrated with crop growth models for more realistic simulation of soil-water flow (Kroes et al. 2000; Luo et al. 2008; van Dam et al. 2008). The literature suggests that a detailed soil-water flow model integrated with a detailed crop model becomes very strong in simulating the dynamics of soil-water flow. The soil hydrology model SWAP which is integrated with a detailed crop model (WOFOST) outperformed its counterparts in studies that compared it with other crop models that also simulate soil-water dynamics. In Eitzenger et al. (2004) the better performance of SWAP was tied to its better representaion of the vertical soil heterogeneity and to the sophisticated root growth and root water uptake modules it uses. Bonfante et al. (2010) explained SWAP's better performance by its ability to handle the ground surface boundary condition and the soil-hydraulic parameterizations better than its counterparts.

The other coupling category to be discussed in this section is the coupling of the soil-water flow and the overland flow models. The literature on the coupling of these two major hydrological flow pathways is constantly growing. Furman (2008) provides a review of the physical and numerical aspects of coupled models and also discusses studies from various disciplines such as irrigation and watershed modeling.

Huang and Yeh (2009) identify two cases of coupled modeling of surface and subsurface flows based on the way the interface between the domains is handled: (i) discontinuous

assumption; and, (ii) continuous assumption. In the discontinuous approach, the interaction between the two domains is modeled by the help of an exchange-flux term at the interface assuming the presence of a separate interface layer (e.g. Ebel et al. 2009; Kolditz et al. 2008; Panday and Huyakorn 2004; VanderKwaak 1999). In the continuous approach, the continuity of pressure heads and fluxes at the interface is enforced (e.g. Dawson 2008; He et al. 2008; Kollet and Maxwell 2006). The coupling approaches can also be categorized according to the numerical solution method adopted as: time lagged coupling (no coupling), iterative coupling, and simultaneous coupling (full coupling) (Furman 2008; Huang and Yeh 2009). In the time-lagged coupling method, practically there is no coupling between the two domains as the solution from the previous time step for one domain is used in the current time step's solution of the other domain (e.g. Bixio et al. 2002; Gandolfi and Savi 2000; Singh and Bhallamudi 1998; Smith and Woolhiser 1971). In iterative coupling, the solution from the previous iteration step for one domain is used in the current iteration step's solution of the other domain (e.g. Morita and Yen 2002; Zerihun et al. 2005a; Zerihun et al. 2005b; Zerihun et al. 2005c). In simultaneous coupling, both systems are simultaneously solved in a single global matrix (e.g. Gunduz and Aral 2005b; Kollet and Maxwell 2006; Kumar et al. 2009; Liang et al. 2007; Panday and Huyakorn 2004; VanderKwaak 1999).

The ground surface boundary condition used in the soil-water model is dependent on the state of the system. In a coupled model of soil-water and overland flows, the ground surface boundary becomes an interfacial boundary between the two flow domains. When overland flow develops, the boundary condition for the soil-water governing equation at

the ground surface has to be switched from a specified flux condition to a specified head condition. When the overland flow recedes, the boundary condition has to be switched back to a specified flux condition. It is reported that this switching may cause numerical problems (Furman 2008).

The evapotranspiration process and the plant growth become important when long term modeling of coupled soil-water and overland flow is required. This adds to the complexity of the integrated model (Maneta et al. 2008). Boegh et al. (2004) present a study that integrates the hydrological model MIKE/SHE with the plant growth model DAISY (Hansen 2002) for distributed hydrological modeling, taking into account a detailed representation of evapotranspiration and plant growth. However, MIKE/SHE uses an uncoupled scheme for the integration of surface and subsurface flows (Furman 2008). The irrigation modelers have only recently been interested in the coupling of soil-water and overland flows. The usual practice has been solving overland flow equations with the infiltration incorporated by algebraic representations such as Kostiakov (Furman et al. 2006) or Green-Ampt (1911) equations (Section 2.5.1). Lecina and Playan (2006a; 2006b) simulate irrigation flows together with crop growth. However, soil-water flow is not modeled and a water balance for the entire soil profile is calculated. Wohling and Schmitz (2007), in their model of furrow irrigation, couple an analytical solution of the one-dimensional zero-inertia overland flow equation with the soil-water model of HYDRUS (Simunek et al. 2006) using an iterative scheme. They have also included a crop growth and evapotranspiration model.

2.6 Contaminant Fate and Transport Processes in Soil-Plant Systems

2.6.1 Contaminant Fate and Transport Models

The contaminant fate and transport processes in soil-plant systems can be divided into three broad domains: (i) plant, (ii) soil; and, (iii) land surface. Plant's contamination has been discussed in Section 2.3. Therefore, in this section, contaminant fate and transport processes within the soil and over the land surface are covered.

The soil domain that falls into the scope of this study is the vadose zone where soil grains and water and air phases co-exist. This region has traditionally been studied by soil and agricultural scientists. More recently, it has also become an important subject of environmental research as it is acknowledged that introduction of contaminants to the subsurface often occurs through this region (Fetter 1999; Simunek and Bradford 2008). Advective – dispersive transport equation (Equation 2.7) is used to model the contaminant transport within the vadose zone. It is common to construct a one-dimensional transport model since the focus is on the shallow soil where the water movement is generally in vertical direction until the groundwater table is reached (e.g. Kroes et al. 2008; Simunek et al. 2008). In vadose zone transport modeling, the contaminant distribution among three different phases has to be considered: soil-solids, soil-water and soil-air. In most cases, it is reasonable to assume that soil-water is the only mobile phase neglecting the advection of soil-air. The partitioning of contaminants between soil-solids and soil-water is modeled by linear or nonlinear adsorption

relationships. The partitioning between soil-water and soil-air can be modeled as an equilibrium or non-equilibrium partitioning process. Reviews of contaminant fate transport mechanisms within the vadose zone and their modeling can be found in Nielsen et al. (1986), Jury and Fluhler (1992), Feyen et al. (1998), Fetter (1999), and Charbeneau (2000).

The contaminant transport over the land surface occurs via overland flow. It facilitates the distribution of the contamination over large areas and the contamination of surface waters as this runoff reaches them. Overland transport is also modeled using the advective – dispersive transport equation (Equation 2.7). Since overland transport is through shallow water flows, two-dimensional modeling is adequate. Overland transport is driven by overland flow and overland flow modeling is a prerequisite for modeling the overland transport process. When one-dimensional modeling of flow is justified (e.g. when modeling furrow irrigation), one dimensional transport modeling is also justified (Abbasi et al. 2003; Wallach et al. 2001; Zerihun et al. 2005b). The discontinuous nature of the overland flow increases the complexity of overland transport modeling as well. Contaminant transfer into the soil through infiltration losses have to be included in the overland transport model equations. The processes of contaminant loss through transformation reactions and volatilization are usually neglected in overland transport models due to the typically short time periods associated with overland flows (Zerihun et al. 2005b). Example modeling studies of the overland transport process can be found in Akan (1987), Garcia-Navarro et al. (2000), Yan and Kahawita (2000), Wallach et al. (2001), Abbasi et al. (2003), Zerihun et al. (2005b), and Kouznetsov et al. (2007).

2.6.2 Coupling the Contaminant Fate and Transport Models

The coupling of the contaminant fate and transport process models of the soil-plant system can be analyzed in two categories: (i) the coupling of the vadose zone contaminant transport models and the plant pathway models; and, (ii) the coupling of the vadose zone contaminant transport models with overland transport models.

There aren't many studies on coupling the vadose zone contaminant transport models with plant pathway models. It was discussed in section 2.3 that most of the multimedia models that include the plant pathway neglect contaminant transport processes in soils by modeling the soil as a single compartment. One of the multimedia models that have attempted to include the soil transport processes is Komprda et al.'s (2009) study. Komprda et al. (2009), in their dynamic compartmental model of the air-soil-plant system, divide the soil compartment into 7 horizontal layers of 1 cm and connect the soil layers through the advection and diffusion processes. However, the advective flux from an upper soil layer to a lower soil layer is simple calculated by assigning the rainfall rate as the mass transfer rate coefficient. Matthies and Behrendt (1995) present one of the rare modeling studies where a plant pathway model (Trapp 1995) is integrated with a soil-water flow and contaminant transport model. However, in this simulation model, the soil and the plant models are solved sequentially with unidirectional data flow from the soil model to the plant model. Moreover, the plant biomass growth is calculated by simply multiplying the root water uptake rate by a transpiration related growth coefficient. Thus, the full integration of models that describe the soil-plant system is not achieved.

In recent years, the number of studies that attempt to couple surface and subsurface transport processes has increased. This field is also (like the coupled flow modeling field) led by watershed and irrigation modelers. From the environmental health standpoint, the quantification of the coupled transport processes at the interface of surface and subsurface is critical as it helps to describe and predict the non-point source pollution due to contaminated runoff. Irrigation modelers are also interested on the subject in order to gain better understanding of the fermigation process which is the application of fertilizers as they are dissolved in the surface irrigation flow (Zerihun et al. 2005b).

The transfer of dissolved contaminants between the overland and soil domains occurs through advective and diffusive/dispersive processes. The advective process is the contaminant transfer between the two domains through water exchange (infiltration/exfiltration). This is the only transport process considered in Zerihun et al. (Zerihun et al. 2005b; Zerihun et al. 2005c) since they have focused on the fermigation modeling. In order to model contamination of the overland flow by the contaminated soil it passes over, diffusive/dispersive exchange processes have to be included. The diffusive/dispersive exchange process is modeled by assuming a diffusive mass transfer through a thin stagnant water film between the soil surface and the moving overland flow (Zerihun et al. 2005b). Although the same approach is adopted by many modelers, there seems to be no consensus in how to determine the thickness of the water film (VanderKwaak 1999). Examples of coupled models of subsurface/surface contaminant transport can be found in Vanderkwaak (1999), Zerihun et al. (2005b; 2005c), Kouznetsov et al. (2007), and He et al. (2009).

CHAPTER 3

PLANT PATHWAY

3.1 Plant Pathway Model

In this study, the contaminant transport through the plant pathway is modeled by representing the above-ground parts of the plant as a single compartment. On the other hand, the plant roots are represented by a root growth and a root density distribution function (Section 3.2.3), which are critical in determining the root water uptake and thus in determining the plant contaminant uptake by the roots.

3.1.1 Mass Transfer Processes

In this section, the mathematical descriptions of the mass transfer processes used in the plant pathway model are given. The mass transfer processes considered when developing the plant pathway model are given in Figure 3.1 where soil is represented as a single compartment.

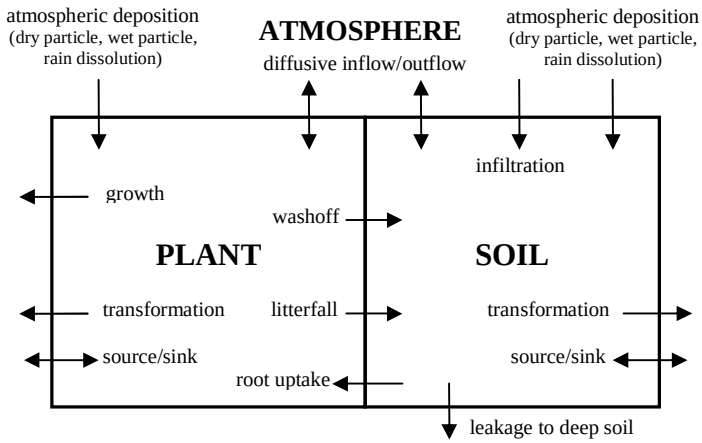

Figure 3.1: Plant pathway mass transfer processes considered in this study.

3.1.1.1 Atmospheric Deposition

Atmospheric deposition is assumed to be the result of three transport processes described as: dissolution in the rainfall, wet deposition and dry deposition. The total atmospheric deposition rate onto the soil and onto the plants is then calculated as:

$$E_{Atm-Soil} = \left[k_{dry-soil} + (1 - f_c)(k_{wet} + k_{rain}) \right] C_A \tag{3.1}$$

$$E_{Atm-Plant} = \left[k_{dry-plant} + f_c (k_{wet} + k_{rain}) \right] C_A \tag{3.2}$$

where $E_{Atm-Soil}$ is the atmospheric deposition onto the soil [M L^{-2} T^{-1}], $E_{Atm-Plant}$ is the atmospheric deposition rate onto the plants [M L^{-2} T^{-1}], $k_{dry\text{-}soil}$ is the mass transfer rate coefficient for dry deposition onto the soil [L T^{-1}], $k_{dry\text{-}plant}$ is the mass transfer rate coefficient for dry deposition onto the plants [L T^{-1}], f_c is the vegetation cover fraction,

k_{wet} is the mass transfer rate coefficient for wet deposition [L T^{-1}], k_{rain} is the mass transfer coefficient for removal by rain dissolution [L T^{-1}], and C_A is the concentration in the atmosphere [M L^{-3}].

The contaminant entry into the soil due to wet deposition and through rain dissolution is hindered as the rainfall is intercepted by the plant. The interception ratio is calculated by using a vegetation cover fraction, f_c. The non-intercepted rainfall and the associated contaminant are considered as inflow from atmosphere to the soil.

The mass transfer rate coefficients for the deposition processes can be defined as (Cousins and Mackay 2000; Ramaswami et al. 2005):

$$k_{dry-soil} = u_{q-soil} F_q K_{qa} \tag{3.3}$$

$$k_{dry-plant} = u_{q-plant} F_q K_{qa} LAI \tag{3.4}$$

$$k_{wet} = u_{rain} S_r F_q K_{qa} \tag{3.5}$$

$$k_{rain} = \frac{q_{rain}}{K_{aw}} \tag{3.6}$$

where $u_{q\text{-}soil}$ is the rate at which particles are settled out of atmosphere onto soil [L T^{-1}], $u_{q\text{-}plant}$ is the rate at which particles are settled out of atmosphere onto plants [L T^{-1}], F_q is the volumetric fraction of air occupied by aerosols [L^3 L^{-3}], K_{qa} is the contaminant specific aerosol-air partition coefficient, LAI is the leaf area index [L^2 L^{-2}], q_{rain} is the

rainfall velocity [L T^{-1}], S_r is the scavenging ratio [L^3 L^{-3}], K_{aw} is the contaminant specific air-water partition coefficient [-].

3.1.1.2 Diffusive Transfers between the Plant and the Atmosphere

The diffusive flux between the plant and the atmosphere can be expressed as:

$$J_{p,a} = k_{a-p}\left(C_A - C_P K_{AP}\right) \tag{3.7}$$

where $J_{p,a}$ is the diffusive flux between the plant and the atmosphere [M L^{-2} T^{-1}], k_{a-p} is the air to plant diffusive mass transfer rate coefficient [L T^{-1}], C_P is the concentration in the plant [M L^{-3}], and K_{AP} is the contaminant specific air-plant partition coefficient [-].

In order to calculate the air to plant diffusive mass transfer rate coefficient, a two resistance model is adopted as proposed in Cousins and Mackay (2000). This model assumes that the exchange of chemicals between the atmosphere and the plant is occurring in series by diffusion through the leaf and then through the air boundary layer. Note that more detailed models do exist in the literature (e.g. see Riederer (1995)). Two resistance in-series model for calculating k_{a-p} can be written as:

$$\frac{1}{k_{a-p}} = \frac{1}{k_{ab-p} LAI} + \frac{1}{k_c LAI} \tag{3.8}$$

where k_{ab-p} is the mass transfer rate coefficient for the diffusive transport across the plant's air boundary layer [L T^{-1}], and k_c is the mass transfer rate coefficient for the diffusive transport through the leaf cuticle [L T^{-1}]. k_{ab-p} can be estimated as (Cousins and Mackay 2000):

$$k_{ab-p} = \frac{D_g^a}{d_{a,p}} \tag{3.9}$$

where $d_{a,p}$ is the air-plant boundary layer thickness [L]. $d_{a,p}$ is an unknown quantity, but Cousins and Mackay (2000) suggest that it should be of the same order as the soil-air boundary thickness (2-6 mm) or lower. And, k_c can be estimated using the expression below (Cousins and Mackay 2001):

$$k_c = P_c\left(\frac{1}{K_{aw}}\right) \tag{3.10}$$

where P_c is the cuticle permeance [L T^{-1}]. In order to estimate P_c, Cousins and Mackay (2000) propose using Equation (3.11) which takes the average of two separate empirical relationships based on fundamental chemical properties of the contaminant:

$$\log P_c = \frac{\left(0.704\log K_{ow} - 11.2\right) + \left(-3.47 - 2.79\log MW + 0.970\log K_{ow}\right)}{2} \tag{3.11}$$

where K_{ow} is the contaminant specific octanol-water partition coefficient [L^3 L^{-3}] and MW is the molecular weight of the contaminant in g/mol.

3.1.1.3 Transformation within the Plant

Assuming a first order decay rate coefficient can explain the contaminant transformations within the plant, the following equation can be written:

$$R_P = \lambda_p C_P V_P \tag{3.12}$$

where R_P is the contaminant decay rate within the plant [M L^2 T^{-1}], λ_p is the first order decay rate coefficient of the contaminant within the plant [T^{-1}], and V_P is the plant volume per unit land area [L^3 L^{-2}]. Then, the mass transfer rate coefficient that describes the contaminant transformation within the plant, k_p [L T^{-1}], is:

$$k_p = \lambda_p V_P \tag{3.13}$$

3.1.1.4 Washoff

Washoff term refers to the process of contaminant transfer from the plant to the surface soil by the erosion occurring at the aboveground parts of the plant. Cousins and Mackay

(2000) chose to neglect this process in their model and the current version of this model also neglects this process.

3.1.1.5 Litterfall and Root Decay

Litterfall is the process of introduction of the dying aboveground plant parts to the surface soil. As a result of this process, the contaminant within those plant parts is transferred to the soil. Some litterfall is expected to occur at every stage of plant life; however, litterfall quantity should increase at the later stages of plant growth as the senescence starts. Thus, a variable litterfall rate that is dependent on the plant's growth stage should be used.

Root decay is a means of contaminant transfer from plant directly to the subsurface soil. Root decay process is similar with the litterfall process in the sense that both of them are occurring at every stage of the plant life but have variable rates depending on the plant's growth stage. However, root decay differs from litterfall since the spatial variations in the amount of root biomass that turns into soil litter have to be considered. Root density changes with the soil depth and the root decay rate should also be variable with depth depending on the root density at that particular depth.

The current model neglects these two processes since the proper mathematical descriptions are not available. In the future, when the increased understanding of these

processes allows doing so, the modules for litterfall and root decay can be included in the model.

3.1.1.6 Root Uptake

If we neglect the diffusive uptake by roots (as in Cousins and Mackay (2000)), and only consider contaminant uptake by mass flow, organic chemical uptake by the roots can be expressed as:

$$R_U = \int_0^{L_R} \left(k_{s-p}\, C_w \right) dz \tag{3.14}$$

$$k_{s-p}\left(z\right) = TSCF \cdot S\left(z\right) \tag{3.15}$$

where R_U is the mass flow rate into the plant via root uptake [M L^{-2} T^{-1}], k_{s-p} is the mass transfer rate coefficient from soil to plant via root uptake [L T^{-1}], *TSCF* is the transpiration stream concentration factor [L^3 L^{-3}], S is the root water uptake rate [T^{-1}], and L_R is the root depth [L].

In order to estimate *TSCF* for nonionized compounds, Dettenmaier et al. (2009) recommend the following empirical relationship based on the octanol-water partition coefficient (K_{ow}) of the specific chemical being studied:

$$TSCF = \frac{11}{11 + 2.6^{\log K_{ow}}} \tag{3.16}$$

3.1.2 Mass Balance Equation

The summary of the mass transfer processes used in the plant pathway model is given in Table 3.1. The resulting mass balance equation for the plant compartment is given in Equation (3.17):

$$\frac{d\left(V_P C_P\right)}{dt} = \left[\begin{array}{l} \left(k_{dry-plant} + k_{wet-plant} + k_{rain-plant} + k_{a-p}\right) C_A - \left(k_{p-a} + k_p\right) C_P \\ + \int\limits_{\substack{\text{root} \\ \text{zone}}} \left(k_{s-p}\, C_w\right) dz \end{array}\right] \tag{3.17}$$

where V_P is the plant volume [L^3 L^{-2}] and C_P is the contaminant concentration in the plant [M L^{-3}].

Table 3.1: Mass transfer processes considered in the resultant plant pathway model.

Process	***Mass Transfer Rate Coefficient [L T^{-1}]***	***Multiplying Concentration [M L^{-3}]***
Dry particle deposition onto plants	$k_{dry-plant}$	C_A
Wet particle deposition onto plants	$k_{wet-plant}$	C_A
Deposition via rain dissolution onto plants	$k_{rain-plant}$	C_A
Diffusive flow from atmosphere to plant	k_{a-p}	C_A
Diffusive flow from plant to atmosphere	k_{p-a}	C_P
Transformation within the plant	k_p	C_P
Root uptake	k_{s-p}	C_w

3.2 Plant Life-Cycle Model

The plant life-cycle model is a critical component of this study since it provides the time dependent values for the leaf area index (*LAI*), the root depth, the root density distribution and the plant volume which are all used by the other models that describe the water flow and transport processes in the terrestrial system that is being analyzed. In this study, the crop growth model that has been successfully applied to agricultural water management by Mailhol, Olufayo et al. (1997), Wohling and Schmitz (2007) and Mailhol and Merot (2008) is adopted.

The plant life-cycle model is a collection of sub-models that describe the different growth stages that the plant go through over time as it continuously interacts with the natural and anthropogenic environmental conditions. The overall plant-life cycle model used in this study can be put into the category of descriptive plant growth models rather than the explanatory models (Section 2.4). The model is composed of relationships that predict various plant characteristics using a set of physically significant parameters. These relationships are simple but they are sophisticated enough to analyze the effects of various feedback processes. The model can dynamically simulate the most fundamental plant life-cycle related parameters required for a fully integrated terrestrial ecosystem model. The effect of climatic conditions on the plant growth is modeled through the use of variables such as thermal time and solar radiation. The model is compatible with macroscopic root water uptake modeling methodology, so it is easy to be integrated with the soil-water flow models in order to analyze the plant response to water stress.

A further advantage of the plant life-cycle model is its flexibility. It is easy to modify the model components and improve the overall model since the model has a modular structure and the relationships that are used are simple but physically meaningful. For instance, the same *LAI* model used in this study had been modified by Mailhol and Merot (2008) to incorporate the impact of solar radiation deficiency by simply adding an extra term to the model equation.

3.2.1 The Leaf Area Index Simulation Model

The *LAI* simulation model calculates the daily average values of *LAI* based on a thermal time concept following the approach of the model PILOTE 1.3 by Mailhol et al. (1997) and Wohling and Schmitz's (2007) generalization of the same model to crop growth. In this model, thermal time is the basic driving force for *LAI* development. The plant response to water stress is modeled by the inclusion of a water stress index (*WSI)* term.

$$LAI(i) = LAI_{\max}\left[\left(\frac{TT(i)-T_s}{T_f}\right)^{\beta} \times \exp\left\{\frac{\beta}{\delta}\left(1-\left(\frac{TT(i)-T_s}{T_f}\right)^{\delta}\right)\right\} - \left(1-\left(WSI(i)\right)^{\lambda}\right)\right] \quad (3.18)$$

$$TT(i) = \sum_{k=1}^{k=i}\left(T(i)-T_b\right) \quad (3.18a)$$

$$WSI(i) = \frac{T_A(i)}{T_P(i)} \quad (3.18b)$$

where i is the number of days past since the day of sowing, $LAI_{\max}$ is the maximum value of the leaf area index [L^2 L^{-2}], $TT(i)$ the thermal time on day i in degree days [$\hat{T}T$] (where $\hat{T}$ is temperature), T_s is the thermal time of emergence [$\hat{T}T$], T_f is the threshold thermal time corresponding to $LAI_{\max}$ [$\hat{T}T$], β and δ are parameters related to the shape of the *LAI* curve, $WSI(i)$ is the water stress index, λ is a dimensionless parameter governing the plant sensitivity to water stress, $T(i)$ is the daily mean air temperature in °C [$\hat{T}$], T_b is the base temperature of the crop [$\hat{T}$], $T_A(i)$ is the actual daily transpiration rate on day i [$L\ T^{-1}$], and $T_P(i)$ is the potential transpiration rate on day i [$L\ T^{-1}$].

The terms T_f and $LAI_{\max}$ are plant specific and are obtained by measurements. The information on how the *LAI* curve changes with time for a crop in certain conditions may be used to determine the parameters β, δ, and λ. Mailhol, Olufayo et al. (1997) propose to change δ with a lower value after $LAI_{\max}$ or after $TT(i) = T_f$ + 40°C in order to simulate slow senescence for crops such as corn. The actual and potential transpiration rates are calculated by coupling the *LAI* model with the soil-water flow model.

3.2.2 The Plant Biomass Model

The plant biomass is calculated as in Mailhol and Merot (2008). In their study, they had modified Mailhol, Olufayo et al.'s (1997) crop yield model and calculated the dry matter

accumulation of hay at daily time steps. They have introduced a new parameter, R_p, to simulate a hindered growth of plant due to decreased *LAI* values.

$$m_p(i) = m_p(i-1) + R_p(i) \cdot RUE \cdot SR(i) \cdot ISR^*(i) \tag{3.19}$$

$$R_p(i) = \frac{CLAI(i-3)}{CLAI^*(i-3)} \tag{3.19a}$$

$$ISR^*(i) = 1 - e^{-\left[c_{ext}^*(i) \cdot LAI^*(i)\right]} \tag{3.19b}$$

$$c_{ext}^*(i) = \min\left\{1.0, 1.43 \cdot \left[LAI^*(i)\right]^{-0.5}\right\} \tag{3.19c}$$

where $m_p(i)$ is the total above ground dry biomass on day *i* [M L^{-2}], *RUE* is the intercepted radiation use efficiency (i.e. the amount of above-ground biomass [M] produced per Joule [M L^2 T^{-2}] of solar energy received) [T^2 L^{-2}], *SR* is the daily incident solar radiation per area [M T^{-2}], $ISR^*(i)$ is the fraction of solar radiation intercepted by the crop on day *i*, $CLAI(i-3)$ is the cumulative leaf area index value on the last 3 days [L^2 L^{-2}], $CLAI^*(i-3)$ is the cumulative leaf area index value calculated assuming no water stress on the last 3 days [L^2 L^{-2}], and $LAI^*(i)$ is the leaf area index value on day *i* calculated assuming no water stress [L^2 L^{-2}].

In the plant pathway model, one of the parameters used is the volume of the plant compartment. The plant volume that corresponds to to the calculated plant biomass is

determined by Equation (3.20) using the relationship between the fresh volume of the plant and plant's water content and dry density (Matthies and Behrendt 1995):

$$V_P = \left(\frac{m_P}{1 - W_P} \right) \frac{1}{\rho_P} \tag{3.20}$$

where W_P is the water content of the plant [L^3 L^{-3}] and ρ_P is the dry density of the plant [M L^{-3}].

3.2.3 The Root Model

The time dependent value of the root depth and the root distribution are required for dynamic representation of the root water uptake rate distribution within the soil column as plants go through different growth stages. In this study, the root depth is estimated using a linear root growth function which is a commonly employed method. Sigmoidal (Yadav et al. 2009b) and sinusoidal (Yadav et al. 2009a) growth functions were also considered as alternative root growth models; however, no significant difference on the overall model output was observed and the linear growth function was selected since it required less input parameters. The daily values of root depth are calculated using Equation (3.21).

$$L_R(t_R) = \begin{cases} L_R(0) + \dfrac{L_{R,\max} - L_R(0)}{t_{R,\max}} t_R & t_R < t_{R,\max} \\ L_{R,\max} & t_R \geq t_{R,\max} \end{cases} \tag{3.21}$$

where $L_R(t_R)$ is the root depth at time t_R [L], $L_R(0)$ is the initial root depth [L], $L_{R,\max}$ is the maximum root depth [L], $t_{R,\max}$ is the time required to reach $L_{R,\max}$ [T].

The root distribution is calculated by using Novak's (1987) exponential root distribution function given in Equation (3.22). Novak (1987) has developed a model to estimate root water extraction rate using this root distribution function that agrees with the experimental measurements when the transpiration is at the potential rate. Novak's (1987) function is in accordance with van den Honert's (1948) hypothesis which is the basis of many "physically and physiologically" correct methods for calculating root water uptake (Novak 1987). However, these methods require the determination of hydraulic resistance to flow from soil to the plant as well as the water potential within the plant, which are difficult to determine in practice. Novak's model on the other hand requires only a single dimensionless empirical parameter and gives results which agree with the experimental measurements:

$$b(z) = \frac{\delta \exp\left[-\delta\left(z / L_R\right)\right]}{L_R\left[1-\exp(-\delta)\right]} \tag{3.22}$$

where $b(z)$ is the normalized root distribution [-] and δ is a dimensionless empirical constant (3.64 for corn).

The term “normalized” root distribution indicates that the returned value by Equation (3.22) is not the actual root density at the given depth but it is the fraction of the total root density residing at that depth. The integration of Equation (3.22) over the total root zone length (L_R) gives 1, so it can be used in a macroscopic root water uptake model without any modifications. The root water uptake model used in this study is described in Chapter 5 when the coupling of the soil-water flow and the plant life-cycle models is discussed.

CHAPTER 4

FLOW AND TRANSPORT MODELS

4.1 Unsaturated Zone Soil-Water Flow Model

4.1.1 Model Development

The governing equation that describes the water flow in the unsaturated zone is the Richards' equation (Richards 1931). The one dimensional mixed form of the Richards' equation, with the root water uptake term represented as a sink term, is given in Equation (4.1):

$$\frac{\partial \theta}{\partial t} = \frac{\partial}{\partial z}\left(K_u \left(\frac{\partial h}{\partial z} - 1 \right) \right) - U \qquad (4.1)$$

where θ is the volumetric water content [L^3 L^{-3}], t is time [T], K_u is the unsaturated hydraulic conductivity [L T^{-1}], h is the soil-water pressure head [L], z is the soil depth [L] (positively directed downward), and U is the root water uptake rate [T^{-1}]. Note that this form of the Richard's equation as given in Equation (4.1) neglects the compressibility of water.

By introducing the specific moisture capacity term, $C = C(h) = (d\theta / dh)$, the pressure based form of the Richard's equation can be written as:

$$C\frac{dh}{dt} = \frac{\partial}{\partial z}\left(K_u\left(\frac{\partial h}{\partial z} - 1\right)\right) - U \tag{4.2}$$

The solution of the Richards' equation requires the knowledge of the appropriate constitutive relationships between θ and K_u, and h. The widely used method to estimate the soil-water retention and hydraulic conductivity relationships in the vadose zone is the van Genuchten equations (1980):

$$S_e(h) = \frac{\theta(h) - \theta_r}{\theta_s - \theta_r} = \left[1 + \left(\alpha_v |h|\right)^{n_v}\right]^{-m_v} \tag{4.3}$$

$$K_u(h) = K_s\left(S_e(h)\right)^{1/2}\left[1 - \left(1 - \left(S_e(h)\right)^{1/m_v}\right)^{m_v}\right]^2 \tag{4.4}$$

where S_e is the effective saturation [$L^3\ L^{-3}$], θ_r is the residual water content [$L^3\ L^{-3}$], θ_s is the saturated water content [$L^3\ L^{-3}$], K_s is the saturated hydraulic conductivity [$L\ T^{-1}$], and α_v [L^{-1}], n_v (dimensionless) and m_v (dimensionless) are constants depending on the soil type, where $m_v = (1 - 1/n_v)$.

In this study the control volume method is used to solve Equation (4.1) (Berg 1999). In this approximation the soil column is divided into N cells in the vertical direction each with a grid point at the center (Figure 4.1). The variation in space and time of the relevant variables is assumed to be described by piecewise continuous profiles determined by their

grid point values (Berg 1999). Then a mass balance for water for each cell is written where the water flux between each cell, q [L T^{-1}], is given by the Darcy's law as:

$$q = -K_u \left(\frac{\partial h}{\partial z} - 1 \right) \tag{4.5}$$

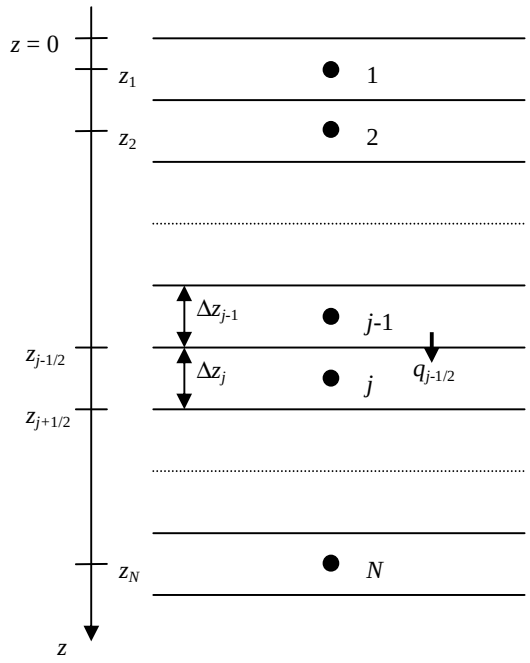

Figure 4.1: Spatial discretization of the soil column. (j: cell number; Δz_j: thickness of cell j; $q_{j-1/2}$: water flux from cell j-1 to cell j)

Following the spatial discretization, the resulting set of equations can be obtained for j = 1,…,N as shown below (See Appendix A for the details):

$$M_j \left(\frac{dh}{dt} \right)_j + S_j^1 h_{j-1} + S_j^2 h_j + S_j^3 h_{j+1} = F_j \tag{4.6}$$

$$M_j = C_j \Delta z_j \tag{4.6a}$$

$$S_j^1 = -\left(\frac{K_{j-1/2}}{0.5\left(\Delta z_j + \Delta z_{j-1}\right)} \right) \tag{4.6b}$$

$$S_j^2 = \left(\frac{K_{j+1/2}}{0.5\left(\Delta z_{j+1} + \Delta z_j\right)} + \frac{K_{j-1/2}}{0.5\left(\Delta z_j + \Delta z_{j-1}\right)} \right) = -\left(S_j^3 + S_j^1\right) \tag{4.6c}$$

$$S_j^3 = -\left(\frac{K_{j+1/2}}{0.5\left(\Delta z_{j+1} + \Delta z_j\right)} \right) \tag{4.6d}$$

$$F_j = \left[-K_{j+1/2} + K_{j-1/2} - U_j \Delta z_j \right] \tag{4.6e}$$

$$C_j = \frac{\left\{\theta_j\right\}_{t+\Delta t} - \left\{\theta_j\right\}_t}{\left\{h_j\right\}_{t+\Delta t} - \left\{h_j\right\}_t} \tag{4.6f}$$

where Δt is the time step size used in the temporal discretization, and $K_{j\pm1/2}$ are the interblock hydraulic conductivity values [L T^{-1}]. The interblock hydraulic conductivity values can be calculated as the arithmetic (Equation 4.7a), geometric (Equation 4.7b) or harmonic (Equation 4.7c) mean of the hydraulic conductivities associated with the adjacent cells:

$$K_{j+1/2} = \frac{K_j + K_{j+1}}{2} \tag{4.7a}$$

$$K_{j+1/2} = \left(K_j K_{j+1}\right)^{1/2} \tag{4.7b}$$

$$K_{j+1/2} = \frac{\left(\Delta z_j + \Delta z_{j+1}\right) K_j K_{j+1}}{\Delta z_j K_{j+1} + \Delta z_{j+1} K_j} \tag{4.7c}$$

There is no consensus in the literature on which method of calculating the interblock hydraulic conductivities is superior. For example, Haverkamp and Vauclin (1979) and Schnabel and Richie (1984) favor using the geometric mean, while Berg (1999) and Manzini and Ferraris (2004) defend using the harmonic mean on the basis of its being able to be derived from physical arguments. On the other hand the SWAP model uses the arithmetic mean to calculate the interblock hydraulic conductivity values (van Dam and Feddes 2000).

In Equtation 4.6, C_j is the representative mean value of the specific water capacity throughout the cell j, $C_j = \left(d\theta/dh\right)_j$. The specific water capacity needs special attention in developing a mass-conservative numerical scheme for the solution of the Richards' equation. The approximation in Equation 4.6f arises naturally in the control volume solution of Berg (1999) and it produces a mass conservative scheme. This approximation is equivalent to the approximations of Cooley (1983) and Milly (1985) using finite element methods.

Finally, an implicit time integration method together with Picard iteration is used to obtain the spatial and the temporal distribution of soil-water pressure head within the soil column. This component of the analysis is standard in the vadose zone analysis literature (Berg 1999; Celia et al. 1990; van Dam and Feddes 2000) and it is explained in more detail in Appendix F.

4.1.2 Model Testing

The unsaturated zone soil-water flow model was first tested with an example problem from Lehman and Ackerer (1998). Lehman and Ackerer (1998) modeled infiltration into a homogeneous porous medium having an initial water content close to the residual one. The soil column length was taken to be 30 cm. The initial water pressure head was set to be -1000 cm throughout the column. The upper boundary condition was h_{top} = -75 cm and the bottom boundary condition was h_{bottom} = -1000 cm (Figure 4.2). The soil hydraulic parameters were K_s = 0.00922 cm/s, θ_s = 0.368, θ_r = 0.102, α = 0.0335 cm^{-1}, and n = 2. The column was divided into 120 cells with 0.25 cm thickness. A 6-hour simulation was performed with a time step size of 30 seconds.

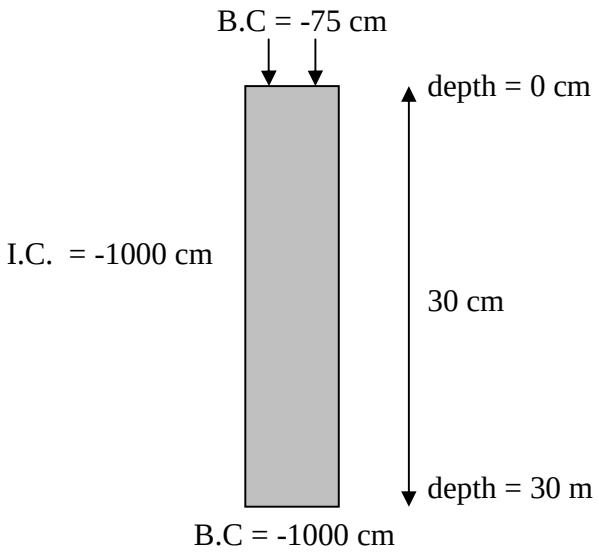

Figure 4.2: The modeling domain and the initial (I.C) and boundary (B.C.) conditions for the example problem of Lehman and Ackerer (1998).

In their study, Lehman and Ackerer (1998) used the semi-analytical solution of Philip (1957) and compared it to the numerical solutions with modified Picard and Newton iterations. The model developed in this study was solved using different methods to calculate interblock hydraulic conductivities: arithmetic mean, geometric mean, and harmonic mean. The results obtained by the model developed in this study are compared to the results of Lehmann and Ackerer (1998) in Figure 4.3. The pressure head profile obtained by calculating the interblock hydraulic conductivities using the arithmetic means is exactly the same as Lehman and Ackerer's results obtained by using the Picard iteration method. This is expected since Picard iteration is also the iteration method used in this study. The profile obtained by using the geometric means is similar to the results obtained by Philip's (1957) solution which predicts a slightly higher infiltration front than the profile obtained by using the arithmetic means. On the other hand, the results obtained by using the harmonic means predict the infiltration front at a much higher depth than the other methods. The results show that the model developed in this study can reproduce the results obtained by Lehman and Ackerer (1998) and the results of Philip's (1957) semi-analytical solution in this infiltration problem when arithmetic and geometric means are used to calculate the interblock hydraulic conductivity values.

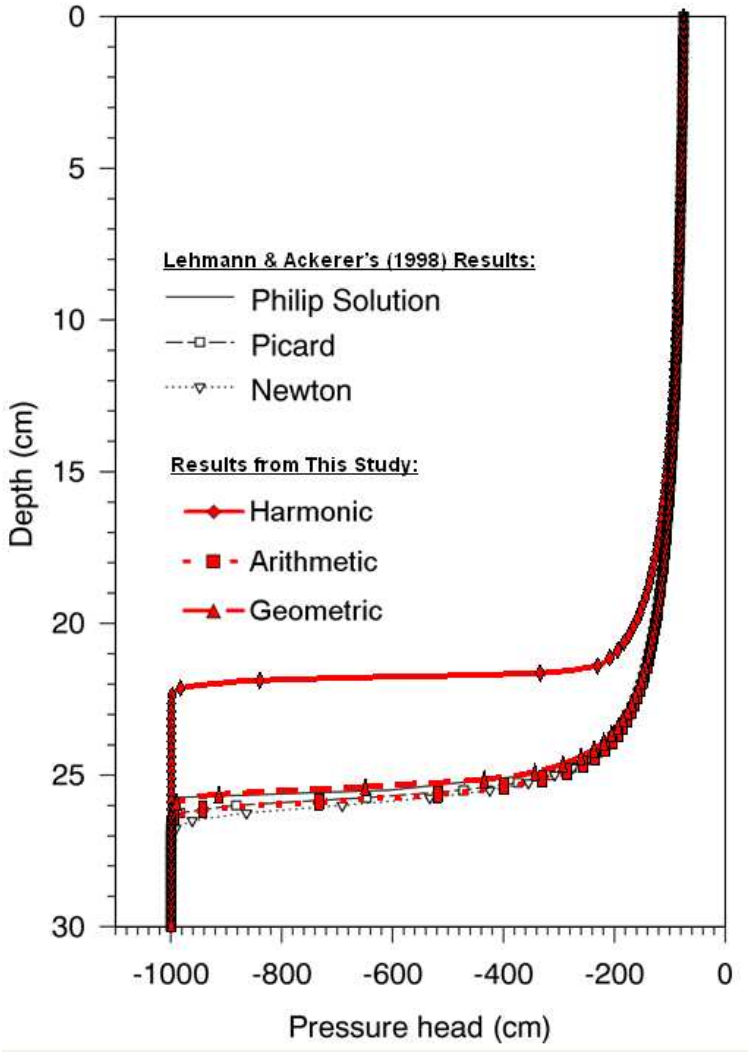

Figure 4.3: Comparison of the results obtained by this study and the results of Lehman and Ackerer (Lehmann and Ackerer 1998).

The produced model was also tested using the steady state infiltration and evaporation scenarios of Vanderborght et al. (2005). Vanderborght et al. (2005) created analytical benchmarks for soil-water flow problems and used them to evaluate a number of numerical models available (i.e. MACRO, HYDRUS, SWAP, WAVE, and MARTHE). Solving the same test problems with the model developed in this study enables a comparison with these numerical models as well as the analytical solution.

The first scenario from Vanderborght et al. (2005) is steady-state infiltration with a flux of 0.5 cm/day through a layered soil profile. Two soil layers were considered: the first one extending through the top 50 cm of the soil column, the second one extending from 50 cm to 200 cm. Three different combinations of soil types were simulated: (i) loam over sand; (ii) sand over loam; and, (iii) clay over sand. The standard soil hydraulic properties for the soil textures of loam, sand, and clay as provided in the soil catalog of HYDRUS 1D software were used (Simunek et al. 2008). An initial pressure head of -200 cm throughout the column was assumed. A zero-gradient boundary condition was assumed at the bottom of the soil column. The soil column was discretized using a cell thickness of 1 cm. The results obtained by the model developed in this study is compared with the results obtained by the analytical benchmark of Vanderborght et al. (2005) and the other numerical models in Figure 4.4 (loam over sand), Figure 4.5 (sand over loam), and Figure 4.6 (clay over sand). The model developed in this study was able to reproduce the pressure head profiles obtained by the analytical benchmark in the simulations with loam over sand (Figure 4.4) and with clay over sand (Figure 4.6). For the simulation with sand over loam (Figure 4.5), the sharp transition at the interface was not exactly

reproduced. However, most of the numerical models tested by Vanderborght et al. (2005) had also simulated a gradual transition at the interface. For this case, the proposed model performed as good as SWAP and better than HYDRUS.

Next, a steady-state evaporation with a constant flux of 0.5 cm/day was simulated. The modeling domain is a loamy soil profile with a depth of 54 cm. A zero pressure head boundary condition at the bottom of the soil profile is assumed. The initial pressure head values varied linearly with 0 cm at the bottom to -54 cm at the top of the column. The spatial discretization was again 1 cm. The model solution is compared with the analytical benchmark of Vanderborght et al. (2005) and the other numerical models' results in Figure 4.7. The model results match with the analytical solution.

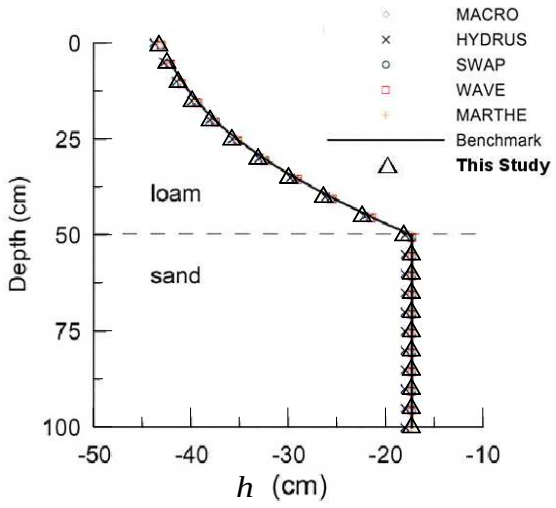

Figure 4.4: Steady-state soil-water pressure head profiles in layered soil (loam over sand) with a constant infiltration rate of 0.5 cm/day. (Comparison with the test in Vanderborght et al. (2005))

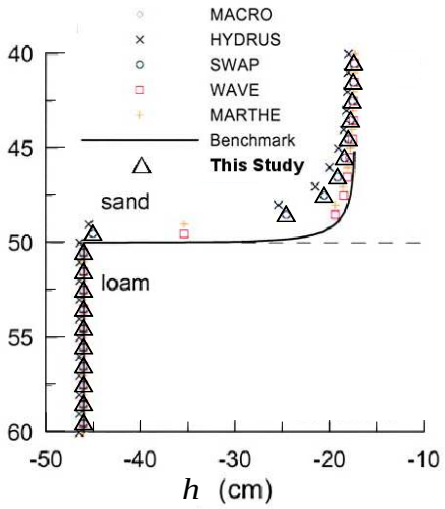

Figure 4.5: Steady-state soil-water pressure head profiles in layered soil (sand over loam) with a constant infiltration rate of 0.5 cm/day. (Comparison with the test in Vanderborght et al. (2005))

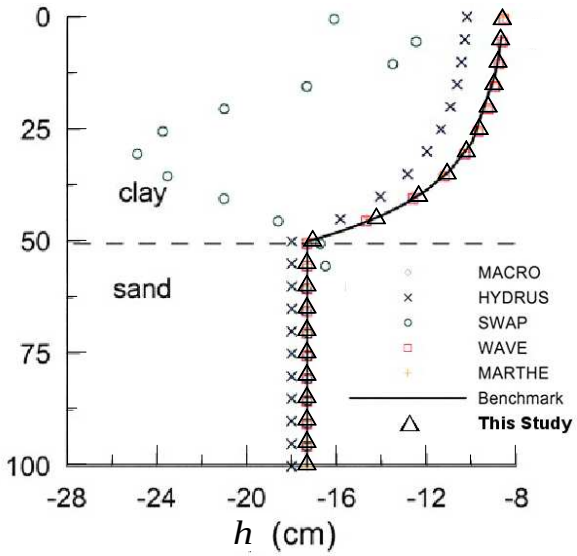

Figure 4.6: Steady-state soil-water pressure head profiles in layered soil (clay over sand) with a constant infiltration rate of 0.5 cm/day. (Comparison with the test in Vanderborght et al. (2005))

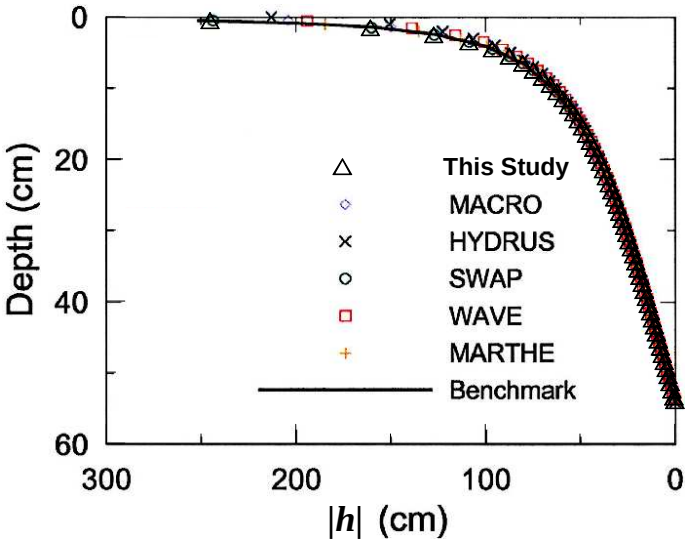

Figure 4.7: Steady-state soil-water pressure head profiles with a constant evaporation rate of 0.5 cm/day. (Comparison with the test in Vanderborght et al. (2005))

4.2 Vadose Zone Contaminant Transport Model

4.2.1 Model Development

To model the contaminant transport in the vadose zone, the advection-dispersion-reaction equation is used. The transport equation for an organic contaminant assuming linear equilibrium partitioning between three phases (i.e. soil-solids, soil-water, and soil-air) is given in Equation (4.8).

$$\frac{\partial}{\partial t}\left[G_1 C_w\right] = \underbrace{\frac{\partial}{\partial z}\left(G_2 \frac{\partial C_w}{\partial z} - G_3 C_w\right)}_{\text{advection-dispersion}} + \underbrace{G_4 C_w + G_5}_{\text{source/sink/transformation}} \tag{4.8}$$

$$G_1 = \rho_b K_d + \phi s_g K_H + \phi s_w \tag{4.8a}$$

$$G_2 = \phi s_w D_w + \phi s_g D_g K_H \tag{4.8b}$$

$$G_3 = q \tag{4.8c}$$

$$G_4 = -\left(\lambda_s \rho_b K_d + \lambda_g \phi s_g K_H + \lambda_w \phi s_w\right) - r_u \tag{4.8d}$$

$$G_5 = M \tag{4.8e}$$

where G_1 is the bulk coefficient for the partitioning processes [L^3 L^{-3}], C_w is the contaminant concentration in soil-water [M L^{-3}], G_2 is the bulk coefficient for the dispersion processes [L^2 T^{-1}], G_3 is the bulk coefficient for the advection process [L T^{-1}], G_4 is the bulk coefficient for the first-order loss processes [T^{-1}], G_5 is the bulk term for the source/sink processes [M L^{-3} T^{-1}], ρ_b is the soil bulk density [M L^{-3}] , K_d is the

partition coefficient between soil-solids and soil-water [L^3 M^{-1}], ϕ is porosity [L^3 L^{-3}], s_g is soil-gas saturation [L^3 L^{-3}], K_H is the dimensionless Henry's Law constant [-], s_w is soil-water saturation [L^3 L^{-3}], D_w is the dispersion coefficient in soil-water [L^2 T^{-1}], D_g is the dispersion coefficient in soil-air [L^2 T^{-1}], λ_s is the first-order transformation rate coefficient in soil-solids [T^{-1}], λ_g is the first-order transformation rate coefficient in soil-air [T^{-1}], λ_w is the first-order transformation rate coefficient in soil-water [T^{-1}], r_u is the root uptake rate [T^{-1}], and M is the source / sink term [M L^{-3} T^{-1}].

In determining the dispersion coefficients in soil-water and soil-air, the tortuosity of the porous medium is taken into account by using the expressions (Chu and Marino 2004):

$$D_w = \frac{(\phi s_w)^{7/3}}{\phi^2} D_l^w + \alpha_L \frac{q}{\phi s_w} \tag{4.9a}$$

$$D_g = \frac{(\phi s_g)^{7/3}}{\phi^2} D_g^a \tag{4.9b}$$

where D_l^w is the molecular diffusion coefficient [L^2 T^{-1}] in water, D_g^a is the molecular diffusion coefficient [L^2 T^{-1}] in free air, α_L is the longitudinal dispersivity [L]. Note that the mechanical dispersion process is included when calculating the dispersion in soil-water through the second term in Equation (4.9a)

The contaminant transport equation is spatially discretized using the finite volume methods after dividing the soil column into N cells similar to the discretization used in

the soil-water flow equation (Figure 4.1). Using cell centered (CC) finite volume method (FVM), the equation is integrated over a control volume (CV), then appropriate approximations are made for fluxes across the boundary of each CV. For this case (one-dimensional problem), control volumes reduce to cell thicknesses. The details of the spatial discretization process are given in Appendix B.

As a result, the following set of equations are obtained for $j = 1,\ldots,N$:

$$\left(\frac{d\left(G_1 C_w\right)}{dt}\right)_j M_j + S_j^1 \left(C_w\right)_{j-1} + S_j^2 \left(C_w\right)_j + S_j^3 \left(C_w\right)_{j+1} = F_j \tag{4.10}$$

$$M_j = \Delta z_j \tag{4.10a}$$

$$S_j^1 = -\left[A_{j-1/2}\left(1-\alpha_{j-1/2}\right) + D_{j-1/2} \right] \tag{4.10b}$$

$$S_j^2 = -\left[A_{j+1/2}\alpha_{j+1/2} + A_{j-1/2}\alpha_{j-1/2} - D_{j+1/2} - D_{j-1/2} + \left(G_4\right)_j \Delta z_j \right] \tag{4.10c}$$

$$S_j^3 = -\left[A_{j+1/2}\left(1-\alpha_{j+1/2}\right) + D_{j+1/2} \right] \tag{4.10d}$$

$$F_j = \left(G_5\right)_j \Delta z_j \tag{4.10e}$$

$$A_{j-1/2} = \left(G_3\right)_{j-1/2} \tag{4.10f}$$

$$A_{j+1/2} = -\left(G_3\right)_{j+1/2} \tag{4.10g}$$

$$D_{j-1/2} = \frac{\left(G_2\right)_{j-1/2}}{\left[\dfrac{\left(\Delta z\right)_j + \left(\Delta z\right)_{j-1}}{2}\right]} \tag{4.10h}$$

$$D_{j+1/2} = \frac{\left(G_2\right)_{j+1/2}}{\left[\frac{\left(\Delta z\right)_{j+1} + \left(\Delta z\right)_j}{2}\right]} \tag{4.10i}$$

where the terms $A_{j\pm1/2}$ represent the "advective strength" between cell j and its neighboring cells, the terms α are the weighting factors used in the discretization of the advection term, and the terms $D_{j\pm1/2}$ represent the "diffusive conductance" between cell j and its neighboring cells (Wheeler et al. 2007). Using the value $\alpha_{j-1/2} = \alpha_{j+1/2} = 1/2$ yields the central differencing scheme which is used in this study.

A separate equation was developed to handle the soil surface boundary in a way similar to the "zero thickness" cell approach applied in Berg, Swaney et al. (2007). This approach enables a more accurate description of the volatilization and atmospheric deposition processes. This equation is written in the same format as the spatially discretized transport equation (Equation 4.9); and, it is added to the equation set with the index $j = 0$ referring to the soil surface boundary located just above cell 1:

$$\left(\frac{d\left(G_1 C_w\right)}{dt}\right)_0 M_0 + S_0^2 \left(C_w\right)_0 + S_0^3 \left(C_w\right)_1 = F_0 \tag{4.11}$$

$$M_0 = \Delta z_0 = 0 \tag{4.11a}$$

$$S_0^2 = -\left[A_{1/2}\alpha_{1/2} - D_{1/2} - D_{Soil-Atm}\right] \tag{4.11b}$$

$$S_0^3 = -\left[A_{1/2}\left(1-\alpha_{1/2}\right) + D_{1/2}\right] \tag{4.11c}$$

$$F_0 = \left[D_{Atm-Soil}\right] C_A + E_{Atm-Soil} + E_0 \tag{4.11d}$$

where $D_{Soil-Atm}$ is the diffusive mass transfer rate coefficient from the soil to the atmosphere (volatilization rate coefficient) [L T^{-1}], $D_{Atm-Soil}$ is the diffusive mass transfer rate coefficient from atmosphere to soil [L T^{-1}] , C_A is the contaminant concentration in the atmosphere [M L^{-3}], $E_{Atm-Soil}$ is the atmospheric deposition rate onto soil [M L^{-2} T^{-1}], and E_0 is the source input rate [M L^{-2} T^{-1}].

The diffusive flux between the soil and the atmosphere can be expressed using a boundary layer model (Chu and Marino 2004) as:

$$J_{s,a} = D_g^a \frac{C_A - K_{aw} C_w(0)}{d} \tag{4.12}$$

where $J_{s,a}$ is the diffusive flux between the soil surface and the atmosphere [M L^{-2} T^{-1}], D_g^a is the diffusion coefficient in free air [L^2 T^{-1}], K_{aw} is the air-water partition coefficient [L^3 L^{-3}], $C_w(0)$ is the water phase contaminant concentration at the soil surface [M L^{-3}], d is the air-soil boundary layer thickness [L]. Then, the diffusive mass transfer rate coefficients between the soil and the atmosphere are determined by rewriting Equation (4.12) as:

$$J_{s,a} = D_{Atm-Soil} C_A - D_{Soil-Atm} C_w(0) \tag{4.13}$$

$$D_{Atm-Soil} = \frac{D_g^a}{d} \tag{4.13a}$$

$$D_{Soil-Atm} = \frac{D_g^a}{d} K_{aw} \tag{4.13b}$$

After the spatial discretization, an implicit time integration method is used to obtain the spatial and the temporal distribution of contaminant concentrations within the soil column. The details of time integration are given in Appendix E.

4.2.2 Model Testing

The soil transport model was tested by comparing it to the analytical solution provided in van Genuchten and Alves (1982) for one-dimensional advective-dispersive transport of solutes in the subsurface. The particular analytical solution used in the test takes into account the retardation and the first-order decay processes as well. The contamination scenario considers continuous source input at the model boundary with a specified constant concentration. The model parameters used in the test are given in Table 4.1. In the model simulation, a zero—gradient boundary condition was assigned at the downstream boundary. The comparison of the model results with the analytical solution is given in Figure 4.8. It is seen that the model results exactly match with the analytical solution.

Table 4.1: Test parameters used in the soil transport model comparison with the analytical solution.

Length of the model domain	100 m
Simulation period	20 days
Spatial discretization, Δx	2 m
Specified contaminant concentration at the boundary, $C_{w,0}$	1 g/m^3
Initial contaminant concentration, $C_{w,i}$	0 g/m^3
Darcy flux, q	1.0×10^{-5} m/s
Porosity, ϕ	0.45
Soil bulk density, ρ_b	1.32×10^{-6} g/m^3
Partition coefficient, K_d	6.8×10^{-8} m^3/g
Dispersion coefficient, G_2	1.0×10^{-4} m^2/s
First-order decay rate coefficient, G_4	1.0×10^{-6} s^{-1}

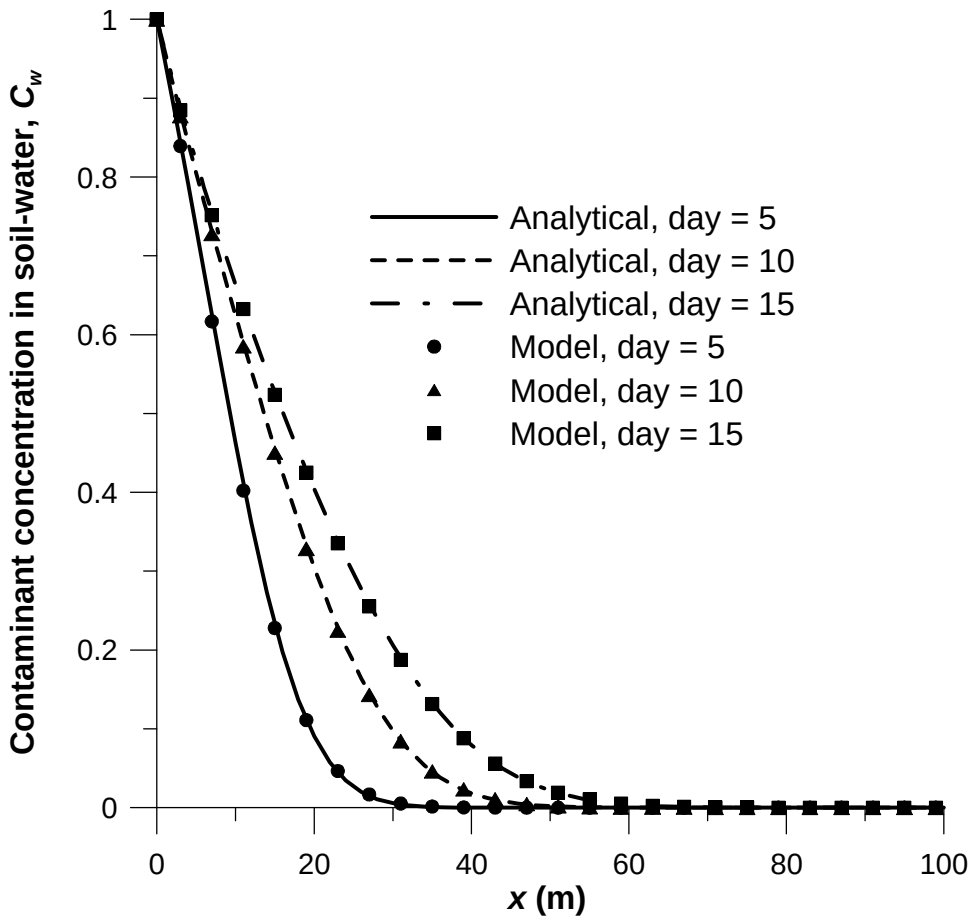

Figure 4.8: Soil transport model comparison with the analytical solution.

4.3 Overland Flow Model

4.3.1 Model Development

The full set of two-dimensional dynamic and unsteady shallow water flow equations (the Saint Venant's equations) are composed of the continuity equation (Equation 4.14) and two momentum equations (Equation 4.15) (Feng and Molz 1997; Hromadka et al. 1987):

$$\frac{\partial H}{\partial t}+\frac{\partial q_x}{\partial x}+\frac{\partial q_y}{\partial y}=0 \tag{4.14}$$

$$\frac{1}{gh}\left[\frac{\partial q_x}{\partial t}+\frac{\partial}{\partial x}\left(\frac{q_x^2}{h}\right)+\frac{\partial}{\partial y}\left(\frac{q_x q_y}{h}\right)\right]+\left(\frac{\partial H}{\partial x}+S_{fx}\right)=0 \tag{4.15a}$$

$$\frac{1}{gh}\left[\frac{\partial q_y}{\partial t}+\frac{\partial}{\partial y}\left(\frac{q_y^2}{h}\right)+\frac{\partial}{\partial x}\left(\frac{q_x q_y}{h}\right)\right]+\left(\frac{\partial H}{\partial x}+S_{fy}\right)=0 \tag{4.15b}$$

where H is the water surface elevation [L] of overland flow $(H=h+Z)$, h is the flow depth [L], Z is the land surface elevation [L], t is time [T], q_x is the water flux [L^2 T^{-1}] (water flow rate per unit width) in x-direction, q_y is the water flux in y-direction [L^2 T^{-1}] (water flow rate per unit width), g is the gravitational acceleration [L T^{-2}], S_{fx} is the friction slope [L L^{-1}] in x-direction (slope of the total energy line), S_{fy} is the friction slope in y-direction [L L^{-1}] (slope of the total energy line).

It is often unnecessary to solve the full set of Saint-Venant equations and various approximations based on neglecting certain terms of the momentum equations have been proposed (Hunter et al. 2007). The zero-inertia (diffusion wave) approximation is obtained by neglecting the local and convective acceleration terms in the momentum equations (These are the three terms in the brackets of Equations (4.15a) and (4.15b)) (Hromadka and Yen 1986). This simplification makes the total energy line and the water surface the same by reducing the momentum equations to:

$$\frac{\partial H}{\partial x} = -S_{fx} \tag{4.16a}$$

$$\frac{\partial H}{\partial y} = -S_{fy} \tag{4.16b}$$

There are various methods to evaluate the friction slopes. The most widely used method is to use the Manning's equation (Dutta et al. 2000):

$$S_{fx} = \frac{n_x^2 u^2}{h^{4/3}} \tag{4.17a}$$

$$S_{fy} = \frac{n_y^2 v^2}{h^{4/3}} \tag{4.17b}$$

where n_x is the Manning's roughness coefficient [T $L^{-1/3}$] in x-direction, n_y is the Manning's roughness coefficient [T $L^{-1/3}$] in y-direction, u is the flow velocity [L T^{-1}] in the x-direction, and v is the flow velocity [L T^{-1}] in the y-direction.

Combining Equations (4.16) and (4.17) yields:

$$\left|\frac{\partial H}{\partial x}\right| = \frac{n_x^2 u^2}{h^{4/3}} \tag{4.18a}$$

$$\left|\frac{\partial H}{\partial y}\right| = \frac{n_y^2 v^2}{h^{4/3}} \tag{4.18b}$$

By rearranging Equation (4.17), the flow velocity expressions are obtained:

$$|u| = \frac{h^{2/3}}{n_x}\left|\frac{\partial H}{\partial x}\right|^{1/2} \tag{4.19a}$$

$$|v| = \frac{h^{2/3}}{n_y}\left|\frac{\partial H}{\partial y}\right|^{1/2} \tag{4.19b}$$

The relationship with the water flux and the flow velocities are:

$$q_x = uh \tag{4.20a}$$

$$q_y = vh \tag{4.20b}$$

So, the water flux terms can be expressed as:

$$|q_x| = \frac{h^{5/3}}{n_x}\left|\frac{\partial H}{\partial x}\right|^{1/2} \tag{4.21a}$$

$$\left|q_y\right| = \frac{h^{5/3}}{n_y}\left|\frac{\partial H}{\partial y}\right|^{1/2} \tag{4.21b}$$

The relationship obtained between the water fluxes and the water surface gradients enables defining the water fluxes in the form of diffusive fluxes:

$$q_x = -\frac{h^{5/3}}{n_x}\frac{1}{\left|\frac{\partial H}{\partial x}\right|^{1/2}}\frac{\partial H}{\partial x} = -D_x\frac{\partial H}{\partial x} \tag{4.22a}$$

$$q_y = -\frac{h^{5/3}}{n_y}\frac{1}{\left|\frac{\partial H}{\partial y}\right|^{1/2}}\frac{\partial H}{\partial y} = -D_y\frac{\partial H}{\partial y} \tag{4.22b}$$

with the diffusion coefficients defined as:

$$D_x = \frac{h^{5/3}}{n_x}\frac{1}{\left|\frac{\partial H}{\partial x}\right|^{1/2}} \tag{4.23a}$$

$$D_y = \frac{h^{5/3}}{n_y}\frac{1}{\left|\frac{\partial H}{\partial y}\right|^{1/2}} \tag{4.23b}$$

where D_x is the diffusion coefficient of flow [$L^2\,T^{-1}$] in *x*-direction, and D_y is the diffusion coefficient of flow [$L^2\,T^{-1}$] in *y*-direction.

When the diffusion-based water flux equations (Equation 4.22) are inserted into the continuity equation, the governing equation for overland flow modeling using the diffusion wave (zero inertia) approximation to the Saint Venant's equations is obtained:

$$\frac{\partial H}{\partial t} - \frac{\partial}{\partial x}\left(D_x \frac{\partial H}{\partial x} \right) - \frac{\partial}{\partial y}\left(D_y \frac{\partial H}{\partial y} \right) = R - I - E \tag{4.24}$$

Note that in Equation (4.24) the source/sink terms of rainfall, R [L T^{-1}], infiltration, I [L T^{-1}], and evaporation, E [L T^{-1}], are also taken into account.

In order to solve Equation (4.24) numerically, the equation is spatially discretized using a finite volume approach. It is assumed that the 2D modeling domain is composed of a finite number of non-overlapping cells and each cell has a grid point at its center (Figure 4.9). It is further assumed that the values of the relevant variables and their variations in space and time within each cell are represented by their values at these grid points. The details of the spatial discretization process are given in Appendix C.

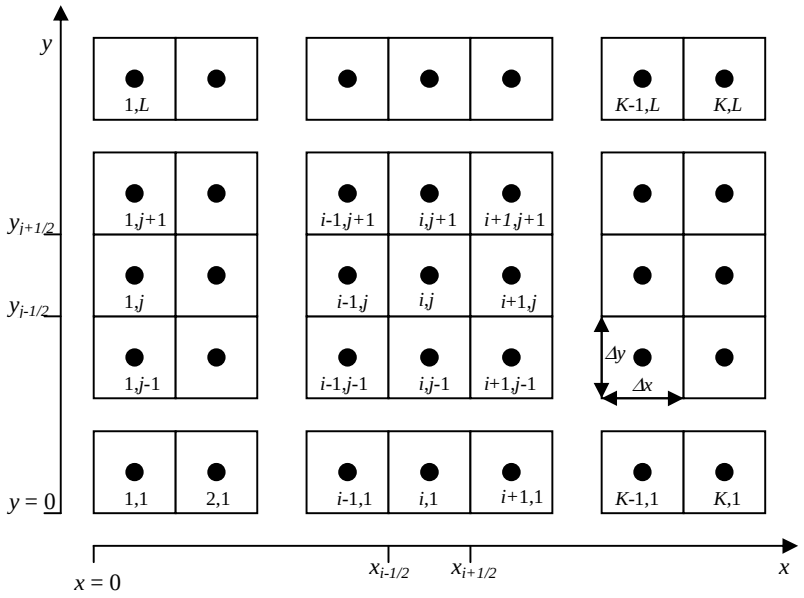

Figure 4.9: The overland flow modeling domain, cells and the grids.

After the spatial discretization, the following ODE system is obtained for i=1,...,K, j=1,…,L (K and L are the number of cells in the x- and y- directions, respectively):

$$\left(\frac{dH}{dt}\right)_{i,j} M_{i,j} + \underbrace{\left[S_{i,j}^{E} + S_{i,j}^{W} + S_{i,j}^{N} + S_{i,j}^{S}\right]}_{S_{i,j}^{0}} H_{i,j} - S_{i,j}^{E} H_{i+1,j} - S_{i,j}^{W} H_{i-1,j} - S_{i,j}^{N} H_{i,j+1} - S_{i,j}^{S} H_{i,j-1} = F_{i,j} \tag{4.25}$$

$$M_{i,j} = \Delta x \Delta y \tag{4.25a}$$

$$S_{i,j}^{E} = D_{i+1/2,j} \frac{\Delta y}{\Delta x} \tag{4.25b}$$

$$S_{i,j}^{W} = D_{i-1/2,j} \frac{\Delta y}{\Delta x} \tag{4.25c}$$

$$S_{i,j}^{N} = D_{i,j+1/2}\frac{\Delta x}{\Delta y} \tag{4.25d}$$

$$S_{i,j}^{S} = D_{i,j-1/2}\frac{\Delta x}{\Delta y} \tag{4.25e}$$

$$F_{i,j} = R\Delta x\Delta y - I\Delta x\Delta y \tag{4.25f}$$

Finally, an implicit time integration method together with Picard iteration is used to obtain the spatial and the temporal variation of overland flow depths. This component of the analysis is explained in more detail in Appendix F.

4.3.2 Model Testing

The developed overland flow model was tested against the one-dimensional analytical solution of the kinematic wave approximation to the Saint Venant equations for a channel of constant slope and roughness (Stephenson and Meadows 1986). The same analytical solution was used by Gottardi and Venutelli (1993), Gunduz (2004b) and Kollet and Maxwell (2006) in testing numerical solutions of overland flow models. The test parameters used in this study was obtained from Kollet and Maxwell (2006) and they are given in Table 4.2.

Table 4.2: Test parameters used in overland flow model comparison with 1D analytical solution.

Slope in x-direction	0.0005
Channel length	400 m
Flow outlet	Zero-gradient outlet at x = 0 m
Manning's roughness coefficient, n	2.3×10^{-7} day/m$^{1/3}$
Rainfall rate, R	R = 0.33 mm/min for $t \leq 200$ min R = 0.00 mm/min for $t > 200$ min
Simulation time	300 min
Spatial discretization, Δx	Case a: 80 m (K = 5) Case b: 10 m (K = 40)

The comparison of the model results to the analytical solution is shown in Figure 4.10. It is noted that the model solution deviates from the analytical solution around the time of concentration and towards the end of the receding phase of flow. However, the smoothed transition to the peak flow is remedied significantly by increasing the grid resolution.

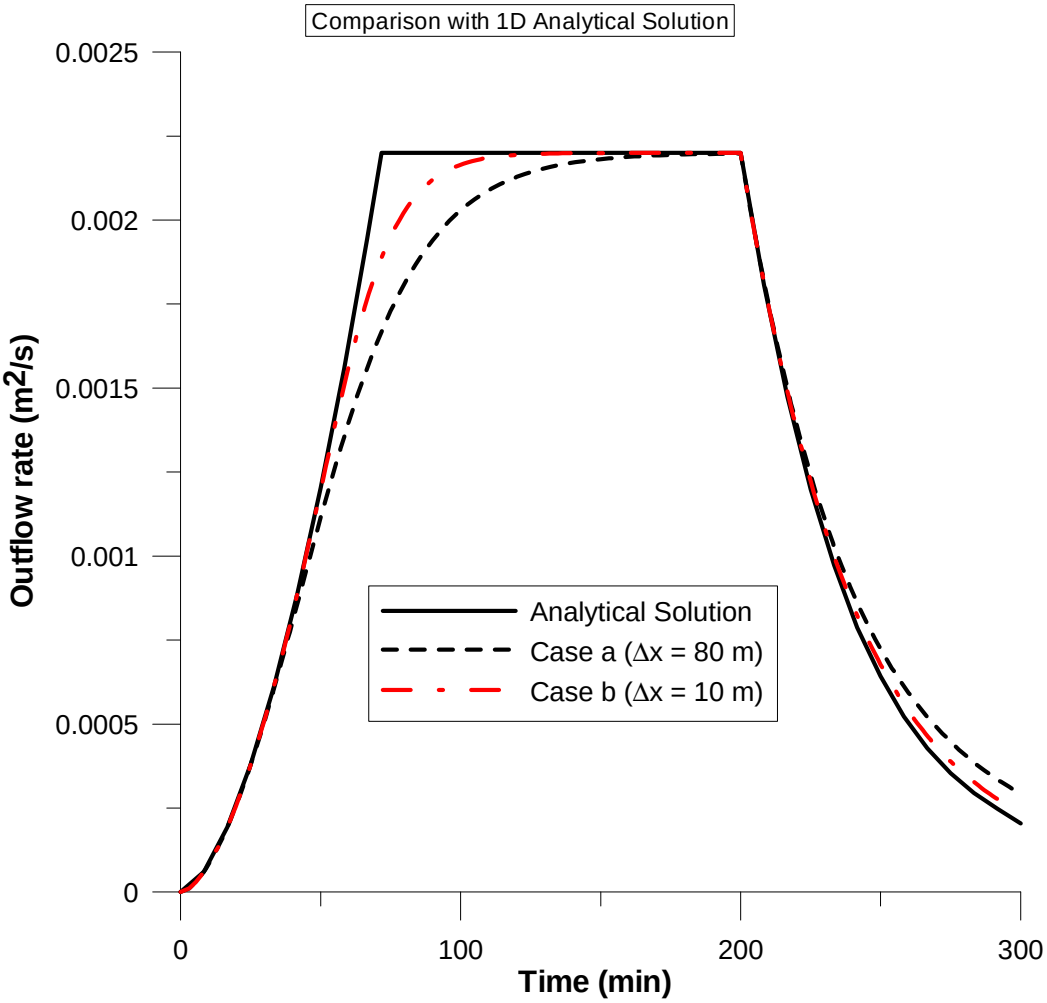

Figure 4.10: Overland flow model comparison with 1D analytical solution.

Next, the overland flow model was tested against the results published by Kollet and Maxwell (2006) of a test problem on a two-dimensional tilted V-catchment. Kollet and Maxwell (2006) compared the results of their model (ParFlow) with the results obtained by a number of other numerical models, namely HEC-1, HSPF, MODHMS (Panday and Huyakorn 2004) and the model by DiGiammarco et al. (1996). The 2D V-catchment domain profile is shown in Figure 4.11 and the test parameters used are given in Table 4.4.

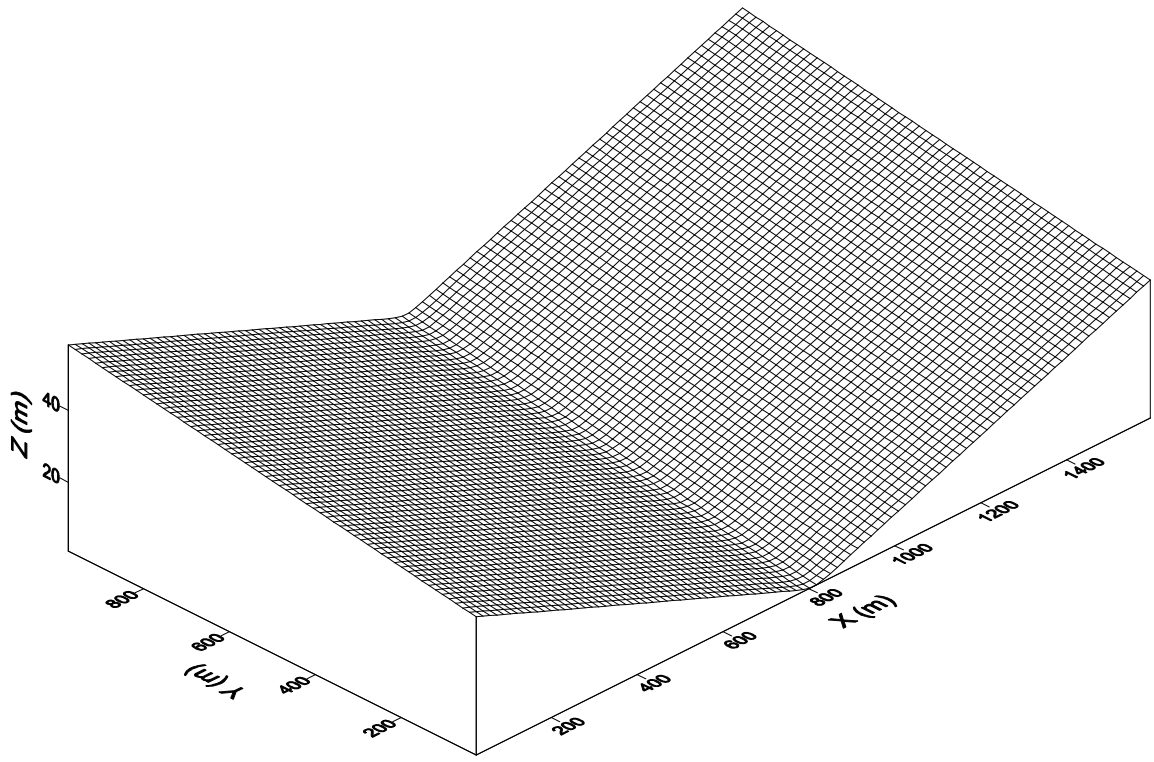

Figure 4.11: The profile of the 2D tilted V-catchment used in the overland flow model testing.

Table 4.3: Test parameters used in the comparison of overland flow model performance with other numerical models for a 2D tilted V-catchment problem.

Flow outlet	800 m ≤ x ≥ 820 m, y = 0 Case a: zero depth gradient Case b: critical depth
Manning's roughness coefficient, *n*	0.015 s/m$^{1/3}$ for the slopes 0.15 s/m$^{1/3}$ for the channel
Rainfall rate, *R*	$R = 3 \times 10^{-6}$ m/s for $t \leq 90$ min (5400 s) $R = 0.00$ m/s for $t > 90$ min (5400 s)
Simulation time	180 min (10800 s)
Spatial discretization	For the slopes: $\Delta x = \Delta y = 50$ m For the channel : $\Delta x = 50$ m, $\Delta y = 50$ m $X = 1620$ m, $Y = 1000$ m $K = 33$, $L = 20$

The model test was performed by assigning two different boundary conditions. In case a, a zero-depth-gradient boundary condition was assigned at the outlet of the model domain, whereas in case b, a critical depth boundary condition was used. The model results as compared with the other numerical models are shown in Figure 4.12 (case a) and Figure 4.13 (case b). It is observed that the results obtained by the model proposed in this study coincide with the results obtained by ParFlow (Kollet and Maxwell 2006) and DiGiammarco et al. (1996).

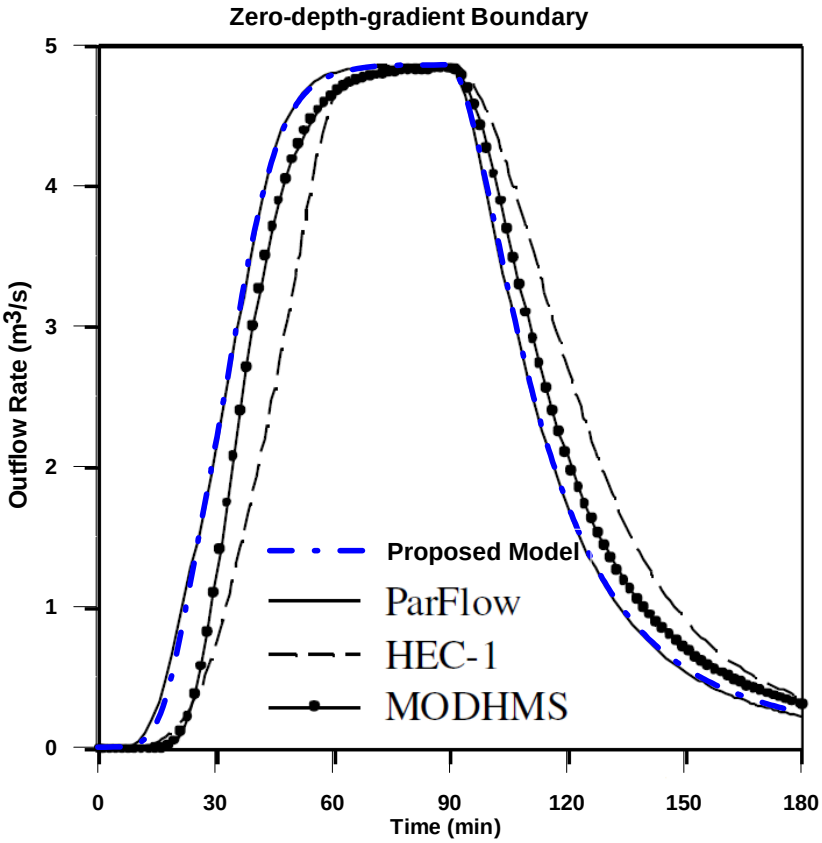

Figure 4.12: Overland flow model results for the 2D V-catchment problem compared with the other numerical models. (Case a: zero depth-gradient boundary condition at the outlet)

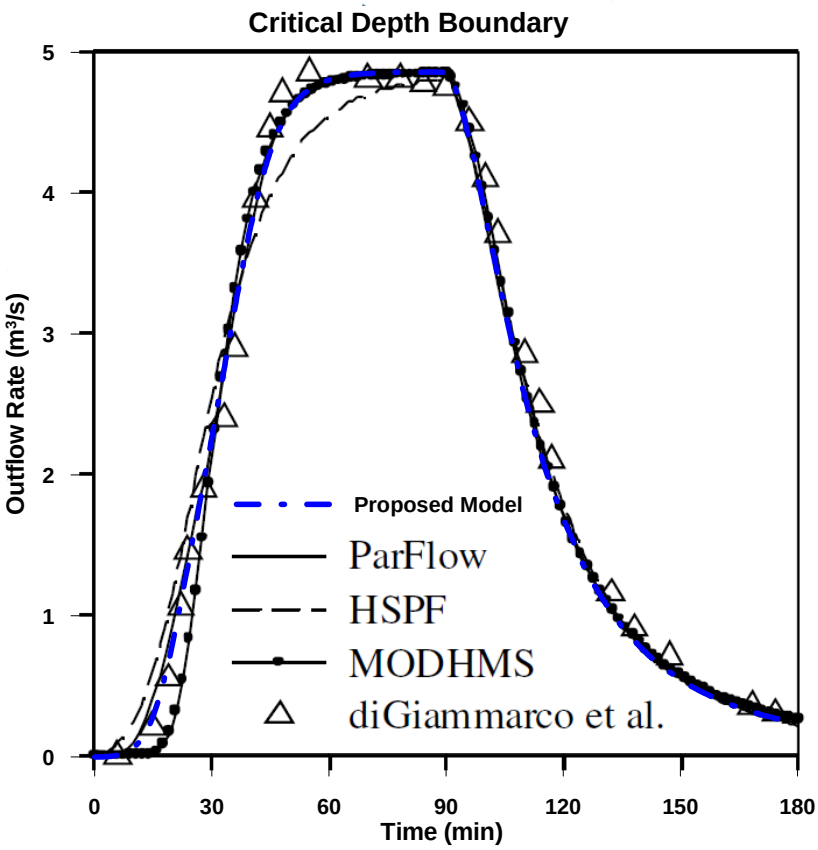

Figure 4.13: Overland flow model results for the 2D V-catchment problem compared with the other numerical models. (Case b: critical depth boundary condition at the outlet)

4.4 Overland Transport Model

4.4.1 Model Development

In order to model the contaminant transport through overland flow, the advection-dispersion-reaction equation is used. The two-dimensional, vertically averaged transport equation for a dissolved phase contaminant is given in Equation 4.25:

$$\frac{\partial (C_o h)}{\partial t} = \underbrace{-\frac{\partial (C_o h v_x)}{\partial x} - \frac{\partial (C_o h v_y)}{\partial y}}_{\text{Advection}} + \underbrace{\frac{\partial}{\partial x}\left(hD_x \frac{\partial C_o}{\partial x} \right) + \frac{\partial}{\partial y}\left(hD_y \frac{\partial C_o}{\partial y} \right)}_{\text{Dispersion}} - \underbrace{\lambda h C_o}_{\text{Reaction}} + \underbrace{M}_{\text{Source}} \tag{4.26}$$

where C_o is the vertically averaged contaminant concentration [M L-3] in the overland flow, h is the overland flow depth [L], t is time [T], v_x is the overland flow velocity [L T^{-1}] in the x-direction, v_y is the overland flow velocity [L T^{-1}] in the y-direction, x is the horizontal spatial direction [L], y is the vertical spatial direction [L], D_x is the dispersion coefficient [L^2 T^{-1}] in the x-direction, D_y is the dispersion coefficient [L^2 T^{-1}] in the y-direction, λ is the first-order decay rate coefficient [T^{-1}], M is the contaminant source input rate [M L^{-2} T^{-1}].

The water depth and the flow velocity information is obtained through the solution of the overland flow model (Section 4.3). The dispersion coefficients are determined by adding the contributions of the hydrodynamic dispersion and molecular diffusion processes:

$$D_i = D_{H,i} + D_l^w \tag{4.27}$$

where i is the flow direction ($i = x,y$) and $D_{H,i}$ is the hydrodynamic dispersion coefficient for flow direction i. The hydrodynamic dispersion coefficient can be estimated from the flow and flow surface characteristics by using the relationship (Zerihun et al. 2005c):

$$D_{H,i} = Ce \cdot hv_i^* \tag{4.28}$$

where Ce is a dimensionless constant and v_i^* is the shear velocity [L T^{-1}]. The shear velocity is described as (Zerihun et al. 2005c):

$$v_i^* = \left(ghS_{f,i}\right)^{1/2} \tag{4.29}$$

Combining Equations (4.28) ,(4.29) and (4.17) yields:

$$D_{H,i} = Ce \cdot n_i \sqrt{g} h^{5/6} v_i \tag{4.30}$$

So, the dispersivity for overland flow in direction i, $\alpha_{o,i}$ [L], can be defined as:

$$\alpha_{o,i} = Ce \cdot n_i \sqrt{g} h^{5/6} \tag{4.31}$$

with

$$D_{H,i} = \alpha_{o,i} v_i \tag{4.32}$$

Equation (4.26) can be rewritten after introducing the bulk terms as:

$$\frac{\partial (G_1 C_w)}{\partial t} = \underbrace{-\frac{\partial (G_{3x} C_w)}{\partial x} - \frac{\partial (G_{3y} C_w)}{\partial y}}_{\text{Advection}} + \underbrace{\frac{\partial}{\partial x}\left(G_{2x} \frac{\partial C_w}{\partial x} \right) + \frac{\partial}{\partial y}\left(G_{2y} \frac{\partial C_w}{\partial y} \right)}_{\text{Dispersion}} + \underbrace{G_4 C_w}_{\text{Reaction}} + \underbrace{G_5}_{\text{Source}} \tag{4.33}$$

$$G_1 = h \tag{4.33a}$$

$$G_{2x} = hD_x \tag{4.33b}$$

$$G_{2y} = hD_y \tag{4.33c}$$

$$G_{3x} = hv_x \tag{4.33d}$$

$$G_{3y} = hv_y \tag{4.33e}$$

$$G_4 = -\lambda h \tag{4.33f}$$

$$G_5 = M \tag{4.33g}$$

The overland transport model uses the same domain, cell and grid structure as the overland flow model (Figure 4.9). Equation 4.33 is spatially discretized using the same finite volume methodology applied in the discretization of the vadose zone transport model. The details can be found in Appendices B and D. The outcome is the following set of equations for i=1,...,K, j=1,…,L (K and L are the number of cells in the x- and y-directions, respectively):

$$\left(\frac{d\left[G_1 C_o\right]}{dt}\right)_{i,j} M_{i,j} + S_{i,j}^{W}\left(C_o\right)_{i-1,j} + S_{i,j}^{S}\left(C_o\right)_{i,j-1} + S_{i,j}^{0}\left(C_o\right)_{i,j} + S_{i,j}^{E}\left(C_o\right)_{i+1,j} + S_{i,j}^{N}\left(C_o\right)_{i,j+1} = F_{i,j} \tag{4.34}$$

$$M_{i,j} = \Delta x_{i,j} \Delta y_{i,j} \tag{4.34a}$$

$$S_{i,j}^{W} = -\left\{\left[A_{i,j}^{W}\left(1-\alpha_{i,j}^{W}\right) + D_{i,j}^{W}\right]\Delta y_{i,j}\right\} \tag{4.34b}$$

$$S_{i,j}^{S} = -\left\{\left[A_{i,j}^{S}\left(1-\alpha_{i,j}^{S}\right) + D_{i,j}^{S}\right]\Delta x_{i,j}\right\} \tag{4.34c}$$

$$S_{i,j}^{0} = -\left\{\begin{array}{l}\left[A_{i,j}^{E}\alpha_{i,j}^{E} + A_{i,j}^{W}\alpha_{i,j}^{W} - D_{i,j}^{E} - D_{i,j}^{W}\right]\Delta y_{i,j} \\ +\left[A_{i,j}^{N}\alpha_{i,j}^{N} + A_{i,j}^{S}\alpha_{i,j}^{S} - D_{i,j}^{N} - D_{i,j}^{S}\right]\Delta x_{i,j} \\ +\left(G_4\right)_{i,j}\Delta x_{i,j}\Delta y_{i,j}\end{array}\right\} \tag{4.34d}$$

$$S_{i,j}^{E} = -\left\{\left[A_{i,j}^{E}\left(1-\alpha_{i,j}^{E}\right) + D_{i,j}^{E}\right]\Delta y_{i,j}\right\} \tag{4.34e}$$

$$S_{i,j}^{N} = -\left\{\left[A_{i,j}^{N}\left(1-\alpha_{i,j}^{N}\right) + D_{i,j}^{N}\right]\Delta x_{i,j}\right\} \tag{4.34f}$$

$$F_{i,j} = \left(G_5\right)_{i,j}\Delta x_{i,j}\Delta y_{i,j} \tag{4.34g}$$

where the terms $A_{i,j}^{E}$, $A_{i,j}^{W}$, $A_{i,j}^{N}$, $A_{i,j}^{S}$ represent the "advective strength" at the east, west, north and south interfaces of cell *i*,*j*, respectively. The terms $\alpha_{i,j}^{E}$, $\alpha_{i,j}^{W}$, $\alpha_{i,j}^{N}$, $\alpha_{i,j}^{S}$ are the weighting factors used in the discretization of the advection term at the east, west, north and south interfaces of cell *i*,*j*, respectively. And the terms $D_{i,j}^{E}$, $D_{i,j}^{W}$, $D_{i,j}^{N}$, $D_{i,j}^{S}$ represent the "diffusive conductance" at the east, west, north and south interfaces of cell *i*,*j*, respectively (Wheeler et al. 2007). The details on how to determine these terms are given in Appendix D.

An implicit scheme is used to solve the ODE system given in Equation (4.34). The details of the time integration procedure can be found in Appendix E.

4.4.2 Model Testing

The overland transport model was tested using the analytical solution to the one dimensional advection-dispersion equation which was provided by van Genuchten and Alves (1982). The contaminant is introduced at x = 0 m with a constant concentration of 50 g/m^3 from the beginning to the end of the simulation. The initially uncontaminated overland flow has a uniform velocity of 0.03 m/s. The parameters used in the test are given in Table 4.4.

Table 4.4: Test parameters used in the comparison of the overland transport model with the analytical solution.

Contaminant concentration at x = 0 m, C_0	50 g/m^3
Initial contaminant concentration, C_i	0 g/m^3
Flow velocity, v_x	0.03 m/s
Dispersivity, $\alpha_{o,i}$	0.5 m
Molecular diffusion coefficient, D_l^w	1.0×10^{-10} m^2/s
Length of the model domain	100 m
Spatial discretization, Δx	1 m

In the context of this study, the overland flow occurs due to runoff and irrigation flow through vegetated land surfaces. Thus, the flow process is slower and shallower when compared with channel flow. This implies that the domination of the advection process in

the overland transport problems this study is interested in is expected to be less pronounced. However, it is not expected to have Peclet numbers (Equation B.13) low enough to be able to implement the central differencing scheme (Equation B.14) when determining the weighing factors used in the advective flux calculations. Therefore the upwind (Equation B.15) and exponential schemes (Equation B.16) are used to describe the advective fluxes in this test problem. The comparison of the model results with the analytical solution is shown in Figures 4.14 and 4.15 for the simulations using the upwind and the exponential schemes, respectively. It is seen that there is excessive numerical dispersion in the results obtained by the upwind scheme (Figure 4.14). The same is also true for the results obtained with the exponential scheme although to a lesser extent (Figure 4.15).

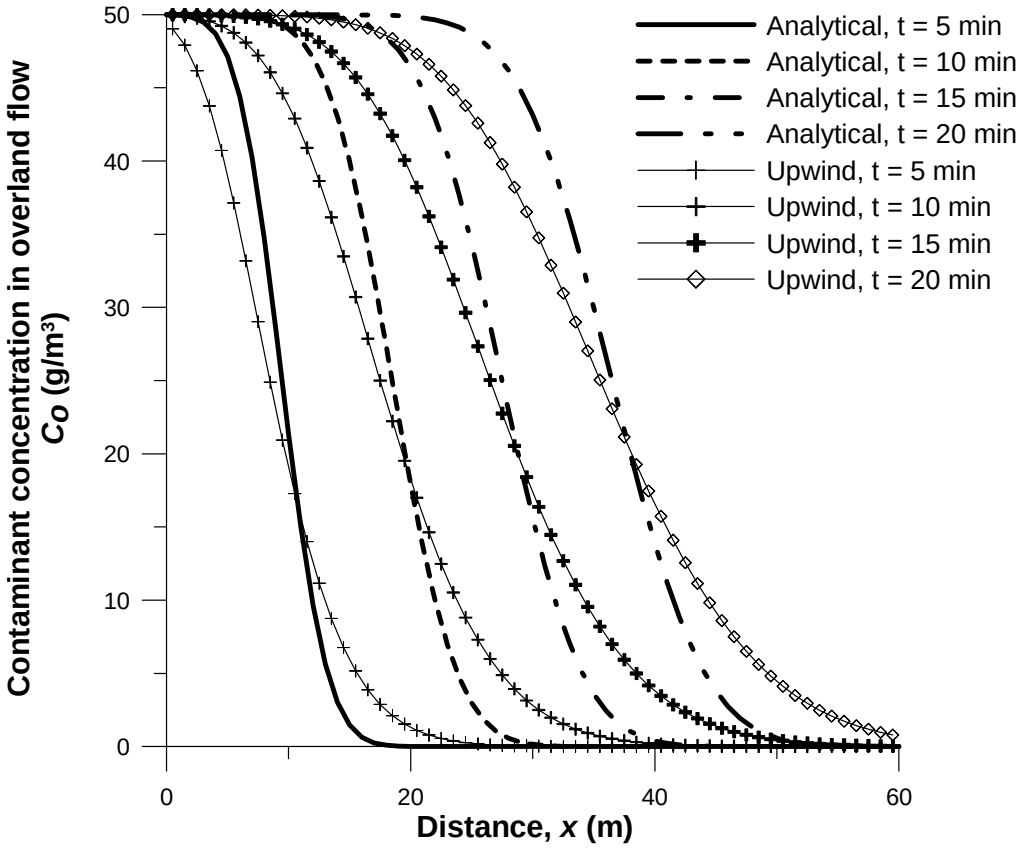

Figure 4.14: Comparison of the overland transport model results with the analytical solution. (Using the *upwind* scheme for the advective flux modeling.)

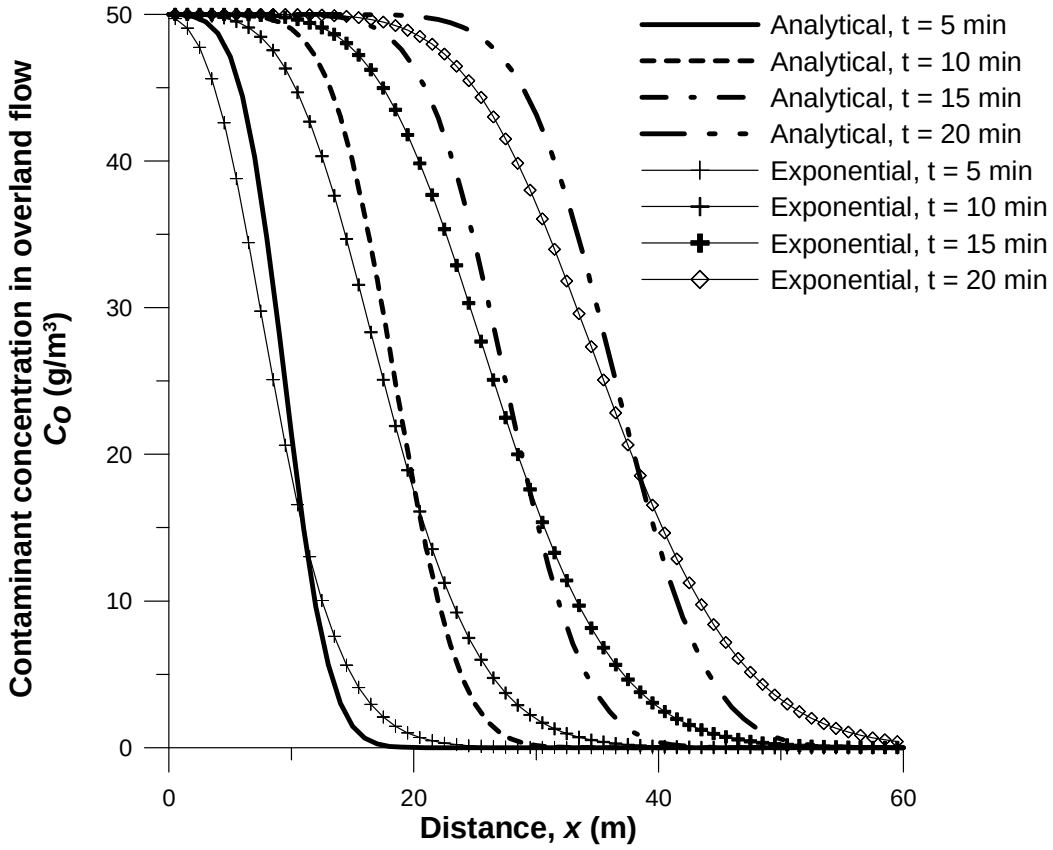

Figure 4.15: Comparison of the overland transport model results with the analytical solution. (Using the *exponential* scheme for the advective flux modeling.)

The advection schemes used in the transport model are first-order approximations. In the approximation of the spatial derivative of the advection term, only the concentration values from the two neighboring cells are used. For more accurate results, higher order approximations to the derivative of the advection term that includes the concentration information from other cells in the vicinity of the neighboring cells are needed. For the advection dominated transport problems (e.g. transport in river systems), multi-point up-wind biased schemes, such as the QUICKEST algorithm, give satisfactory results (Gokgoz Kilic 2008; Gunduz 2004a). On the other hand, increased stability as well as minimization of numerical diffusion can be achieved by employing nonlinear methods, such as flux limiters (e.g. van Leer limiter) (Chu and Mariño 2006; van Leer 1974; VanderKwaak 1999). However, in this study, these higher order methods are not explored.

In Figures 4.16 and 4.17, the model results obtained by simulations that neglect the contaminant fluxes due to hydrodynamic dispersion are compared with the analytical solution. It is seen that the model results have improved after this modification. This shows that the contribution of the numerical dispersion due to the advective schemes is higher than the contribution of the hydrodynamic dispersion included in the dispersive flux calculations. Especially, the results obtained by the exponential scheme (Figure 4.17) are in good agreement with the analytical solution. Note that the exponential scheme still uses the Peclet number calculated by taking into account the hydrodynamic dispersion when determining the weighing factors for the neighboring cells' concentrations (Equation B.13). Also, although the hydrodynamic dispersion is neglected in calculating

the dispersive fluxes, the molecular diffusion is not. In practice, this would allow contaminant dispersion even when the overland water is stagnant. Considering the discontinuous nature of the overland flow and the generally large time scales considered in this study (on the order of days versus minutes), this simple modification to neglect fluxes due to hydrodynamic dispersion when calculating the dispersive fluxes can be accepted to be a reasonable compromise between model simplicity and accuracy.

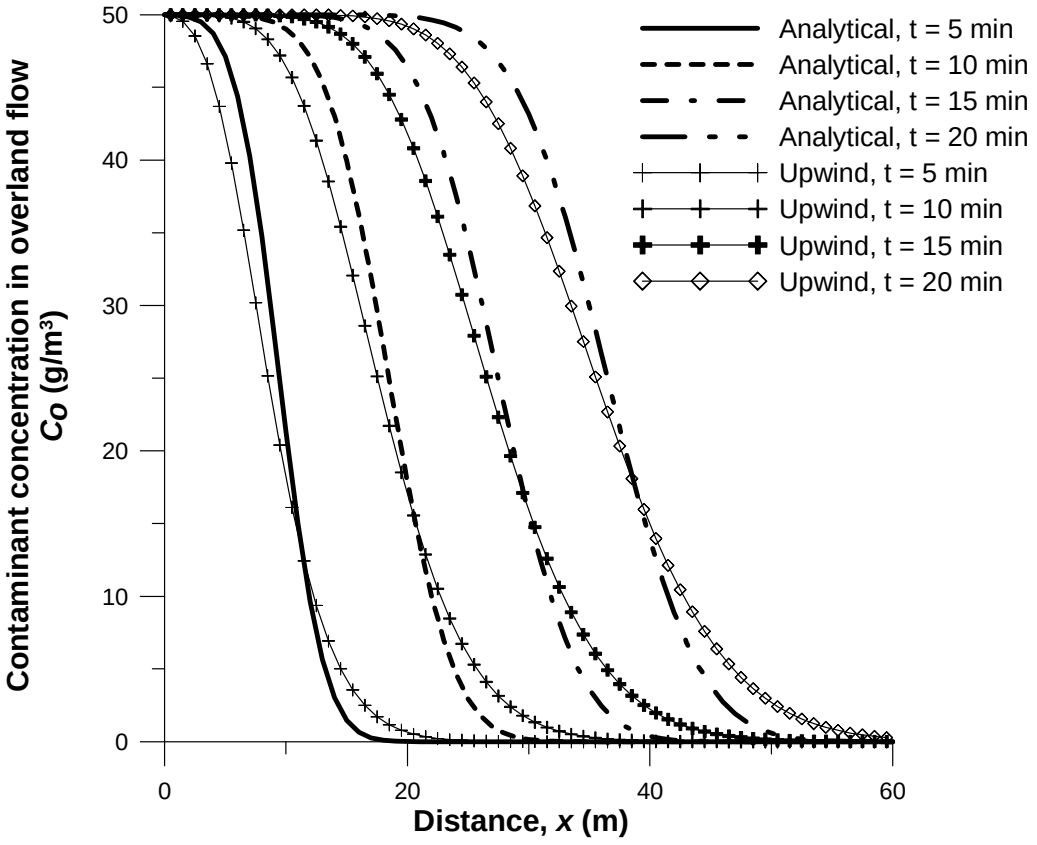

Figure 4.16: Comparison of the overland transport model results with the analytical solution. (Using the *upwind* scheme for the advective flux modeling) (Fluxes due to hydrodynamic dispersion are neglected.)

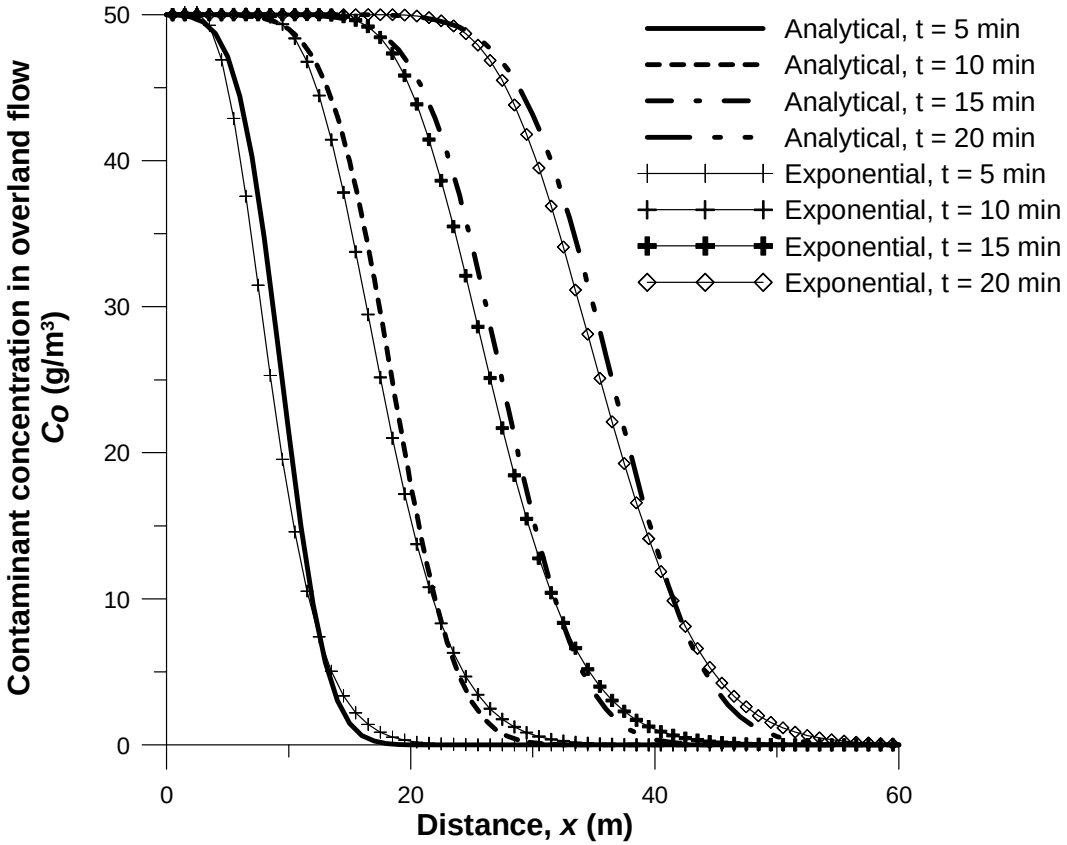

Figure 4.17: Comparison of the overland transport model results with the analytical solution. (Using the *exponential* scheme for the advective flux modeling) (Fluxes due to hydrodynamic dispersion are neglected.)

CHAPTER 5

INTEGRATED DYNAMIC MODELING OF THE SOIL-PLANT SYSTEM

5.1 Introduction

In Sections 2.3 and 2.6.2, it was discussed that in most of the multimedia models that have incorporated the plants, the soil that is in interaction with the plant is modeled as a single compartment. When the soil is modeled as a single compartment, this particular type of multimedia model does not take into account the spatial distribution of the moisture and the contaminant within the soil. This simplification has important consequences when determining the contaminant transfer between the soil and the plant and between the soil and the atmosphere. Contaminant uptake by plants is dependent on the root water uptake rate and the soil contaminant concentration, both of which may be highly variable throughout the soil depth. Contaminant transfer processes between the atmosphere and the soil are highly dependent on the near surface characteristics of the soil. These issues can be addressed by integrating the plant root uptake model with a contaminant transport model that tracks the spatial and the temporal distribution of contaminants within the soil.

In recent literature contaminant transport modeling within the vadose zone is well developed although the plant related processes are not satisfactorily incorporated to these models. The HYDRUS Software Series (HYDRUS 1D, 2D, 3D) is a widely used simulation tool that models vadose zone flow and contaminant transport in great detail

(Simunek et al. 2008; Simunek et al. 2006). However, plants are treated as external entities, thus plant growth and plant pathway models are not considered. SWAP model has much in common with HYDRUS but its more recent versions also include a generic crop growth model (Kroes et al. 2008; van Dam et al. 2008) although the plant pathway is again not a part of the modeling domain. The agricultural-oriented detailed crop models such as CropSyst (Stöckle et al. 2003) and DAISY (Abrahamsen and Hansen 2000) perform water flow and nutrient transport modeling as well. However, they are aimed at determining the crop yield response to different environmental conditions and management scenarios, and are not oriented to perform pollution analysis.

A modeling framework that would integrate the vadose zone contaminant transport models with the dynamic plant root uptake models would significantly improve the comprehensive understanding of the vadose zone plant-soil system under study. In this chapter, the conceptualization and the analytical framework of such an integration is discussed and the outcome is presented through several applications.

5.2 Integrated Model Development

In order to build the integrated model, the plant models that have been described in Chapter 3 have to be coupled with the unsaturated zone soil-water flow model (Section 4.1) and the vadose zone contaminant transport model (Section 4.2). This coupling is established at multiple interfaces and at different levels of solution steps (i.e. model development phase vs. numerical solution phase). The overall coupling scheme can be

divided into two main categories: (i) coupling the unsaturated zone soil-water flow and the plant life-cycle models; and, (ii) coupling the vadose zone contaminant transport and the plant pathway models.

5.2.1 Coupling the Unsaturated Zone Water Flow and the Plant Life-Cycle Models

The coupling of the unsaturated zone soil-water flow and the plant life-cycle models is achieved by special handling of two modules: (i) the ground surface boundary (top boundary of the soil column); and, (ii) the root water uptake. In both of these modules, *LAI* is the key parameter that defines the interaction between the two models.

5.2.1.1 Ground Surface Boundary

In the treatment of the ground surface boundary when solving for the soil-water flow, the algorithm used in the SWAP model formed the foundation (van Dam and Feddes 2000). At each time step of the numerical solution, the algorithm determines whether evaporation or infiltration conditions prevail at the soil surface. Then, the head or flux that defines the boundary condition is specified according to the weather conditions and soil moisture availability near the ground surface. The interaction with the plant growth model occurs when determining the potential water flux at the ground surface. The potential flux at the ground surface is dependent on the precipitation that is not intercepted by the plants covering the soil surface and on the potential soil evaporation rate:

$$q_{top} = (1 - f_{\text{int}})\, q_{rain} - E_p \tag{5.1}$$

where q_{top} is the potential flux at the ground surface [L T^{-1}], f_{int} is the fraction of the precipitation that is intercepted by the vegetation, q_{rain} is the precipitation rate [L T^{-1}], and E_p is the potential soil evaporation rate [L T^{-1}].

The intercepted fraction of the precipitation for a certain time period is determined by comparing the volume of precipitation during that time period with the available volume for interception storage for the same time period. In order to estimate the available volume for interception storage, water budget calculations that take into account the maximum interception storage capacity, precipitation, and the evaporation from interception are carried out. The maximum interception storage capacity is assumed to be dependent on *LAI* and a specific storage capacity for the plant.

The intercepted fraction of the precipitation, f_{int}, in Equation (5.1) is determined as:

$$f_{\text{int}} = \begin{cases} 1 & \text{if } V_{rain} \le S_{def} \\ \dfrac{S_{def}}{V_{rain}} & \text{if } V_{rain} > S_{def} \end{cases} \tag{5.2}$$

where V_{rain} is the volume of rainfall over the area of concern [L], and S_{def} is the available volume for interception storage for that area [L].

In order to determine S_{def}, the interception storage capacity of the plants and the current volume of the intercepted water on the plants need to be known. For this purpose, Panday and Huyakorn (2004) calculated a water balance over the interception storage volume. In this model, the intercepted water volume at each time step of the numerical solution is calculated by taking into account the rainfall input and evaporative flux during that time step. The interception storage at the current time step *t* is calculated by adding the rainfall volume to the previously available intercepted water volume. However, the interception storage is limited by its maximum capacity which is assumed to be dependent on *LAI* and a specific storage capacity, S_L [L]. S_L is a plant-specific parameter that can be determined by measurements.

$$\left(S_{\text{int}}\right)^{t,*} = \min\left(S_{\text{int,max}}, \left(S_{\text{int}}\right)^{t-1} + q_{rain}\Delta t\right) \tag{5.3}$$

$$S_{\text{int,max}} = LAI \cdot S_L \tag{5.4}$$

$(S_{\text{int}})^{t,*}$ is the interception storage at time *t* without taking evaporation into consideration. The evaporation during the current time step is assumed to be the vegetation cover fraction (f_c) times a potential evaporation rate from free water surfaces for the site conditions, $E_{w,p}$ [L T^{-1}]. However, the total evaporated volume from the interception storage is not allowed to exceed the currently available intercepted water volume:

$$E_{\text{int}}\Delta t = \min\left(\left(S_{\text{int}}\right)^{t,*}, f_c E_{w,p}\Delta t\right) \tag{5.5}$$

where E_{int} is the evaporation rate from interception [L T^{-1}].

Finally, the net interception storage for the current time step is calculated as:

$$\left(S_{\text{int}}\right)^{t} = \left(S_{\text{int}}\right)^{t,*} - E_{\text{int}}\Delta t \tag{5.6}$$

Based in this, the interception storage deficit can be determined as:

$$\left(S_{def}\right)^{t} = S_{\text{int,max}} - \left(S_{\text{int}}\right)^{t-1} + E_{\text{int}}\Delta t \tag{5.7}$$

and,

$$V_{rain} = q_{rain}\Delta t \tag{5.8}$$

An alternative form of Equation (5.2) without using the bulk terms is:

$$f_{\text{int}} = \begin{cases} 1 & \text{if } \left[\left(S_{\text{int}}\right)^{t-1} + q_{rain}\Delta t\right] \le \left[S_{\text{int,max}} + E_{\text{int}}\Delta t\right] \\ \dfrac{S_{\text{int,max}} - \left(S_{\text{int}}\right)^{t-1} + E_{\text{int}}\Delta t}{q_{rain}\Delta t} & \text{if } \left[\left(S_{\text{int}}\right)^{t-1} + q_{rain}\Delta t\right] > \left[S_{\text{int,max}} + E_{\text{int}}\Delta t\right] \end{cases} \tag{5.9}$$

Another critical parameter, which is related to the ground surface boundary conditions and which is also dependent on the plant's growth stage, is the potential soil evaporation rate. Potential soil evaporation rate is determined using the following relationship:

$$E_p = (1 - f_c) E_{p,0} \tag{5.10}$$

where f_c is the vegetation cover fraction, and $E_{p,0}$ is the potential evaporation rate [L T^{-1}] for bare, wet soil according to the site conditions. Equation (5.10) is the same relationship used in the SWAP model (Kroes et al. 2008) for determining the potential evaporation rate from partially covered soil when f_c is calculated based on the Beer-Lambert equation that describes the radiation attenuation as a function of *LAI* (van Dijk and Bruijnzeel 2001a):

$$f_c = 1 - e^{-\kappa LAI} \tag{5.11}$$

where κ is the plant specific extinction coefficient (dimensionless) which most commonly varies in the range 0.5 – 0.7.

The actual flux occurring at the ground surface may be less than the potential flux that is calculated in Equation (5.1) due to physical limits to soil-water flow near the surface. The maximum flux allowed at the soil surface ($q_{top,\max}$) is calculated by using the Darcy's law:

$$q_{top,\max} = -K_{1/2} \left(\frac{h_1 - h_{top}}{0.5\Delta z_1} - 1 \right) \tag{5.12}$$

where h_{top} is the soil-water pressure head at the ground surface [L]. Its value depends on the environmental conditions at the specific time step it is being calculated. If $q_{top} > 0$, which indicates that infiltration prevails, h_{top} is assigned the water depth value at the ground surface ($h_{top} = h_{surf}$). If $q_{top} < 0$, h_{top} becomes the soil-water pressure head in equilibrium with the prevailing relative humidity in the atmosphere ($h_{top} = h_{atm}$). The h_{top} value also identifies the limit of the soil-water pressure head at the soil surface as it becomes the boundary condition when the potential flux exceeds the maximum flux (i.e. when $\left|q_{top}\right| > \left|q_{top,\max}\right|$). In that case, the top boundary condition switches to a specified head boundary condition and equals to h_{surf} or h_{atm} as infiltration or evaporation, respectively, dominates. A schematical description of the ground surface boundary condition selection algorithm is given in Figure 5.1. Note that in the case of infiltration conditions the allowable top boundary flux is also compared with the saturated hydraulic conductivity (K_s) value. This helps in stabilizing the iterative numerical solution of the unsaturated flow equation with switching boundary conditions since $q_{top,\max}$ is calculated using only a first-order approximation in Equation (5.12) (van Dam and Feddes 2000).

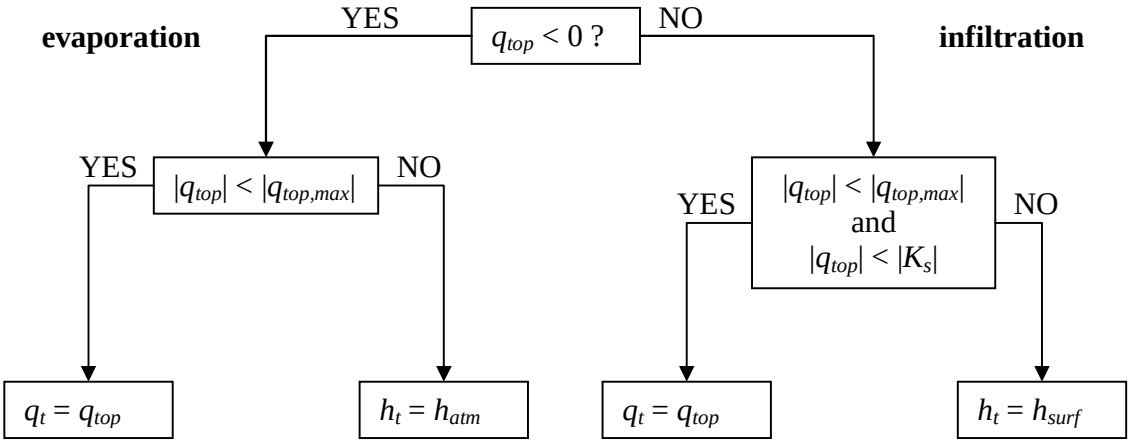

Figure 5.1: Schematical description of the ground surface boundary condition selection algorithm.

5.2.1.2 Root Water Uptake

In this study, a macroscopic root water uptake model is adopted. The macroscopic root water uptake models assume a soil-plant-atmosphere continuum and conceptualize plant roots as channels that convey soil-water into the atmosphere. This conceptualization is not far from reality since “only about 2% of the water absorbed into plant roots is used in photosynthesis” (Spellman 2008) while the rest is transpired into the atmosphere. Following this conceptualization, the macroscopic root water uptake models distribute the potential transpiration rate throughout the soil column by considering the spatial distribution of the roots (Section 2.5.1).

The potential transpiration rate is calculated by multiplying the potential evapotranspiration rate by the vegetation cover fraction:

$$T_p = f_c ET_p - E_{\text{int}} \tag{5.13}$$

where ET_p is the potential evapotranspiration rate [L T^{-1}] representing the combined effect of the evaporation and transpiration processes occurring at the site. When Equation (5.13) gives a negative potential transpiration rate, potential transpiration is set to be zero. Thus, it is assumed that there is no transpiration while there is evaporation from interception.

The crop coefficient approach detailed in the report of by Allen, Pereira et al. (1998) is used to determine the potential evapotranspiration. The crop coefficient approach is based on modifying a reference evapotranspiration value using a crop specific coefficient:

$$ET_p = K_c ET_0 \tag{5.14}$$

where K_c is the dimensionless crop coefficient. K_c is related with the growth state of the crop and can be calculated as (Mailhol et al. 1997):

$$K_c = K_{c,\max}\left(1 - e^{-x_k \cdot LAI}\right) \tag{5.15}$$

where $K_{c,\max}$ is the maximum value of K_c for the crop depending on the local site conditions and x_k is a parameter that reflects the crop's water consumption characteristics.

The potential root water uptake rate, S_p, is obtained by distributing the potential transpiration throughout the root zone by using the root distribution function (Equation 3.22) discussed in Section 3.2.3:

$$S_p = b(z)T_P \tag{5.16}$$

The soil column may not be able to satisfy this potential root water uptake demand due to water scarcity and the actual root water uptake may be less than the potential value, creating water stress on the plant. In this case, the macroscopic root water uptake models employ various functions to model the reduction in water uptake rates at depths where the soil-water content is relatively lower.

The actual root water uptake rate, *S*, is calculated from the potential uptake rate by employing the water stress reduction and the water stress compensation functions as shown below:

$$S = \alpha\beta_c S_p \tag{5.17}$$

where α is the function that accounts for the reduced water uptake by the roots, and β_c is the water stress compensation function.

Feddes, Kowalik et al. (1978) proposed calculating α as a function of the soil-water pressure head:

$$\alpha(h) = \begin{cases} 0 & \text{for } h > h_a \\ \dfrac{h - h_{opt}}{h_a - h_{opt}} & \text{for } h_a > h > h_{opt} \\ 1 & \text{for } h_{opt} \geq h > h_d \\ \dfrac{h - h_{wp}}{h_d - h_{wp}} & \text{for } h_d \geq h > h_{wp} \end{cases} \qquad \left(h_a > h_{opt} > h_d > h_{wp}\right) \tag{5.18}$$

In Equation (5.18), h_a indicates the anaerobiosis point, above which the soil is assumed to be waterlogged and the root water uptake is zero. h_{opt} is the optimal pressure head for root water uptake. h_d is the pressure head associated with the turgor pressure below which the plant starts closing the stomata (Wohling and Schmitz 2007). And, h_{wp} is the wilting point, below which plants cannot extract water from soil.

In order to model the water stress compensation, Li, De Jong et al. (2001) proposed a function that is basically a weighted stress index calculated based on water availability and root distribution, which was later tested by Braud, Varado et al. (2005) and found robust. Li, De Jong et al. (2006a) successfully applied a generalized version of this function:

$$\beta_c(h,z) = \frac{\alpha(h)}{\int_{L_R} \alpha(h) b(z)\, dz} \tag{5.19}$$

Combining Equations (5.16)-(5.19), the root water uptake rate distribution can be obtained by:

$$S(h,z) = \alpha(h)\beta_c(h,z)b(z)T_P \tag{5.20}$$

After the root water uptake distribution throughout the soil column is determined, it is included into the soil-water flow model as a sink term. The coupling between the unsaturated zone soil-water flow model and the plant life-cycle model occurs over this sink term. The potential transpiration is estimated based on the environmental conditions and the plant's growth stage. Thus, the plant life-cycle model is critical in calculating the spatially distributed root water uptake sink term in the flow equation as it provides the potential transpiration rate and the root distribution. On the other hand, the solution of the soil-water flow model provides the water distribution over the soil depth which in turn determines if the plant will experience water stress. When the plant experiences water stress, its growth is impeded. The actual transpiration rate will be given by the integration of the root water uptake rates over the root zone.

$$T_A = \int_{L_R} S(h,z)dz = \int_{L_R} \alpha(h)\beta_c(h,z)b(z)T_P dz = T_P \int_{L_R} \alpha(h)\beta_c(h,z)b(z)dz \tag{5.22}$$

As given in Equation (3.18b), the ratio of the actual transpiration rate to the potential transpiration rate gives the water stress index (*WSI*) used in the *LAI* simulation. Thus, over the root water uptake calculations, there is a two-way interaction between the unsaturated zone soil-water flow model and the plant life-cycle model; and, the coupled solution of them requires an iterative approach (Wohling and Schmitz 2007).

The iterative coupling algorithm is shown in Figure 5.2. The algorithm starts with the estimate of *LAI* equal to LAI_{pot}, which is calculated by assuming there is no water stress (*WSI* = 1). Then the iteration starts with solving the soil-water flow model to calculate the actual transpiration value. Note that while the *LAI* model runs in daily time steps, the soil-water flow model will most probably have smaller time step sizes. Thus, the actual transpiration is calculated by accumulating the integrated root water uptake rates over successive time intervals until the end of the day. Then, the calculated transpiration rate is used to calculate the water stress index which is applied to the *LAI* model to give a new estimate of the *LAI*. If the new estimate is not sufficiently close to the previous *LAI* estimate, the daily iteration starts again by using the new *LAI* to calculate the potential transpiration and evaporation rates to run the soil-water flow model. The iteration stops when the *LAI* estimates converge.

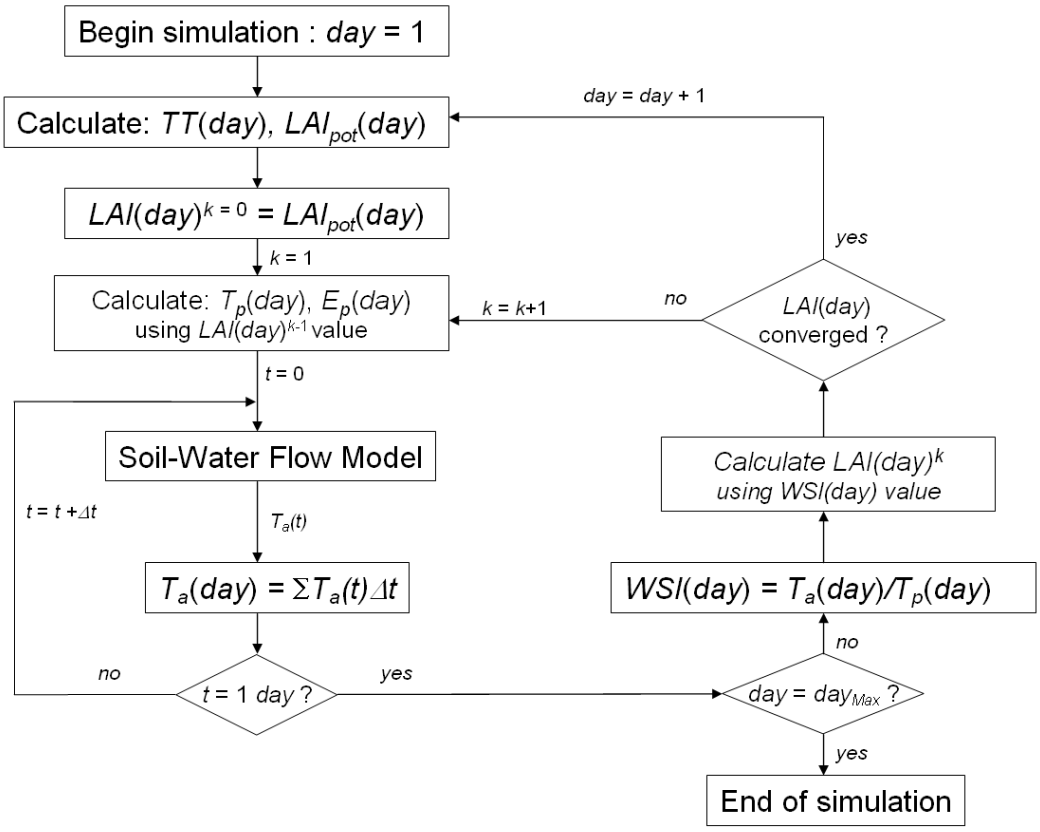

Figure 5.2: Iterative coupling of the LAI simulation model and the soil-water flow model. (k : iteration index)

5.2.2 Coupling the Vadose Zone Contaminant Transport and the Plant Pathway Models

The coupling of the soil contaminant transport and the plant pathway models occurs at the numerical solution phase, more specifically, at the time discretization phase. In Section 2.2 where the vadose zone contaminant transport model is described, the numerical solution of the partial differential equation of contaminant transport was advanced up to the end of the spatial discretization phase where finite volume spatial discretization has been applied. After the vadose zone contaminant transport model is spatially discretized (Equation 4.10), the solution of the contaminant transport and plant pathway models proceeds together. The plant pathway equation is an ordinary differential equation (ODE) as shown in Equation (3.17) and can be rewritten in a format that is compatible with the format of Equation (4.10) obtained after the finite volume discretization of the contaminant transport equation:

$$\frac{d\left(V_P C_P\right)}{dt} + S_{N+1}^{N+1} C_P + \sum_{j=0}^{N} S_{N+1}^{j} \left(C_w\right)_j = F_{N+1} \tag{5.23}$$

$$S_{N+1}^{N+1} = k_{p-a} + k_p \tag{5.23a}$$

$$S_{N+1}^{j} = -\left(r_u\right)_j \Delta z_j \quad \text{for } j = 0, \ldots, N \tag{5.23b}$$

$$F_{N+1} = \left(k_{dry-plant} + k_{wet-plant} + k_{rain-plant} + k_{a-p}\right) C_A \tag{5.23c}$$

In Equation (5.23), the coefficients are assigned the subscript N+1 to indicate the rank of the plant's contamination equation within the set of equations that describe the contaminant fate and transport in the whole soil-plant system. Now, the complete system

can be compactly represented in the same matrix-vector format which has been used in the solutions of the individual flow and transport models as shown in the Appendices:

$$\mathbf{M}\left(\frac{\mathbf{d}(\mathbf{G_1}\mathbf{C})}{\mathbf{dt}}\right) + \mathbf{SC} = \mathbf{F} \tag{5.24}$$

with

$$\mathbf{M} = \begin{pmatrix} M_0 & & & & & & \\ & M_1 & & & & & \\ & & \ddots & & & & \\ & & & M_{N-1} & & & \\ & & & & M_N & & \\ & & & & & 1 \end{pmatrix}; \mathbf{G_1} = \begin{pmatrix} (G_1)_0 & & & & & & \\ & (G_1)_1 & & & & & \\ & & \ddots & & & & \\ & & & (G_1)_{N-1} & & & \\ & & & & (G_1)_N & & \\ & & & & & V_P \end{pmatrix};$$

$$\mathbf{S} = \begin{pmatrix} S_0^0 & S_0^1 & & & & & & & \\ S_1^0 & S_1^1 & S_1^2 & & & & & & \\ & S_2^1 & S_2^2 & S_2^3 & & & & & \\ & & & \ddots & & & & & \\ & & & & S_{N-1}^{N-2} & S_{N-1}^{N-1} & S_{N-1}^N & & \\ & & & & & S_N^{N-1} & S_N^N & & \\ S_{N+1}^0 & S_{N+1}^1 & S_{N+1}^2 & S_{N+1}^3 & \cdots & S_{N+1}^{N-2} & S_{N+1}^{N-1} & S_{N+1}^N & S_{N+1}^{N+1} \end{pmatrix}; \mathbf{C} = \begin{pmatrix} (C_w)_0 \\ (C_w)_1 \\ \vdots \\ (C_w)_{N-1} \\ (C_w)_N \\ C_P \end{pmatrix};$$

and $\mathbf{F} = \begin{pmatrix} F_0 \\ F_1 \\ \vdots \\ F_{N-1} \\ F_N \\ F_{N+1} \end{pmatrix}$.

The solution of Equation (5.24) will give the time evolution of the contaminant concentrations in each soil cell and in the plant compartment simultaneously. This single-

matrix, simultaneous solution approach adds significant flexibility to the modeling framework. By this way, the feedback mechanisms between the plant compartment and the soil system do not have to be one-way. Additional mass transfer processes can be modeled by modifying the relevant elements of matrix **S**, and additional compartments (e.g. fruit, leaves etc.) can be incorporated by adding extra rows to the matrix-vector system. Any suitable ODE solution method can be applied to solve the set of equations. In this study, one-step implicit time integration is employed to obtain the solution (Appendix E).

5.3 Model Application

In this section, several applications are presented to demonstrate the integrated modeling methodology developed in Section 5.2. These examples are structured around analyzing the effects of plant life-cycle modeling on the water and the contaminant distribution within the soil, and in turn, on the evolution of plant's contamination. Simple weather data and simple irrigation schedule are used to facilitate the interpretation of the results. The crop data is obtained from the literature. Mass balance analysis is carried out to identify the accurate fate of the contaminant once it is introduced to the system. Finally, a sensitivity analysis investigates the importance of model input parameters on the plant pathway outcome.

5.3.1 Modeling Domain and the Model Parameters

In all applications a hypothetical heterogeneous soil column of 2 m length is used. The soil media information was adopted from Wohling and Mailhol (2007) as determined at a site in Montpellier, France. The soil profile was divided into three layers that are occupied by different types of soil. The soil characteristics within each layer are given in Table 5.1.

Table 5.1: Soil types and their characteristics used in the applications (Wohling and Mailhol 2007).

Soil Type No.	***Layer (m)***	θ_s	θ_r	$\alpha\ (m^{-1})$	***n***	$K_s\ (m\ s^{-1})$	$\rho_b\ (g\ m^{-3})^a$
1	0.0 – 0.55	0.35	0.05	1.5	1.46	7.5×10^{-6}	1.50×10^{6}
2	0.55 – 0.95	0.38	0.05	1.3	1.45	1.85×10^{-6}	1.45×10^{6}
3	0.95 – 2.0	0.41	0.05	1.9	1.31	5.2×10^{-7}	1.40×10^{6}

[a]: Assumed

An initial soil-water pressure head of -10 m throughout the column was assumed so that it would be possible to see the effect of evapotranspiration more distinctively. In the flow simulations, the top boundary condition was variable dependent on the weather conditions and a free drainage boundary condition was applied at the bottom of the soil column (Figure 5.3).

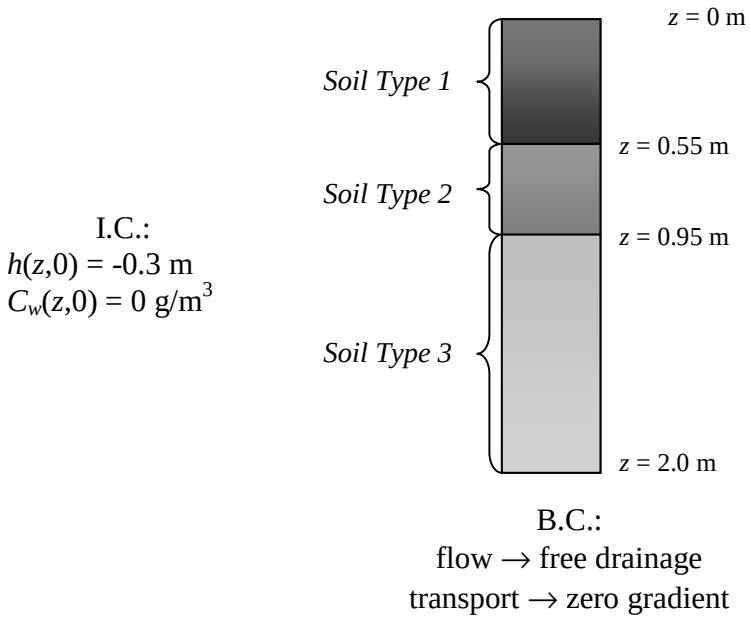

Figure 5.3: The modeling domain and the initial (I.C) and boundary (B.C.) conditions.

In order to facilitate the interpretation of the results, a simplified weather data set is used. Air temperature, reference evapotranspiration (ET_0), h_{atm} (soil surface pressure head in equilibrium with atmospheric water vapor) and daily solar radiation (SR) values are assigned constant values throughout the simulation (Table 5.2).

Table 5.2: Weather data used in the simulations.

Air temperature (T)	20°C
Reference evapotranspiration (ET_0)	2.5 mm/day
h_{atm}	-160 m
Daily incident solar radiation (SR)	2×10^7 J/m^2

Simulation time was set as 120 days to be able to cover a sufficiently long period of time to include the full crop growth and the subsequent senescence. A cycle of 30 days of no rainfall followed by 30 days of constant rainfall (6 mm/day) was repeated until the end of the simulation (Figure 5.4). This simple rainfall pattern creates distinct dry and wet periods. The crop related model parameters were adopted from Mailhol, Olufayo et al. (1997) and Wohling and Mailhol (2007) for corn (Table 5.3). The specific interception storage capacity, S_L, was taken as 0.075 mm (van Dijk and Bruijnzeel 2001b).

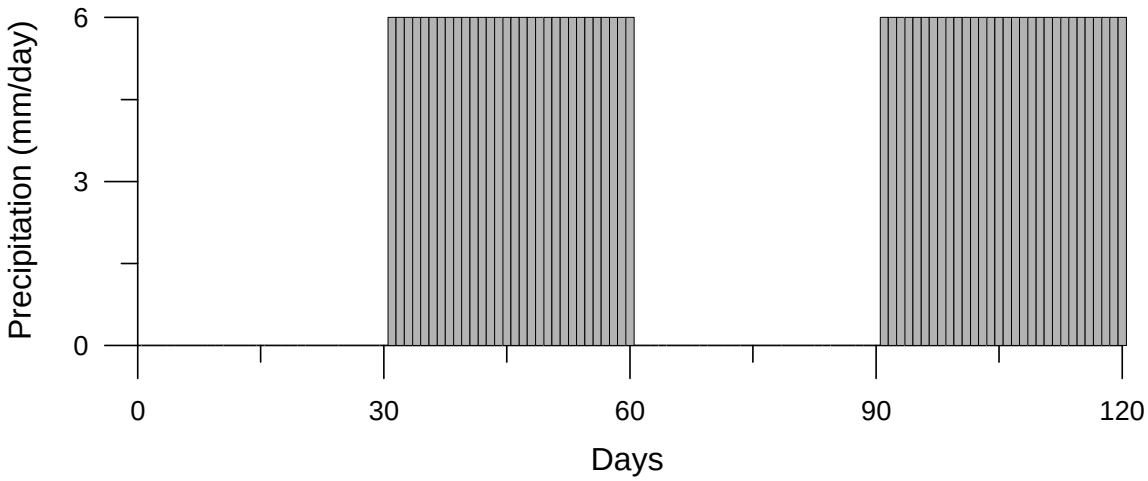

Figure 5.4: Precipitation data.

Table 5.3: Crop parameters (corn). (Mailhol et al. 1997; Wohling and Mailhol 2007)

	Parameter	***Value***
LAI related	LAI_{max}	4.5 m^2m^{-2}
	T_b	6°C
	T_s	100°C
	T_f	1005°C
	λ	1.25
	β	2.4
	δ_1	1.4
	δ_2	0.2
Biomass related	T_{mat}	1925°C
	RUE	1.32 gMJ^{-1}
Root related	$L_R(0)$	0.1 m
	$L_{R,\max}$	1.2 m
	$t_{R,\max}$	72 days
Evapotranspiration related	$K_{c,max}$	1.2
	x_k	1.0
	κ	0.7
Feddes et al.'s (1978) water stress response function parameters	h_a	-0.15 m
	h_{opt}	-0.3 m
	h_{d1}	-3.0 m
	h_{d2}	-35.0
	h_{wp}	-130.0 m
	$TP(h_{d1})$	6.0×10^{-8} m s^{-1}
	$TP(h_{d2})$	1.6×10^{-8} m s^{-1}

The top 20 cm of the soil column is divided into cells with a thickness (Δz) of 0.01 m while a Δz value of 0.05 m was used throughout the rest of the soil column. The initial time step size was set as 1 *hr*. During the simulation, the time step size is allowed to change between 1 *s* and 1 *day* according to the convergence properties of the water flow model. The variable time step size algorithm works similarly to the one explained in van Dam and Feddes (2000). The algorithm doubles the time step size when the number of iterations in the previous time step is less than 3. When the number of iterations needed in the previous time step is more than 6, the time step size is halved for the current time step. If, during the current time step, the solution hasn't converged after 10 iterations, the iterations start over with the time step size halved.

The model parameters used to run the multimedia contaminant fate and transport model are given in Table 5.4. The pesticide diazinon was selected to be the contaminant of concern for the example runs. Its physicochemical properties were compiled from the literature and typical values are used for the soil, plant, and atmosphere related transport parameters.

Table 5.4: Multimedia contaminant fate and transport model parameters.

Contaminant properties (diazinon)		
Molecular weight	304.36 g/mol	(Mackay 2001)
Soil-water partition coefficient, K_d	2.0 cm^3/g	(Chu and Marino 2004)
Air-water partition coefficient OR Dimensionless Henry's law constant, K_{aw} OR K_H	5.0×10^{-5} (dimensionless)	(Chu and Marino 2004)
Log of octanol-water partitioning coefficient, log K_{ow}	3.3 (K_{ow} is dimensionless)	(Mackay 2001)
Water solubility, S_w	60.0 mg/l	(Mackay 2001)
Vapor pressure, P_V	0.008 Pa	(Mackay 2001)
Diffusion coefficient in free air, D_g^a	0.43 m^2/day	(Chu and Marino 2004)
Diffusion coefficient in water, D_l^w	0.000043 m^2/day	(Chu and Marino 2004)
Degradation half life in air	550 h	(Mackay 2001)
Degradation half life in water	1700 h	(Mackay 2001)
Degradation half life in soil	1700 h	(Mackay 2001)
Degradation half life in plant	283 h	Assumed 1/16 of the degradation half life in soil. (Juraske et al. 2008)
Soil related transport parameters		
Longitudinal dispersivity, α_L	0.05 m	(Chu and Marino 2004)
Air boundary layer thickness, d	0.005 m	(Chu and Marino 2004)
Plant related transport parameters		
Air-plant boundary layer thickness	0.002 m	(Cousins and Mackay 2000)
Water content, W_p	0.75 m^3 water / m^3 total plant	Assumed
Density of the dry plant	9×10^5 g/m^3	Assumed

The contamination scenario included the surface application of diazinon one time on the 45th day of the simulation. The application quantity was set as 15 g/m^2 which seemed to be compatible with the actual areal diazinon application rates given in Chu and Marino (2004). The atmospheric concentration is assumed to be zero all throughout the simulation so there would be no contaminant input to the system via atmospheric deposition processes. An initially uncontaminated soil column and plant was assumed. A zero-gradient boundary condition was applied at the bottom of the soil-column.

5.3.2 Description of Simulations

A set of simulations was designed to analyze the effect of vegetation on the water and contaminant distribution within the soil over time, to investigate how the plant growth modeling complexity affects the overall model outcome, and to observe the plant pathway response to different modeling assumptions. The simulation set details are given in Table 5.5 in which the simulations are ranked by the level of detail they incorporate in handling the presence of plants. In the first simulation (*No Plant*), the model is run without a plant compartment. All the subsequent simulations contain the plant compartment but differ in the way they model plant *LAI*, plant biomass (m_P), root growth and root water uptake. In the second simulation (*Const. Plant*), plant life-cycle is not modeled but constant values are assigned to the related parameters. The third simulation (*No Stress*) considers daily variation in plant life-cycle related parameters but ignores the effect of water stress on them. During the fourth simulation (*No Compensation*), the effect of water stress on plant life-cycle is considered but the compensation of this stress

via modified root water uptake distribution is neglected. Finally, the fifth simulation (*Full*) increase the complexity over the fourth simulation by adding the water compensated root water uptake modeling. In Section 5.3.3, the results obtained from this set of example simulations are compared and discussed.

Table 5.5: Tabulated summary of the simulation set.

	Plant Life-Cycle	***Root Water Uptake***
1. No Plant	No plant. $LAI = 0$, $m_P = 0$	No root water uptake.
2. Const. Plant	No plant life-cycle modeling. (Constant *LAI*, plant biomass, and plant volume throughout the simulation) $LAI = 3.0\ m^2m^{-2}$ $m_P = 1000\ g/m^2$, $L_R = 1.2$ m	Root water uptake modeling ignoring water stress compensation. $\beta_c = 1$
3. No Stress	Plant life-cycle modeling ignoring the effect of water stress on *LAI* variation. $WSI = 1$, $LAI = LAI_{pot}(t)$ $m_P = m_P(t)$, $L_R = L_R(t)$	Root water uptake modeling ignoring water stress compensation. $\beta_c = 1$
4. No Compensation	Plant life-cycle modeling considering the effect of water stress on *LAI* variation $WSI = WSI(t)$, $LAI = LAI(t)$, $m_P = m_P(t)$, $L_R = L_R(t)$	Root water uptake modeling ignoring water stress compensation. $\beta_c = 1$
5. Full	Plant life-cycle modeling considering the effect of water stress on *LAI* variation $WSI = WSI(t)$, $LAI = LAI(t)$, $m_P = m_P(t)$, $L_R = L_R(t)$	Root water uptake modeling considering water stress compensation. $\beta_c = \beta_c(h,z,t)$

5.3.3 Results and Discussion

5.3.3.1 Plant Life-Cycle

The different modeling approaches to plant growth by the individual model applications described in the Section 5.3.2 (Table 5.5) are easily distinguished by the *LAI* and plant biomass simulation results shown in Figure 5.5. *Const. Plant* simulation uses constant specified values of *LAI* and biomass while in the other simulations the plant life-cycle is modeled. The simulations start at the day of sowing and the first emergence of plant and hence the first nonzero *LAI* value appears on the 8^{th}, 18^{th} and 22^{nd} days in the *No Stress*, *Full* and the *No Compensation* simulations, respectively (Figure 5.5a). Apparently, the delayed emergence in the *No Compensation* and the *Full* simulations are due to the water stress experienced by the plant during this period. The *Full* simulation with its activated water stress compensation mechanism partially mitigates the impact of the water stress enabling an earlier emergence than the one observed in the *No Compensation* simulation. As the wet period starts on day 30, the difference between the different simulations regarding *LAI* values vanishes.

The results of different simulations deviate after about day 70 (about 10 days later than the end of the first wet period) (Figure 5.5a). After this date, the available moisture in the soil column starts to become inadequate to sustain the plants, which are now in their early senescence period with high *LAI* and biomass. This situation is ignored in the *No Stress* simulation and its *LAI* stays at its potential value. The decreasing *LAI* curve is much

steeper for the *No Compensation* simulation than it is for the *Full* simulation since the compensation mechanism in the *Full* simulation enables plant to make more efficient use of the water available in the root zone. This second period of water stress ends after day 90 as the precipitation input resumes. Please note that the thermal time corresponding to LAI_{max} (T_f = 1005°C) is reached on day 79. This is the start of the natural senescence period and *LAI* values start to decrease even with no water stress. However, the decrease in the *LAI* values is at a slower rate since a smaller δ value is used during this period (δ_1 = 1.4 vs. δ_2 = 0.2) to simulate slow senescence observed in the corn plant (Mailhol et al. 1997).

The response of the plant biomass growth model to water stress is also obvious when the results from different simulations are compared (Figure 5.5b). The *No Stress* simulation ignores the effect of water stress and biomass increase is continued at the same rate throughout the simulation. The *No Compensation* and the *Full* simulations respond to the water stress by decreasing the rate of biomass growth. This is more pronounced during the initial dry period until day 30. As expected, the growth rate is the lowest for the *No Compensation* simulation. Due to the decreased growth rate in this initial dry period and the late emergence, the biomass values from the *No Compensation* simulation are lower than that of the *Full* simulation throughout the whole period. Note that a constant daily solar radiation value was used to simulate plant growth and hence the potential biomass growth from the *No Stress* simulation follows a straight line. Also, the plant biomass values continue to increase even after *LAI* senescence has begun since a different and later maturation point (T_{mat} = 1925°C) is adopted for stopping the biomass growth. As the

plants start experiencing increased water stress, towards the end of the second dry period, only a subtle decrease in biomass growth rate is observed in the *No Compensation* and the *Full* simulations since this is a brief period and ends on day 90.

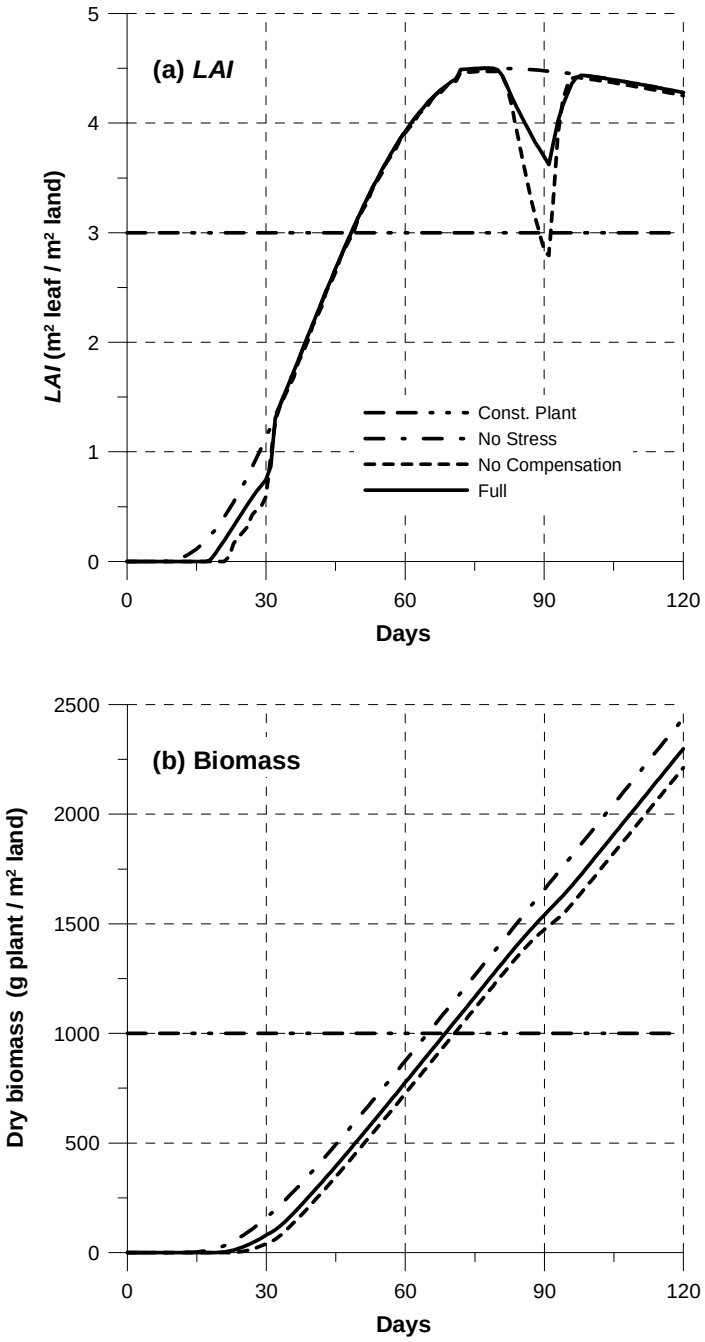

Figure 5.5: Daily variation of *LAI* (a) and plant biomass (b) as obtained from different model simulations. (See Table 5.5 for the model simulation details.)

5.3.3.2 Soil-water Distribution

Since the plant life-cycle model and the soil-water flow model are in close interaction, the results from both models should be analyzed together. Soil-water pressure head profiles given in Figure 5.6 show the effect of plant growth on the soil-water distribution. The profile snapshots in Figure 5.6 are plotted at the times corresponding to the start and the end of the wet periods. The root water uptake rate distributions at the start and the end of the wet periods are shown in Figure 5.7.

The highest soil-water pressure heads are observed in the *No Plant* simulations since the only means of water depletion is evaporation from soil surface (Figure 5.6). On the other hand, the lowest soil-water pressure head values are observed in the *Const. Plant* simulation results due to the fact that a high and constant transpiration demand is imposed throughout the simulation. When the root water uptake rate profiles (Figure 5.7) are compared with the soil-water pressure head profiles (Figure 5.6), it is consistently observed that there is reduced water uptake within the zones of low soil-water pressure head for the corresponding simulations.

For the simulations that model plant growth (*No Stress*, *No Compensation*, *Full*), very similar soil-water pressure head profiles are obtained at the end of the wet periods (day 60 and day 120) whereas the soil-water pressure head profiles for these simulations are slightly different at the end of the dry periods (day 30 and day 90) (Figure 5.6). Analyzing the corresponding root water uptake rate profiles (Figure 5.7) and also

comparing the corresponding *LAI* values (Figure 5.5a) are helpful for a better interpretation of these discrepancies. On day 30, the *No Stress* simulation has the highest *LAI* among the simulations that model plant growth so it simulates higher root water uptake and thus higher water depletion in the root zone. The same is true for the 90^{th} day. However, as a result of root growth, the effect of the compensated root water uptake model is more pronounced in the *Full* simulation results as the active water uptake region is moved to deeper soil compared to the other simulations. Of course, this more efficient water uptake is reflected in the simulated *LAI* value which is higher for the *Full* simulation than it is for the *No Compensation* simulation on day 90.

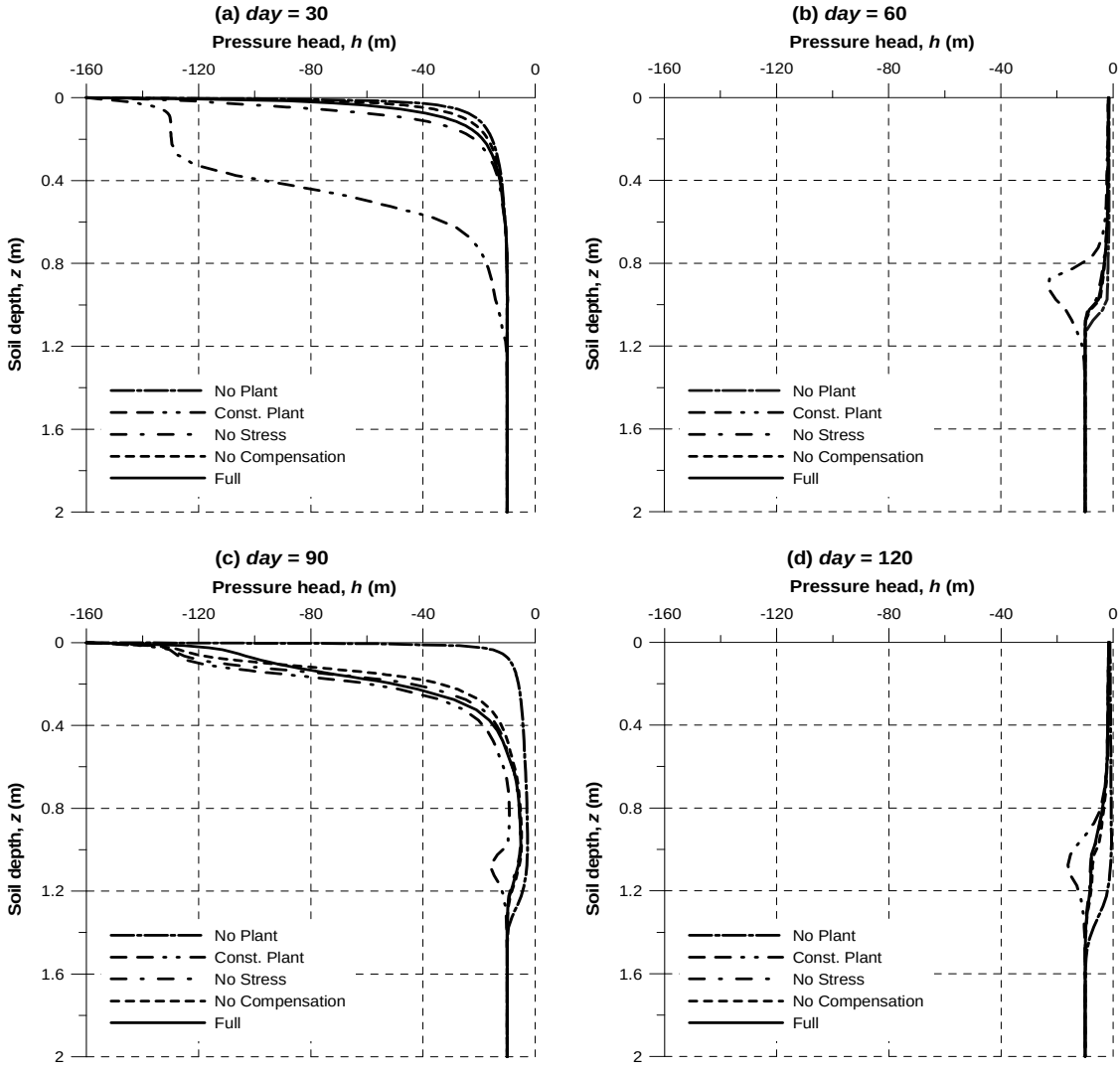

Figure 5.6: Pressure head profiles obtained by different model simulations at the beginning and at the end of the wet periods.

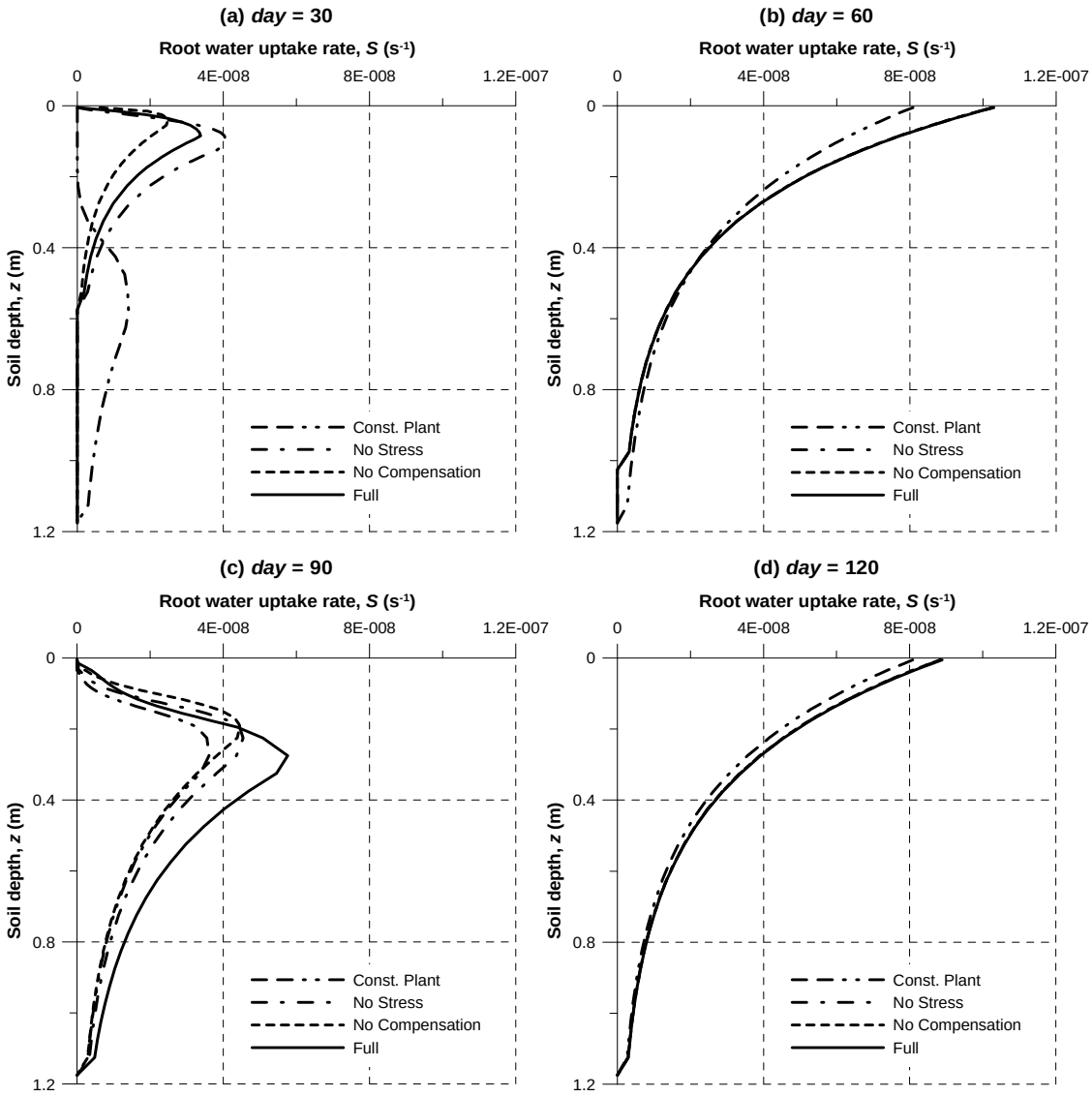

Figure 5.7: Root water uptake rate distributions at the beginning and at the end of the wet periods.

5.3.3.3 Contaminant Distribution in Soil

The bulk soil concentration profiles obtained by different simulations are given in Figure 5.8. Note that the contaminant cannot penetrate to deeper soil layers during the simulation period. The concentration profiles given in Figure 5.8 for the simulations that include plants are similar while the profile for the *No Plant* simulation is easily distinguished from the others. This discrepancy can be explained by the combined effect of volatilization and root contaminant uptake. As it is discussed in the *Mass Balance Analysis* section (Section 5.3.3.5), the volatilization loss is higher in the *No Plant* simulation resulting in a decrease in the contaminant mass available to migrate within the soil. On the other hand, for the other simulations, the soil contaminant concentration is decreased by the root contaminant uptake processes. The combined effect is the concentration profile in Figure 5.8a with deeper contaminant migration with a lower peak value for the simulations that consider the presence of plants compared to the concentration profile given by the *No Plant* simulation.

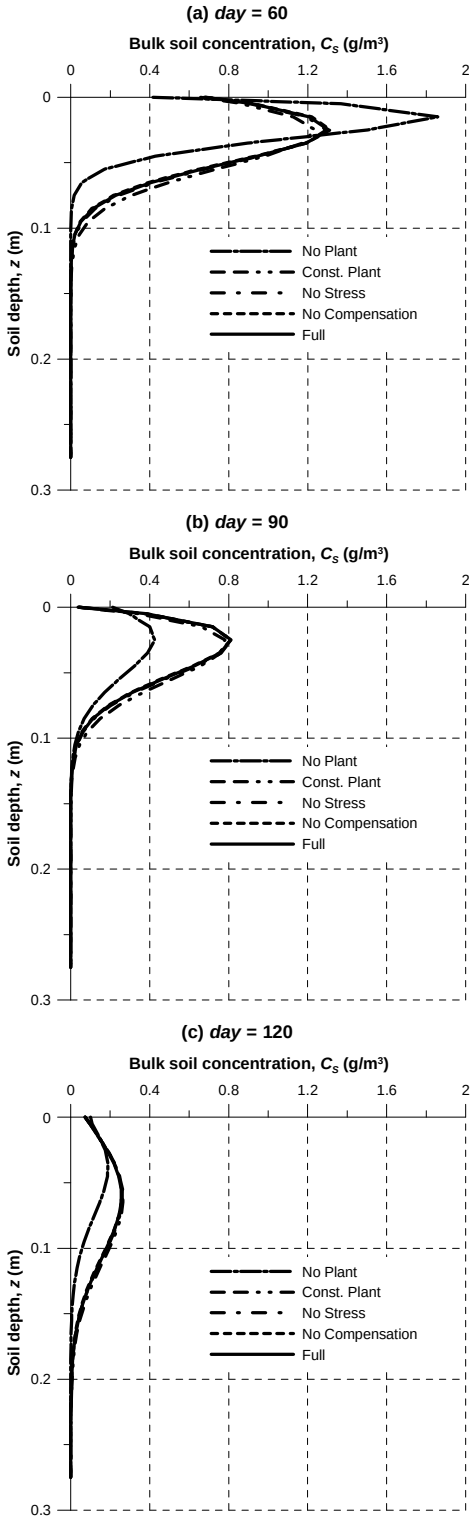

Figure 5.8: Contaminant concentration profiles obtained by different model simulations.

A better picture of the contaminant concentration change with respect to time in the soil is provided by Figure 5.9. A sharp increase in the contaminant concentration is observed at the soil surface on the day of contaminant input, which is immediately followed by a sharp decrease (Figure 5.9a). Volatilization and infiltration, acting together, rapidly decrease the contaminant concentration at the soil surface. The peaks get less sharp in the lower soil layers. (Note the scale difference in the *y*-axis of the figures belonging to different depths.) Among the simulations with plants, in the deeper soil layers (Figures 5.9c-d) the contaminant concentrations are always higher for the *Const. Plant* simulation compared to the simulations that model plant growth (*No Stress*, *No Compensation*, *Full*). The contaminant concentration distribution and its change with time are similar for the simulations that model plant growth. The effect of increased contaminant migration to deeper soil due to increased infiltration is visible in Figure 5.9d where the contaminant concentrations start to increase with the start of the second wet period after day 90.

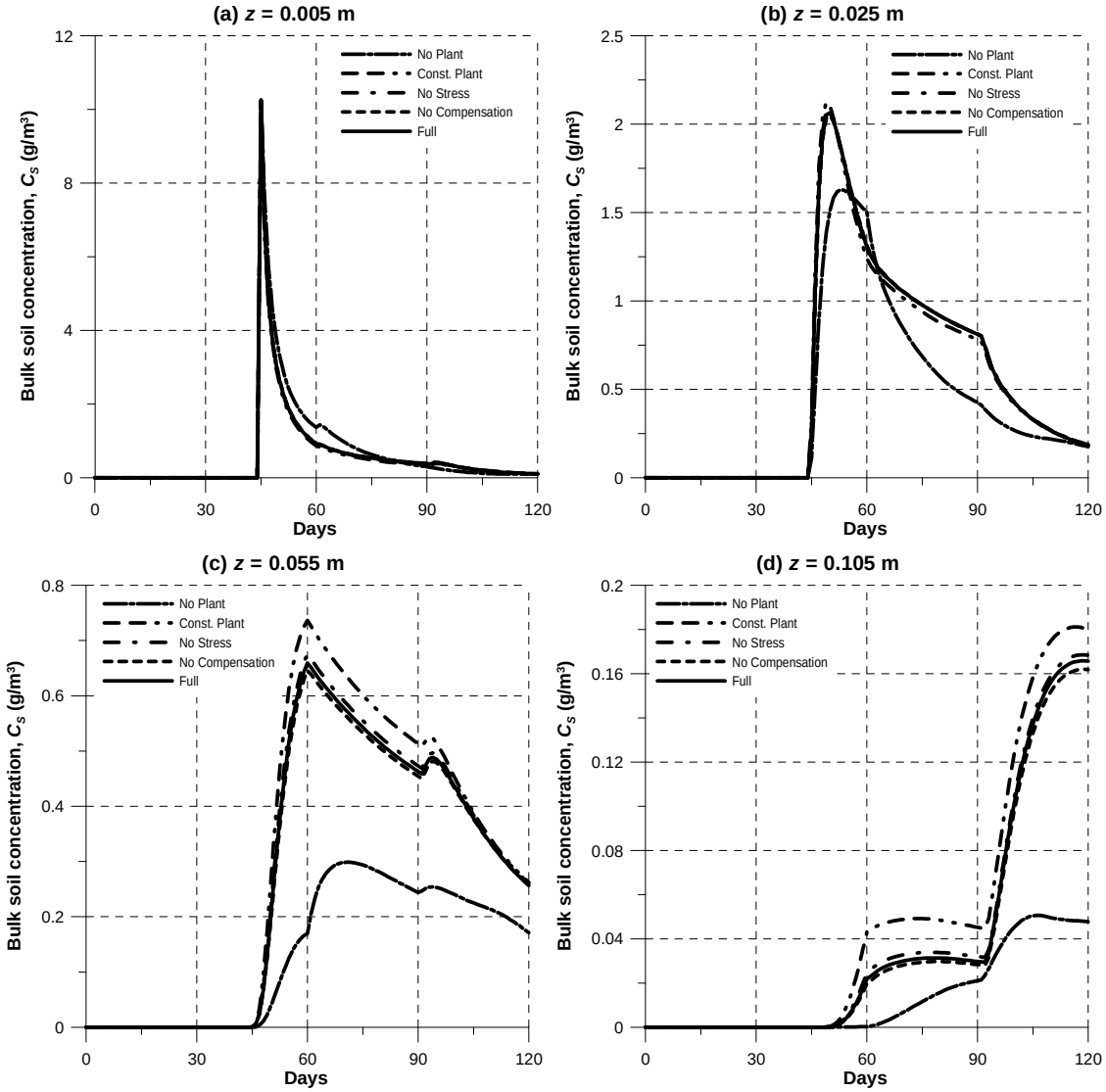

Figure 5.9: The bulk soil concentration change with respect to time at various soil depths.

5.3.3.4 Plant Pathway

The contaminant concentration evolution within the plant throughout the simulation period for different simulations is shown in Figure 5.10. In the contamination scenario applied in this example, the only route for plant's contamination is the root uptake. Since the atmospheric concentration is assumed to be equal to zero all throughout the simulations, no atmospheric deposition has occurred. However, volatilization to the atmosphere as well as decay acted as routes of contaminant loss from the plant. The concentrations estimated by the simulations that model plant growth (*No Stress*, *No Compensation*, *Full*) are similar to each other. Although there are slight differences in the peak concentrations obtained by these simulations, they agree at the timing of the peak. On the other hand, the peak concentration for the *Const. Plant* is much lower than those of the rest of the simulations. Towards the second half of the dry period (days 75-90), contaminant concentration values converge in all of the simulations as they decrease due to the loss processes together with a decrease in root uptake. This decreasing trend of concentration with time is disturbed in all the simulations by the start of the second wet period. After day 90, the increase in concentration for the *Const. Plant* is higher than that of the other simulations and the *Const. Plant* simulation ends up with a higher in-plant concentration than that of the others.

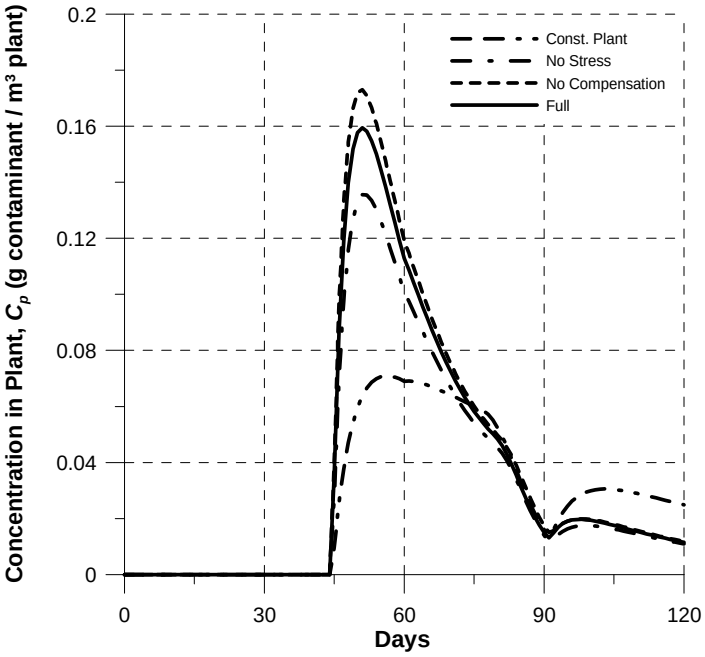

Figure 5.10: Contaminant concentration within the plant with respect to time according to different simulations.

Since the contaminant does not penetrate into deep soil, root uptake is occurring near the soil surface. So, the differences between the simulations regarding the in-plant concentrations can be explained by the differences in root water uptake patterns and the available soil concentrations in this region. The higher concentration increase after the start of the second wet period for the *Const. Plant* simulation can be explained by the combined effect of two factors. First is the increased root water uptake due to new soil-water that has become available because of the precipitation. The second is the generally higher contaminant soil concentrations for this simulation especially for deeper soil layers. However, it should also be noted that the contaminant concentration within the plant is dependent on the plant volume. The plant volume is calculated from the plant biomass which is assigned a constant value for the *Const. Plant* simulation but which is calculated using the plant growth model (Equation 3.19) for the other simulations (Figure

5.5b). In the following section, a mass balance analysis is carried out and the simulation results are compared on the basis of contaminant mass.

5.3.3.5 Mass Balance Analysis

At any time during the simulation, the equation below for the whole system must hold:

$$\begin{pmatrix}\text{Mass in the soil}\\ \text{+ Mass in the plant}\end{pmatrix}_t = \left[\begin{pmatrix}\text{Cumulative inflow to the soil}\\ \text{- Cumulative outflow from the soil}\end{pmatrix} + \begin{pmatrix}\text{Cumulative inflow to the plant}\\ \text{- Cumulative outflow from the plant}\end{pmatrix}\right]_t \quad (5.25)$$

$$\left(\text{Cumulative inflow to the soil}\right)_t = \left(\text{Cumulative surface input to the soil }\right)_t \quad (5.25a)$$

$$\left(\text{Cumulative outflow from the soil}\right)_t = \begin{pmatrix}\text{Cumulative volatilization from the soil}\\ \text{+ Cumulative decay in the soil}\\ \text{+ Cumulative root uptake}\end{pmatrix}_t \quad (5.25b)$$

$$\left(\text{Cumulative inflow to the plant}\right)_t = \left(\text{Cumulative root uptake }\right)_t \quad (5.25c)$$

$$\left(\text{Cumulative outflow from the plant}\right)_t = \begin{pmatrix}\text{Cumulative volatilization from the plant}\\ \text{+ Cumulative decay in the plant}\end{pmatrix}_t \quad (5.25d)$$

The change of contaminant mass within the soil and the plant is shown in Figure 5.11; and, the daily cumulative values of the amount of mass transferred via the relevant processes given in Equation (5.25) are plotted in Figures (5.12-13). In the contamination scenario applied in this study, the only inflow to the system is through the contaminant input onto the soil surface. The outflows from the system are volatilization and decay, which occur both in the soil and in the plant (Figure 5.12). On the other hand, root uptake

transfers the contaminant from the soil to the plant, so it is an intermedia mass transfer process within the system (Figure 5.13).

The mass balance error is calculated for the whole system and also for the plant compartment and the soil column by using the following generic equation:

$$MBE_t = 100 * \left| 1.0 - \frac{\left[\begin{array}{l} \left(\text{Cumulative mass inflow to the system}\right)_t \\ - \left(\text{Cumulative mass outflow from the system}\right)_t \end{array} \right]}{\left(\text{Mass in the system}\right)_t} \right| \qquad (5.26)$$

where MBE_t is the percentage mass balance error at time *t.* The cumulative mass balance error for the plant compartment, the soil column and the whole system at the end of the simulation do not exceed 5.6×10^{-4} %, 2.4×10^{-6} % and 2.3×10^{-11} %, respectively, for any of the simulations.

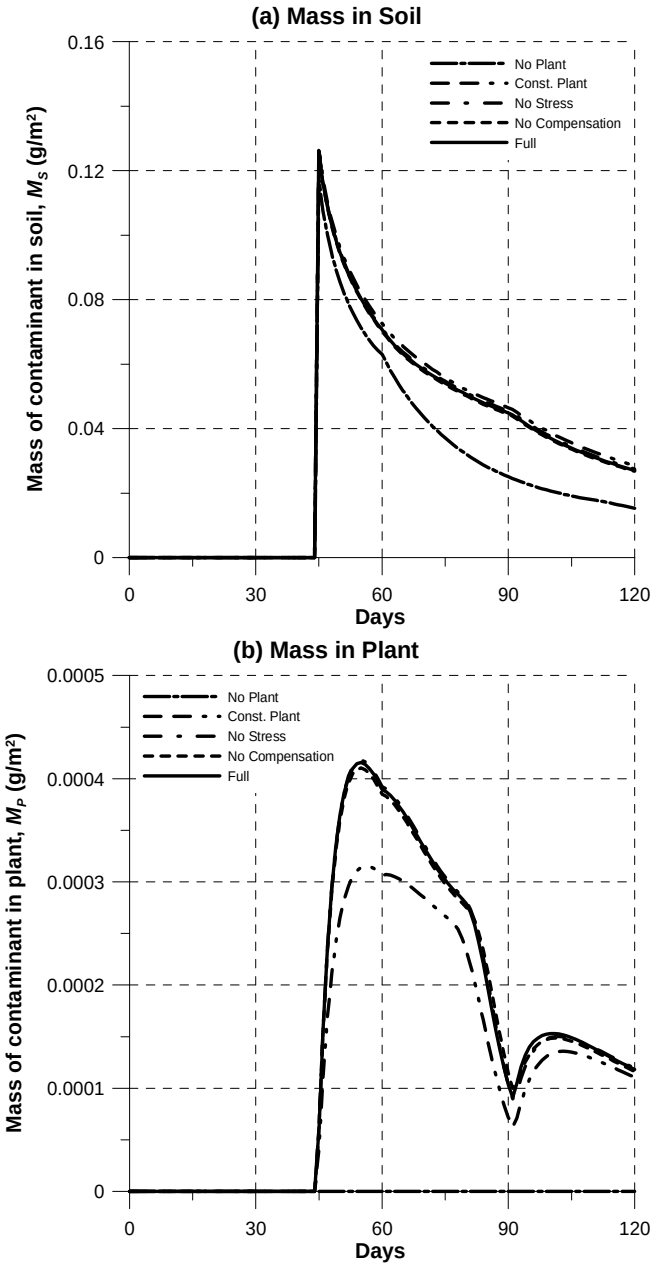

Figure 5.11: Change of contaminant mass in soil (a) and plant (b) with time.

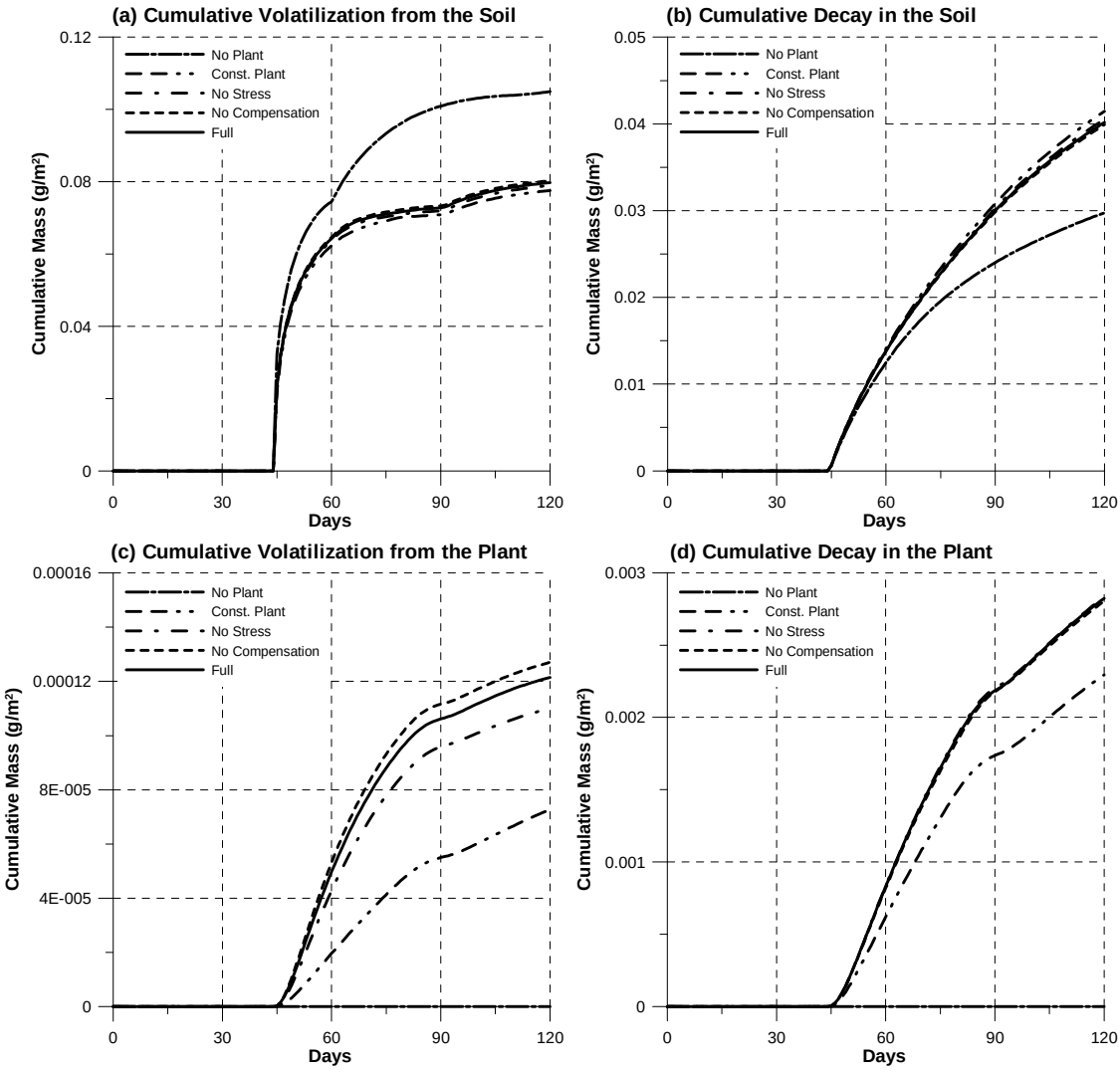

Figure 5.12: Cumulative mass removed from the system via volatilization and decay.

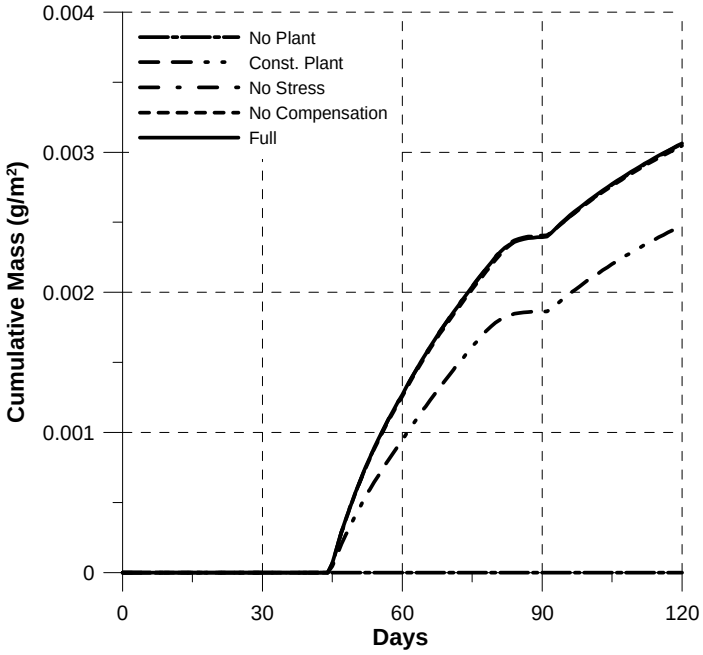

Figure 5.13: Cumulative mass of contaminant transferred via root uptake.

The mass balance analysis results reveal the importance of volatilization as a contaminant loss process from the soil (Figure 5.12a). The highest contaminant loss occurs through volatilization in all of the simulations and the *No Plant* simulation gives the highest amount of volatilization loss. As a result, the total contaminant mass within soil for the *No Plant* simulation decreases more rapidly than it does in the other simulations (Figure 5.11a). Further analysis of the simulation results revealed that there is higher accumulation of contaminant at the soil surface for the case of *No Plant* due to lower infiltration rates in this simulation causing higher volatilization. The reason for the lower infiltration rate is attributed to the lower pressure head gradient at the soil surface due to the relatively more moist conditions in the *No Plant* simulation. The pressure gradient near the soil surface is higher for the simulations that consider the presence of plants since root water uptake consumes soil-water in the root zone.

The contaminant mass within the plant is similar for the simulations that model plant life-cycle (*No Stress*, *No Compensation*, *Full*) whereas it is lower for the *Const. Plant* simulation (Figure 5.11b). This can be explained by the lower root uptake due to lower *LAI* for the *Const. Plant* simulation compared to the other simulations (Figures 5.13, 5.5).

5.3.3.6 Sensitivity Analysis

In this section, the sensitivity of the contaminant concentration within the plant to a selected set of contaminant fate and transport parameters is analyzed. In the analysis, different values were assigned to the parameter of interest while keeping all the other model parameters constant. The sensitivity to a 20% variation in the parameter of interest was investigated for all the selected parameters. However, greater variation was also included in the analysis if the literature indicated a higher uncertainty in the parameter value.

The sensitivity of the contaminant concentration within the plant to the longitudinal dispersivity, retardation factor, bulk decay rate in soil, *TSCF*, contaminant half life within the plant and the air to plant diffusive mass transfer rate coefficient were analyzed. Among these parameters, it was found out that the longitudinal dispersivity, bulk decay rate in soil and air to plant diffusive mass transfer rate coefficient did not effect the in-plant concentrations significantly for the example application problem implemented in this study. The sensitivity of the contaminant concentration within the plant to the

variation of the retardation factor, *TSCF* and contaminant half life within the plant is shown in Figure 5.14. The *Full* simulation was used as the base case in this analysis.

The retardation factor (R) in unsaturated soil can be defined as:

$$R = 1 + \frac{\rho_b K_d + \phi s_g K_H}{\phi s_w} \tag{5.27}$$

R values are variable both spatially and temporally. The main uncertainty in the R value comes from the uncertainty in the value of the partition coefficient, K_d. A K_d value of 2.0 cm^3/g was used in the original simulation. In Figure 5.14a, the plant contaminant concentration variation with time is compared for the model simulations that increased and decreased the original R value by 20%. It is seen that the plant contaminant concentration is higher for the low R value. This is expected since lower R value increases the water availability of the contaminant, facilitating its uptake through plant roots. The effect of R value is significant for the periods of wet soil conditions since there is increased root water uptake.

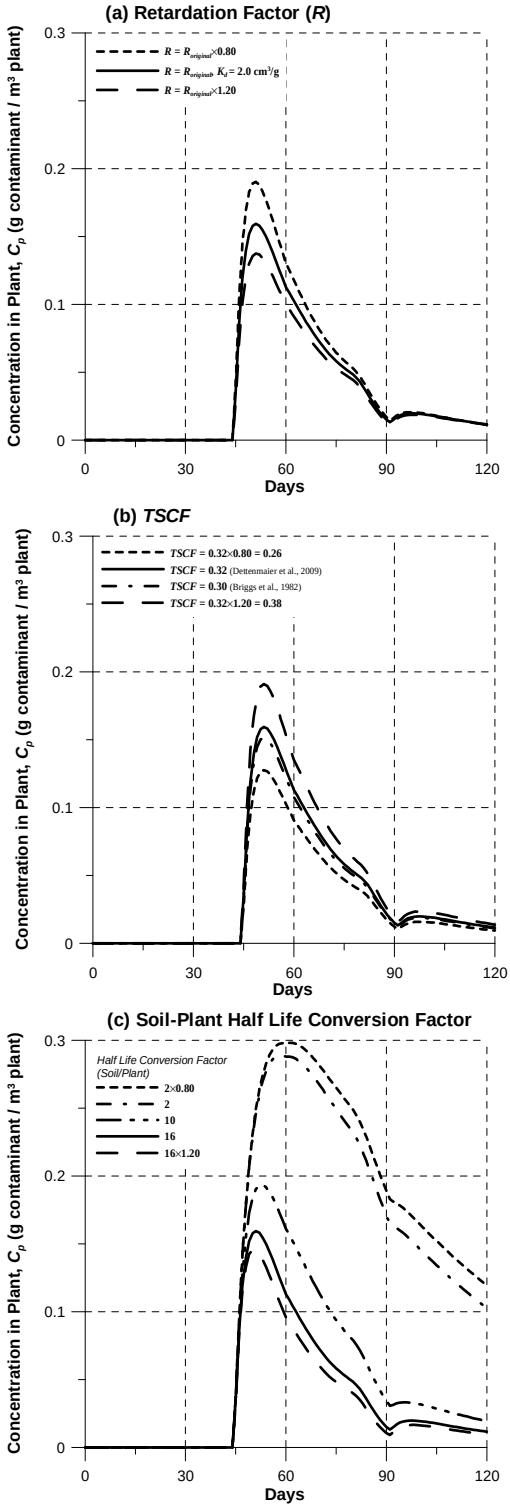

Figure 5.14: Sensitivity of the in-plant contaminant concentration to (a) retardation factor (*R*), (b) *TSCF*, and (c) soil-plant half-life conversion factor.

In the example application, the relationship of Dettenmaier et al. (2009) was used to estimate the *TSCF* value (Equation 3.16) from the log K_{ow} value of the contaminant. This is not the only relationship that is used to estimate *TSCF*. Another popular but older equation to estimate *TSCF* is the one developed by Briggs et al. (1982):

$$TSCF = 0.784 \exp\left[-\left(\log K_{ow} - 1.78\right)^2 / 2.44\right] \tag{5.28}$$

The above equation produces a bell-shaped relationship between *TSCF* and log K_{ow}, which estimates reduced *TSCF* for highly polar (low log K_{ow}) and highly lipophilic (high log K_{ow}) substances. Trapp (2007) discusses the accuracy of the Briggs et al.'s (1982) relationship in case of polar compounds since there are studies who contradict with the predicted reduced uptake by Equation (5.28). Dettenmaier et al. (2009) have also observed high uptake of polar compounds in their extended study of *TSCF* measurements in order to re-evaluate the relationship and produced a new empirical relationship which is nearly sigmoidal (Equation 3.16).

The compound that was used in the application simulations, diazinon, with its log K_{ow} value of 3.3, is slightly lipophilic and both of the relationships estimate similar values as the *TSCF* for diazinon (0.30 with Briggs et al.'s (1982) relationship, 0.32 with Dettenmaier et al.'s (2009) relationship). It is common to measure a range of *TSCF* values for a specific compound due to variations in the experimental setup (Dettenmaier et al. 2009). There is also evidence that supports that *TSCF* is in fact not a constant but a variable that is affected by the environmental conditions (Trapp 2007). In Figure 5.14b,

the effect of *TSCF* variation on the plant pathway outcome is shown. It is seen that the variation in *TSCF* is immediately reflected in the contaminant concentration values within the plant as increased *TSCF* allows more contaminant uptake. However, this effect is also dependent on the water and contaminant availability in the soil and it is more pronounced in the earlier stages of the contamination which is also governed by wet conditions in this example.

The contaminant half life within the plant is one of the parameters with the greatest uncertainty. In the absence of data, extrapolation from degradation half-lives in soil is a commonly used method to estimate in-plant half-lives. However, there is a lot of uncertainty in the results of these extrapolations and there is no consensus in the literature on the conversion factors to be used (Juraske et al. 2008). Juraske et al. (2008) report studies that assume in-plant half lives that are half of that of the soil half life (a conversion factor of 2) as well as studies that assume a conversion factor of 10. They have determined a conversion factor 16 for in-plant half lives through their own field experiments. Following their suggestion, a conversion factor of 16 was used as the basis in determining the in-plant degradation rate in this example. In Figure 5.14c, the outcome of using the lower conversion factors is shown.

5.4 Conclusion

In this chapter, a methodology that unifies single media continuous models with multimedia compartmental models in a flexible framework has been developed for

analyzing the contaminant transport in a soil-plant system. Multiple models, each describing a different set of processes that belong to the system, were integrated within this framework. Together with the contaminant fate and transport models, water flow and plant life-cycle models were also included into the integrated model. The resultant model was applied to a hypothetical contamination scenario where the effect of the presence of plants on the contaminant distribution within the system was investigated. The model outcomes obtained by employing multiple levels of complexity to the plant growth and root water uptake models were compared.

The results obtained from the applications showed the close interaction between plants and the soil-water flow. The presence of plants considerably modified the spatial and temporal water distribution within the root zone. When the fact that plants are dynamic biological systems with a capability to grow and to regulate their interaction with the soil (regarding the root water uptake) was taken into account, the results were further modified and they became dependent on the way the plant's response to the environmental conditions are modeled. When the model of contaminant transport within the soil was integrated with the plant life-cycle and the soil-water flow models, the results became difficult to interpret by intuition as a result of the complexity involved. The plant's contamination modeling as coupled with plant life-cycle, soil-water flow and soil contaminant transport models showed that contaminant concentrations within the plant were highly variable with time indicating potentially important consequences when assessing the risk associated with this exposure pathway.

This work presented in this chapter should serve as a basis for integrating physically based models that describe the various processes related to contaminant fate and transport in the soil-plant system. The individual modules (e.g. *LAI* simulation) used in this study may be easily replaced with others. The mathematical definitions of the processes can be changed. Even adding new expressions for processes that are absent in this study would be straightforward. New compartments can be added to increase the detail if the proper expressions to define mass transfer between the other compartments being modeled can be developed. For example, adding a litter compartment residing at the soil surface would be trivial if the litterfall rate to model mass transfer between the plant and the litter compartments, and the litter decomposition rate to model mass transfer between the litter compartment and the uppermost soil cell can be defined. On the other hand, the model itself can be used as a tool in developing the definitions for these processes. Various hypotheses that describe different processes related to the soil-plant system can be tested using the model. These tests can be performed on field data as well as on the laboratory data since the model is capable of describing soil heterogeneity together with soil hydraulics.

CHAPTER 6

INTEGRATED MODELING OF WATER FLOW IN A TERRESTRIAL SYSTEM

6.1 Introduction

In this chapter, the hydrological counterpart of the soil-plant system model developed in Chapter 5 is extended to cover larger spatial areas. The objective is to develop a model of water flow in a terrestrial system that can describe water flow dynamics on the land surface and within the shallow soil for extended periods of time. Particular attention is given to the effects of the presence of vegetation on the overall water flow dynamics within the system. The vegetation is treated as a dynamic entity considering its life cycle and its response to the water availability within the system. Thus, the key characteristics of the soil-plant system model previously developed are preserved. This is accomplished by representing the modeling domain as a collection of soil-plant system units. These multiple soil-plant system units are coupled by implementing an overland flow model that describes the ground surface processes. Furthermore, the subsurface lateral fluxes between neighboring soil columns are accounted for. The aim is to develop a tool that provides all the hydrological information needed for contaminant fate and transport analysis in heterogeneous soil-plant systems.

In the following sections, the integrated model framework is described and the resultant model's capability in describing the water flow dynamics in a spatially heterogeneous soil-plant system is demonstrated through several applications.

6.2 Integrated Model Development

A schematic view of the integration approach is given in Figure 6.1. The unsaturated zone water flow model coupled with the plant life-cycle model is treated as a single unit of the new integrated model. The details of the water flow modeling within a single soil column have been described in Chapter 5. The other major components of the integrated model are the two-dimensional overland flow model (Section 4.3) and subsurface lateral fluxes between adjacent soil columns calculated using Darcy's law. The coupling of the overland flow model with the unsaturated zone soil-water flow model is described in Section 6.2.1. The method used in determining the subsurface lateral fluxes and incorporating them into the integrated model is explained in Section 6.2.2. Finally, the effect of vegetation on the overland flow processes is discussed in Section 6.2.3.

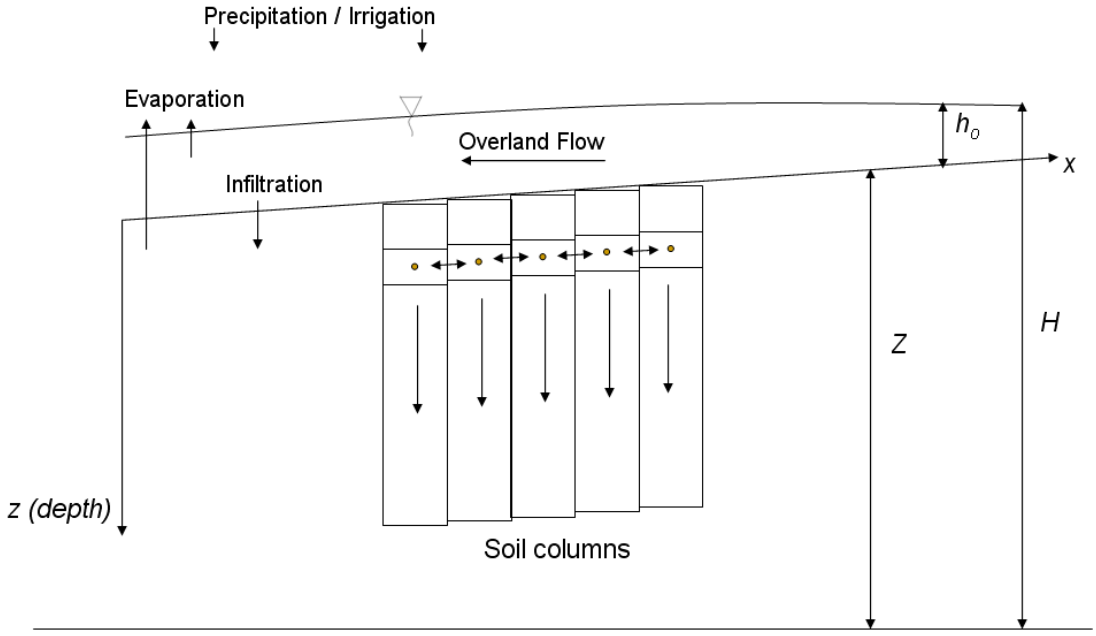

Figure 6.1: A schematic view of the integrated model.

6.2.1 Coupling Overland Flow and Unsaturated Zone Soil-Water Flow Models

The coupling of the overland flow and the soil-water flow models is achieved by the simultaneous solution of the model equations in a single global matrix. The interaction between the two domains is handled by enforcing the continuity of the pressure heads and the fluxes at the interface (i.e. ground surface).

The two-dimensional overland flow model solves for the flow height variation over each overland cell (Section 4.3). Each overland cell is in interaction with a soil column that lies underneath it (Figure 6.1). The one-dimensional soil-water flow model solves for the pressure-head distribution over the soil depth with time within each column (Section 4.1). The global matrix-vector equation when there are P overland cells and N soil cells within each soil column can be represented as below:

$$\mathbf{M}_{\mathbf{global}}\left(\frac{\mathbf{dh}_{\mathbf{global}}}{\mathbf{dt}}\right)+\mathbf{S}_{\mathbf{global}}\mathbf{h}_{\mathbf{global}}=\mathbf{F}_{\mathbf{global}} \tag{6.1}$$

$$\text{with}\ \mathbf{F}_{\mathbf{global}}=\begin{pmatrix}\{\mathbf{F}_{\mathbf{overland}}\}_{P}\\ \{\mathbf{F}_{\mathbf{subsurface},1}\}_{N+1}\\ \vdots\\ \{\mathbf{F}_{\mathbf{subsurface},j}\}_{N+1}\\ \vdots\\ \{\mathbf{F}_{\mathbf{subsurface},P}\}_{N+1}\end{pmatrix};\ \mathbf{M}_{\mathbf{global}}=\begin{pmatrix}\{\mathbf{M}_{\mathbf{overland}}\}_{P}\\ \{\mathbf{M}_{\mathbf{subsurface},1}\}_{N+1}\\ \vdots\\ \{\mathbf{M}_{\mathbf{subsurface},j}\}_{N+1}\\ \vdots\\ \{\mathbf{M}_{\mathbf{subsurface},p}\}_{N+1}\end{pmatrix};\ \mathbf{h}_{\mathbf{global}}=\begin{pmatrix}\{\mathbf{H}\}_{P}\\ \{\mathbf{h}_{1}\}_{N+1}\\ \vdots\\ \{\mathbf{h}_{j}\}_{N+1}\\ \vdots\\ \{\mathbf{h}_{p}\}_{N+1}\end{pmatrix};\ \text{and,}$$

$$\mathbf{S}_{\mathbf{global}} = \begin{pmatrix} \left[\mathbf{S}_{\mathbf{overland}}\right]_{P\times P} & & & & & \\ \left[\mathbf{S}_{\mathbf{o\text{-}s},1}\right]_{(N+1)\times P} & \left[\mathbf{S}_{\mathbf{subsurface},1}\right]_{(N+1)\times(N+1)} & & & & \\ & & \ddots & & & \\ & & \left[\mathbf{S}_{\mathbf{o\text{-}s},j}\right]_{(N+1)\times P} & \left[\mathbf{S}_{\mathbf{subsurface},j}\right]_{(N+1)\times(N+1)} & & \\ & & & & \ddots & \\ & & & & \left[\mathbf{S}_{\mathbf{o\text{-}s},P}\right]_{(N+1)\times P} & \left[\mathbf{S}_{\mathbf{subsurface},P}\right]_{(N+1)\times(N+1)} \end{pmatrix};$$

$$\left[\mathbf{S}_{\mathbf{o\text{-}s},j}\right]_{(N+1)\times P} = \begin{pmatrix} 1 & \cdots & 0 \\ \vdots & \ddots & \vdots \\ 0 & \cdots & 0 \end{pmatrix};$$

$$\left[\mathbf{S}_{\mathbf{subsurface},j}\right]_{(N+1)\times(N+1)} = \begin{pmatrix} -1 & & & & & & & \\ \left(S_1^1\right)_j & \left(S_1^2\right)_j & \left(S_1^3\right)_j & & & & & \\ & \left(S_2^1\right)_j & \left(S_2^2\right)_j & \left(S_2^3\right)_j & & & & \\ & & & \ddots & & & & \\ & & & \left(S_j^1\right)_j & \left(S_j^2\right)_j & \left(S_j^3\right)_j & & \\ & & & & & \ddots & & \\ & & & & & \left(S_N^1\right)_j & \left(S_N^2\right)_j \end{pmatrix};$$

$$\left\{\mathbf{F}_{\mathbf{subsurface},j}\right\}_{N+1} = \begin{pmatrix} z_j \\ \left(F_1\right)_j \\ \left(F_2\right)_j \\ \vdots \\ \left(F_N\right)_j \end{pmatrix}; \left\{\mathbf{M}_{\mathbf{subsurface},j}\right\}_{N+1} = \begin{pmatrix} 0 \\ \left(M_1\right)_j \\ \left(M_2\right)_j \\ \vdots \\ \left(M_1\right)_N \end{pmatrix}; \left\{\mathbf{h}_j\right\}_{N+1} = \begin{pmatrix} \left(h_o\right)_j \\ \left(h_1\right)_j \\ \left(h_2\right)_j \\ \vdots \\ \left(h_N\right)_j \end{pmatrix}.$$

The first row of the subsurface equations as given in Equation (6.1) serves for the purpose of enforcing the pressure head continuity at the ground surface, and also, for converting the overland flow height values (H) into overland flow depths (h_o) by imposing $\left(H\right)_j - \left(h_o\right)_j = z_j$, where z_j is the land surface elevation [L]. In matrix $\mathbf{S}_{\mathbf{subsurface},j}$, the term $\left(S_1^1\right)_j$ is determined as given in Equation (A.15b). It is equal to zero

when there is no overland flow development. In that case, the right-hand-side of the equation for cell 1 is adjusted according to the type of boundary condition applied at the top of the soil column. See Appendix A for the details of handling the top boundary condition in the solution of the soil-water flow model. The algorithm that determines the ground surface conditions in the implementation of the integrated flow model is described below.

In the formulation of the overland flow model (Equation C.10), the F_p term on the right-hand-side of the mass balance equation for cell *p* represents the vertical water fluxes for the cell. Since the current soil-water flow model contains a detailed top boundary condition handling algorithm which is capable of calculating all the vertical fluxes occurring at the soil surface (Figure 5.1), this top boundary condition handling algorithm of the soil water flow model is used as a key component of the interaction algorithm that links the overland flow and soil-water flow models. The overland flow model supplies the surface water depth to the top boundary algorithm and it receives the vertical flux value in return. Thus, in the integrated model, the soil-water flow model previously developed can be used without any modifications, except the small adjustments required to the top boundary condition algorithm that ensure that the continuity assumption at the overland / subsurface interface is realized. The algorithm that handles the interaction between the two domains is schematically described in Figure 6.2.

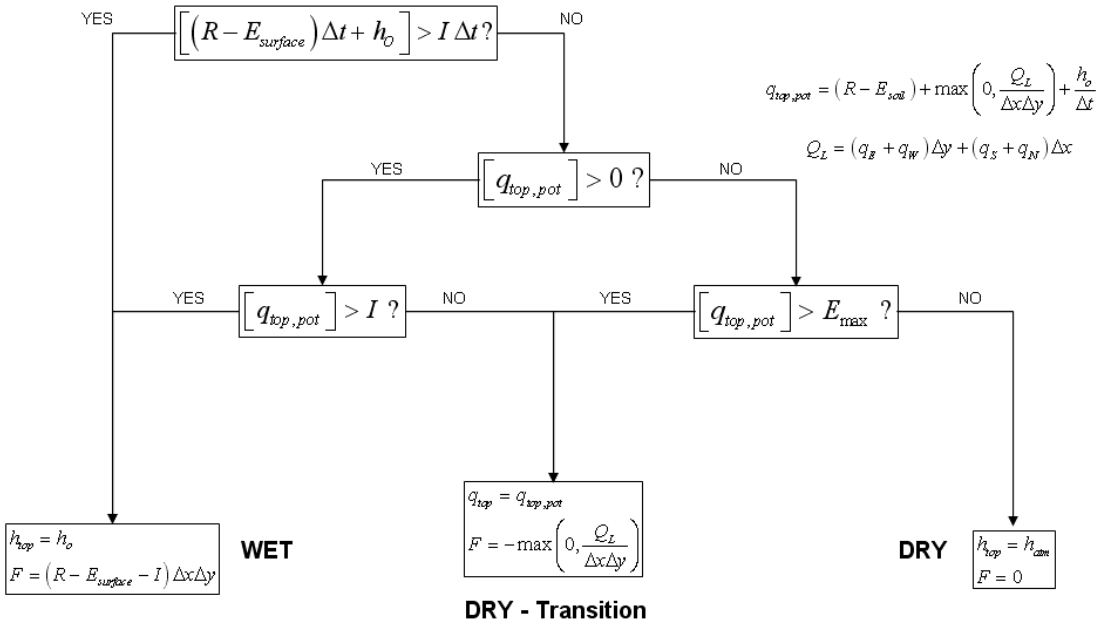

Figure 6.2: Overland / subsurface interaction algorithm implemented in the integrated water flow model.

The algorithm first checks the available water volume at the overland cell for the current time step and compares it with the potential infiltration volume. The available water volume is determined by taking into account the contributions of the rainfall or irrigation flows (R), the evaporation from the overland flow ($E_{surface}$), and the currently available ponded water (h_o). The potential infiltration rate (I) is calculated using the Darcy's law:

$$I = \left[-K_{1/2}\left(\frac{h_1 - h_o}{0.5\Delta z_1} - 1\right)\right] \tag{6.2}$$

where $K_{1/2}$ is the hydraulic conductivity [L T^{-1}] between the soil surface and the center of the top soil cell, h_1 is the soil-water pressure head value [L] at the top soil cell and Δz_1 is the thickness [L] of the top soil cell. If the available water volume is higher than the water volume that can potentially infiltrate, the overland cell is denoted as a wet cell and the top boundary condition for the soil column becomes the overland flow depth (h_{top} = h_o), and the vertical fluxes (F) for the overland cell becomes:

$$F = \left(R - E_{surface} - I\right)\Delta x \Delta y \tag{6.3}$$

where Δx and Δy are the lengths [L] of the overland cell sides in the x- and y-directions, respectively.

If the water volume balance analysis determines that the available water volume during the current time step is not enough to satisfy the infiltration demand, the potential flux at the ground surface ($q_{top,pot}$) is calculated by taking into account all the available water that can infiltrate into the soil cell:

$$q_{top,pot} = \left(R - E_{soil}\right) + \max\left(0, \frac{Q_L}{\Delta x \Delta y}\right) + \frac{h_o}{\Delta t} \tag{6.4}$$

where Q_L is the total lateral fluxes [L^3 T^{-1}] into the overland cell through overland flow during the current time step:

$$Q_L = (q_E + q_W)\Delta y + (q_S + q_N)\Delta x \tag{6.5}$$

where q_E, q_W, q_S, and q_N are the water flux per width [L^2 T^{-1}] from the east, west, south and north neighboring overland cells into the current cell. The incorporation of this second level of comparison and taking into account the lateral overland fluxes and the currently available ponded water in determining the potential ground surface flux, effectively avoid the convergence problems that may be encountered during the iterative numerical solution by making the boundary condition switching a relatively smooth process.

A positive $q_{top,pot}$ indicates infiltration conditions and in this case $q_{top,pot}$ is also compared with the potential infiltration rate, I. If $q_{top,pot}$ is larger than I, the cell is denoted as a wet cell. Otherwise, the cell is assumed to be in transition conditions with a specified flux boundary condition for the soil column being equal to $q_{top,pot}$ and the vertical flux for the overland flow cell being equal to the lateral fluxes that have infiltrated into the soil column.

A negative $q_{top,pot}$ indicates evaporation conditions and in this case $q_{top,pot}$ is compared with the maximum evaporation rate, E_{max}:

$$E_{\max} = -K_{1/2}\left(\frac{h_1 - h_{atm}}{0.5\Delta z_1} - 1\right) \tag{6.6}$$

where h_{atm} is the soil-water pressure head [L] in equilibrium with the prevailing relative humidity in the atmosphere. If $q_{top,pot}$ is larger than E_{max}, the overland cell is denoted as a transition cell with a specified flux boundary condition for the soil column. Otherwise the overland cell is dry with no overland flow and a specified head boundary condition is applied at the top of the soil column ($h_{top} = h_{atm}$).

The overland / subsurface interaction algorithm, by allowing smooth transitions between the wet and dry conditions at the ground surface interface, effectively minimizes the convergence problem that can be encountered in the numerical solution of the integrated flow model.

In case of extended overland flow development, the upper portions of the soil column start to saturate. This may also cause a convergence problem in the numerical solution of the Richards' equation for a fine-textured soil when the van Genuchten equations (1980) (vGM Model) are used to estimate the soil-water retention and hydraulic conductivity relationships (Vogel et al. 2001).

For fine-textured soils (n_v close to 1) , van Genuchten's $K(h)$ (Equation 4.4) exhibits an extremely non-linear behavior close to saturation (Vogel et al. 2001) (Figure 6.3). The accuracy of the vGM model in describing the soil hydraulic properties near saturation for fine-textured soils has been questioned (Vanderborght et al. 2006; Vogel et al. 2001). Modifications have been proposed to the vGM model in order to mitigate these problems (Vogel et al. 2001). The modification that has been analyzed in detail in Vogel et al.

(2001) successfully mitigates the numerical stability problem and also seems to increase the agreement between the predicted and measured conductivity values. However, it also results in a significantly different hydraulic conductivity curve. Consequently, the modeled infiltration rates are higher when the modified vGM model is used.

Although the modified vGM model is recommended to be used by Vogel et al. (2001), the conversion of the original vGM model parameters into the modified vGM model parameters is not straightforward, and also, the modified vGM model parameters have to be estimated from the observed water retention or hydraulic conductivity values. So, until there is a consensus on the required modification on the vGM model and the parameter values for the accepted new model are available, the linearization approach as applied in the SWAP model (Groenendijk et al. 2006) may be adopted. In the SWAP model, when the effective saturaton (*Se*) is larger than 0.99, the hydraulic conductivity value is calculated by a linear interpolation between the hydraulic conductivity value (*K*) corresponding to *Se* = 0.99 and K_s (*K* corresponding to *Se* = 1) (Figure 6.3).

The linearized *K* value corresponding to pressure head, *h* is calculated using the relationship:

$$\frac{h - h^{0.99}}{0 - h^{0.99}} = \frac{K(h)^{*} - K\left(h^{0.99}\right)}{K_s - K\left(h^{0.99}\right)} \tag{6.7}$$

where $h^{0.99}$ is the pressure head [L] corresponding to Se = 0.99, $K(h)^*$ is the linearized hydraulic conductivity value [L T^{-1}], $h^{0.99}$ is calculated using the inverse of the $Se(h)$ function (Equation 4.3):

$$h(Se) = -\frac{\sqrt[n_v]{Se^{-1/m_v} - 1}}{\alpha_v} \tag{6.8}$$

The linear interpolation approach described above is implemented in the model developed in this study as an option to be used when working with fine-textured soils.

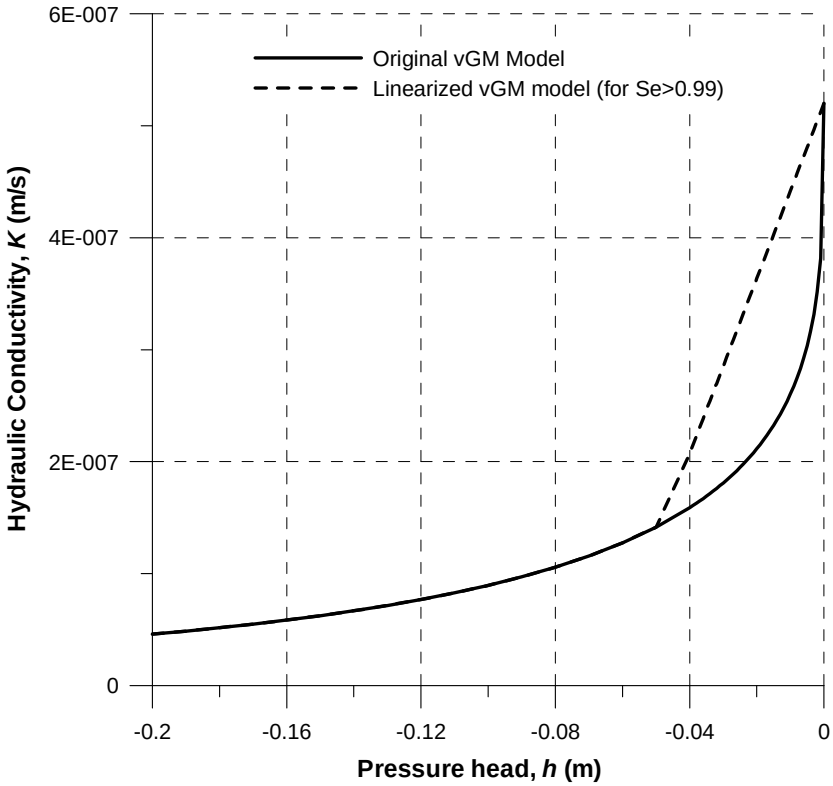

Figure 6.3: The comparison of the linearized vGM model and the original vGM model for a fine-textured soil. Soil hydraulic parameters are θ_s = 0.41, θ_r = 0.05, n_v = 1.31, α_v = 1.9, $K_s = 5.2 \times 10^{-7}$ m/s.

6.2.2 Incorporating the Subsurface Lateral Fluxes

The subsurface lateral fluxes between the corresponding cells in adjacent soil columns are calculated using the Darcy's law (Figure 6.4). The lateral flux into cell *j* from the east interface q_j^E is determined as:

$$q_j^E = K_j^E \frac{h_j^E - h_j}{\Delta x_{j,E}} \tag{6.9}$$

where K_j^E is the interblock hydraulic conductivity [L T^{-1}] at the east interface of cell *j*, h_j is the pressure head value [L] at cell *j*, h_j^E is the pressure head value [L] at the east neighbor of cell *j*, and $\Delta x_{j,E}$ is the distance [L] between the centers of cell *j* and its east neighbor.

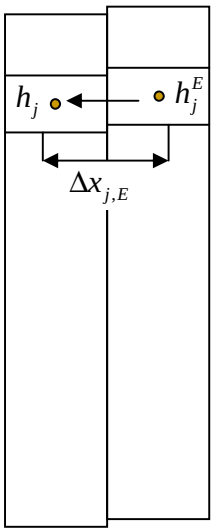

Figure 6.4: The subsurface lateral water flux calculation between two adjacent soil cells.

The calculated lateral fluxes are subsequently incorporated into the spatially discretized soil-water equation (Equation 4.6) as source / sink terms:

$$M_j \left(\frac{dh}{dt} \right)_j + S_j^1 h_{j-1} + S_j^2 h_j + S_j^3 h_{j+1} = F_j + q_j^E + q_j^W + q_j^N + q_j^S \qquad (6.10)$$

6.2.3 Effect of Plants on Overland Flow

The effect of plants on the soil-water flow is modeled through the coupled models of unsaturated zone soil-water flow and plant life-cycle as described in Chapter 5. The effect of plants on the overland flow process is addressed in this section by taking into consideration the dependency of the surface roughness on the characteristics and growth stage of the plants. In this study, Manning's roughness coefficient is used to characterize the surface roughness when modeling the overland flow processes. The Manning's

roughness coefficient variation due to plant growth is determined using Equation 6.11 which is adopted from Mailhol and Merot (2008):

$$n = \left(n_{\max} - n_{\min}\right)\left[1 - \exp\left(-LAI\right)\right] + n_{\min} \tag{6.11}$$

where n is the Manning's roughness coefficient [T $L^{-1/3}$], $n_{\max}$ is the maximum value of n [T $L^{-1/3}$] when the plants are mature (when $LAI = LAI_{max}$), $n_{\min}$ is the minimum value of n [T $L^{-1/3}$] when there are no plants (when $LAI = 0$). When determined using Equation 6.11, the change in the value of the Manning's roughness coefficient with respect to increasing *LAI* values will be as shown in Figure 6.5.

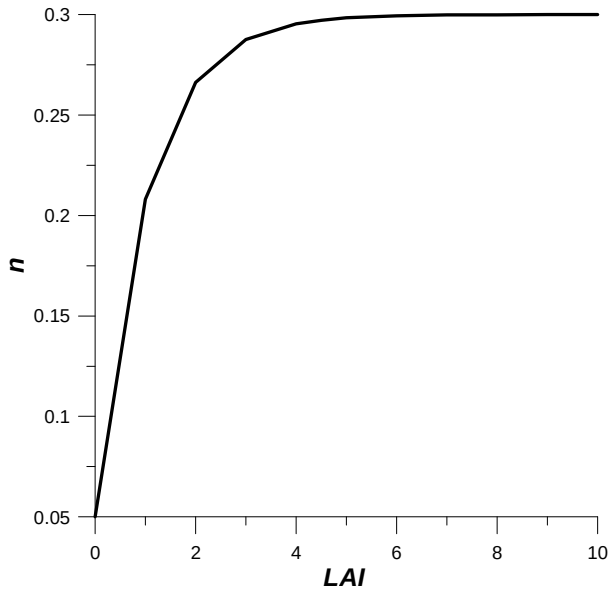

Figure 6.5: Variation in Manning's roughness coefficient values with respect to the variation in *LAI* values as determined by Equation (6.11). (n_{max} = 0.3, n_{min} = 0.05).

Implementation of the relationship given in Equation 6.11 requires the plant specific parameter of n_{max} and a roughness coefficient value for bare soil as n_{min}. In the literature, there is conflicting information regarding the appropriate range of Manning's roughness coefficient values to be used in flow modeling over vegetated soil surfaces. Chow (1959) recommends a range of 0.02-0.05 for cultivated areas in floodplains. Gillies and Smith (2005) have calibrated an irrigation flow model (SIRMOD) for Manning's roughness coefficient and found values that change between 0.016 and 0.05 similar to the tabulated values given in Chow (1959). Clemmens et al. (2001) and Clemmens (2009) discuss Manning's roughness coefficient variation due to vegetation, flow depth and the flow time. In one of their examples they model a hypothetical irrigation field with a Manning's *n* value of 0.08 later decreased to 0.03 due to surface smoothing by flowing water.

On the other hand, there are a significant number of studies that use much higher Manning's *n* values in modeling irrigation flow. Mailhol and Merot (2008) use *n* values that change between 0.15 and 0.3 for border-irrigated grassland fields. Robertson et al. (2004) also report high *n* values (0.2-0.36) and give a discussion of their finding in relation to other literature on this. Maheshwari and McMahon (1993a; 1993b) report high *n* values (0.2-0.5) as well. Liong et al. (1989) also report high Manning's *n* values for overland flow (modeled by the kinematic wave approach) on pervious sub-catchments.

There are criticisms to using Manning's *n* in modeling overland flow on irrigated soils (especially for agricultural fields) based on it's being highly variable in space and time (Esfandiari and Maheshwari 1998; Strelkoff et al. 2009; Turner and Chanmeesri 1984).

Strelkoff et al. (2009) suggest calculating two individual components for the resistance to flow: (i) soil surface resistance; and, (ii) vegetative drag. They suggest adding these two as a first approximation to come up with a measure of the resistance to flow in surface irrigation systems. They present a formulation for boundary drag to represent soil surface resistance to flow by the use of an absolute roughness coefficient rather than the Manning's *n*. And, for the vegetative drag calculations they present a formulation that uses a drag coefficient and vegetation density as parameters. However, they conclude that there is not enough experience to assign appropriate values for the absolute roughness coefficient and vegetation density and also not enough knowledge to assess the accuracy obtained by employing this approach. They state that Manning's *n* remains the most common measure of resistance to flow. They refer to the National Resources Conservation Service's (NRCS) design manuals for suggested values of *n*.

NRCS (2008) suggests the following values for *n* for border irrigation, based on field experience until more information is available through more studies:

- 0.04 for smooth, bare soil surfaces, for row crops irrigated by the level border method,
- 0.10 for drilled small grain crops if the drill rows run lengthwise of the border strip,
- 0.15 for alfalfa, mint, broadcast small grain, and similar crops,
- 0.25 for dense sod crops and small grain crops that are drilled across the border strip.

6.3 Model Application

In this section, several applications are presented to demonstrate the integrated modeling methodology developed in Section 6.2. These examples are structured around analyzing the effects of plant life-cycle modeling and the spatial heterogeneity regarding the vegetation characteristics on the water distribution within the modeling domain. The response of the soil-plant system to different water input regimes is also demonstrated. Simple weather data and simple irrigation schedule are used to facilitate the interpretation of the results. The crop data is obtained from the literature.

6.3.1 Modeling Domain and the Model Parameters

In all applications, an overland flow domain of 400 m width by 400 m length is used. A mild slope (0.0005) is assumed in the x-direction whereas no slope was assumed in the y-direction. The domain is spatially discretized by creating overland cells with $\Delta x = \Delta y =$ 100 m. The overland domain parameters are given in Table 6.1 and a schematic representation of the spatial discretization is given in Figure 6.6.

Table 6.1: Overland domain model parameters.

Slope in *x*-direction	0.0005
Slope in *y*-direction	0.0
Length in *x*-direction	400 m
Length in *y*-direction	400 m
Boundary condition	Zero-depth gradient outlet at x = 400 m Other sides are no-flow boundaries
Initial condition	Dry
Spatial discretization, Δy	100 m (K = 4)
Spatial discretization, Δx	100 m (L = 4)

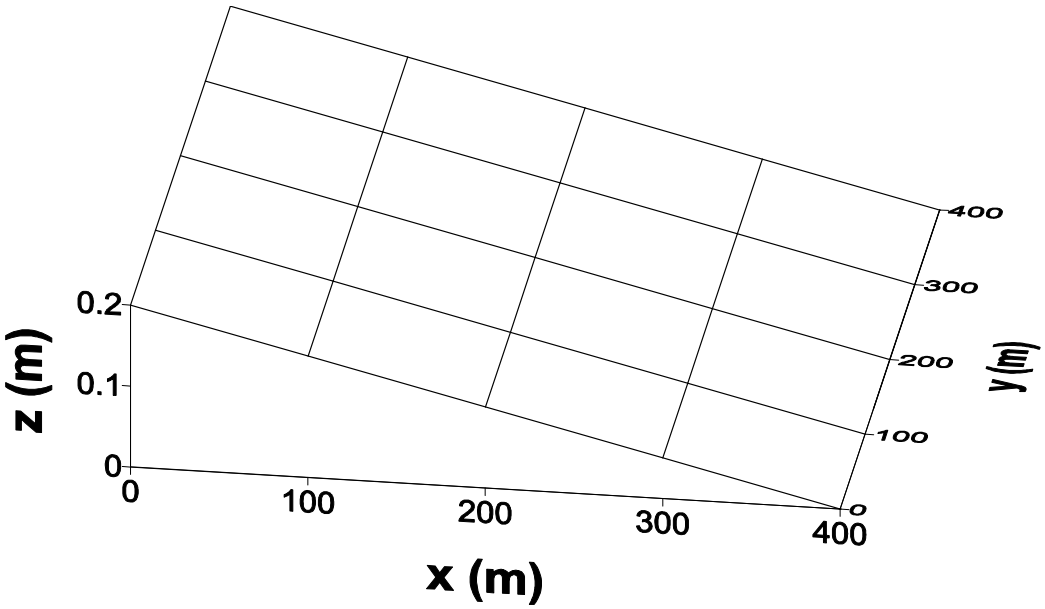

Figure 6.6: The spatial discretization of the overland flow domain.

Each overland cell corresponds to a soil column having a depth of 2 m. The soil cells at the top 20 cm of the column are assigned a thickness of 1 cm. Below 20 cm depth, the cell thicknesses gradually increase, the maximum thickness being 16.51 cm for the bottom 50^{th} cell (Figure 6.7).

Homogeneous soil characteristics are applied throughout the soil columns. The hydraulic parameters of the soil are assigned the average values for a silt loam type soil as reported from Carsel and Parrish (1988) in Vogel et al. (2001) (Table 6.2).

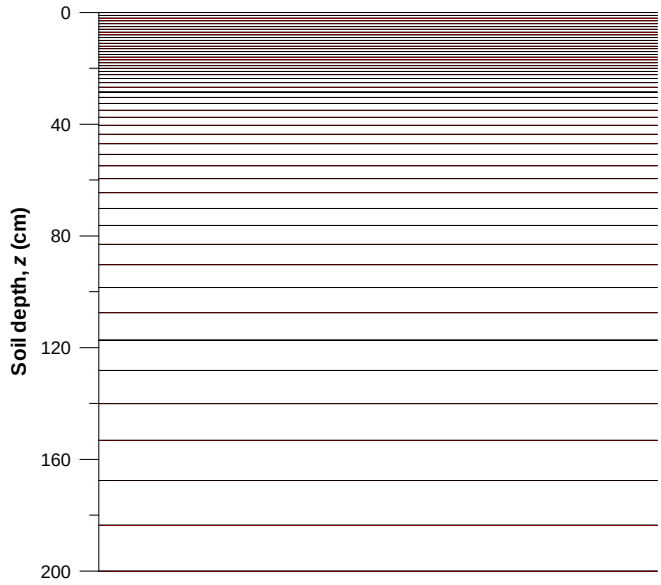

Figure 6.7: The spatial discretization of the soil columns.

Table 6.2: The soil hydraulic parameters for a silt loam type soil (Vogel et al. 2001).

Saturated hydraulic conductivity, K_{sat}	1.25×10^{-6} m/s
van Genuchten parameters	n = 1.41 α = 2.0 m^{-1} θ_{res} = 0.067 θ_{sat} = 0.45

The initial conditions were set assuming a linear variation of the water content throughout the soil column, from 0.5 at the top to 0.8 at the bottom (Figure 6.8). For a silt loam type soil, the pressure head profile corresponding to the water content profile in Figure 6.8 is given in Figure 6.9.

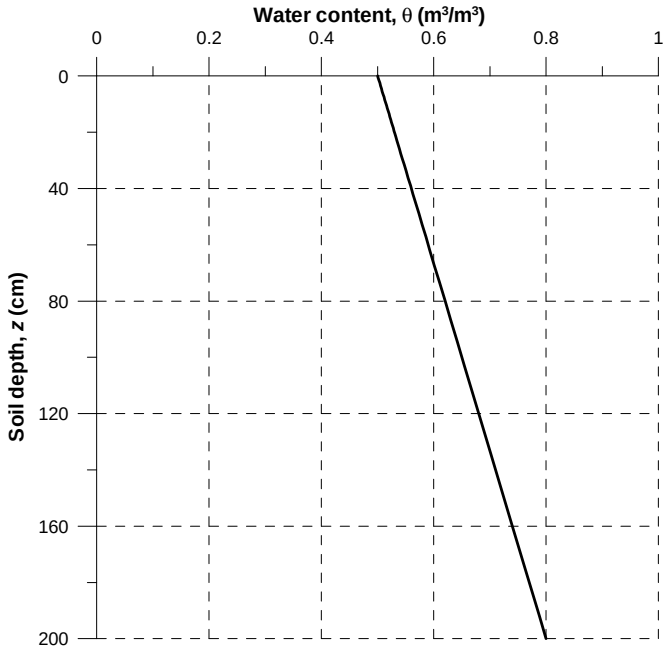

Figure 6.8: The initial distribution of water content used in the simulations.

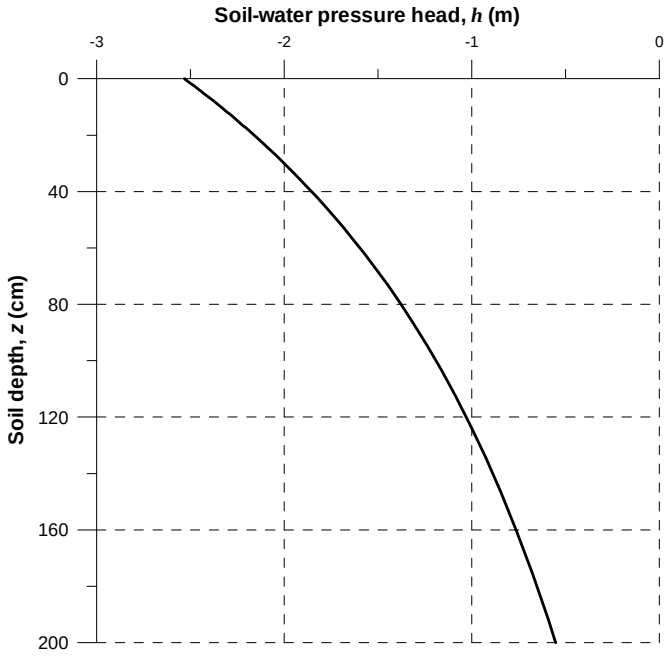

Figure 6.9: The soil-water pressure head profile used as the initial condition in the simulations.

Heterogeneity in the plant presence is established by dividing the modeling domain into two sections and assigning different types of crop to each section. The upstream half of the modeling domain is planted with corn and the downstream half is planted with hay. The crop parameters used in the simulations are given in Table 6.3.

Table 6.3: Crop parameters used in the simulations.

	Parameter	**Corn**	**Hay**
		(Mailhol, Olufayo et al., 1997; Wohling and Mailhol, 2007)	**(Mailhol & Merot, 2008)**
LAI related	LAI_{max} (m^2m^{-2})	4.5	8
	T_b(°C)	6	0
	T_s(°C)	100	0
	T_f(°C)	1005	900
	λ	1.25	10
	β	2.4	3
	δ_1	14	3.7
	δ_2	0.2	4.4
Biomass related	T_{mat}(°C)	1925	1020
	RUE(gMJ^{-1})	1.32	0.37
Root related	L_R (0)	0.1	0.1 (assumed)
	$L_{R,.max}$ (m)	1.2	0.5 (assumed)
	t_R (days)	72	50
Evapotranspiration related	$K_{c,max}$	1.2	1
	x_k	1	1
	k	0.7	0.65
Overland flow related	n_{max}	0.15 (Assumed)	0.3

In order to facilitate the interpretation of the results, a simplified weather data set is used. Air temperature, reference evapotranspiration (ET_0), h_{atm} (soil surface pressure head in equilibrium with atmospheric water vapor) and daily solar radiation (SR) values are assigned constant values throughout the simulation (Table 6.4).

Table 6.4: Weather data used in the simulations.

Air temperature (T)	20°C
Reference evapotranspiration (ET_0)	2.5 mm/day
Reference evaporation rate from bare soil, ($E_{p,0}$)	2.0 mm/day
Evaporation rate from free water surfaces ($E_{w,0}$)	3.0 mm/day
h_{atm}	-160 m

The irrigation schedule is comprised of 6-hour irrigation periods every 10 days starting with day 1. Two types of irrigation methods that are equivalent in terms of the applied water volume are applied (Table 6.5). In the border irrigation, the water is input to the upper cells that are bordering the x = 0 m boundary (with a discharge rate of 0.30 m^3 / s). In the sprinkler irrigation, the water is distributed uniformly to the whole overland domain with a rate of 6.75 mm/hour.

Table 6.5: The comparison of the two types of irrigation methods applied.

Border Irrigation		**Sprinkler Irrigation**	
Discharge rate (m^3/s)	**0.3**	**Discharge rate (mm/hour)**	**6.75**
Discharge time (hours)	6	Discharge time (hours)	6
Border cells area (m^2)	40000	Area (m^2)	160000
Discharge Volume (m^3)	6480	Discharge volume (m^3)	6480

6.3.2 Description of the Simulations

The set of simulations can be classified in three different ways based on different simulation characteristics. Based on the length of the simulation period, two different types of simulations are defined: (i) Daily simulations (simulation length is 1 day); and, (ii) Seasonal simulations (simulation length is 120 days). According to the irrigation method applied, there are again two different types of simulations: (i) Border irrigation; and, (ii) Sprinkler irrigation. And, finally, based on the plant life-cycle model characteristics, the simulations can be classified as belonging to either of these three categories: (i) No Plant (bare soil with no plants); (ii) Const. Plant (constant *LAI* assumed throughout the simulations); and, (iii) Plant (plant life-cycle simulated). In the Const. Plant simulations, the *LAI* of corn is assumed to be 3.0 and the *LAI* of hay is assumed to be 5.0.

6.3.3 Results and Discussion

In this section, the results obtained from the model simulations are presented. The results of the daily simulations are given first, followed by the results of seasonal simulations. The effect of different irrigation methods and the effect of plants on the water flow dynamics within the soil-plant system are discussed. The simulation results are plotted for the strip of overland flow cells and the corresponding soil columns neighboring the $y = 0$ boundary of the model domain. In Figure 6.10, the overland cell and soil column numbers that are used in reporting and discussing the results are shown.

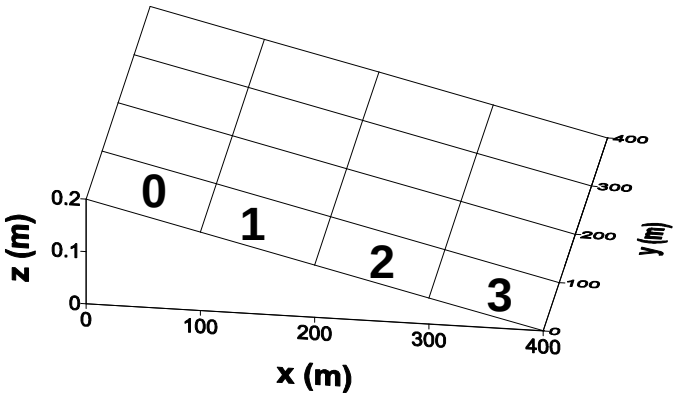

Figure 6.10: The numbering system used for the overland cells and the corresponding soil columns when reporting the simulation results.

6.3.3.1 Daily Simulations

The daily simulation results for border irrigation are given in Figures 6.11-6.16. The overland flow depth variation with time for the No Plant simulation is shown Figure 6.11. It is seen that overland flow development is observed in all the overland cells except the most downstream cell (cell 3). In Figure 6.12, the pressure head variation with time at the top soil cell (soil cell 1) of different soil columns is given for the No Plant simulation. Soil cell 1 of each column is in interaction with the corresponding soil cell and the pressure head variation at this cell gives information about this interaction process. In Figure 6.12, it is observed that, although overland cell 3 doesn't turn into a wet cell, infiltration is occurring from this cell into column 3 starting at about hour 4.

The Const. Plant simulation results are shown in Figures 6.13-6.14. When compared with the No Plant simulation, it is observed that the overland flow depths reach higher levels in the Const. Plant simulation. This is due to the increased surface roughness in the presence of a plant cover that impedes the water flow over the land surface. In Figure 6.14, it is seen that less infiltration occurs at column 3 compared to the No Plant simulation due to less water being able to travel to this downstream column.

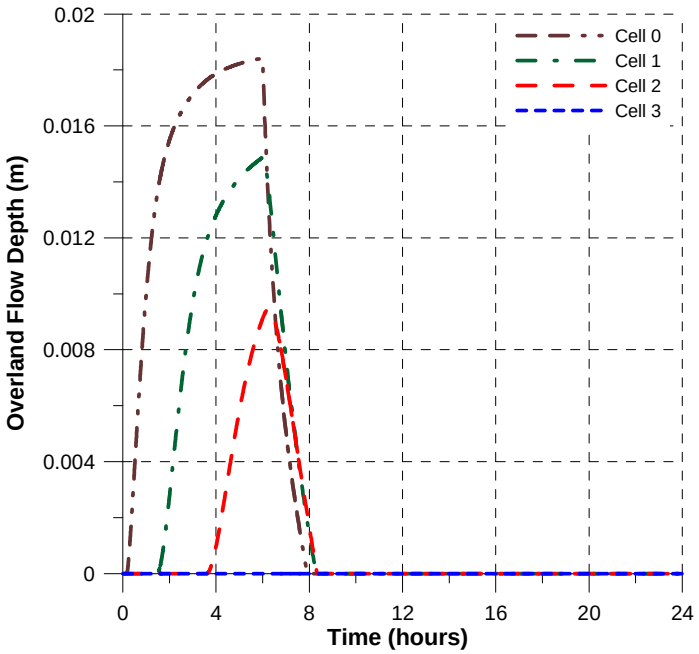

Figure 6.11: Overland flow depth variation with time for the daily simulation of border irrigation (No Plant).

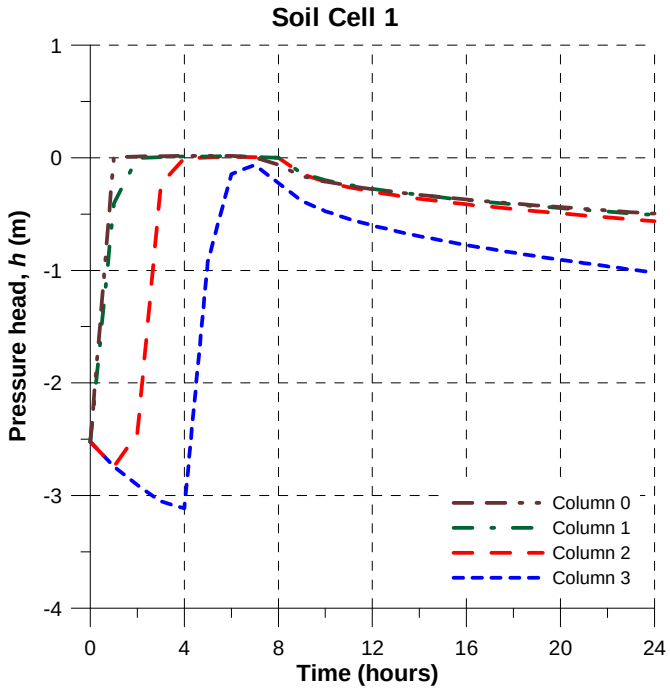

Figure 6. 12: Pressure head variation with time within the top soil cell for daily border irrigation simulation. (No Plant)

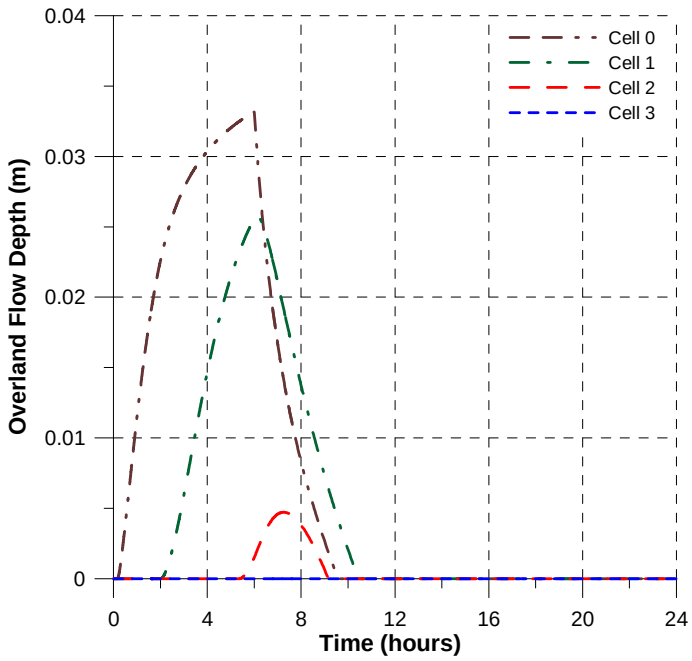

Figure 6. 13: Overland flow depth variation with time for daily border irrigation simulations. (Const. Plant)

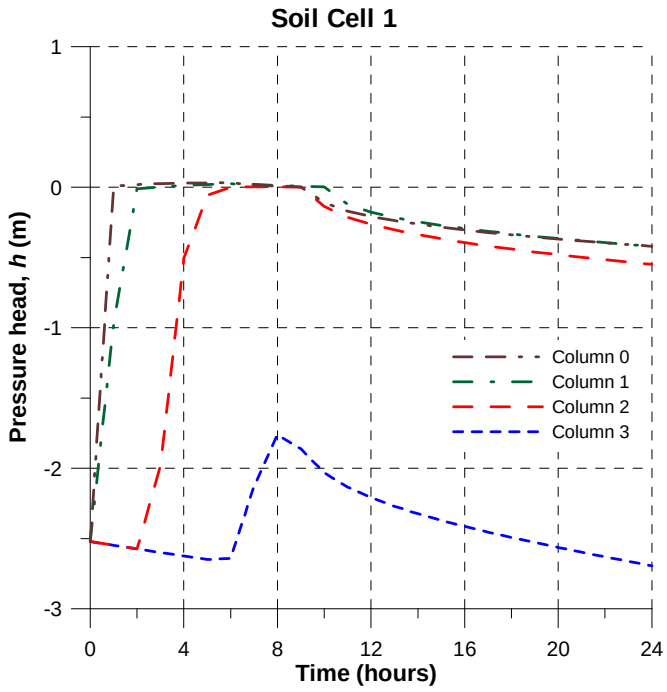

Figure 6.14: Pressure head variation with time at the top soil cell for daily border irrigation simulation. (Const. Plant)

In Figures 6.15 and 6.16, the soil pressure head profiles in the soil columns are given for the No Plant and Const. Plant simulations, respectively. In Figure 6.15, it is seen that the infiltration front reaches the highest depth in column 0. As the columns get further away from the water input, the infiltration front appears gradually at shallower depths. The effect of evaporation is also observed as pressure heads start to decrease at the upper soil sections after the end of the irrigation period (after the 6^{th} hour). In Figure 6.16, the lack of infiltration into column 3 is visible while the infiltration fronts for the other columns reach higher depths compared to the No Plant simulation results (Figure 6.15).

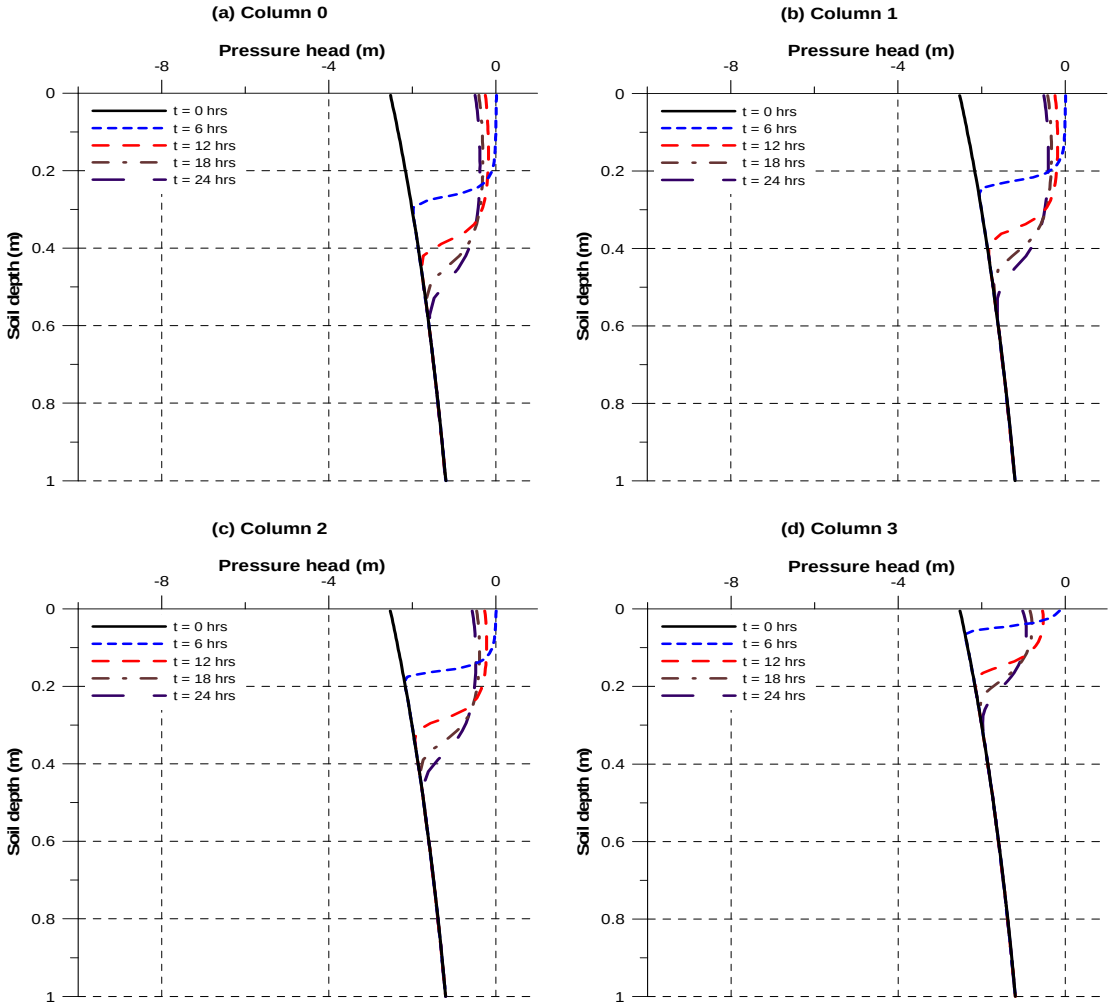

Figure 6.15: Pressure head profiles within different soil columns for daily simulations of border irrigation. (No Plant)

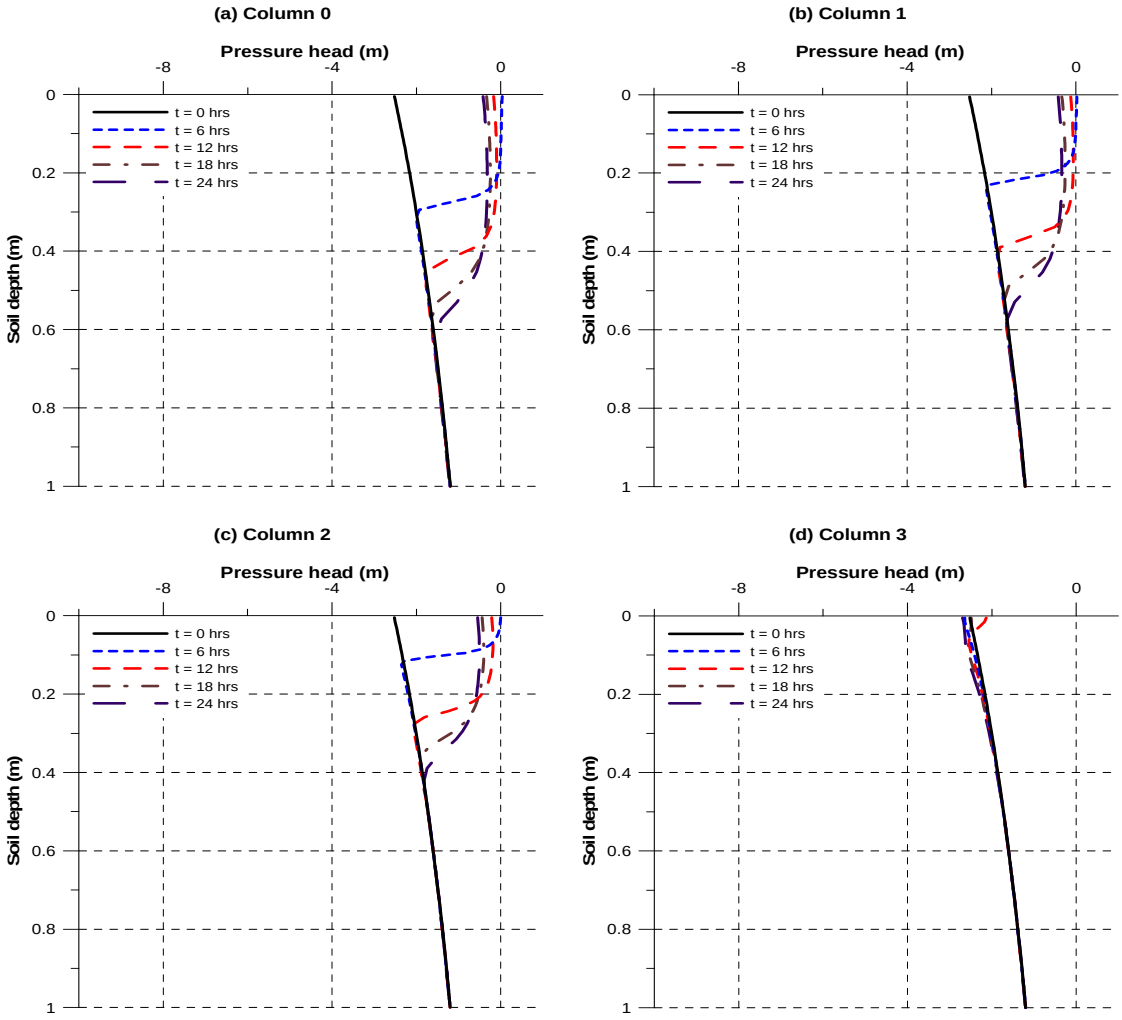

Figure 6.16: Pressure head profiles within different soil columns for daily simulations of border irrigation. (Const. Plant)

The daily simulation results for sprinkler irrigation are given in Figures 6.17-6.21. In Figure 6.17, it is seen that a shallow overland flow develops on all the overland cells during the later parts of the irrigation period in the No Plant simulation. The pressure head variation at soil cell 1 in every column is identical for the No Plant simulation since the irrigation is distributed uniformly over the whole modeling domain (Figure 6.18). In the Const. Plant simulations, on the other hand, no overland flow is observed since the irrigation water is intercepted by the plants, thus decreasing the amount of water that reaches the ground surface (Figure 6.19). The pressure head variation at soil cell 1 is identical for the columns that contain the same type of plant. The pressure head at soil cell 1 of columns 0 and 1 reaches higher values compared to that of columns 2 and 3 (Figure 6.19). This is expected since columns 2 and 3 contain hay with a higher *LAI* value (*LAI* = 5.0 for hay versus *LAI* = 3.0 for corn) resulting in higher interception storage.

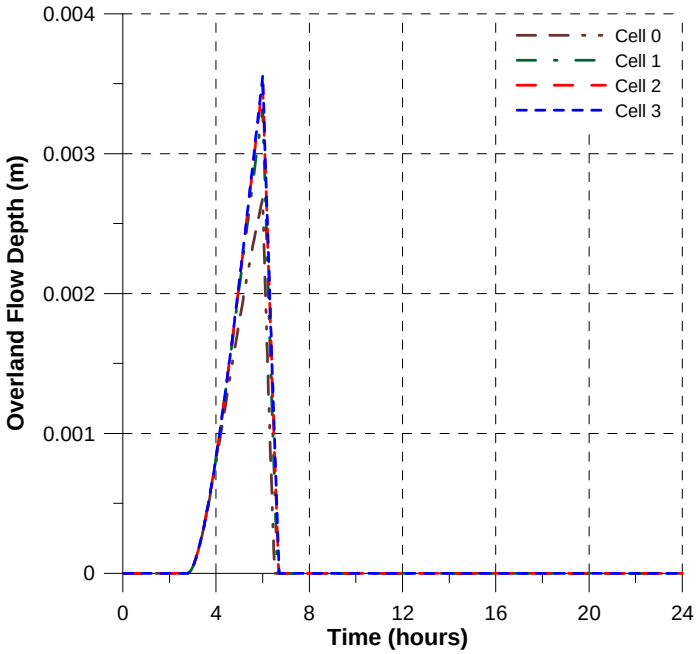

Figure 6.17: Overland flow depth variation with time for daily simulation of sprinkler irrigation. (No Plant)

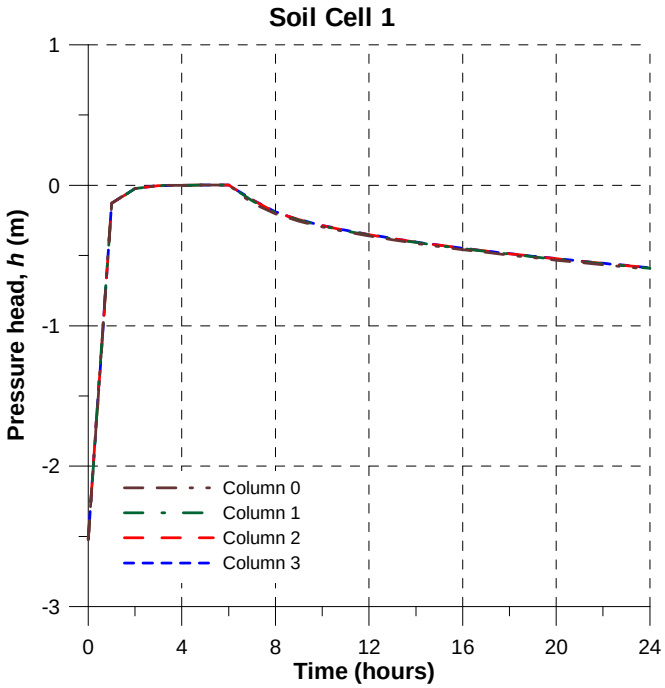

Figure 6. 18: Pressure head variation with time at the top soil cell for daily simulation of sprinkler irrigation. (No Plant)

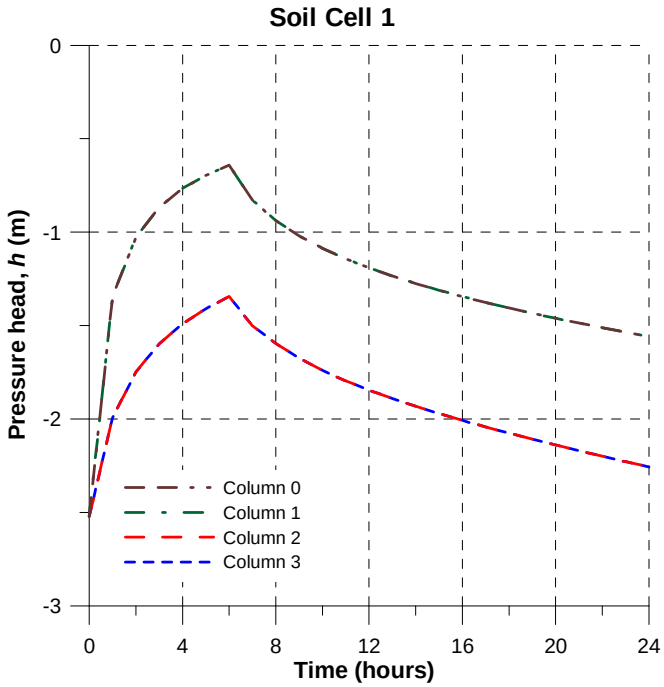

Figure 6.19: Pressure head variation with time at the top soil cell for daily simulation of sprinkler irrigation. (Const. Plant)

In Figures 6.20 and 6.21, the soil pressure head profiles in the soil columns are given for the No Plant and Const. Plant simulations, respectively. The pressure head profiles are identical in No Plant simulations for all the soil columns (Figure 6.20). The pressure head profiles in the Const. Plant simulations show the decreased infiltration in the presence of plants when compared to the No Plant simulations (Figure 6.21). Again, the infiltration is even less in columns 2 and 3 due to higher interception.

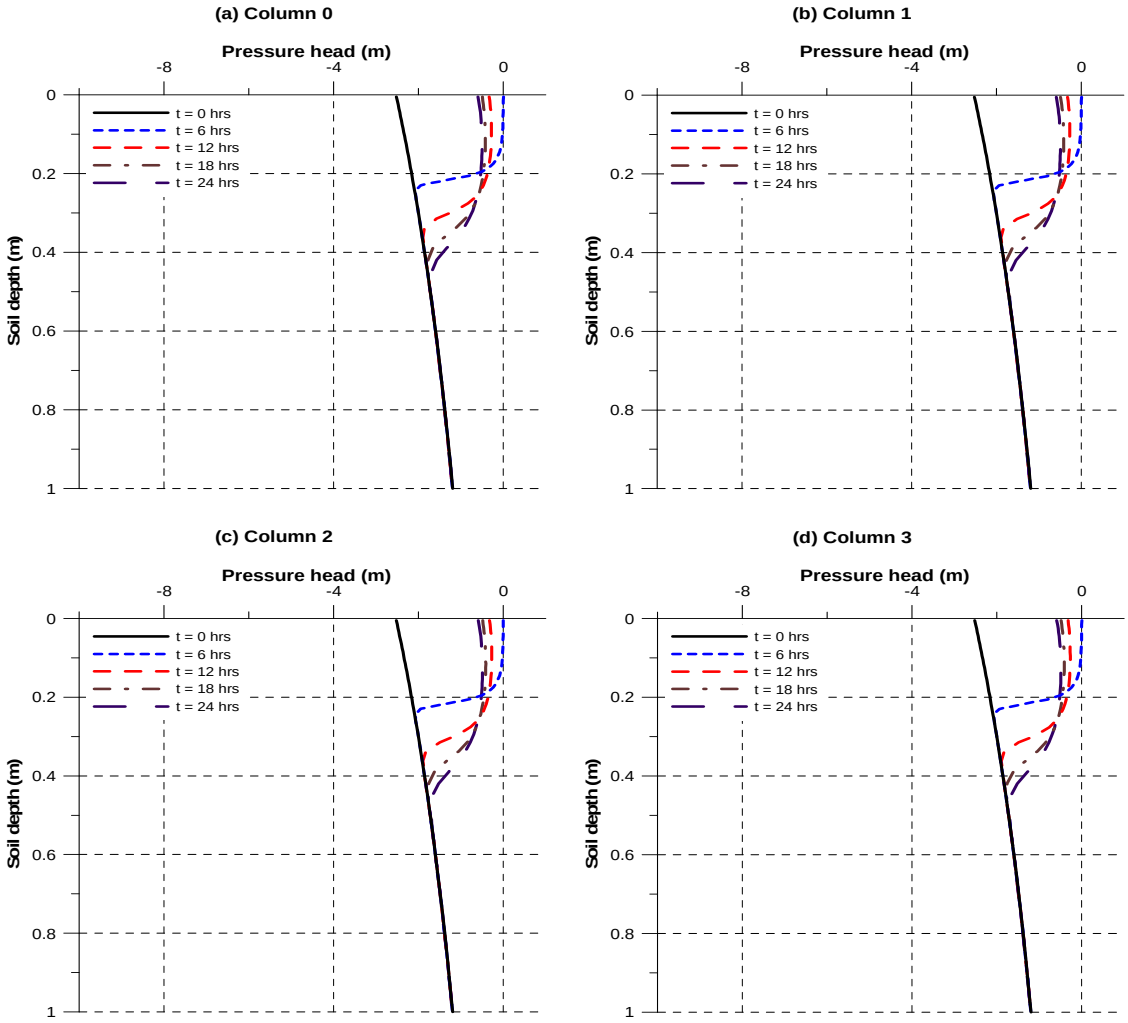

Figure 6.20: Pressure head profiles within different soil columns for daily simulations of sprinkler irrigation. (No Plant)

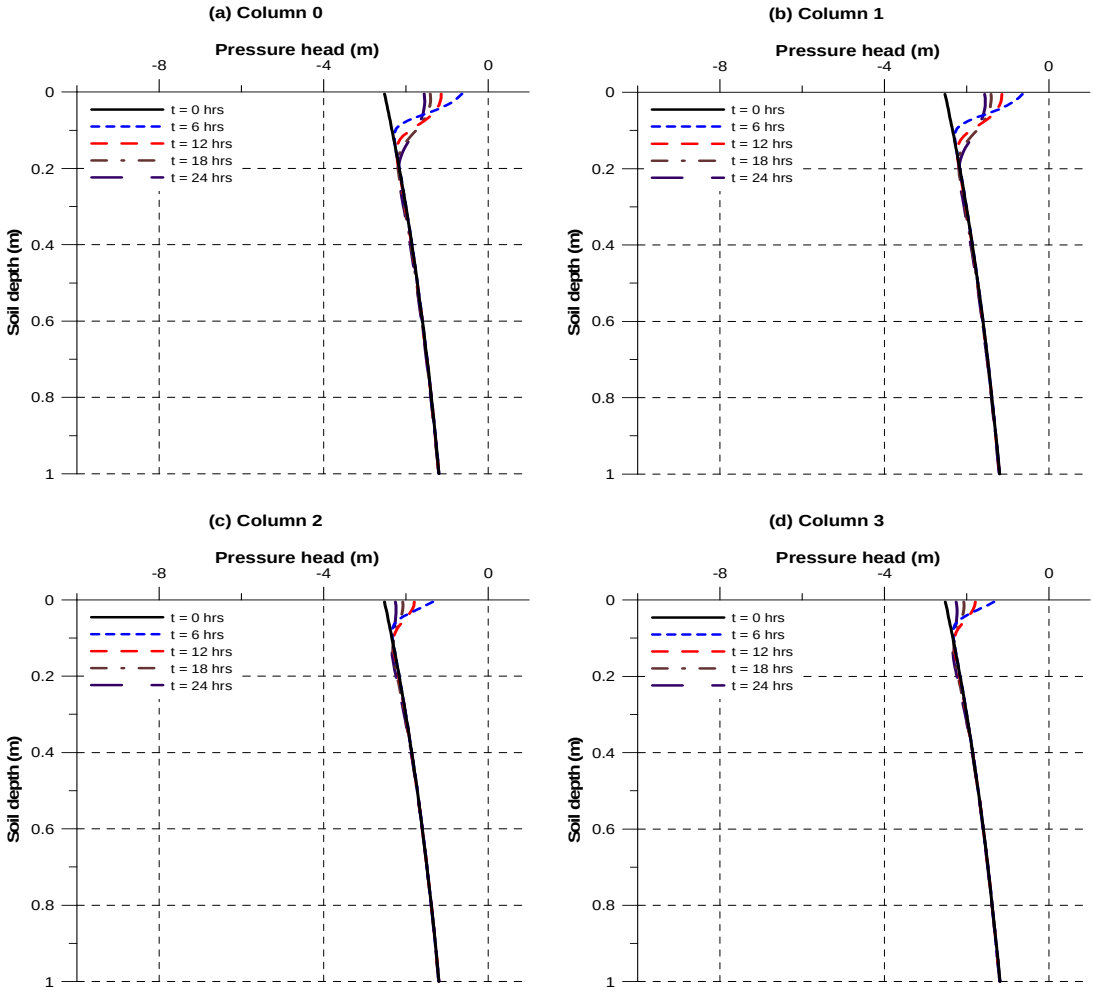

Figure 6.21: Pressure head profiles within different soil columns for daily simulations of sprinkler irrigation. (Const. Plant)

6.3.3.2 *Seasonal Simulations*

The seasonal simulation results for border irrigation are given in Figures 6.22-6.28. The change of overland flow depths with time for the No Plant, Const. Plant, and Plant simulations are shown in Figures 6.22, 6.24, and 6.26, respectively. The overland flow formations are seen as spikes that correspond to the irrigation periods occurring every 10 days. It can be seen that the overland flow depths reach higher values in the Const. Plant simulation compared to the No Plant simulation due to the increased surface roughness. And, the variable surface roughness due to plant growth is manifested in Figure 6.26 as the overland flow depths follow an increasing trend at cells 0 and 1.

The pressure head variation with time at soil cell 1 is plotted for the No Plant, Const. Plant, and Plant simulations in Figures 6.23, 6.25, and 6.27, respectively. It can be seen that no infiltration occurs in column 3 during the Const. Plant simulation (Figure 6.25). The irrigation water is impeded by the presence of plants on the surface of other columns and cannot reach to column 3.

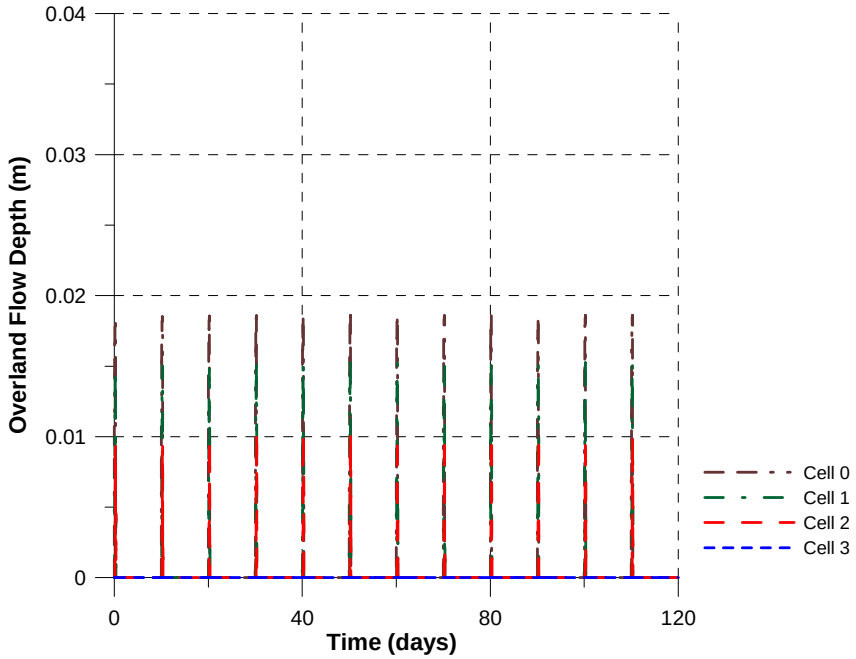

Figure 6.22: Overland flow depth variation with time for seasonal simulation of border irrigation. (No Plant)

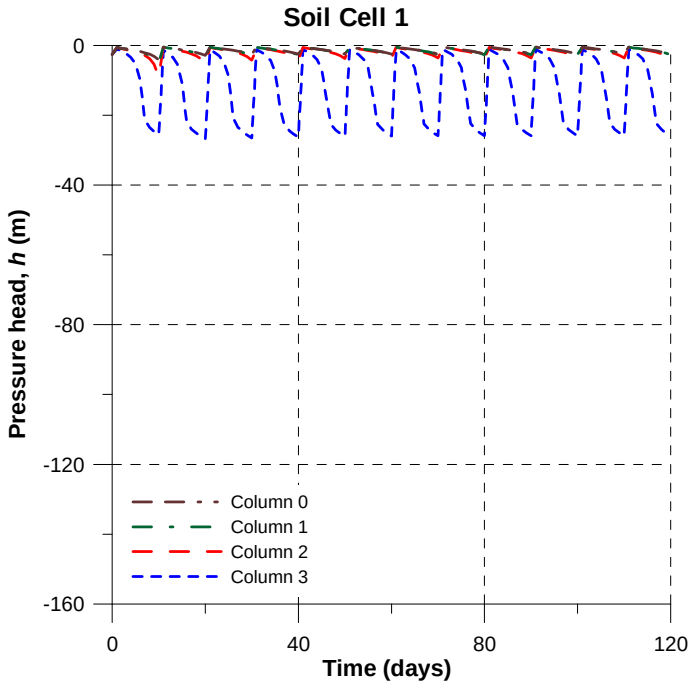

Figure 6.23: Pressure head variation with time at the top soil cell for seasonal simulation of border irrigation. (No Plant)

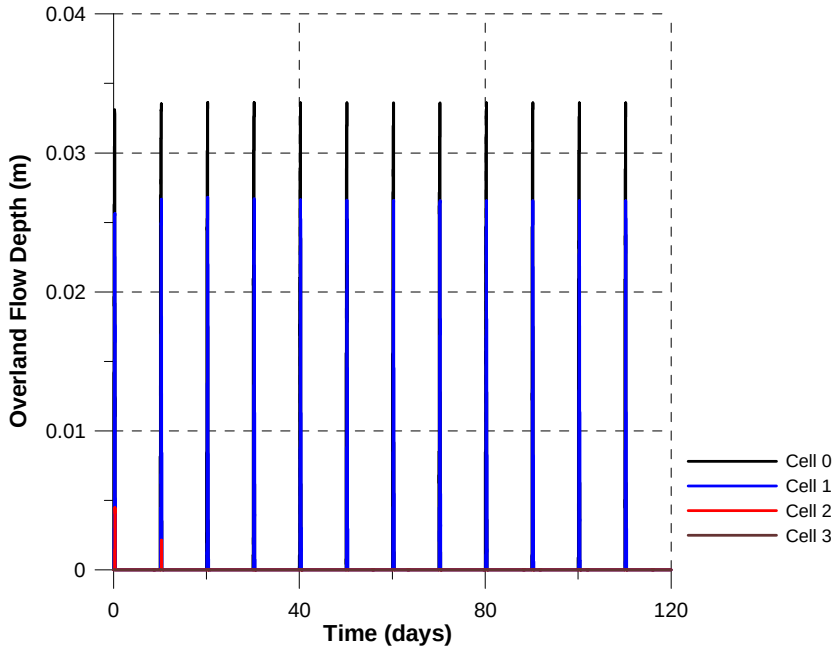

Figure 6.24: Overland flow depth variation with time for seasonal simulation of border irrigation. (Const. Plant)

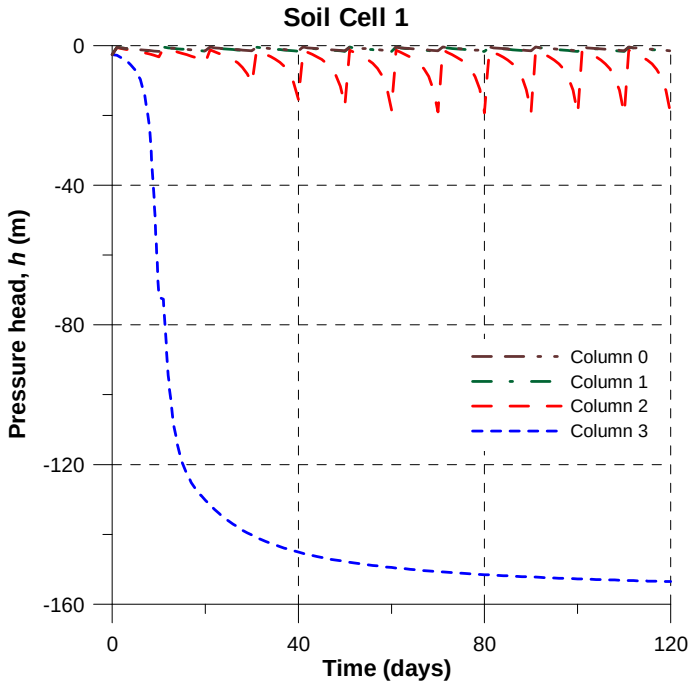

Figure 6.25: Pressure head variation with time at the top soil cell for seasonal simulation of border irrigation. (Const. Plant)

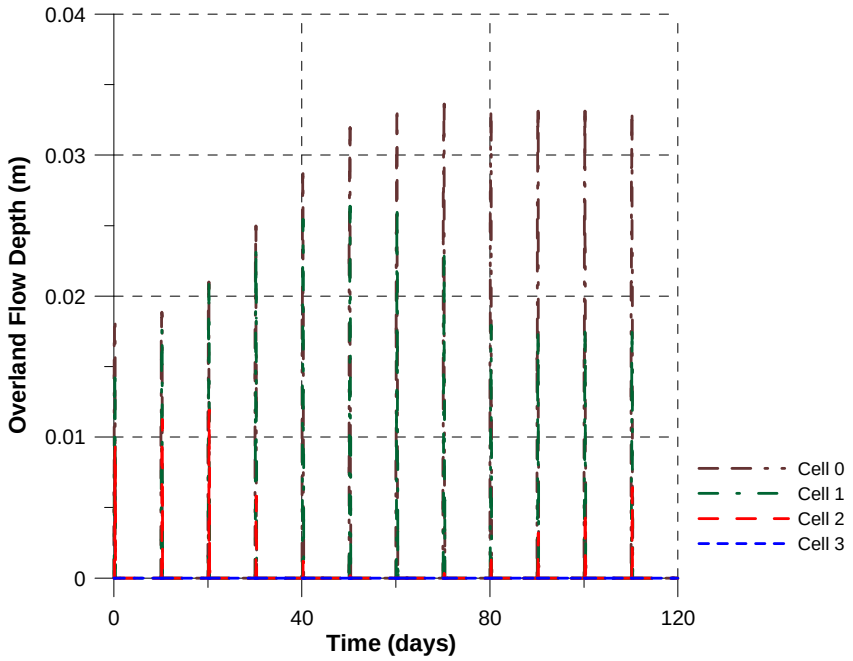

Figure 6.26: Overland flow depth variation with time for seasonal simulation of border irrigation. (Plant)

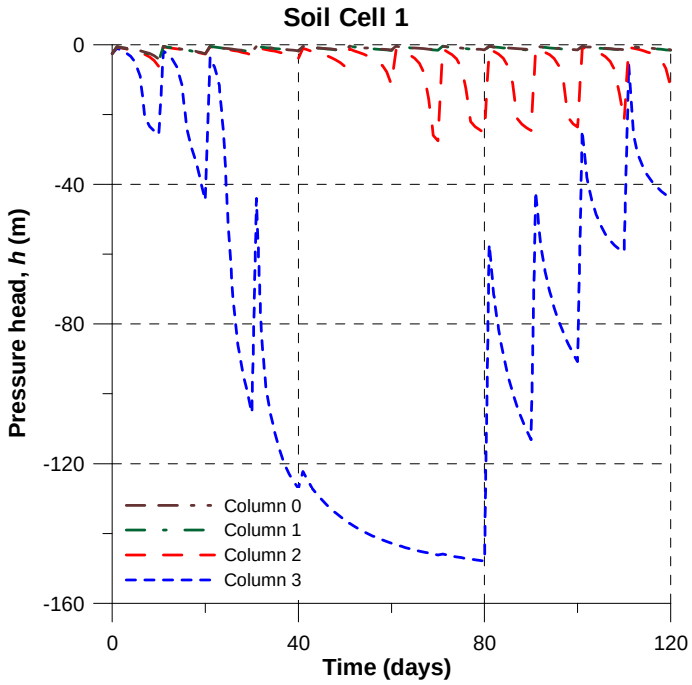

Figure 6.27: Pressure head variation with time at the top soil cell for seasonal simulation of border irrigation. (Plant)

Variable infiltration into column 3 is observed during the Plant simulation (Figure 6.27). During the early and later stages of the simulation, irrigation water can reach down to column 3. However, as the plants in the upstream columns mature, less water is available for column 3. So, Figure 6.27 should be analyzed together with Figure 6.28 where the *LAI* variation with time is plotted for all the columns. It is observed that corn in columns 0 and 1 reach its maturation later than the hay in column 2 and 3. Plants in columns 0, 1 and 2 do not experience water stress and mostly follow their potential *LAI* curve. There are only short water stress periods corresponding to the irrigation days which are caused by water logging. It is seen that plants in column 3 experience extensive water stress. The *LAI* plots also suggest that the increased infiltration into column 3 towards the end of the simulation is a result of the disappearance of hay in column 2 due to senescence and thus making it easier for the irrigation flow to reach down to column 3.

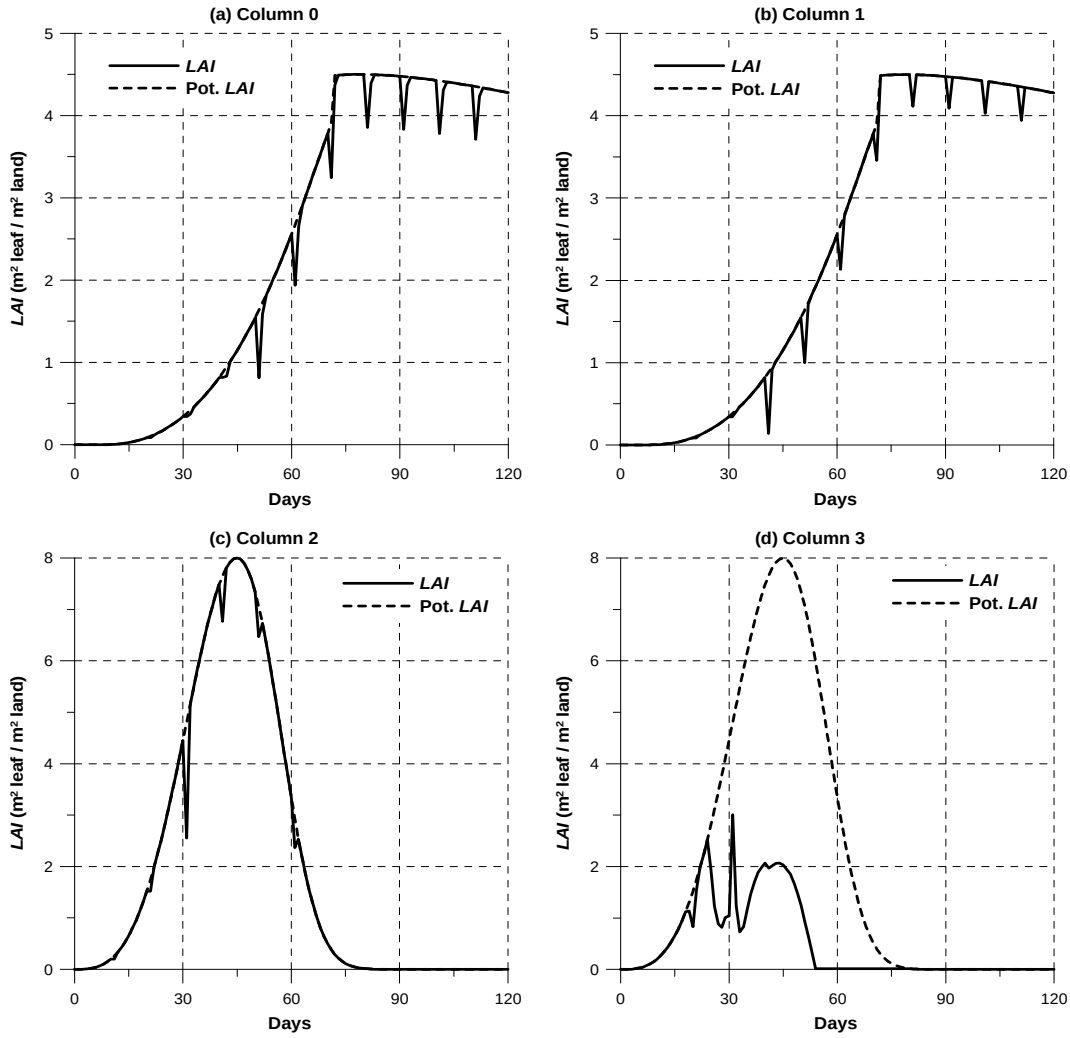

Figure 6.28: *LAI* simulation results for seasonal simulation of border irrigation. (Columns 0 and 1: corn, Columns 2 and 3: hay)

The seasonal simulation results for sprinkler irrigation are given in Figures 6.29-6.34. Shallow overland flows develop during the No Plant (Figure 6.29) and Plant (Figure 6.32) simulations. However, practically no overland flow is observed during the Const. Plant simulation. The absence of overland flow during the whole period of the Const. Plant simulation and also during the period that spans day 30 to day 60 in the Plant simulation can be explained by decreased water availability due to interception losses. When Figure 6.32 is analyzed together with the *LAI* curves (Figure 6.34), the occurrence of overland flow on individual overland cells can be correlated with the low *LAI* values on the corresponding columns.

The pressure head variation at soil cell 1 with time is given in Figures 6.30, 6.31, and 6.33 for the No Plant, Const. Plant and Plant simulations, respectively. It is seen that for the No Plant simulation (Figure 6.30) the pressure head variation is identical in all the columns while for the Const. Plant simulations (Figure 6.31), it is identical for the columns that contain the same type of plant. Lower pressure heads occur in the Const. Plant (Figure 6.31) and Plant (Figure 6.33) simulations due to water losses by interception and root water uptake. This is better observed during the Plant simulation (Figure 6.33) since the lower pressure head values at the soil cell 1 is correlated with the high *LAI* values (Figure 6.34) for that soil column.

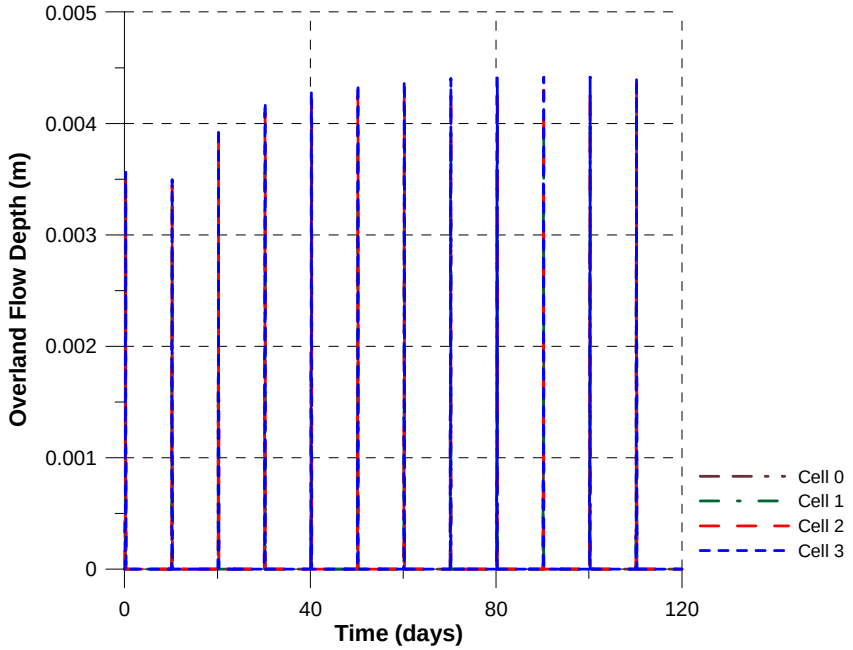

Figure 6.29: Overland flow depth variation with time for seasonal simulation of sprinkler irrigation. (No Plant)

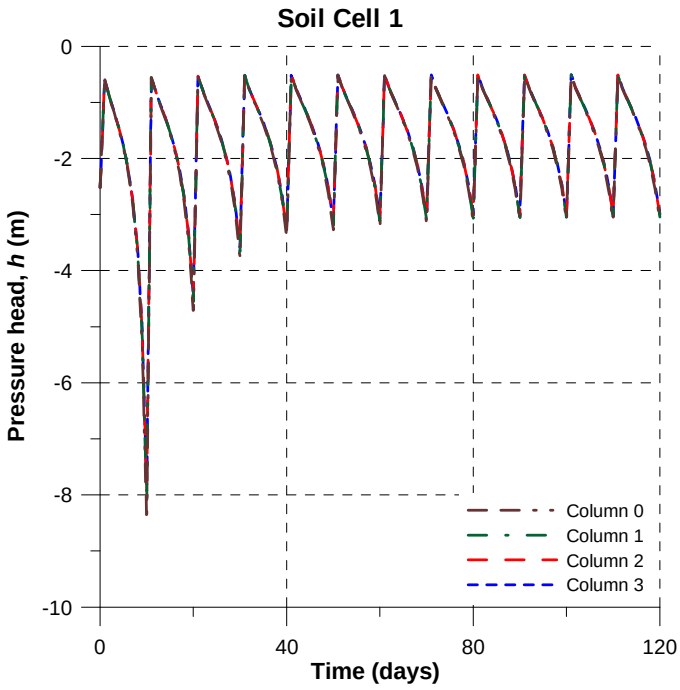

Figure 6.30: Pressure head variation with time at the top soil cell for seasonal simulation of sprinkler irrigation. (No Plant)

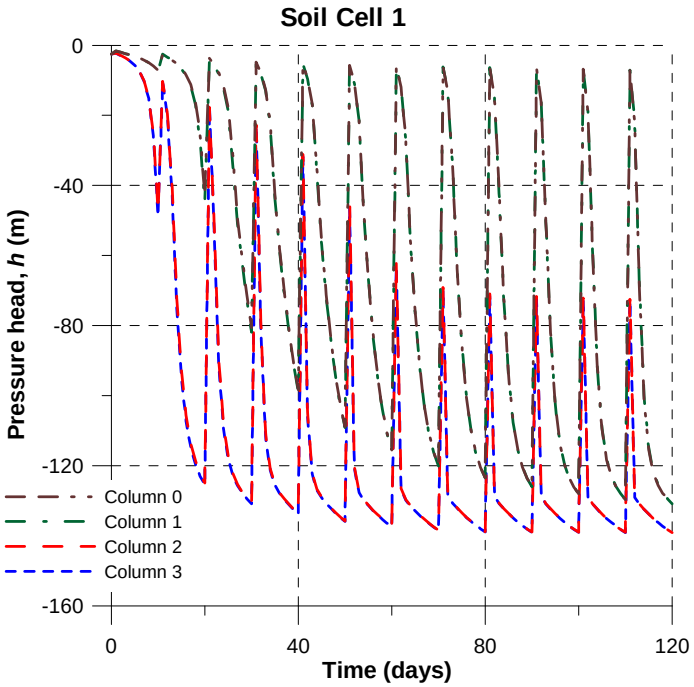

Figure 6.31: Pressure head variation with time at the top soil cell for seasonal simulation of sprinkler irrigation. (Const. Plant)

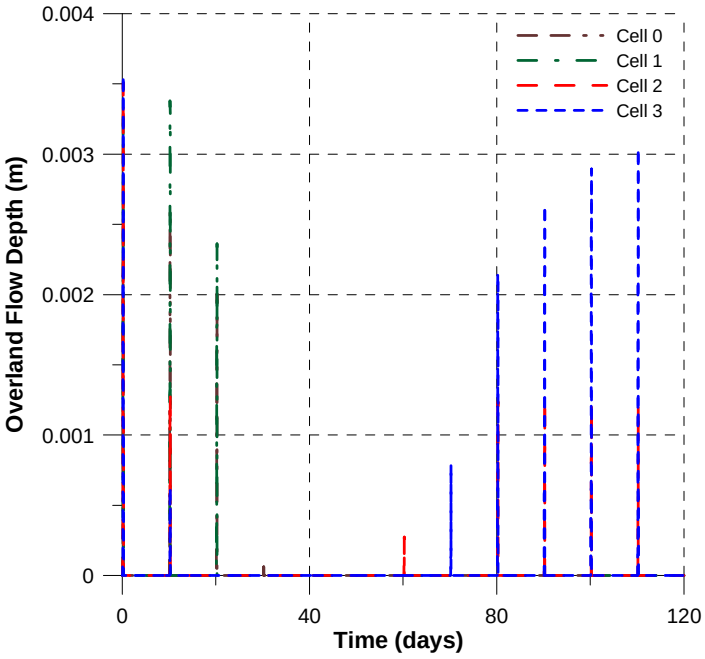

Figure 6.32: Overland flow depth variation with time for seasonal simulation of sprinkler irrigation. (Plant)

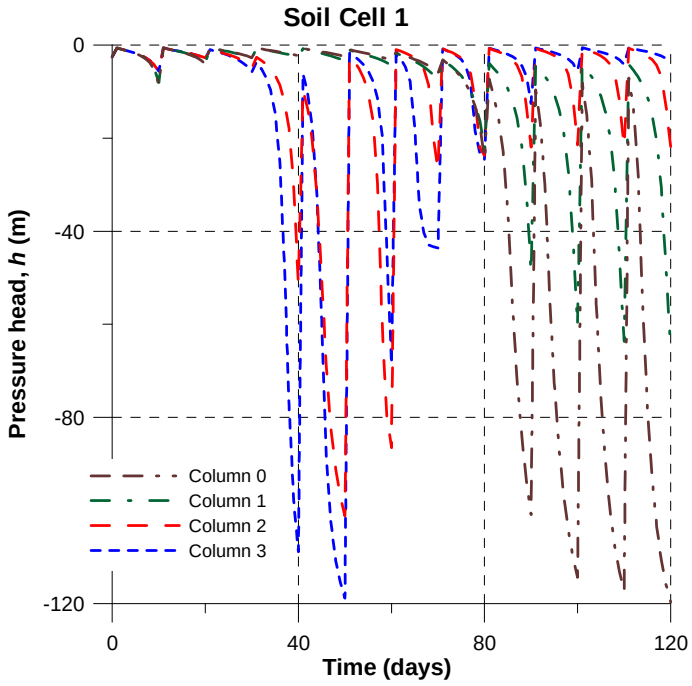

Figure 6.33: Pressure head variation with time at the top soil cell for seasonal simulation of sprinkler irrigation. (Plant)

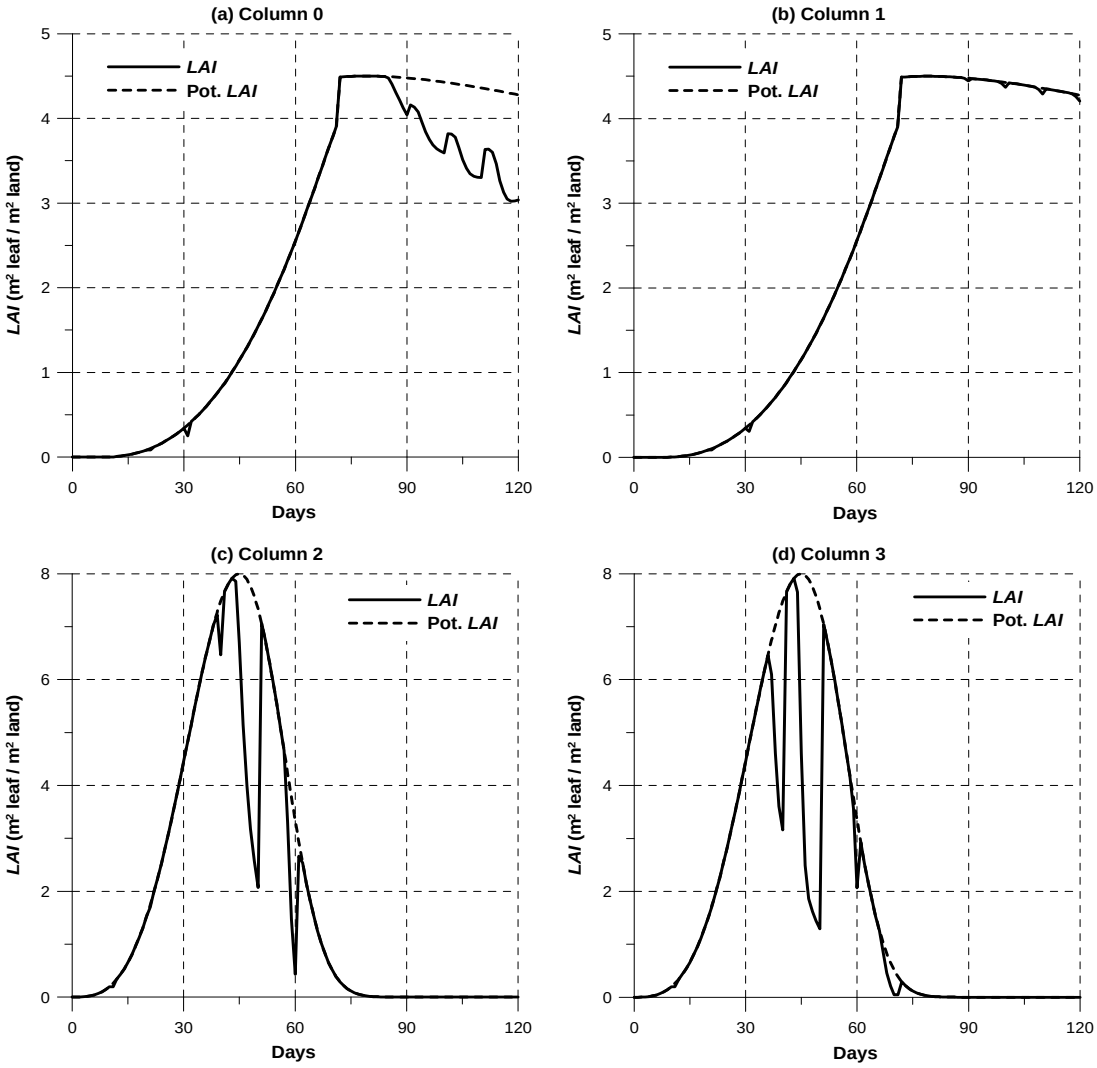

Figure 6.34: *LAI* simulation results for seasonal simulation of sprinkler irrigation. (Columns 0 and 1: corn, Columns 2 and 3: hay)

6.4 Conclusion

In this chapter, an integrated model of water flow in a terrestrial system has been developed by using the soil-plant system model developed in Chapter 5 as a building block. With this extension, the hydrological counterpart of the soil-plant system model is applicable to fields that have heterogeneous vegetation and soil characteristics.

The model applications presented in this chapter demonstrated the ability of the model to describe interactions between the overland flow and the soil-water dynamics. Also, the effects of the presence of vegetation and its dynamic nature on the overland flow occurrence and soil-water availability are shown.

The developed model is able to provide an integrated analysis of water flow dynamics in terrestrial systems. It can be combined with a contaminant transport model for an integrated contaminant fate and transport analysis.

CHAPTER 7

INTEGRATED MODELING OF CONTAMINANT FATE AND TRANSPORT IN A TERRESTRIAL SYSTEM

7.1 Introduction

In this chapter, the contaminant fate and transport counterpart of the soil-plant system model that was developed in Chapter 5 is extended to cover larger spatial areas. Combined with the integrated flow model developed in Chapter 6, this extension to the soil-plant system model provides a tool for describing the contaminant fate and transport processes in areas that contain heterogeneities regarding vegetation, land surface, soil and hydrological characteristics. Following the same approach that was used in the development of the integrated water flow model, the modeling domain is conceptualized as a collection of soil-plant system units. These multiple soil-plant system units are coupled by implementing an overland transport model that describes the ground surface processes. Furthermore, the subsurface lateral fluxes of contaminants between neighboring soil columns are incorporated to allow interaction between the soil columns beneath the ground surface.

In the following sections, the integrated model framework is described and the resultant model's capability in describing the contaminant fate and transport in a spatially heterogeneous soil-plant system is demonstrated through several applications.

7.2 Integrated Model Development

A schematic view of the integration approach is given in Figure 7.1. The vadose zone transport model coupled with the plant pathway model is treated as a single unit of the new integrated model. The details of the contaminant fate and transport modeling within a single soil column have been described in Chapter 5. The other major components of the integrated transport model are the two-dimensional overland transport model (Section 4.4) and the advective and dispersive contaminant fluxes between adjacent soil columns. The coupling of the overland transport model with the vadose zone transport model is described in Section 7.2.1. The method used in determining the subsurface lateral fluxes and incorporating them into the integrated model is explained in Section 7.2.2.

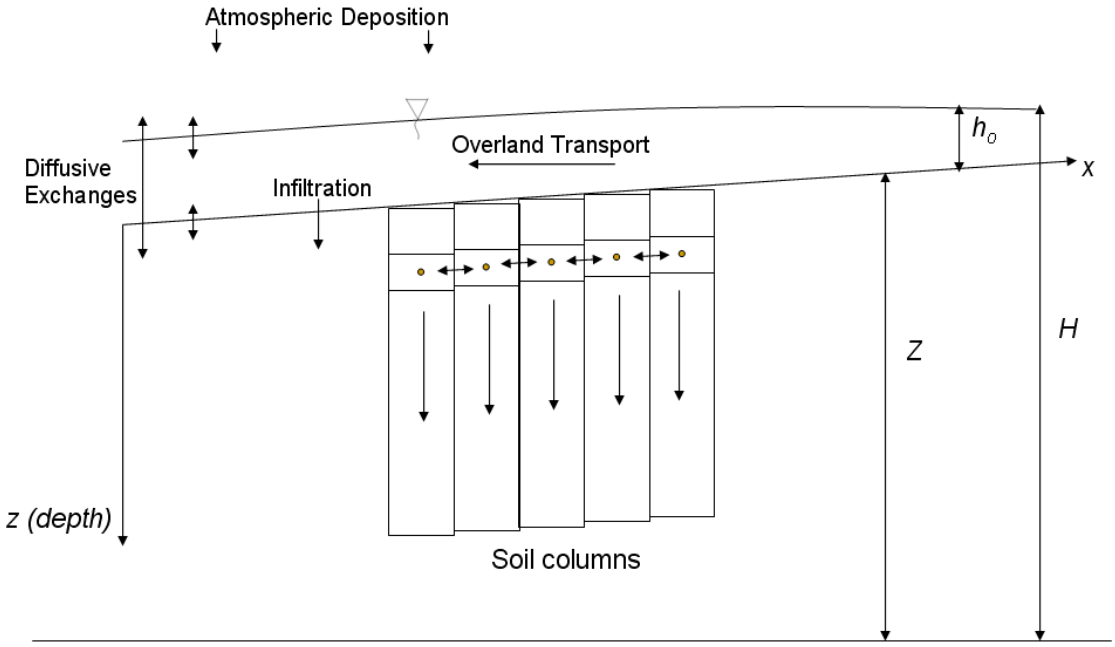

Figure 7.1: A schematic view of the integrated transport model.

7.2.1 Coupling Overland Transport and Vadose Zone Transport Models

The coupling of the overland transport and the vadose zone transport models is achieved by the simultaneous solution of the model equations in a single global matrix. In this section, the governing equations for the overland transport and the vadose zone transport model and their spatially discretized versions are rewritten. Then, the terms that describe the interactions between the two domains are incorporated into the governing equations. Finally, the structure of the global matrix for the integrated transport model is given.

The governing equation for the overland transport model is (1D version is given for ease of demonstration):

$$\frac{\partial\left(C_o h\right)}{\partial t} = -\frac{\partial\left(C_o h v_x\right)}{\partial x} + \frac{\partial}{\partial x}\left(hD_x \frac{\partial C_o}{\partial x}\right) + M \tag{7.1}$$

The set of model equations for $i = 1,...,K$ (K is the number of cells in the x- direction) after spatial discretization are:

$$\left(\frac{d\left[hC_o\right]}{dt}\right)_i \Delta x_i \Delta y_i - \left\{\left[\left(hv_x\right)_i^W \left(1-\alpha_i^W\right)+\left(\frac{hD_x}{\Delta x}\right)_i^W\right]\Delta y_i\right\}\left(C_o\right)_{i-1}$$
$$-\left\{\begin{bmatrix}\left(-hv_x\right)_i^E \alpha_i^E + \left(hv_x\right)_i^W \alpha_i^W \\ -\left(\frac{hD_x}{\Delta x}\right)_i^E - \left(\frac{hD_x}{\Delta x}\right)_i^W\end{bmatrix}\Delta y_i\right\}\left(C_o\right)_i \qquad (7.2)$$
$$-\left\{\left[\left(-hv_x\right)_i^E \left(1-\alpha_i^E\right)+\left(\frac{hD_x}{\Delta x}\right)_i^E\right]\Delta y_i\right\}\left(C_o\right)_{i+1} \quad = M_i \Delta x_i \Delta y_i$$

After introducing the bulk terms (i = 1,...,K), the following compact representation is obtained:

$$\left(\frac{d\left[G_o C_o\right]}{dt}\right)_i \left(M_o\right)_i + \left(S_o\right)_i^W \left(C_o\right)_{i-1} + \left(S_o\right)_i^0 \left(C_o\right)_i + \left(S_o\right)_i^E \left(C_o\right)_{i+1} = \left(F_o\right)_i \qquad (7.3)$$

$$\left(G_o\right)_i = \left(h_o\right)_i \qquad (7.3a)$$

$$\left(M_o\right)_i = \Delta x_i \Delta y_i \qquad (7.3b)$$

$$\left(S_o\right)_i^W = -\left[\left(hv_x\right)_i^W \left(1-\alpha_i^W\right)+\left(\frac{hD_x}{\Delta x}\right)_i^W\right]\Delta y_i \qquad (7.3c)$$

$$\left(S_o\right)_i^0 = -\begin{bmatrix}\left(-hv_x\right)_i^E \alpha_i^E + \left(hv_x\right)_i^W \alpha_i^W \\ -\left(\frac{hD_x}{\Delta x}\right)_i^E - \left(\frac{hD_x}{\Delta x}\right)_i^W\end{bmatrix}\Delta y_i \qquad (7.3d)$$

$$\left(S_o\right)_i^E = -\left[\left(-hv_x\right)_i^E \left(1-\alpha_i^E\right)+\left(\frac{hD_x}{\Delta x}\right)_i^E\right]\Delta y_i \qquad (7.3e)$$

$$\left(F_o\right)_i = \left(Q_o\right)_i \Delta x_i \Delta y_i \qquad (7.3f)$$

The governing equation for the vadose zone transport model can be rewritten as in Equation 7.4 (reaction processes are not shown for ease of demonstration):

$$\frac{\partial}{\partial t}\left[R\theta C_w\right] = \frac{\partial}{\partial z}\left(D_s \frac{\partial C_w}{\partial z} - qC_w\right) + M \tag{7.4}$$

$$R = 1 + \frac{\rho_b K_d + \phi s_g K_H}{\phi s_w} \tag{7.4a}$$

$$\theta = \phi s_w \tag{7.4b}$$

$$D_s = \phi s_w D_w + \phi s_g D_g K_H \tag{7.4c}$$

After spatial discretization, the following set of equations are obtained for $j = 1,\ldots,N$ (where N is the total number of cells in the soil column):

$$\begin{aligned}\left(\frac{d\left(R\theta C_w\right)}{dt}\right)_j \Delta z_j &- \left[q_j^U\left(1-\alpha_j^U\right) + \left(\frac{D_s}{\Delta z}\right)_j^U\right]\left(C_w\right)_{j-1} \\ &- \left[q_j^U \alpha_j^U - q_j^D \alpha_j^D - \left(\frac{D_s}{\Delta z}\right)_j^U - \left(\frac{D_s}{\Delta z}\right)_j^D\right]\left(C_w\right)_j \\ &- \left[-q_j^D\left(1-\alpha_j^D\right) + \left(\frac{D_s}{\Delta z}\right)_j^D\right]\left(C_w\right)_{j+1} = F_j \Delta z_j\end{aligned} \tag{7.5}$$

After introducing the bulk terms ($j = 1,...,N$), the following compact representation is obtained:

$$\left(\frac{d\left(G_S C_w\right)}{dt}\right)_j \left(M_S\right)_j + \left(S_S\right)_j^U \left(C_w\right)_{j-1} + \left(S_S\right)_j^0 \left(C_w\right)_j + \left(S_S\right)_j^D \left(C_w\right)_{j+1} = \left(F_S\right)_j \tag{7.6}$$

$$\left(G_S\right)_j = \left(R\theta\right)_j \tag{7.6a}$$

$$\left(M_S\right)_j = \Delta z_j \tag{7.6b}$$

$$\left(S_S\right)_j^U = -\left[q_j^U\left(1-\alpha_j^U\right)+\left(\frac{D_s}{\Delta z}\right)_j^U\right] \tag{7.6c}$$

$$\left(S_S\right)_j^0 = -\left[q_j^U\alpha_j^U - q_j^D\alpha_j^D - \left(\frac{D_s}{\Delta z}\right)_j^U - \left(\frac{D_s}{\Delta z}\right)_j^D\right] \tag{7.6d}$$

$$\left(S_S\right)_j^D = -\left[-q_j^D\left(1-\alpha_j^D\right)+\left(\frac{D_s}{\Delta z}\right)_j^D\right] \tag{7.6e}$$

$$\left(F_S\right)_j = \left(Q_S\right)_j \Delta z_j \tag{7.6f}$$

The handling of the top boundary condition for a specified concentration condition is summarized below. In the integrated model, the specified concentration at the top boundary is replaced with the overland flow concentration.

The mass balance equation for the soil cell 1 is:

$$\left(\frac{d\left(G_S C_w\right)}{dt}\right)_1\left(M_S\right)_1 + \left(S_S\right)_1^U\left(C_w\right)_0 + \left(S_S\right)_1^0\left(C_w\right)_1 + \left(S_S\right)_1^D\left(C_w\right)_2 = \left(F_S\right)_1 \tag{7.7}$$

$$\left(G_S\right)_1 = \left(R\theta\right)_1 \tag{7.7a}$$

$$\left(M_S\right)_1 = \Delta z_1 \tag{7.7b}$$

$$\left(S_S\right)_1^U = -\left[q_{\text{inf}}\left(1-\alpha_1^U\right)+\frac{\left(D_s\right)_1^U}{\Delta z/2}\right] \tag{7.7c}$$

$$\left(S_S\right)_1^0 = -\left[q_{\inf}\alpha_1^U - q_1^D\alpha_1^D - \frac{\left(D_s\right)_1^U}{\Delta z/2} - \left(\frac{D_s}{\Delta z}\right)_1^D \right] \tag{7.7d}$$

$$\left(S_S\right)_1^D = -\left[-q_1^D\left(1-\alpha_1^D\right) + \left(\frac{D_s}{\Delta z}\right)_1^D \right] \tag{7.7e}$$

$$\left(F_S\right)_1 = \left(Q_S\right)_1 \Delta z_1 \tag{7.7f}$$

where $q_{\inf}$ is the infiltration rate [L T^{-1}]and $\left(D_s\right)_1^U$ is the dispersion coefficient [L^2 T^{-1}] at the upper interface of soil cell 1.

After incorporating the boundary condition $\left(C_w\right)_0 = \left(C_w\right)_{top}$:

$$\left(\frac{d\left(G_S C_w\right)}{dt}\right)_1 \left(M_S\right)_1 + \left(S_S\right)_1^U \left(C_w\right)_{top} + \left(S_S\right)_1^0 \left(C_w\right)_1 + \left(S_S\right)_1^D \left(C_w\right)_2 = \left(F_S\right)_1 \tag{7.8}$$

Since $\left(C_w\right)_{top}$ is known, it can be moved to the right-hand-side:

$$\left(\frac{d\left(G_S C_w\right)}{dt}\right)_1 \left(M_S\right)_1 + \left(S_S\right)_1^0 \left(C_w\right)_1 + \left(S_S\right)_1^D \left(C_w\right)_2 = \left(F_S\right)_1 - \left(S_S\right)_1^U \left(C_w\right)_{top} \tag{7.9}$$

A modified source term for soil cell 1 can be defined as:

$$\left[\left(F_S\right)_1\right]' = \left(F_S\right)_1 - \left(S_S\right)_1^U \left(C_w\right)_{top} \tag{7.10}$$

Then, the mass balance equation for soil cell 1 takes the following form:

$$\left(\frac{d\left(G_S C_w\right)}{dt}\right)_1 \left(M_S\right)_1 + \left(S_S\right)_1^0 \left(C_w\right)_1 + \left(S_S\right)_1^D \left(C_w\right)_2 = \left[\left(F_S\right)_1\right]' \tag{7.11}$$

In case of an atmospheric boundary condition (when instantaneous equilibrium is assumed between the water phase concentration at the soil surface and the atmospheric concentration), the top boundary concentration is:

$$\left(C_w\right)_{top} = \frac{C_{Atm}}{K_{aw}} \tag{7.12}$$

where C_{Atm} is the contaminant concentration [M L^{-3}] in the atmosphere, and K_{aw} is the air-water partition coefficient [L^3 L^{-3}].

Assuming that the overland / subsurface contaminant transfer occurs through the soil layer between the soil surface and the center of the uppermost soil cell (soil cell 1) the interaction between the two domains is conceptualized as shown in Figure 7.2.

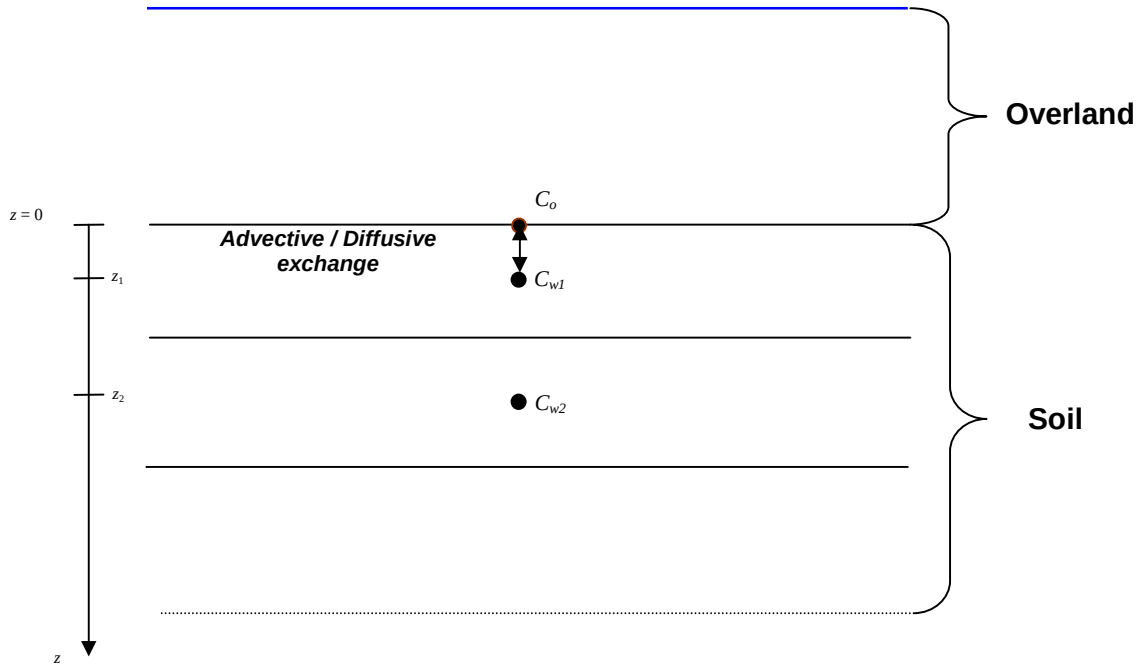

Figure 7.2: Conceptual representation of the overland / subsurface interactions.

Mass balance equation for the overland cell *i* above column *i* after the interaction terms are included is written as in Equation (7.13). (The terms that describe transport processes between the two domains are shown in red.)

$$\left(\frac{d\left[hC_o\right]}{dt}\right)_i \Delta x_i \Delta y_i - \left\{\left[\left(hv_x\right)_i^W \left(1-\alpha_i^W\right)+\left(\frac{hD_x}{\Delta x}\right)_i^W\right]\Delta y_i\right\}\left(C_o\right)_{i-1}$$
$$-\left\{\begin{bmatrix}\left(-hv_x\right)_i^E \alpha_i^E + \left(hv_x\right)_i^W \alpha_i^W \\ -\left(\frac{hD_x}{\Delta x}\right)_i^E - \left(\frac{hD_x}{\Delta x}\right)_i^W\end{bmatrix}\Delta y_i \right.$$
$$\left. + \left[-\left(q_{\text{inf}}\right)_i \alpha_i^D - \left(\frac{\left(D_s\right)^D}{\Delta z_1/2}\right)_i\right]\Delta x_i \Delta y_i \right\}\left(C_o\right)_i \qquad (7.13)$$
$$-\left\{\left[\left(-hv_x\right)_i^E \left(1-\alpha_i^E\right)+\left(\frac{hD_x}{\Delta x}\right)_i^E\right]\Delta y_i\right\}\left(C_o\right)_{i+1}$$
$$-\left\{\begin{bmatrix}-\left(q_{\text{inf}}\right)_i\left(1-\alpha_i^D\right) \\ +\left(\frac{\left(D_s\right)^D}{\Delta z_1/2}\right)_i\end{bmatrix}\Delta x_i \Delta y_i\right\}\left[\left(C_w\right)_1\right]_i = M_i \Delta x_i \Delta y_i$$

Mass balance equation for soil cell 1 in column *i* is only slightly changed from its specified boundary condition version given in Equation (7.9). In the integrated model, the soil surface concentration is equal to the overland concentration and the terms associated with this unknown concentration are moved to the left-hand-side of the equation (The terms that describe transport processes between the two domains are shown in red.):

$$\left\{\left(\frac{d\left(R\theta C_w\right)}{dt}\right)_1 \Delta z_1 - \left[q_{\text{inf}}\left(1-\alpha_1^U\right)+\frac{\left(D_s\right)_1^U}{\Delta z_1/2}\right]C_o \right.$$
$$-\left[q_{\text{inf}}\alpha_1^U - q_1^D\alpha_1^D - \frac{\left(D_s\right)_1^U}{\Delta z_1/2} - \left(\frac{D_s}{\Delta z}\right)_1^D\right]\left(C_w\right)_1 \qquad (7.14)$$
$$\left. -\left[-q_1^D\left(1-\alpha_1^D\right)+\left(\frac{D_s}{\Delta z}\right)_1^D\right]\left(C_w\right)_2 = F_1\Delta z_1\right\}_i$$

The overland transport equation that includes the subsurface interaction terms can be rewritten as below after defining the bulk terms:

$$\left(\frac{d[G_oC_o]}{dt}\right)_i (M_o)_i + (S_o)_i^W (C_o)_{i-1} + \left[(S_o)_i^0\right]' (C_o)_i + (S_o)_i^E (C_o)_{i+1} + (S_o)_i^D \left[(C_w)_1\right]_i = (F_o)_i \tag{7.15}$$

$$(G_o)_i = (h_o)_i \tag{7.15a}$$

$$(M_o)_i = \Delta x_i \Delta y_i \tag{7.15b}$$

$$(S_o)_i^W = -\left[(hv_x)_i^W (1-\alpha_i^W) + \left(\frac{hD_x}{\Delta x}\right)_i^W\right]\Delta y_i \tag{7.15c}$$

$$\left[(S_o)_i^0\right]' = \left[(S_o)_i^0 + (S_o)_i^{0,D}\right] \tag{7.15d}$$

$$(S_o)_i^0 = -\begin{bmatrix}(-hv_x)_i^E \alpha_i^E + (hv_x)_i^W \alpha_i^W \\ -\left(\frac{hD_x}{\Delta x}\right)_i^E - \left(\frac{hD_x}{\Delta x}\right)_i^W\end{bmatrix}\Delta y_i \tag{7.15e}$$

$$(S_o)_i^{0,D} = \left[-(q_{\text{inf}})_i \alpha_i^D - \left(\frac{(D_s)^D}{\Delta z_1/2}\right)_i\right]\Delta x_i \Delta y_i \tag{7.15f}$$

$$(S_o)_i^E = -\left[(-hv_x)_i^E (1-\alpha_i^E) + \left(\frac{hD_x}{\Delta x}\right)_i^E\right]\Delta y_i \tag{7.15g}$$

$$(S_o)_i^D = -\left\{\left[-(q_{\text{inf}})_i (1-\alpha_i^D) + \left(\frac{(D_s)^D}{\Delta z_1/2}\right)_i\right]\Delta x_i \Delta y_i\right\} \tag{7.15h}$$

$$\left(F_o\right)_i = \left(Q_o\right)_i \Delta x_i \Delta y_i \tag{7.15i}$$

Similarly, the mass balance equation for soil cell 1 after incorporating the overland interaction terms can be rewritten as:

$$\left(\frac{d\left(G_S C_w\right)}{dt}\right)_1 \left(M_S\right)_1 + \left(S_S\right)_1^U C_o + \left(S_S\right)_1^0 \left(C_w\right)_1 + \left(S_S\right)_1^D \left(C_w\right)_2 = \left(F_S\right)_1 \tag{7.16}$$

$$\left(G_S\right)_1 = \left(R\theta\right)_1 \tag{7.16a}$$

$$\left(M_S\right)_1 = \Delta z_1 \tag{7.16b}$$

$$\left(S_S\right)_1^U = -\left[\left(q_{\text{inf}}\right)_i \left(1-\alpha_1^U\right) + \frac{\left(D_s\right)_1^U}{\Delta z_1 / 2}\right] \tag{7.16c}$$

$$\left(S_S\right)_1^0 = -\left[\left(q_{\text{inf}}\right)_{\text{inf}} \alpha_1^U - q_1^D \alpha_1^D - \frac{\left(D_s\right)_1^U}{\Delta z_1 / 2} - \left(\frac{D_s}{\Delta z}\right)_1^D\right] \tag{7.16d}$$

$$\left(S_S\right)_1^D = -\left[-q_1^D \left(1-\alpha_1^D\right) + \left(\frac{D_s}{\Delta z}\right)_1^D\right] \tag{7.16e}$$

$$\left(F_S\right)_1 = \left(Q_S\right)_1 \Delta z_1 \tag{7.16f}$$

Finally, the global matrix-vector system for the integrated model can be represented as:

$$[\mathbf{M}]\left(\frac{\mathbf{d}[\mathbf{GC}]}{\mathbf{dt}}\right) + [\mathbf{S}]\{\mathbf{C}\} = \{\mathbf{F}\} \tag{7.17}$$

with $[\mathbf{M}] = \begin{pmatrix} [\mathbf{M_o}] & & & \\ & [\mathbf{M_S}]_1 & & \\ & & \ddots & \\ & & & [\mathbf{M_S}]_K \end{pmatrix}$; $[\mathbf{G}] = \begin{pmatrix} [\mathbf{G_o}] & & & \\ & [\mathbf{G_S}]_1 & & \\ & & \ddots & \\ & & & [\mathbf{G_S}]_K \end{pmatrix}$;

$\{\mathbf{C}\} = \begin{pmatrix} \{\mathbf{C_o}\} \\ \{\mathbf{C_w}\}_1 \\ \vdots \\ \{\mathbf{C_w}\}_N \end{pmatrix}$; $\{\mathbf{F}\} = \begin{pmatrix} \{\mathbf{F_o}\} \\ \{\mathbf{F_S}\}_1 \\ \vdots \\ \{\mathbf{F_S}\}_N \end{pmatrix}$; $[\mathbf{S}] = \begin{pmatrix} [\mathbf{S_o}] & [\mathbf{S_{o\text{-}1}}] & \cdots & [\mathbf{S_{o\text{-}K}}] \\ [\mathbf{S_{1\text{-}o}}] & [\mathbf{S_S}]_1 & & \\ \vdots & & \ddots & \\ [\mathbf{S_{K\text{-}o}}] & & & [\mathbf{S_S}]_K \end{pmatrix}$; and the sub-

matrices that describe the interaction between the overland and subsurface domains:

$$[\mathbf{S_{o\text{-}1}}] = \begin{pmatrix} (S_o)_1^D & & 0 \\ & \ddots & \\ 0 & & 0 \end{pmatrix}_{(K\times N)}; \quad [\mathbf{S_{o\text{-}K}}] = \begin{pmatrix} 0 & & 0 \\ & \ddots & \\ 0 & & (S_o)_K^D \end{pmatrix}_{(K\times N)};$$

$$[\mathbf{S_{1\text{-}o}}] = \begin{pmatrix} (S_S)_1^U & \cdots & 0 \\ \vdots & \ddots & \\ 0 & & 0 \end{pmatrix}_{(N\times K)}; \quad [\mathbf{S_{K\text{-}o}}] = \begin{pmatrix} 0 & \cdots & 0 \\ \vdots & \ddots & \\ 0 & & (S_S)_K^U \end{pmatrix}_{(N\times K)}.$$

The ODE system represented in Equation (7.17) is solved by using the time integration scheme explained in Appendix E.

The condition of the overland cell falls into one of these four categories with respect to the overland / subsurface flow interaction:

1- WET: Overland flow developed; infiltration at its maximum rate.

2- Transition (Infiltration): Overland flow not developed; infiltration equal to the potential vertical flux at the soil surface.

3- Transition (Evaporation): No overland flow; evaporation equal to the potential vertical flux at the soil surface.
4- DRY: No overland flow, evaporation at its maximum rate.

For conditions 1 and 2, there is interaction between the overland and subsurface domains. However, for conditions 3 and 4, the overland and soil transport solutions are decoupled. In this case the boundary condition at the top of soil columns are expressed as specified concentrations and the condition is imposed as it has been explained through Equations (7.8-7.11) by modifying the *F* term on the right hand side of the mass balance equation for the uppermost soil cell (cell 1). And, the decoupled versions of the overland and vadose zone transport equations are used in building the global matrix-vector system. During the actual solution, the condition of any overland cell is determined individually and the overland cell / soil column interactions are handled in a case by case basis.

The overland transport solution described in this section (and also in Section 4.4) is valid for non-zero water depths ($h>0$). During the actual solution of the integrated overland / subsurface system, non-zero overland flow depths are only seen when the overland flow cell is in condition 1 (WET). In order to avoid the numerical difficulties that are encountered with zero overland flow depths, the overland flow depth is artificially modified so that it doesn't fall below a specified small value (ε_{depth}):

$$h = \begin{cases} h_o & \text{if } h > \varepsilon_{depth} \\ \varepsilon_{depth} & \text{if } h \le \varepsilon_{depth} \end{cases} \tag{7.18}$$

A ε_{depth} value of 10^{-4} m is assumed in this study.

7.2.2 Incorporating the Subsurface Lateral Fluxes

The subsurface lateral fluxes are incorporated by calculating the advective and dispersive fluxes between the corresponding soil cells in adjacent soil columns (Figure 7.3). The total lateral flux into cell *j* from its east neighbor residing at the same depth can be represented as:

$$J_j^E = \underbrace{-q_j^E \left[\left(1-\alpha_j^E\right) C_{w,j}^E + \alpha_j^E C_{w,j} \right]}_{\text{Advective Inflow}} + \underbrace{\left(\frac{D_s}{\Delta x}\right)_j^E \left(C_{w,j}^E - C_{w,j}\right)}_{\text{Dispersive Inflow}} \tag{7.19}$$

where J_j^E is the total contaminant flux [L T^{-1}] into cell *j* through its east interface, q_j^E is the lateral flow rate [L T^{-1}] at the east interface of *j*, α_j^E is the advective scheme weighting factor at the east interface of *j*, $C_{w,j}^E$ is the soil-water contaminant concentration [M L^{-3}] at *j*'s east neighboring cell, and $C_{w,j}$ is the soil-water contaminant concentration [M L^{-3}] at *j*.

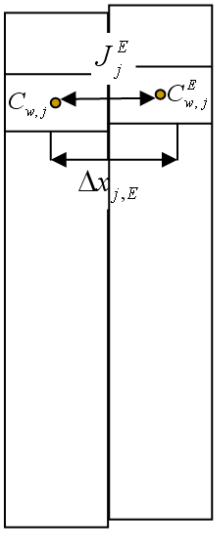

Figure 7.3: The subsurface lateral contaminant flux calculation between two adjacent soil cells.

Including the lateral fluxes from all directions (only east and west directions are given here for ease of demonstration), the spatially discretized vadose zone transport equation is modified as in Equation (7.20) where the superscript *W* is used to denote the terms associated with the west neighbor of cell *j*.

$$\left(\frac{d\left(G_S C_w\right)}{dt}\right)_j \left(M_S\right)_j + \left(S_S\right)_j^U \left(C_w\right)_{j-1} + \left(S_S\right)_j^D \left(C_w\right)_{j+1} + \left[\left(S_S\right)_j^0\right]' \left(C_w\right)_j + \left(S_S\right)_j^E \left(C_w\right)_j^E + \left(S_S\right)_j^W \left(C_w\right)_j^W = \left(F_S\right)_j \tag{7.20}$$

$$\left(G_S\right)_j = \left(R\theta\right)_j \tag{7.20a}$$

$$\left(M_S\right)_j = \Delta z_j \tag{7.20b}$$

$$\left(S_S\right)_j^U = -\left[q_j^U\left(1-\alpha_j^U\right)+\left(\frac{D_s}{\Delta z}\right)_j^U\right] \tag{7.20c}$$

$$\left(S_S\right)_j^D = -\left[-q_j^D\left(1-\alpha_j^D\right)+\left(\frac{D_s}{\Delta z}\right)_j^D\right] \tag{7.20d}$$

$$\begin{aligned}\left[\left(S_S\right)_j^0\right]' &= \left[\left(S_S\right)_j^0+\left(S_S\right)_j^{0,E}+\left(S_S\right)_j^{0,W}\right] \\ &= -\left[q^U\alpha_j^U - q_j^D\alpha_j^D - \left(\frac{D_s}{\Delta z}\right)_j^U - \left(\frac{D_s}{\Delta z}\right)_j^D\right] \\ &\quad -\left[-q_j^E\alpha_j^E - \left(\frac{D_s}{\Delta x}\right)_j^E\right] - \left[-q_j^W\alpha_j^W - \left(\frac{D_s}{\Delta x}\right)_j^W\right]\end{aligned} \tag{7.20e}$$

$$\left(S_S\right)_j^0 = -\left[q_j^U\alpha_j^U - q_j^D\alpha_j^D - \left(\frac{D_s}{\Delta z}\right)_j^U - \left(\frac{D_s}{\Delta z}\right)_j^D\right] \tag{7.20f}$$

$$\left(S_S\right)_j^{0,E} = -\left[-q_j^E\alpha_j^E - \left(\frac{D_s}{\Delta x}\right)_j^E\right] \tag{7.20g}$$

$$\left(S_S\right)_j^{0,W} = -\left[-q_j^W\alpha_j^W - \left(\frac{D_s}{\Delta x}\right)_j^W\right] \tag{7.20h}$$

$$\left(S_S\right)_j^E = -\left[-q_j^E\left(1-\alpha_j^E\right)+\left(\frac{D_s}{\Delta x}\right)_j^E\right] \tag{7.20i}$$

$$\left(S_S\right)_j^W = -\left[-q_j^W\left(1-\alpha_j^W\right)+\left(\frac{D_s}{\Delta x}\right)_j^W\right] \tag{7.20j}$$

$$\left(F_S\right)_j = \left(Q_S\right)_j\Delta z_j \tag{7.20k}$$

The matrix **S** in the global ODE system (Equation 7.17) has the following structure after incorporating the lateral flux terms:

$$[\mathbf{S}] = \begin{pmatrix} [\mathbf{S_o}] & [\mathbf{S_{o\text{-}1}}] & [\mathbf{S_{o\text{-}2}}] & \cdots & [\mathbf{S_{o\text{-}K}}] \\ [\mathbf{S_{1\text{-}o}}] & [\mathbf{S_S}]_1 & [\mathbf{S_S}]_1^{\mathbf{E}} & & \\ [\mathbf{S_{2\text{-}o}}] & [\mathbf{S_S}]_2^{\mathbf{W}} & [\mathbf{S_S}]_2 & & \\ \vdots & & & \ddots & [\mathbf{S_S}]_{\mathbf{K\text{-}1}}^{\mathbf{E}} \\ [\mathbf{S_{K\text{-}o}}] & & & [\mathbf{S_S}]_{\mathbf{K}}^{\mathbf{W}} & [\mathbf{S_S}]_{\mathbf{K}} \end{pmatrix} \tag{7.21}$$

where $[\mathbf{S_S}]_{\mathbf{1}}^{\mathbf{E}} = \begin{pmatrix} \left[(S_S)_1^E\right]_1 & & \\ & \ddots & \\ & & \left[(S_S)_N^E\right]_1 \end{pmatrix}_{(N\times N)}$;

$[\mathbf{S_S}]_{\mathbf{2}}^{\mathbf{W}} = \begin{pmatrix} \left[(S_S)_1^W\right]_2 & & \\ & \ddots & \\ & & \left[(S_S)_N^W\right]_2 \end{pmatrix}_{(N\times N)}$;

$[\mathbf{S_S}]_{\mathbf{K\text{-}1}}^{\mathbf{E}} = \begin{pmatrix} \left[(S_S)_1^E\right]_{K-1} & & \\ & \ddots & \\ & & \left[(S_S)_N^E\right]_{K-1} \end{pmatrix}_{(N\times N)}$;

$[\mathbf{S_S}]_{\mathbf{K}}^{\mathbf{W}} = \begin{pmatrix} \left[(S_S)_1^W\right]_{K-1} & & \\ & \ddots & \\ & & \left[(S_S)_N^W\right]_{K-1} \end{pmatrix}_{(N\times N)}$.

7.3 Model Application

In this section, several applications are presented to demonstrate the integrated modeling methodology developed in Section 7.2. These examples are structured around analyzing the effects of plant life-cycle modeling and the spatial heterogeneity regarding the vegetation characteristics on the contaminant distribution within the modeling domain. The response of the soil-plant system to different water input regimes is also demonstrated. Simple weather data and simple irrigation schedule are used to facilitate the interpretation of the results. The crop data is obtained from the literature.

7.3.1 Modeling Domain and the Model Parameters

In the model applications, the same modeling domain and the same model parameters used in the integrated flow model applications are used. So, the modeling domain description and the model parameters related with the system's hydraulic properties (Table 6.2, Figure 6.9), spatial discretization of the domain (Figures 6.6 and 6.7), weather conditions (Table 6.4), crop parameters (Table 6.3) and the irrigation schedule (Table 6.5) are as given in Section 6.3.1.

The same contaminant (diazinon) used in the single-column soil-plant system model applications (Section 5.3) is used in the applications. The chemical properties of the contaminant together with the required multimedia contaminant fate and transport model parameters can be found in Table 5.4.

The contamination scenarios included the application of diazinon one time on the first day of the simulation into the irrigation flow. Therefore, the contamination scenario is dependent on the irrigation method used. In the border irrigation simulations, at total of 12 kg of contaminant is applied throughout the 6-hour irrigation period. In the sprinkler irrigation simulations, the same total amount of contaminant was applied homogeneously onto the upstream half of the modeling domain where the corn crop is planted.

The atmospheric concentration is assumed to be zero all throughout the simulations so there is no contaminant input to the system via atmospheric deposition processes. Initially uncontaminated soil columns and plants were assumed. A zero-gradient boundary condition was applied at the bottom of the soil-columns.

7.3.2 Description of the Simulations

As in the integrated flow model applications, the set of simulations can be classified in three different ways based on different simulation characteristics:

1) Simulation length:
    a. Daily simulations (Simulation length = 1 day)
    b. Seasonal simulations (Simulation length = 120 days)
2) Irrigation method:
    a. Border irrigation (Contaminant input at the upstream border)
    b. Sprinkler irrigation (Homogeneous contaminant input throughout the upper half of the domain where the corn crop is planted)

3) Plant life-cycle modeling:

   a. No Plant (Plants are not present, bare soil)

   b. Const. Plant (Plant growth not modeled. Constant mass and *LAI* throughout the simulations. Corn: *LAI* = 3.0, biomass = 1000 g/m^2; Hay: *LAI* = 5.0, biomass = 200 g/m^2)

   c. Plant (Plant life-cycle simulated)

7.3.3 Results and Discussion

In this section, the results obtained from the model simulations are presented. The results of the daily simulations are given first, followed by the results of the seasonal simulations. The effect of different irrigation methods and the effect of plants on the contaminant distribution within the system are discussed. The simulation results are plotted for the strip of overland flow cells and the corresponding soil columns neighboring the $y = 0$ boundary of the model domain (Figure 6.10).

7.3.3.1 Daily Simulations

The daily simulation results for border irrigation are given in Figures 7.4-7.9. In Figures 7.4 and 7.6, the variation of the contaminant concentration in the overland flow is given for the No Plant and the Const. Plant simulations, respectively. In Figures 7.5 and 7.7, the variation of contaminant mass per unit area is plotted for the No Plant and the Const. Plant simulations, respectively. The contaminant mass per unit area at each column is

calculated by multiplying the overland concentration value with the corresponding overland flow depth value. It is observed that the overland mass plots are more informative since they provide the absolute amount of contaminant available in the overland flow. Also, it is seen that the overland contaminant mass variation plots follow a similar trend to the overland depth variation plots for the corresponding simulations given in Chapter 6 (Figures 6.11 and 6.13). There is a higher accumulation of the contaminant in the overland flow over the columns 0 and 1 in the Const. Plant simulation (Figure 7.7) compared to the No Plant simulation (Figure 7.5). This is due to overland flow accumulation over the upstream columns in the presence of plants. Note that the less amount of contaminant reaches column 2 in the Const. Plant simulation compared to the No Plant simulation. This phenomenon is also observed in the soil column concentration profiles given in Figures 7.8 and 7.9 for the No Plant and Const. Plant simulations, respectively. Some minor amount of contamination reaches column 3 in the No Plant simulation while almost no contamination reaches to this most downstream column in the Const. Plant simulation. Also, in Figure 7.9, the concentration profile for the 12^{th} hour indicates contaminant infiltration even after the end of the irrigation period (6^{th} hour) in Const. Plant simulations while it does not for the No Plant simulations (Figure 7.8) for which the contaminant concentrations start to decrease at an earlier time.

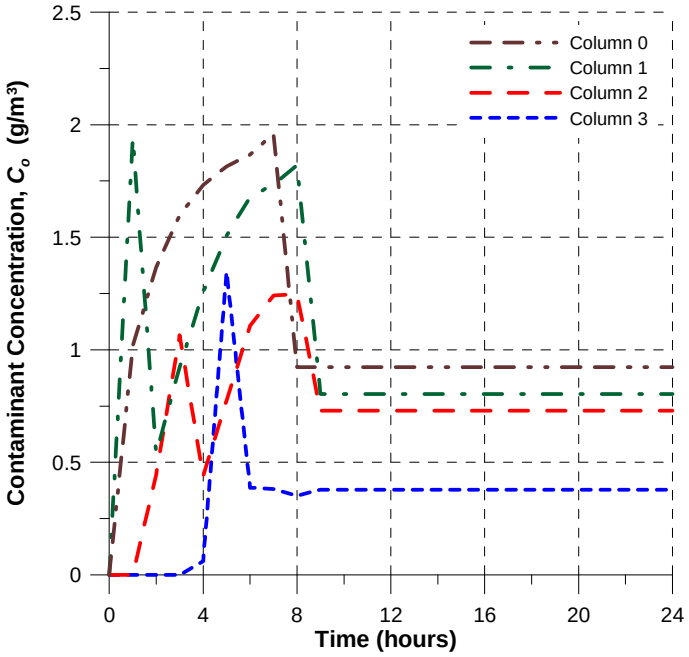

Figure 7.4: Contaminant concentration in the overland flow for the daily simulation of border irrigation. (No Plant)

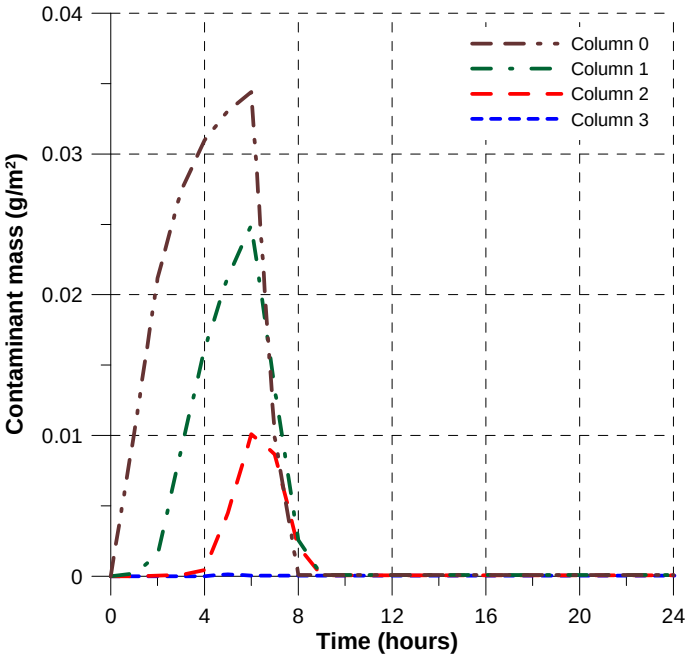

Figure 7.5: Contaminant mass in the overland flow for the daily simulation of border irrigation. (No Plant)

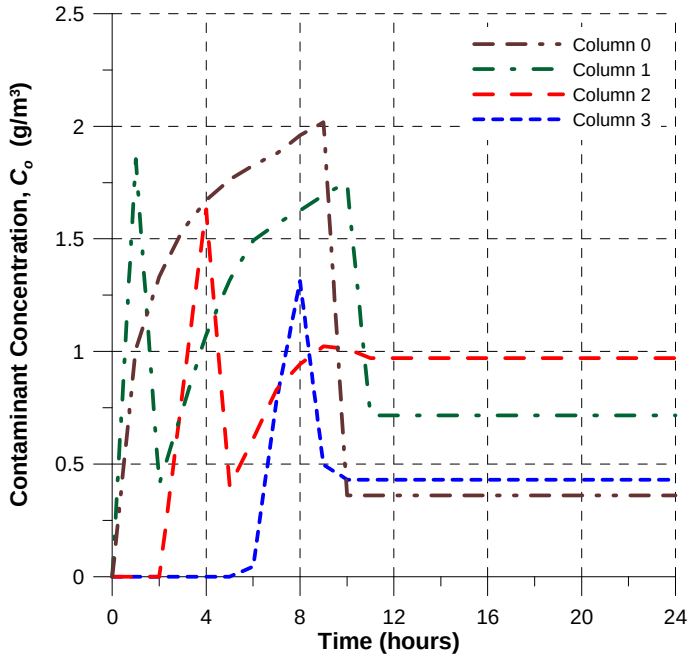

Figure 7.6: Contaminant concentration in the overland flow for the daily simulation of border irrigation. (Const. Plant)

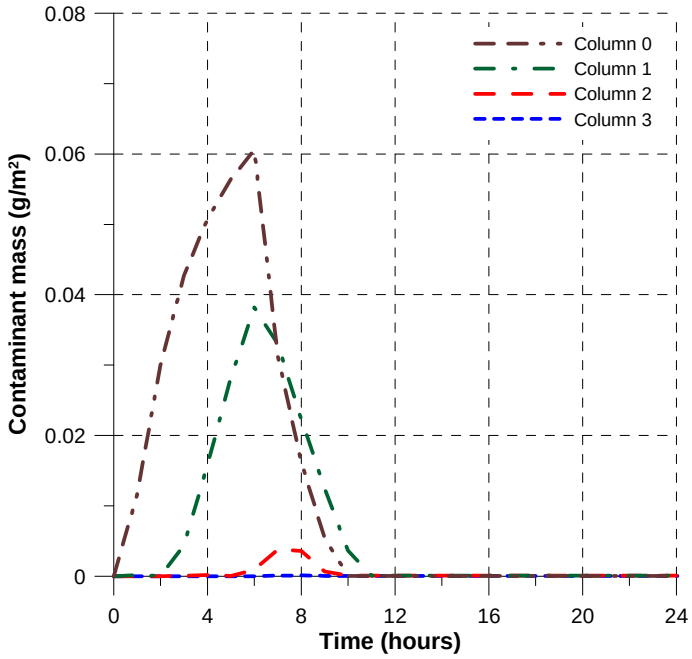

Figure 7.7: Contaminant mass in the overland flow for the daily simulation of border irrigation. (Const. Plant)

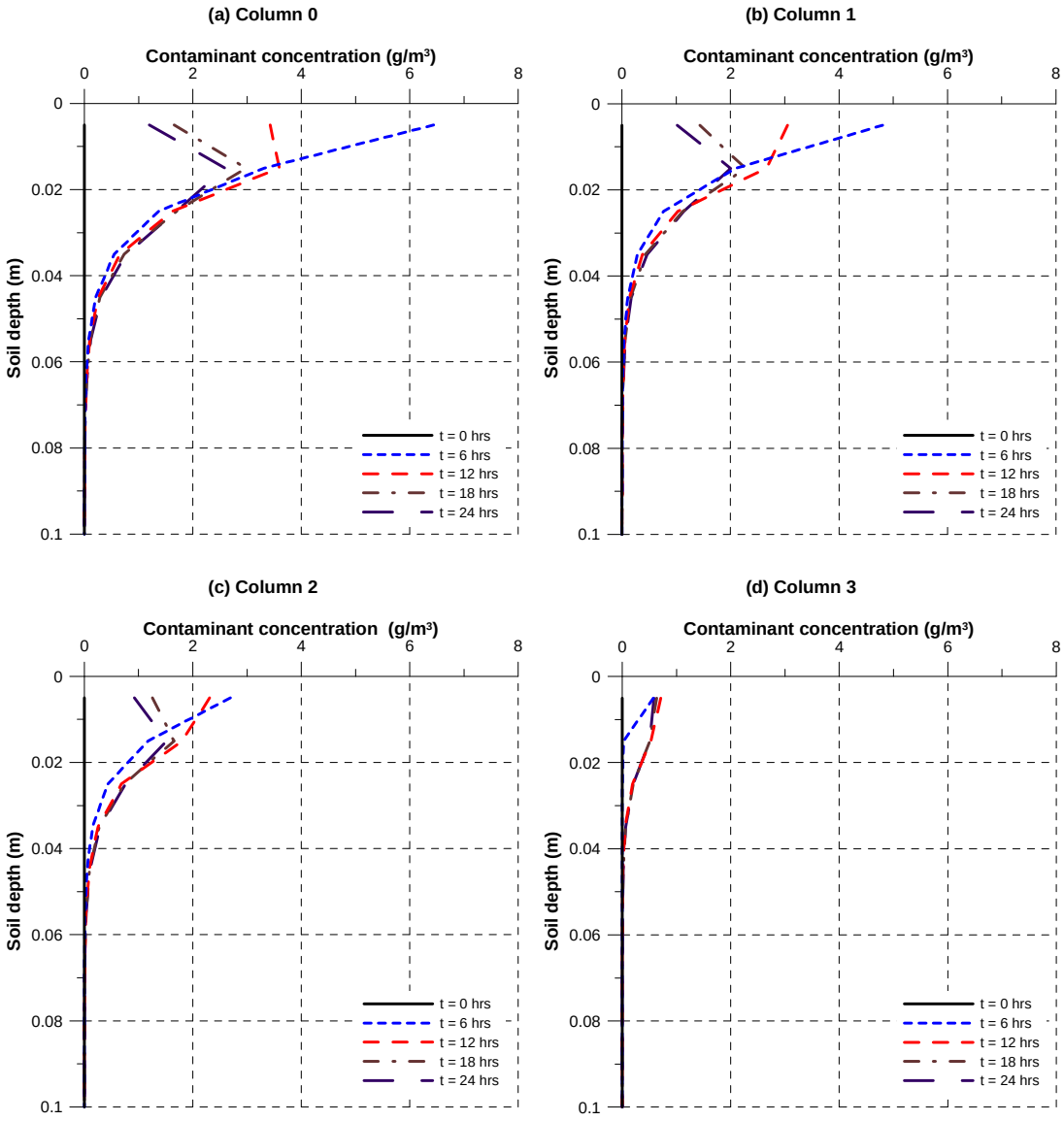

Figure 7.8: Contaminant concentration profiles within the soil columns for the daily simulation of border irrigation. (No Plant)

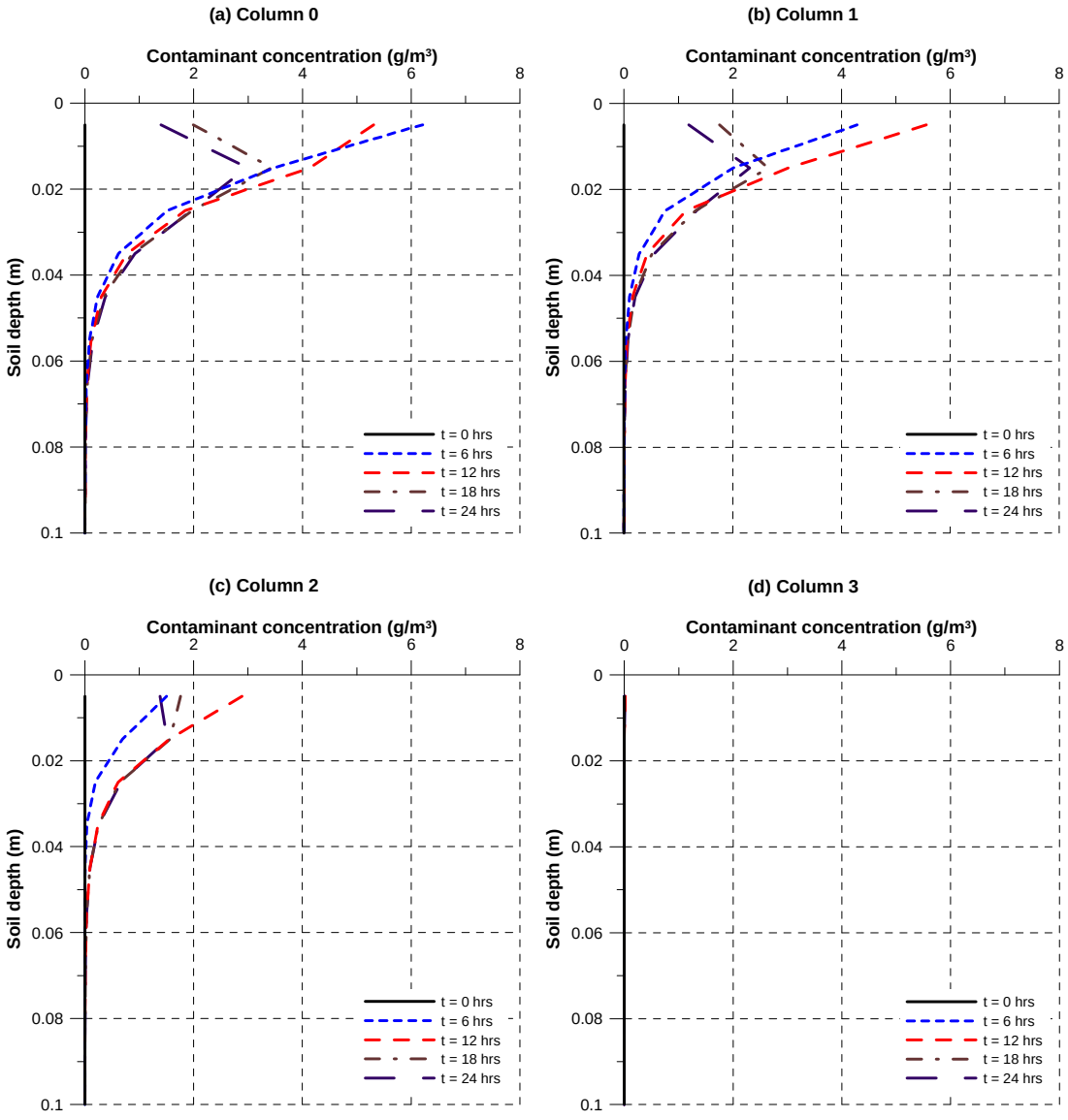

Figure 7.9: Contaminant concentration profiles within the soil columns for the daily simulation of border irrigation. (Const. Plant)

The daily simulation results for sprinkler irrigation are given in Figures 7.10-7.15. In the sprinkler irrigation simulations the contaminant is introduced over columns 0 and 1 homogeneously. The variation of the contaminant mass with time follows the same trend as the corresponding overland flow depth variation with time for the No Plant simulation (Figures 7.11 and 6.17). For the Const. Plant simulation, no overland flow is developed, therefore the contaminant is not distributed to columns 2 and 3 and accumulates on columns 1 and 2 (Figure 7.13) and then percolates into the soil columns. When the concentration profiles within the soil columns are compared for the No Plant and the Const. Plant simulations (Figures 7.14 and 7.15), it can be seen that higher concentrations are reached during the Const. Plant simulations due to overland contaminant accumulation. On the other hand, the contamination does not reach into as deep layers as it does in the No Plant simulation due to decreased infiltration rate as a result of interception of the irrigation water by the plant cover.

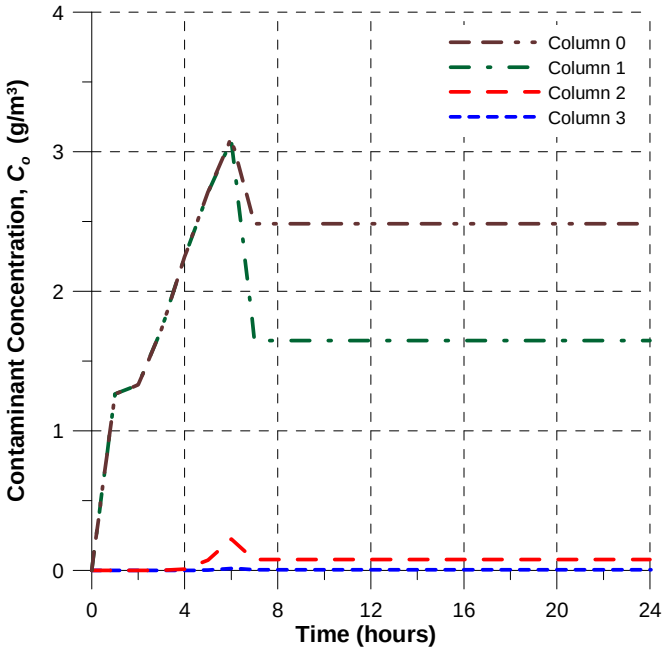

Figure 7.10: Contaminant concentration in the overland flow for the daily simulation of sprinkler irrigation. (No Plant)

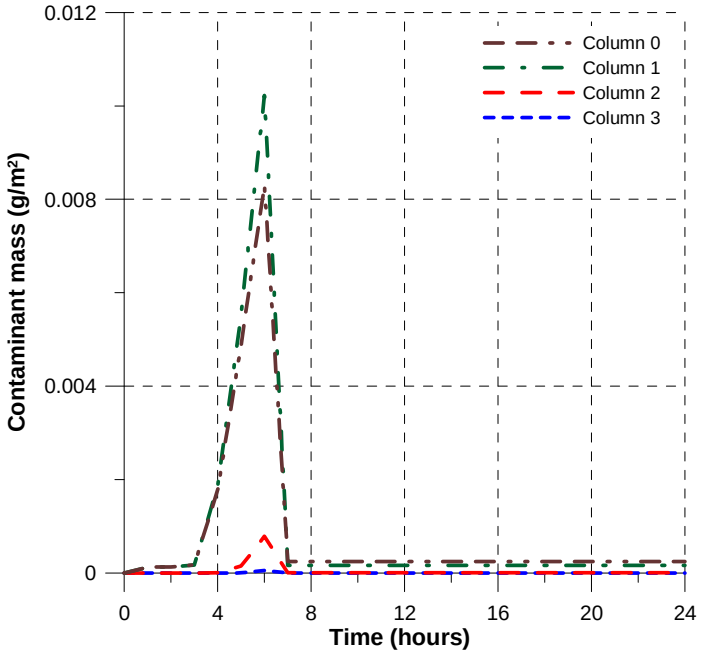

Figure 7.11: Contaminant mass in the overland flow for the daily simulation of sprinkler irrigation. (No Plant)

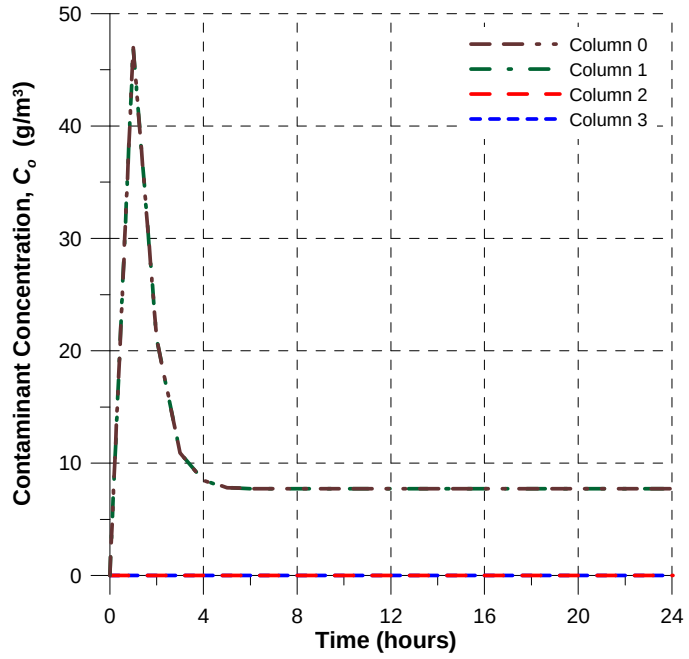

Figure 7.12: Contaminant concentration in the overland flow for the daily simulation of sprinkler irrigation. (Const. Plant)

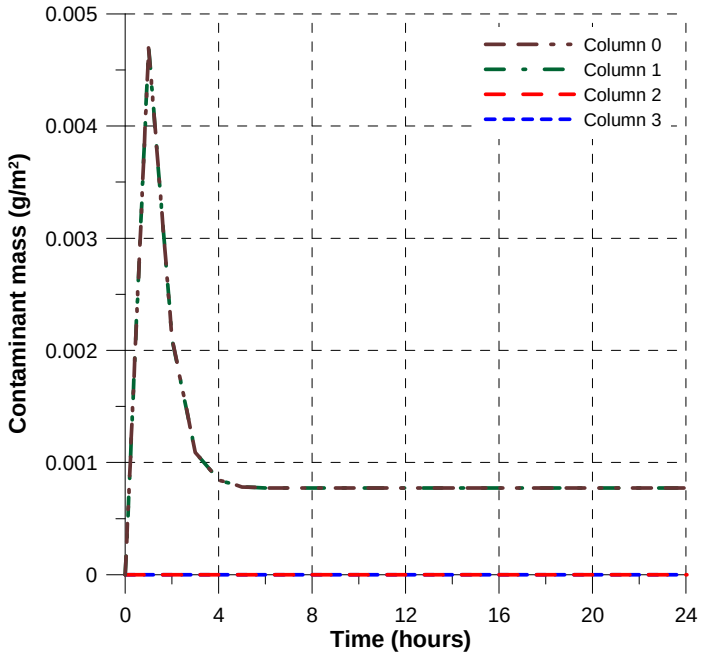

Figure 7.13: Contaminant mass in the overland flow for the daily simulation of sprinkler irrigation. (Const. Plant)

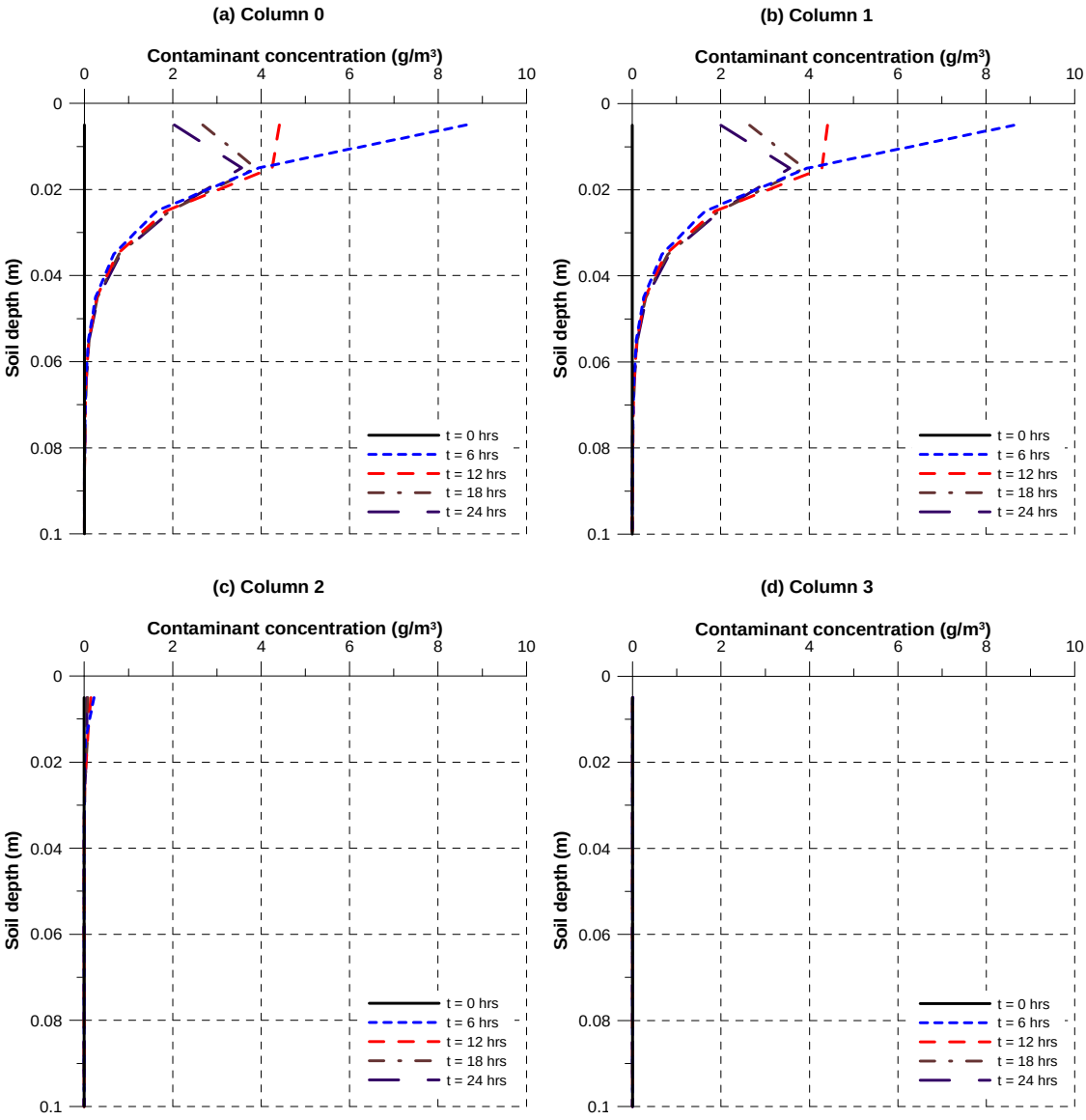

Figure 7.14: Contaminant concentration profiles within the soil columns for the daily simulation of sprinkler irrigation. (No Plant)

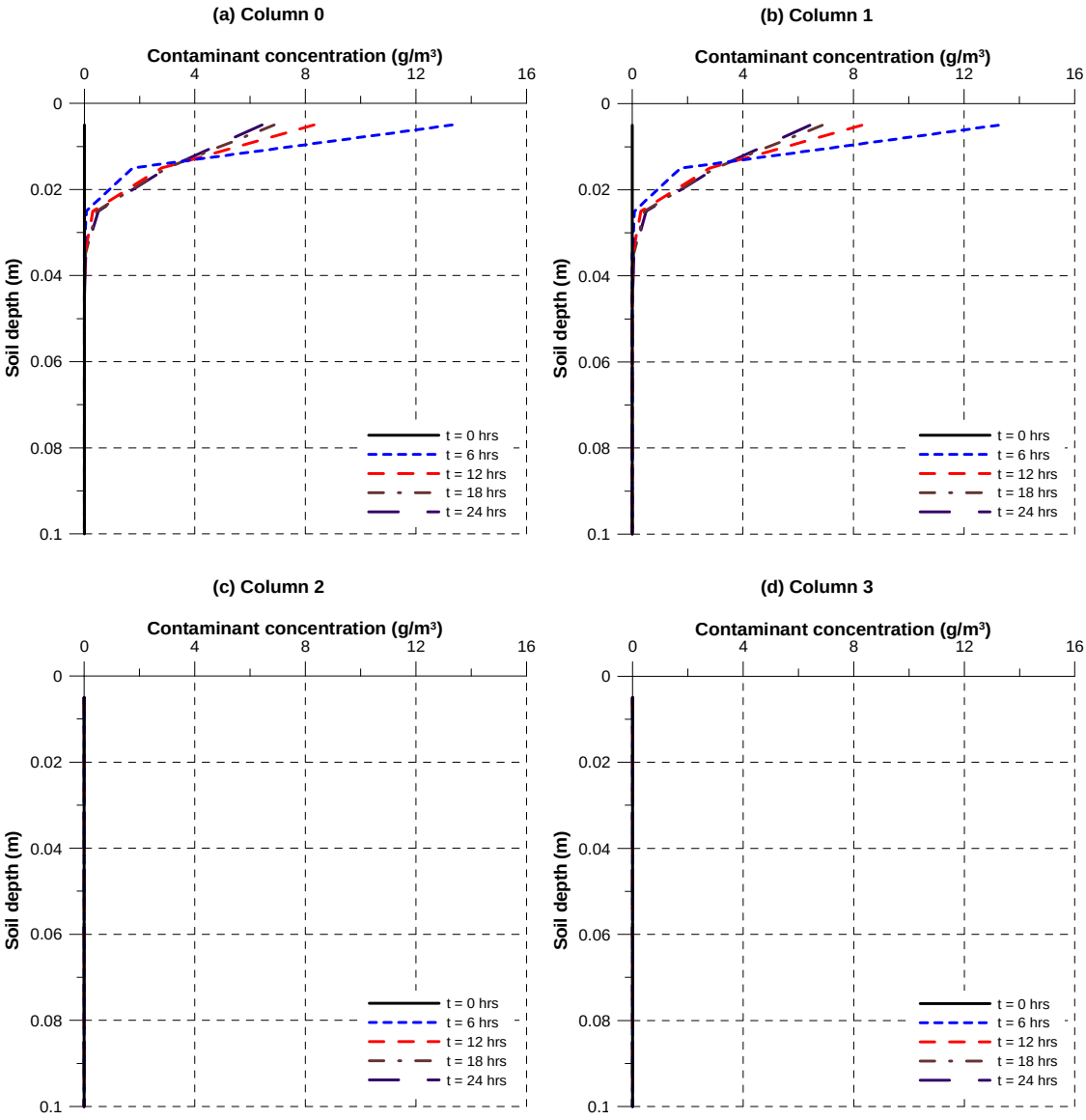

Figure 7.15: Contaminant concentration profiles within the soil columns for the daily simulation of sprinkler irrigation. (Const. Plant)

7.3.3.2 Seasonal Simulations

The seasonal simulation results for border irrigation are given in Figures 7.16-7.26. The variation with time of the contaminant mass in the overland flow is shown in Figures 7.16, 7.17, and 7.18 for the No Plant, Const. Plant and Plant simulations, respectively. The spikes in these figures correspond to the irrigation events. Other than on day 1, the irrigation flows are contaminant-free. However, as the overland flow develops and infiltrates during the irrigation events, it gets contaminated through its interaction with contaminated soil. The level of contamination of the overland flow due to this process decreases with time as the contaminant at the soil surface is removed by the processes of percolation, decay, and volatilization. The spikes of overland flow contaminant mass reach slightly higher values during the Const. Plant simulations (Figure 7.17) compared to the No Plant and Plant simulations. This can be explained by the slightly higher contaminant accumulation over columns 0, 1 and 2 during the Const. Plant simulation due to impeded runoff and decreased evaporation in the presence of plants. This is also confirmed by the snapshots of concentration profiles within the soil columns as given with 20-day intervals through Figures 7.19-7.24.

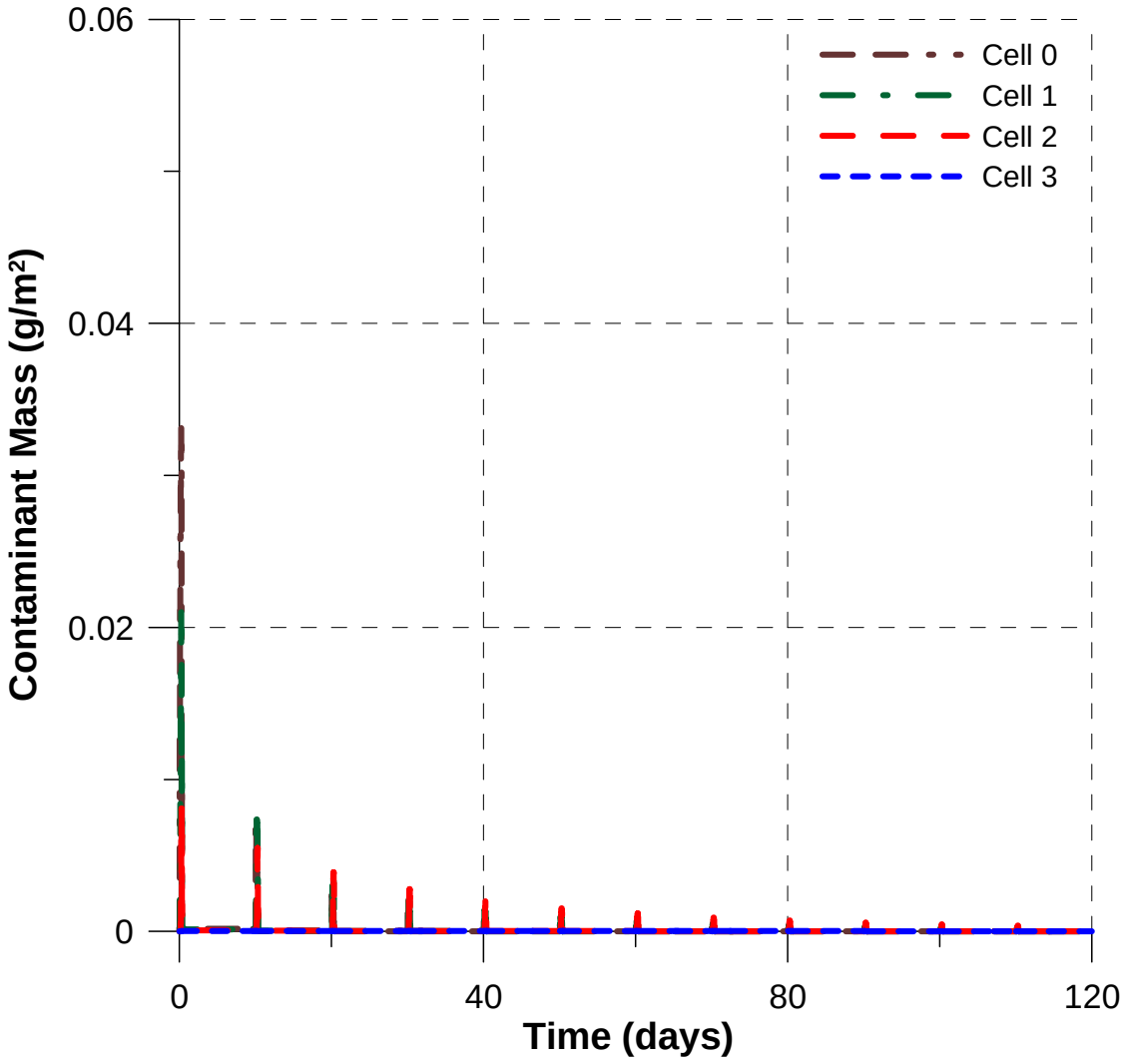

Figure 7.16: Contaminant mass in the overland flow for the seasonal simulation of border irrigation. (No Plant)

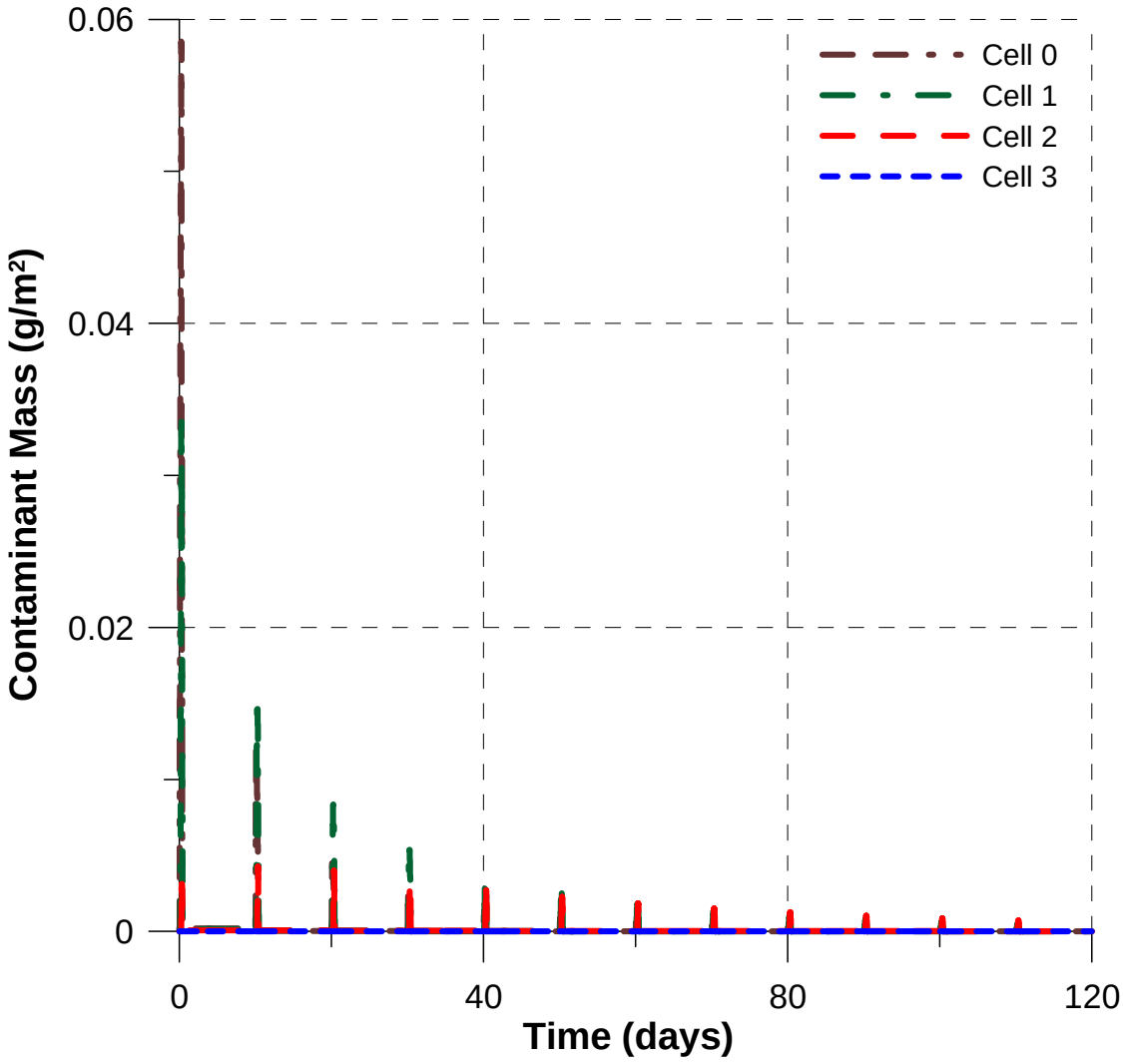

Figure 7.17: Contaminant mass in the overland flow for the seasonal simulation of border irrigation. (Const. Plant)

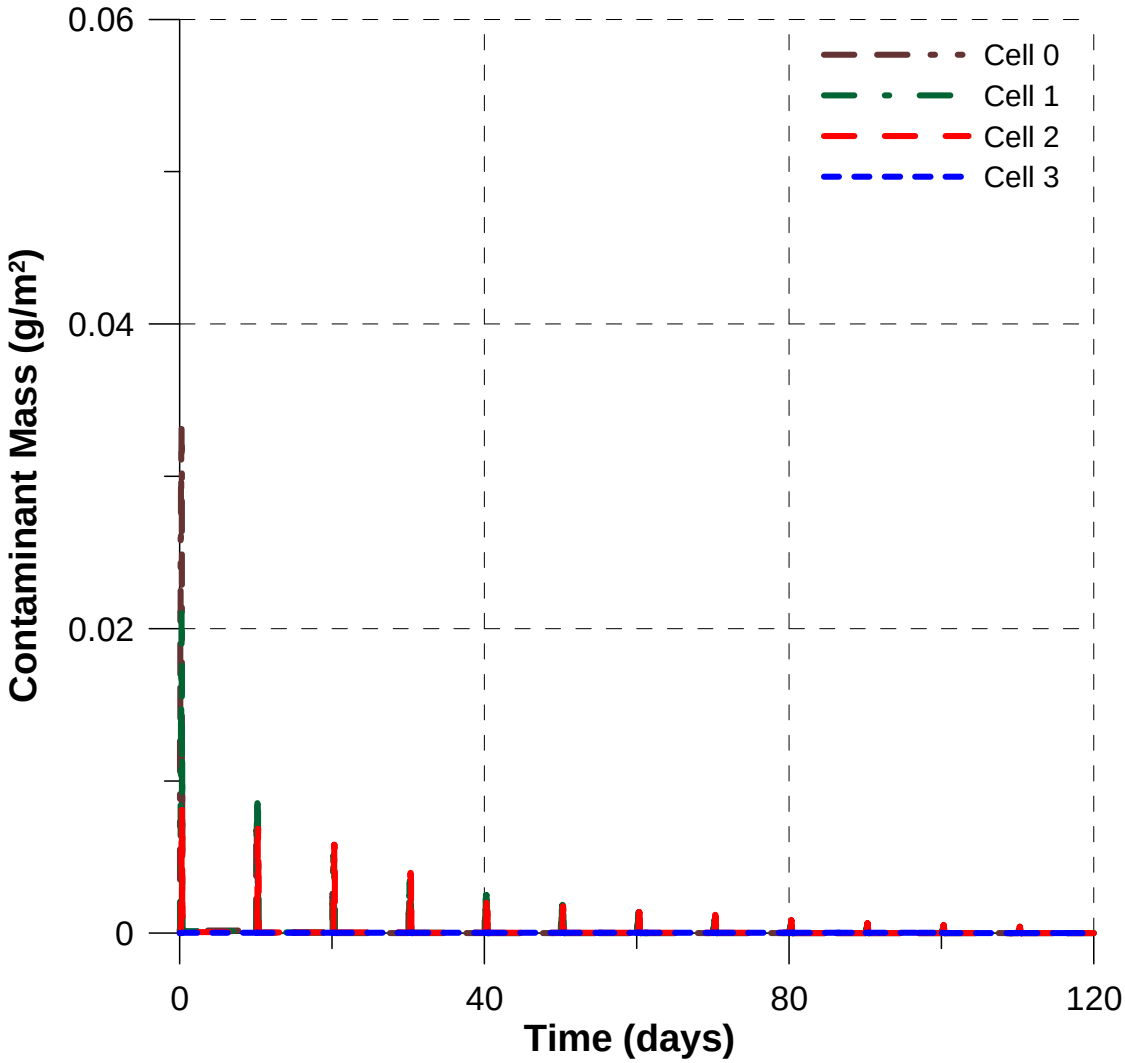

Figure 7.18: Contaminant mass in the overland flow for the seasonal simulation of border irrigation. (Plant)

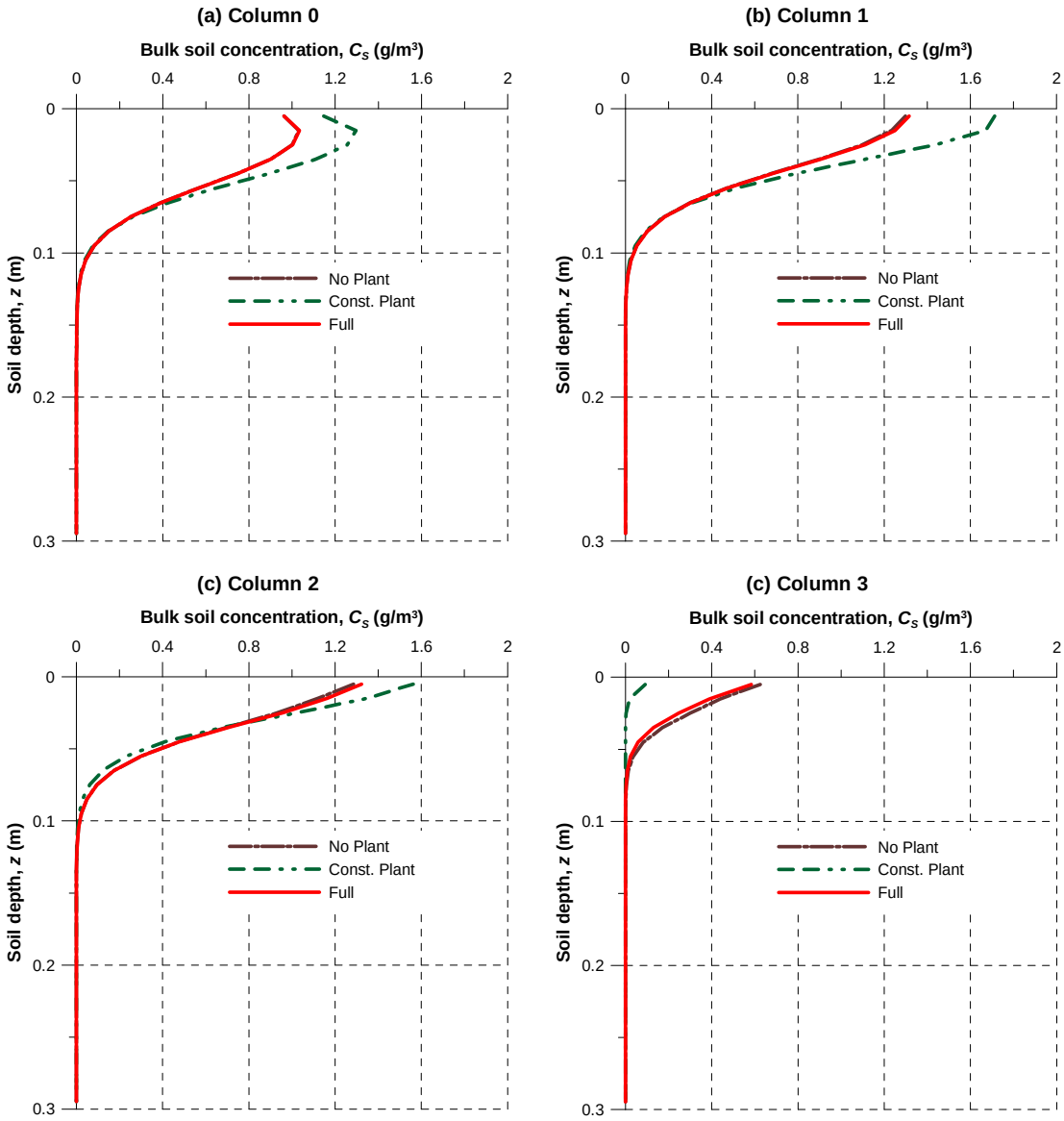

Figure 7.19: Contaminant concentration profiles within the soil columns for the seasonal simulation of border irrigation. (day = 20)

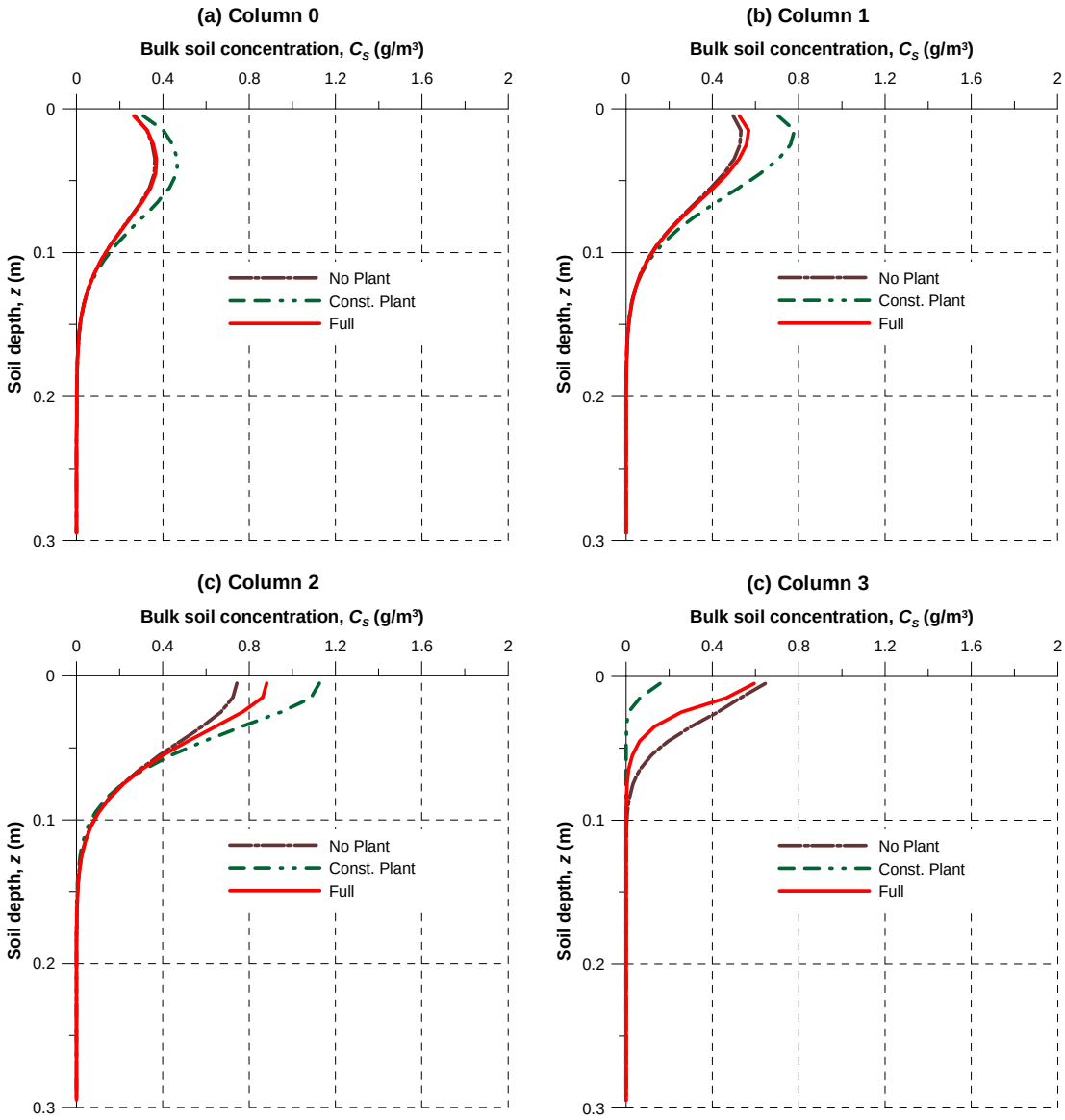

Figure 7.20: Contaminant concentration profiles within the soil columns for the seasonal simulation of border irrigation. (day = 40)

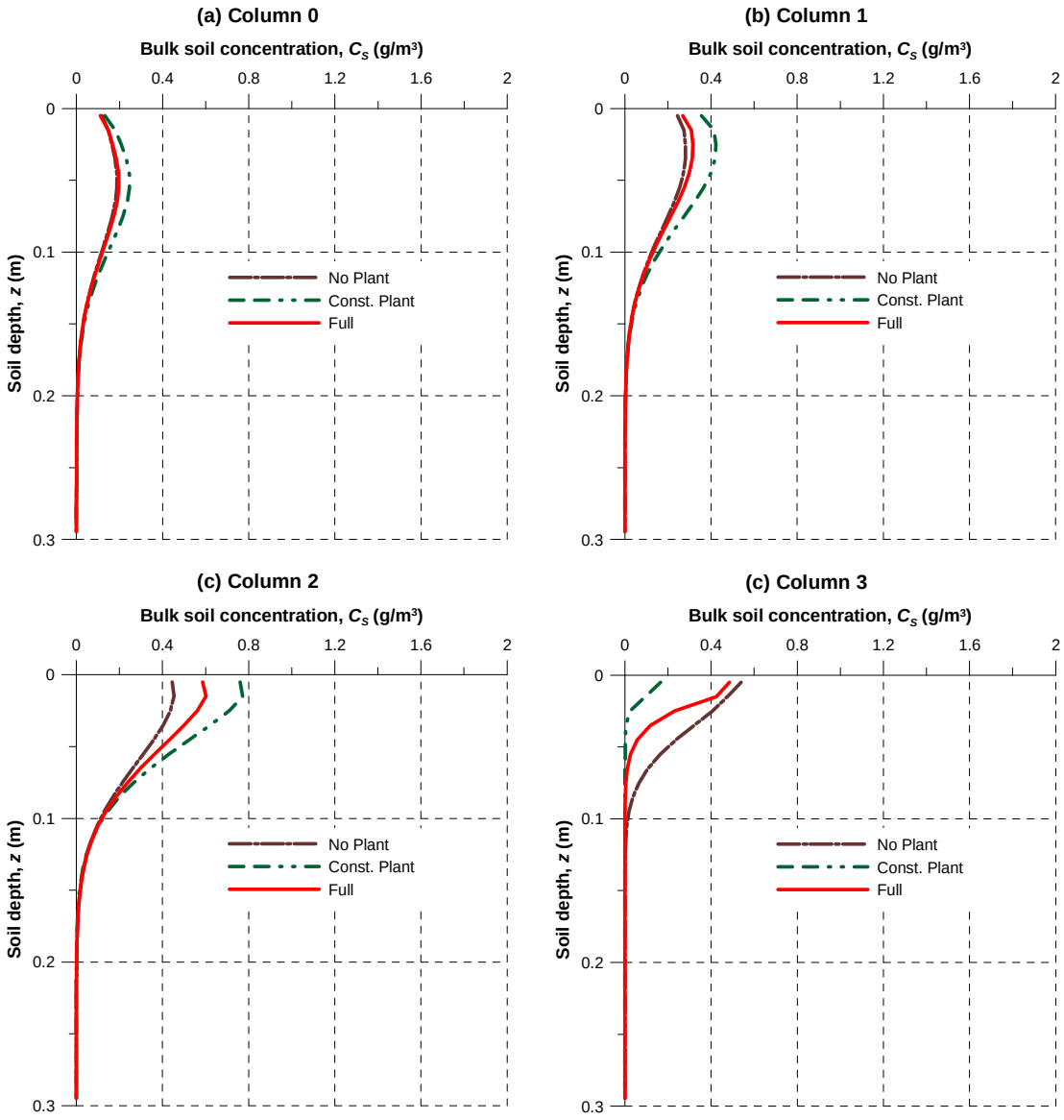

Figure 7.21: Contaminant concentration profiles within the soil columns for the seasonal simulation of border irrigation. (day = 60)

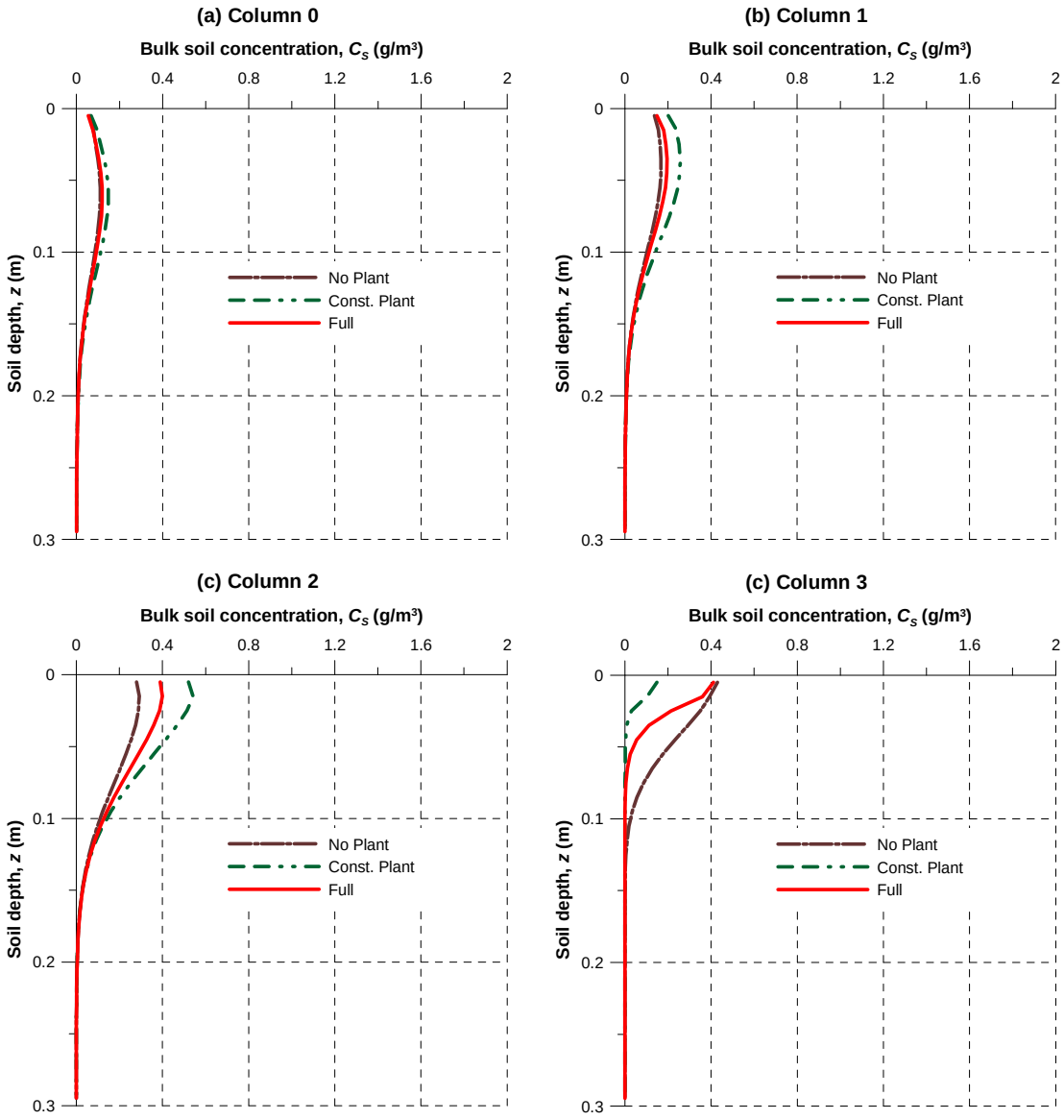

Figure 7.22: Contaminant concentration profiles within the soil columns for the seasonal simulation of border irrigation. (day = 80)

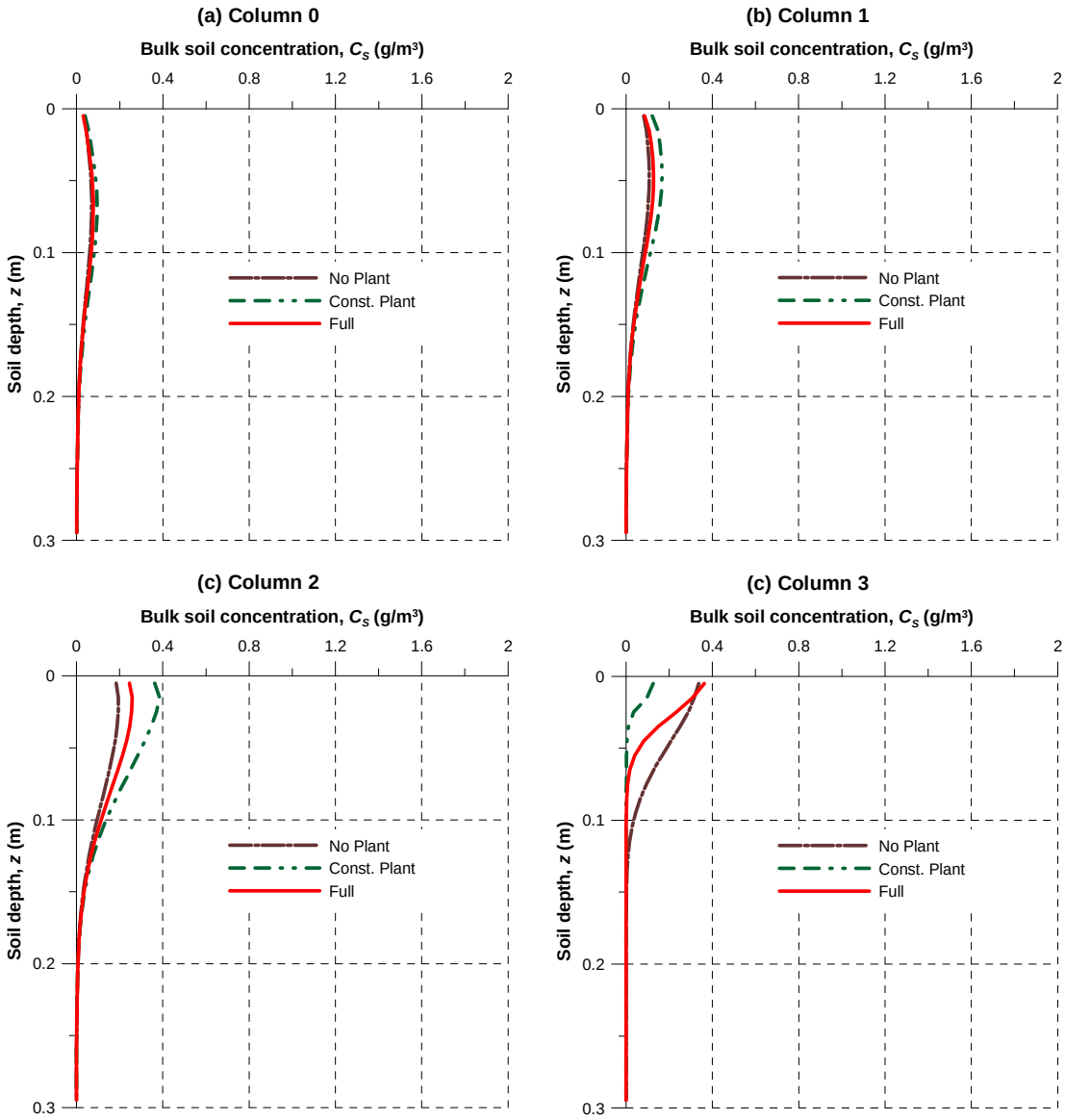

Figure 7.23: Contaminant concentration profiles within the soil columns for the seasonal simulation of border irrigation. (day = 100)

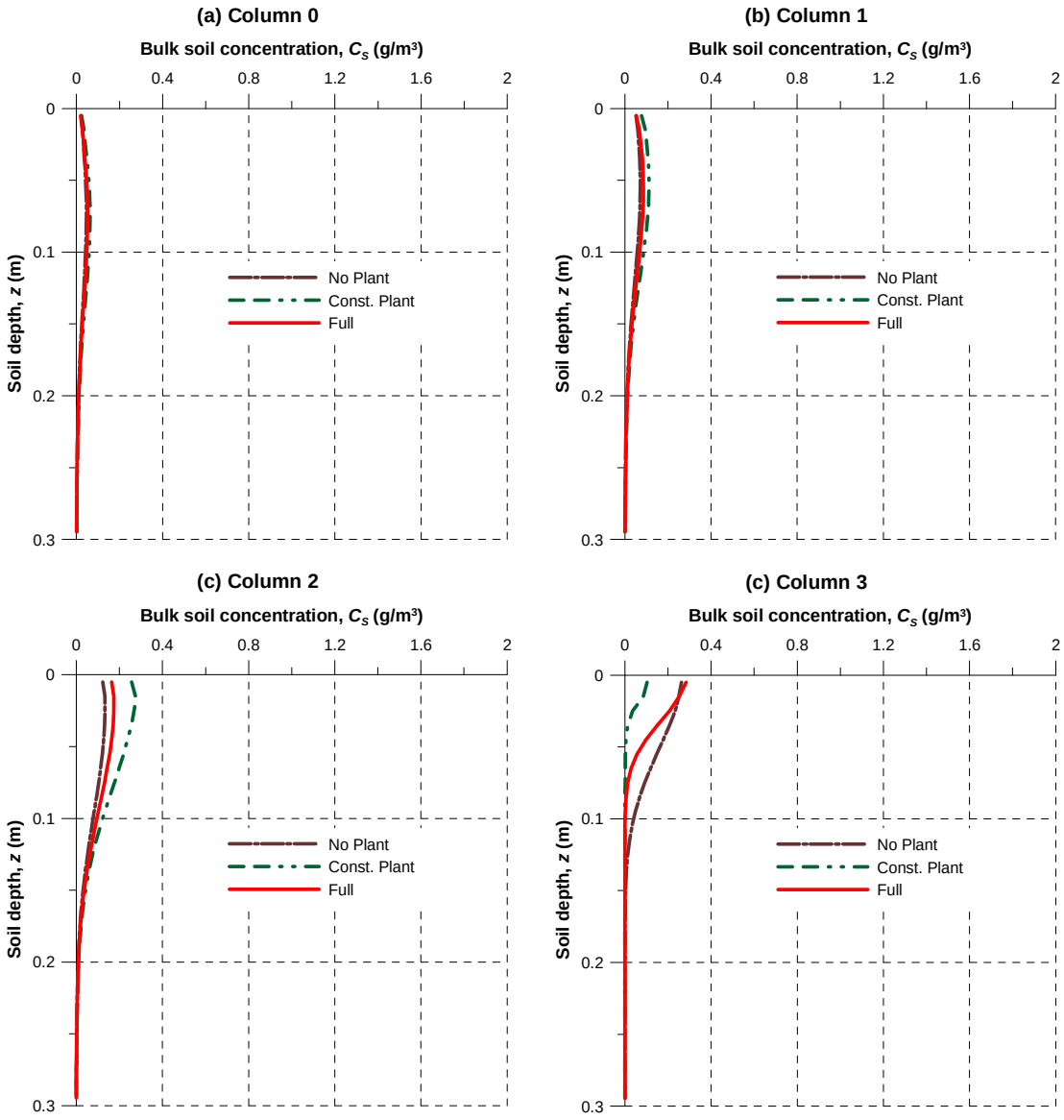

Figure 7.24: Contaminant concentration profiles within the soil columns for the seasonal simulation of border irrigation. (day = 120)

It is seen that the most downstream column (column 3) is the least contaminated column in all the simulations (Figures 7.19d, 7.20d, 7.21d, 7.22d, 7.23d, 7.24d). It is contaminated to an even lesser degree during the Const. Simulation compared to the others since the contaminant has been accumulated in the upstream columns before it could reach down to this column by transport through runoff. Another interesting point is that the soil surface concentration change is negligible for column 3 through Figures 7.19-7.24 although it is decreasing in other columns as time progresses. This is due to the fact that column 3 receives a small but continuous amount of contaminant through runoff that has originated from the upstream soil columns.

The plant biomass simulation results are given in Figure 7.25. It is seen that in columns 0, 1 and 2, biomass increase is smooth and continuous since a constant solar radiation value is applied throughout the simulation and the plants in these columns do not experience water stress as it was demonstrated in the *LAI* simulation results in Figure 6.28 in the previous chapter. On the other hand, the effect of water stress on the growth of the plant in column 3 is demonstrated in Figure 7.25d. The decrease in plant biomass in column 2 is due to senescence. The thermal time when hay reaches maturation is much less than the thermal time required for corn (1020 °C vs 1925 °C) (Table 6.3). Thus, in this simulation hay reaches its maturation on day 51 and litterfall should start. The original biomass simulation model does not model litterfall. In this example application, litterfall rate for hay was estimated by decreasing the biomass value proportional to the decrease in the *LAI* value as simulated by the *LAI* model, after the thermal time for maturation is reached.

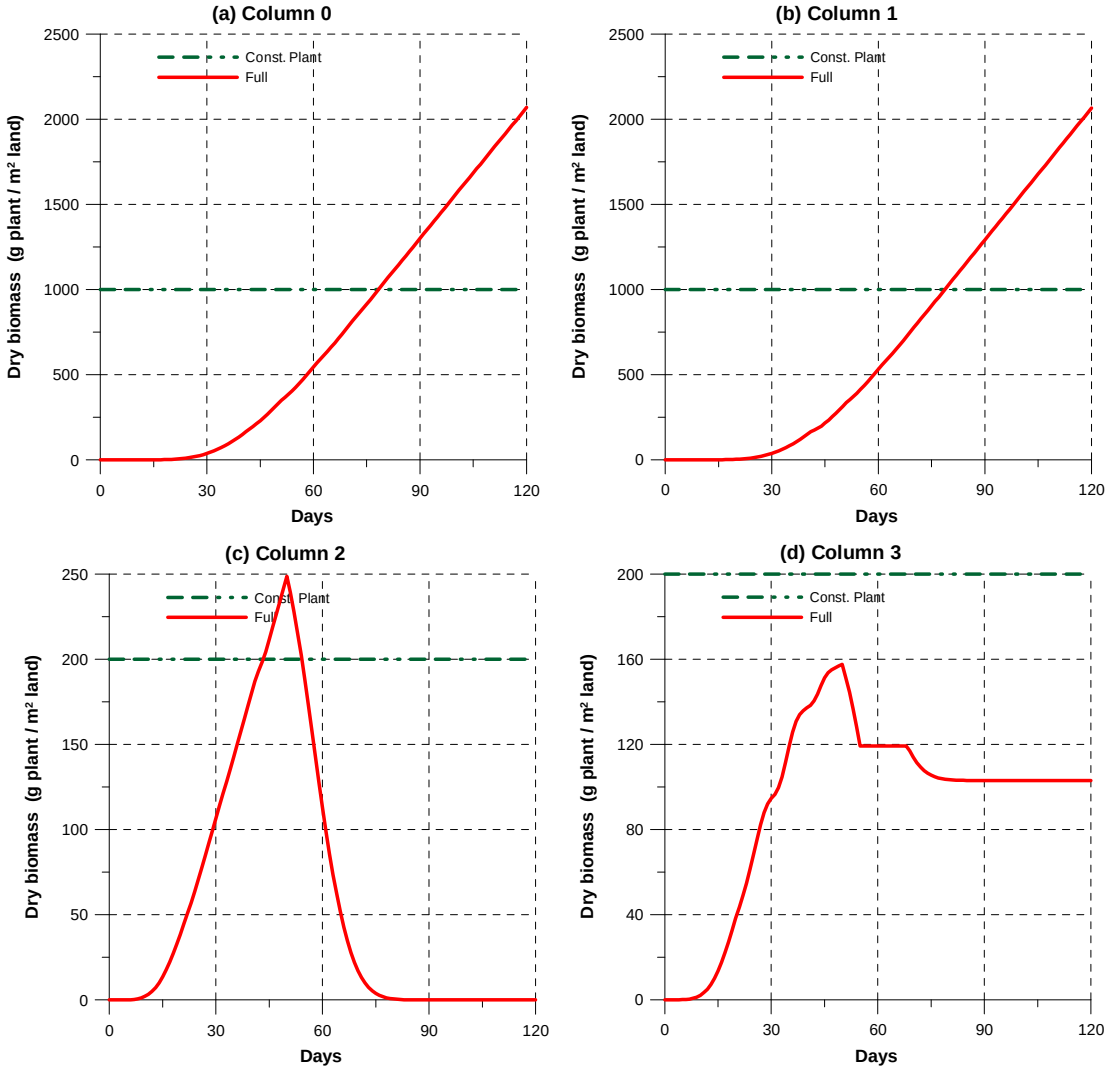

Figure 7.25: Plant biomass simulation results for the seasonal simulation of border irrigation. (Columns 0 and 1: corn, Columns 2 and 3: hay)

The variation with time of the contaminant concentration within the plant for different simulations is shown in Figure 7.26. It is seen that higher values are reached in the Const. Plant simulations in all columns except column 3. This is due to the fact that, in Const. Plant simulations, plants are already present when the contaminant is released at the beginning of the simulation. Therefore, they are exposed to the highest amount of contamination during the early periods of the simulations and the contaminant concentration within the plant rapidly increases. On the other hand, the Plant simulations start with zero plant biomass and zero root uptake values, and the root uptake rates only gradually increase as the plants grow. In these simulations, the plants reach maturation only after the contaminant concentrations in the soil have decreased. The lower in-plant concentrations associated for column 3 during the Const. Plant simulation are due to the lesser contaminant availability in this column.

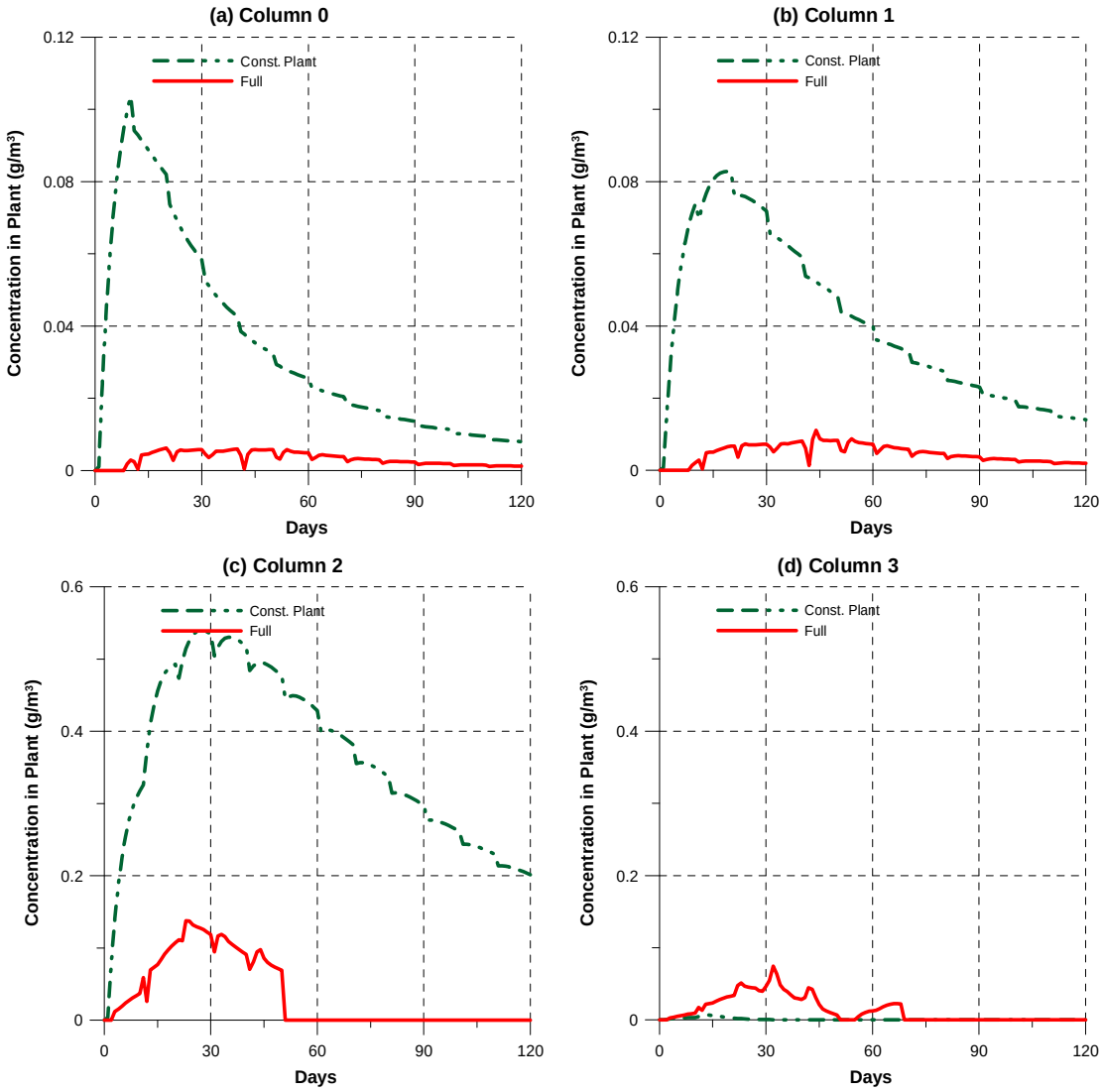

Figure 7.26: Contaminant concentration within the plant for the seasonal simulation of border irrigation. (Columns 0 and 1: corn, Columns 2 and 3: hay)

The seasonal simulation results for sprinkler irrigation are given in Figures 7.27-7.37. In the sprinkler irrigation simulations the contaminant is introduced over columns 0 and 1 homogeneously. The variation of the contaminant mass in the overland flow with time is shown in Figures 7.27, 7.28, and 7.29 for the No Plant, Const. Plant and Plant simulations, respectively. The spikes in these figures correspond to the irrigation events. As it was also seen in the results of the border irrigation simulations, the spikes of overland flow contaminant mass reach slightly higher values during the Const. Plant simulation (Figure 7.28) compared to the No Plant and Plant simulations. This is also consistent with the higher concentration values near the soil surface observed in Const. Plant simulation as shown in Figures 7.30-7.35 where the snapshots of concentration profiles within the soil columns are given with 20-day intervals. As it was discussed in the application section of the previous chapter (Section 6.3.3.2), in the sprinkler irrigation simulations negligible overland flow development is occurring (Figures 6.29-6.33). Therefore, the contaminant transfer to columns 3 and 4 is almost negligible in the sprinkler irrigation simulations (Figures 7.30-7.35).

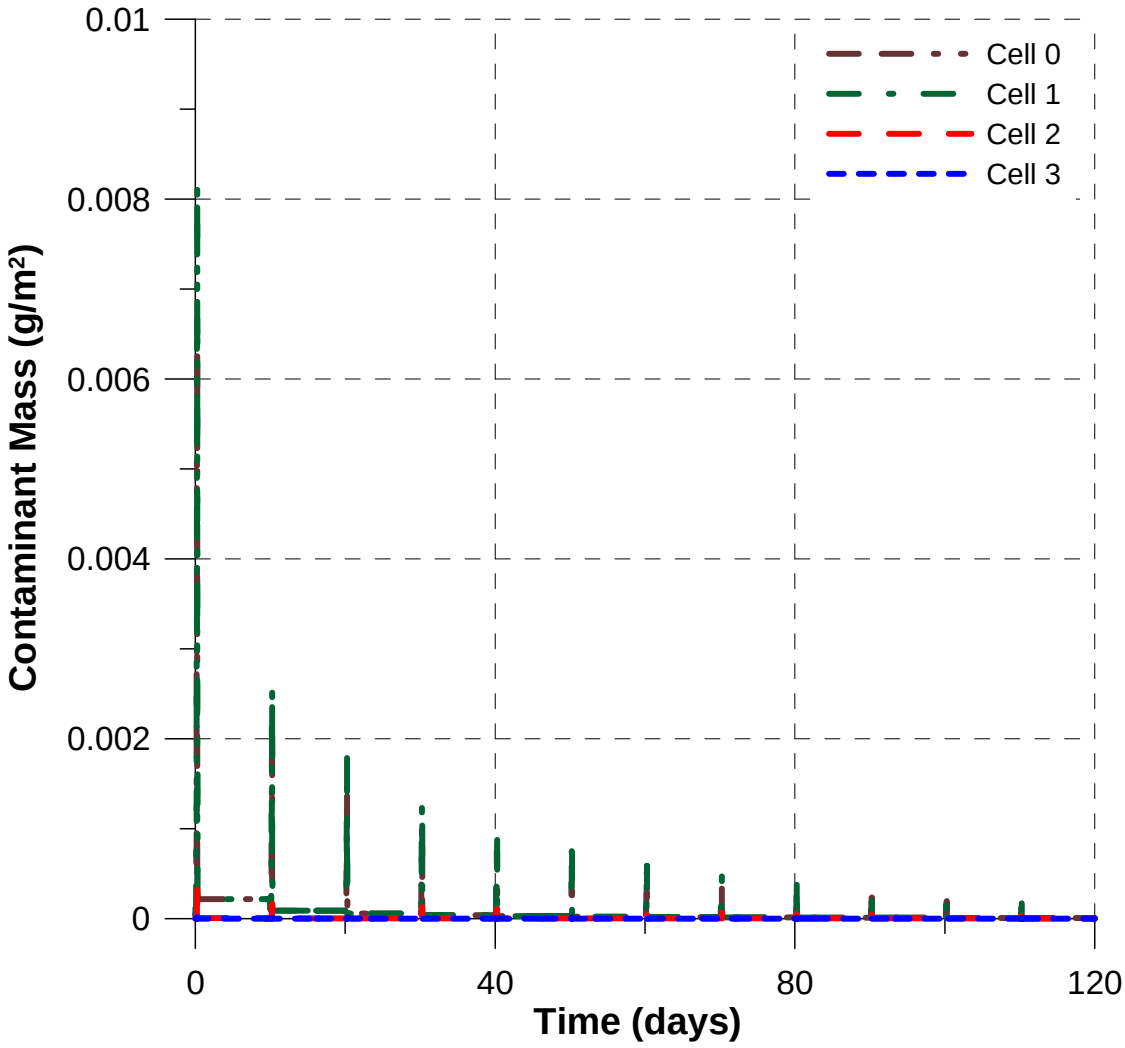

Figure 7.27: Contaminant mass in the overland flow for the seasonal simulation of sprinkler irrigation. (No Plant)

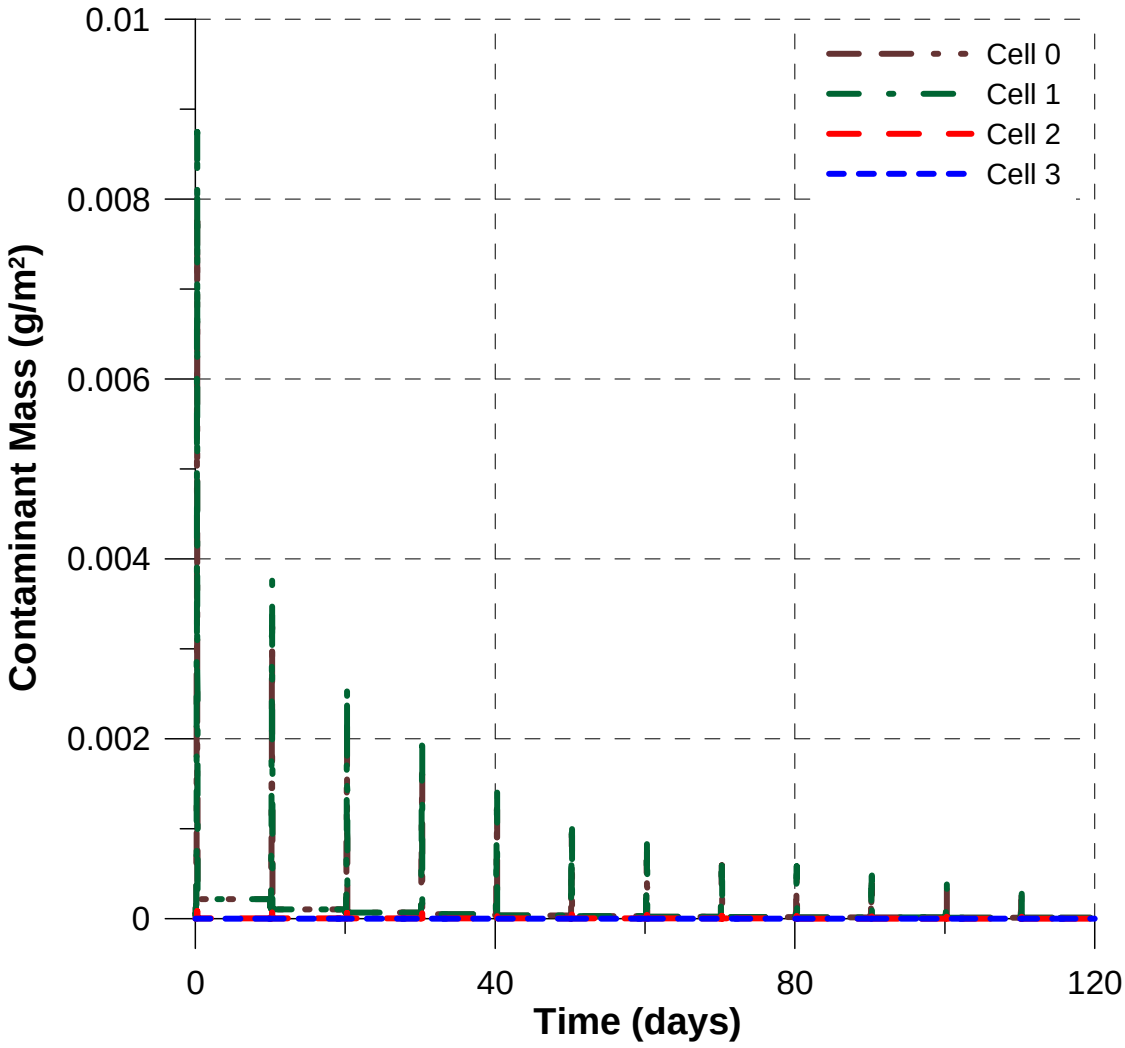

Figure 7.28: Contaminant mass in the overland flow for the seasonal simulation of sprinkler irrigation. (Const. Plant)

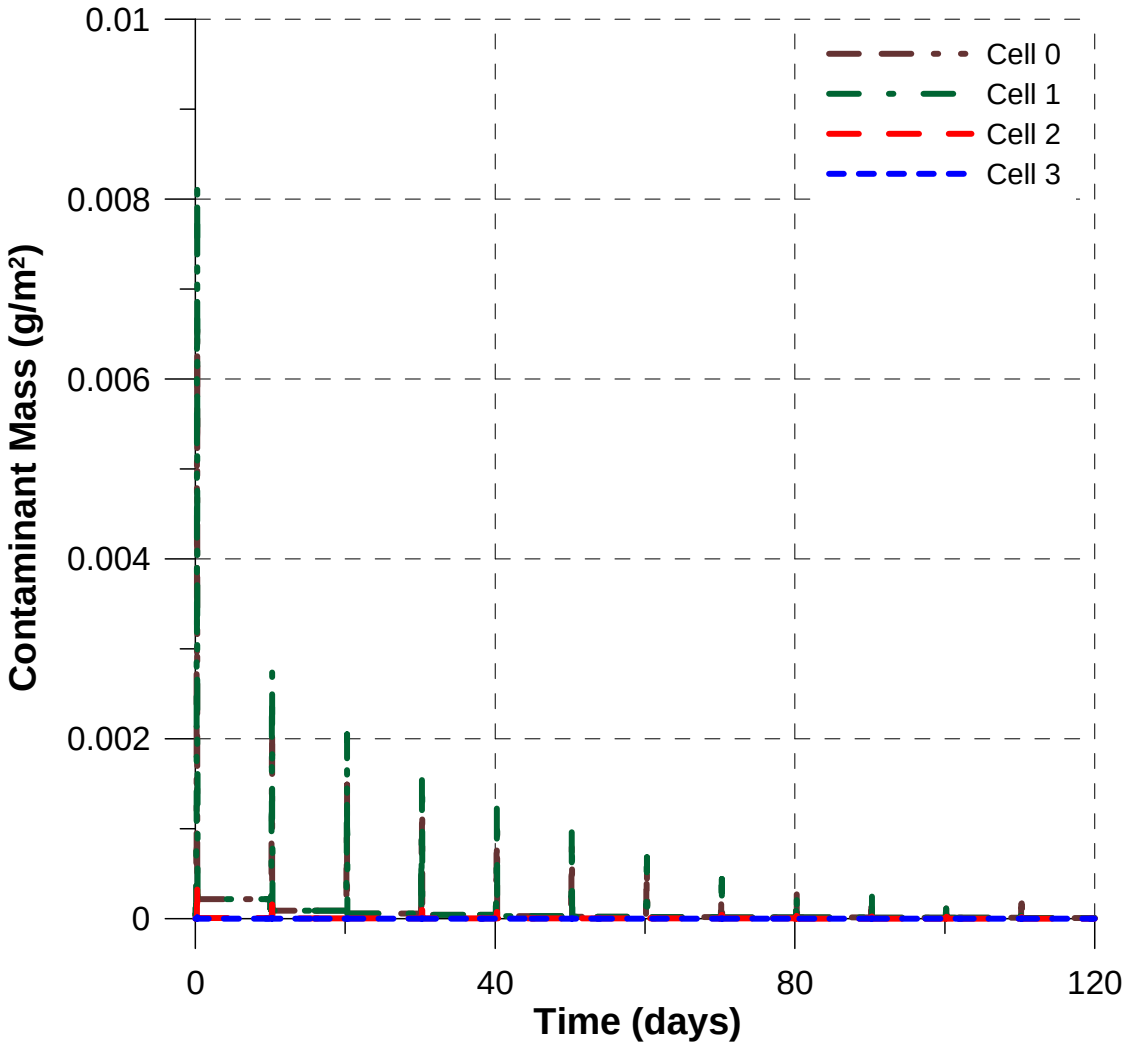

Figure 7.29: Contaminant mass in the overland flow for the seasonal simulation of sprinkler irrigation. (Plant)

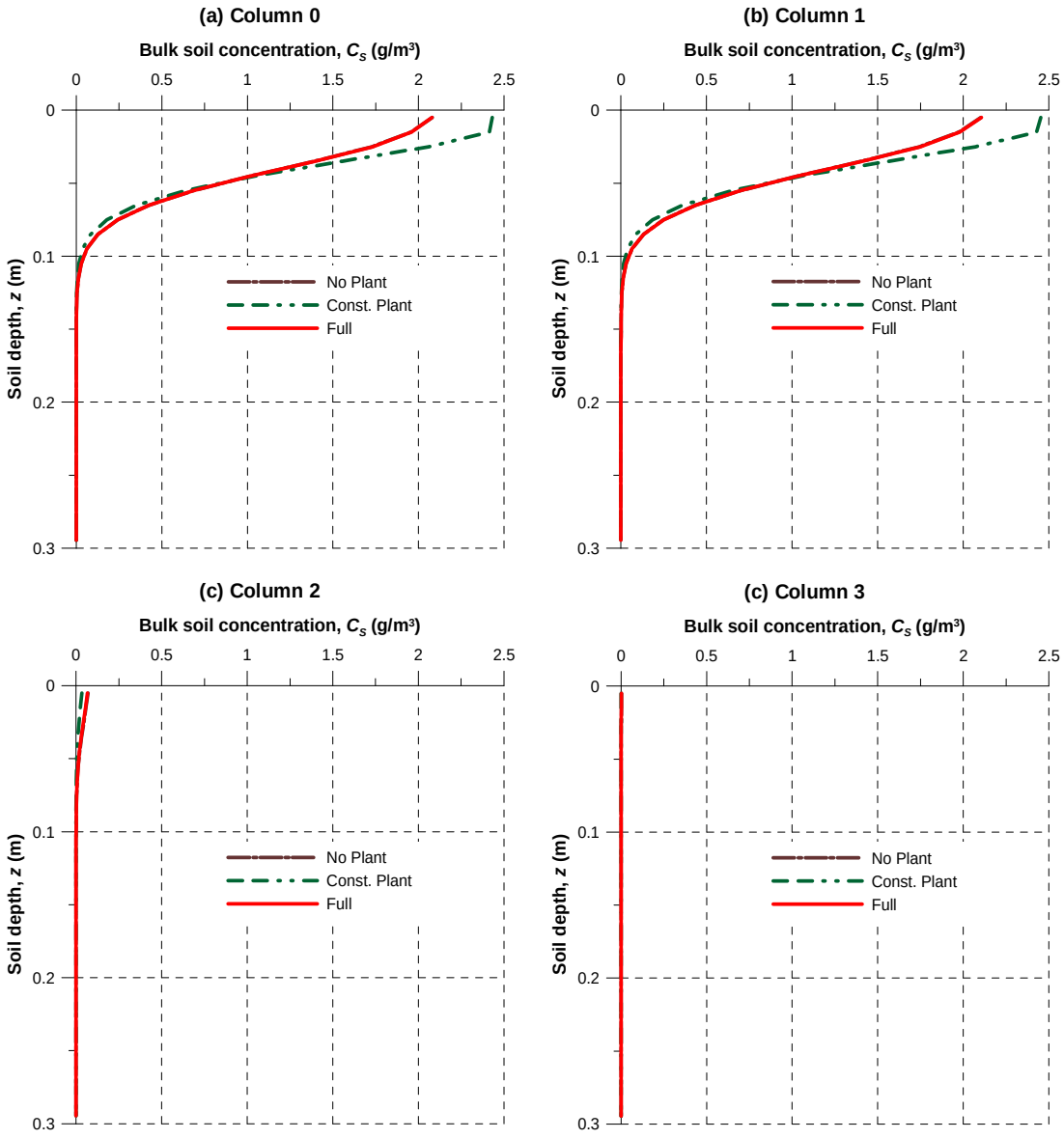

Figure 7.30: Contaminant concentration profiles within the soil columns for the seasonal simulation of sprinkler irrigation. (day = 20)

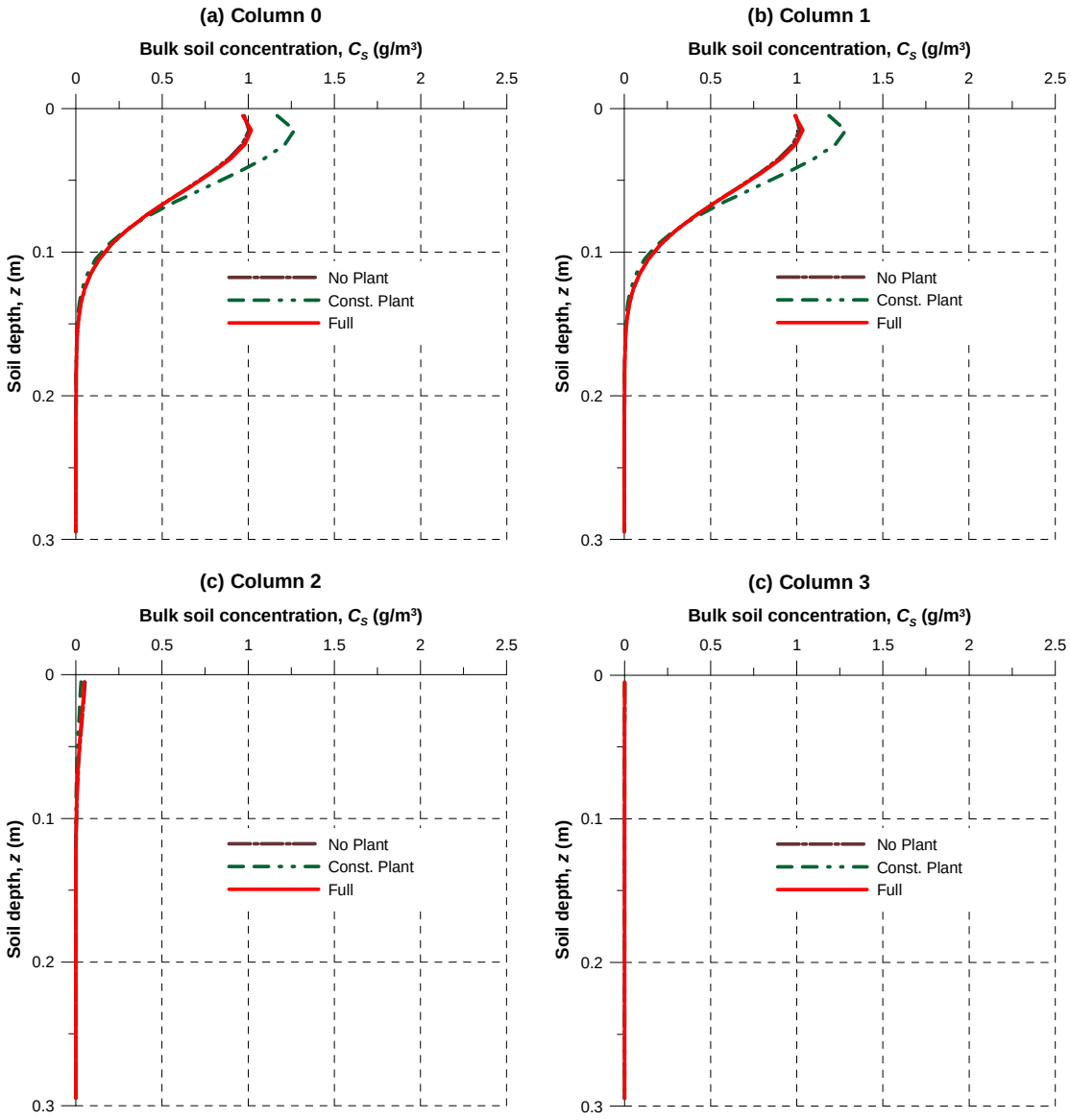

Figure 7.31: Contaminant concentration profiles within the soil columns for the seasonal simulation of sprinkler irrigation. (day = 40)

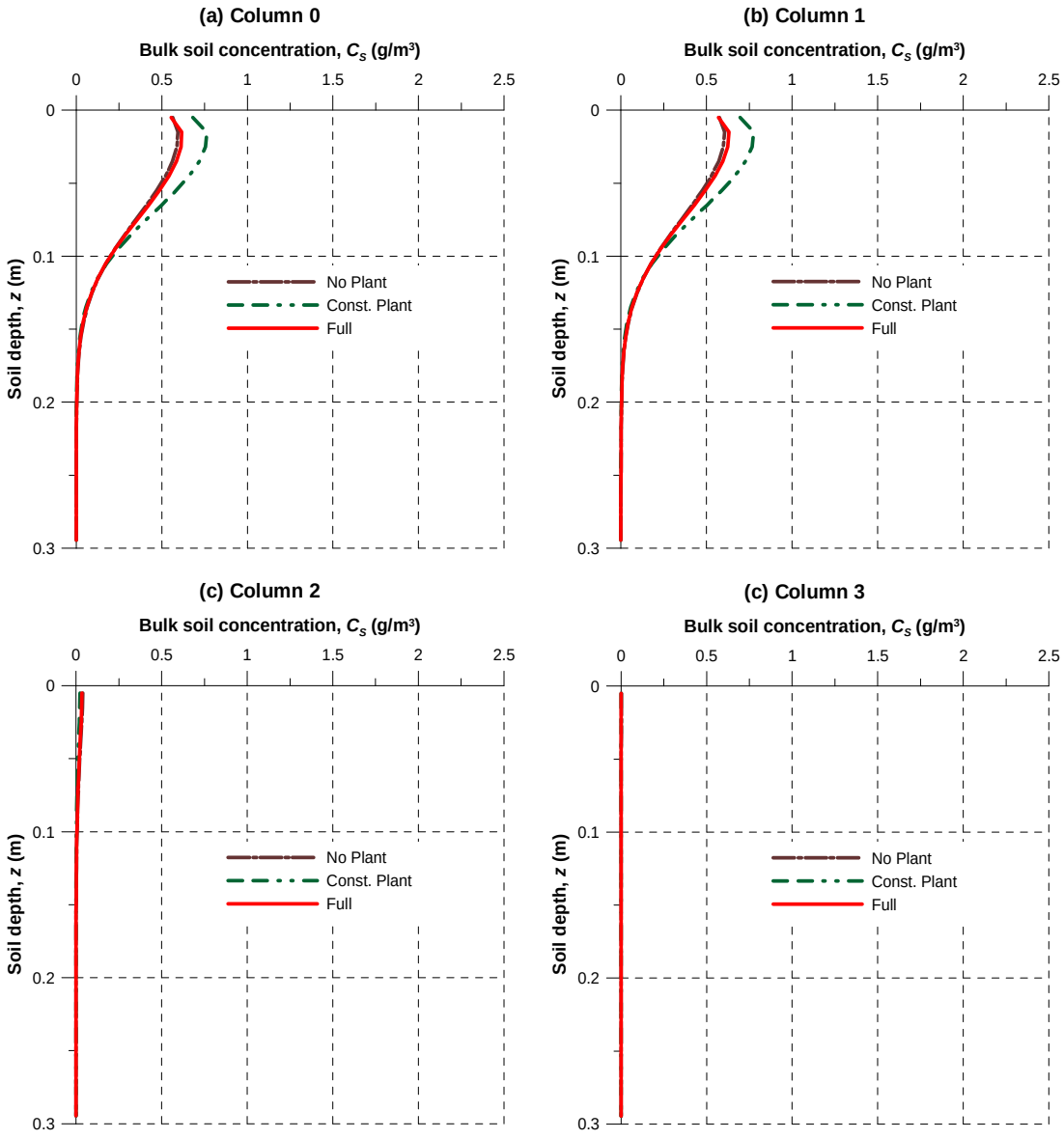

Figure 7.32: Contaminant concentration profiles within the soil columns for the seasonal simulation of sprinkler irrigation. (day = 60)

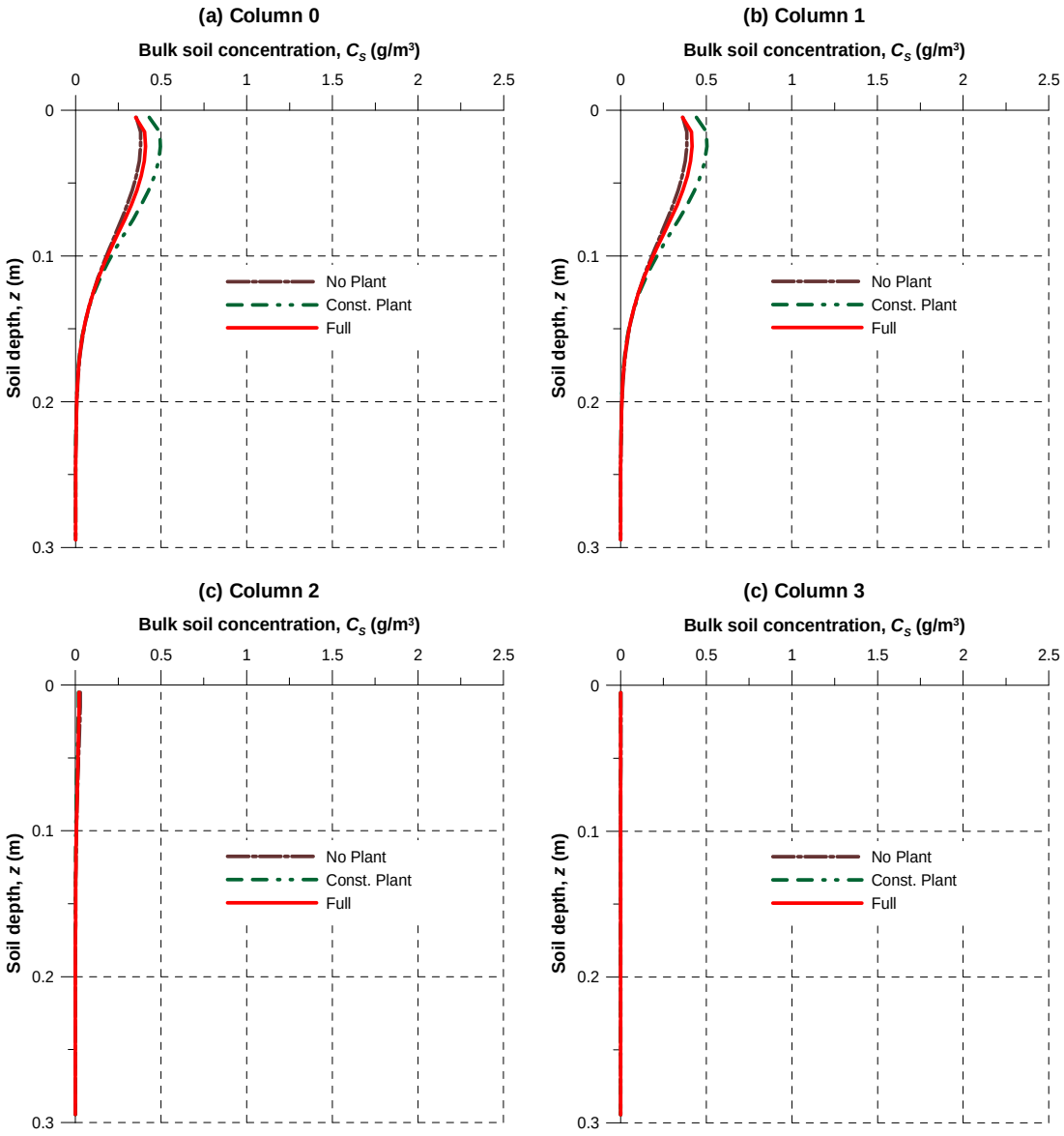

Figure 7.33: Contaminant concentration profiles within the soil columns for the seasonal simulation of sprinkler irrigation. (day = 80)

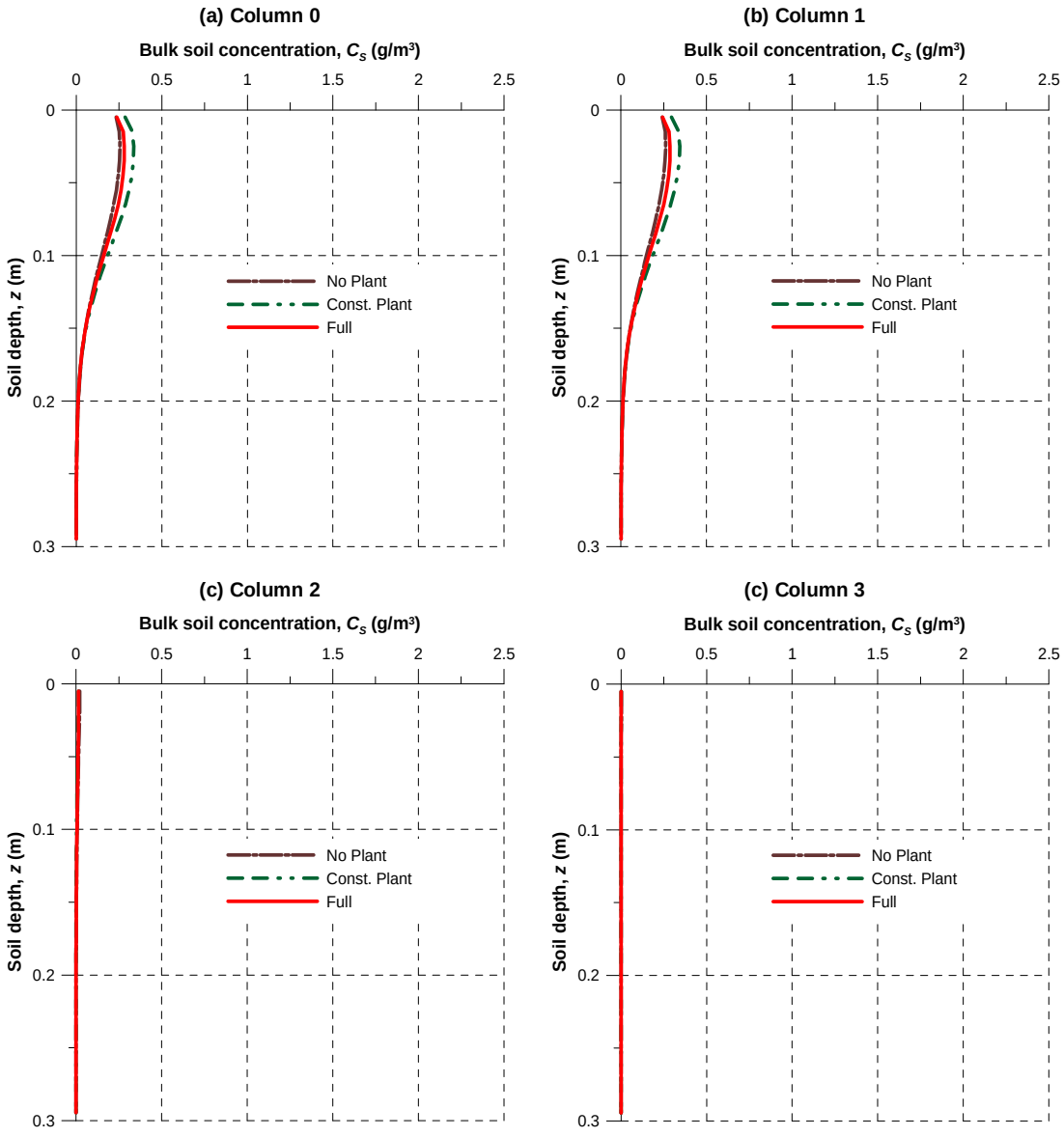

Figure 7.34: Contaminant concentration profiles within the soil columns for the seasonal simulation of sprinkler irrigation. (day = 100)

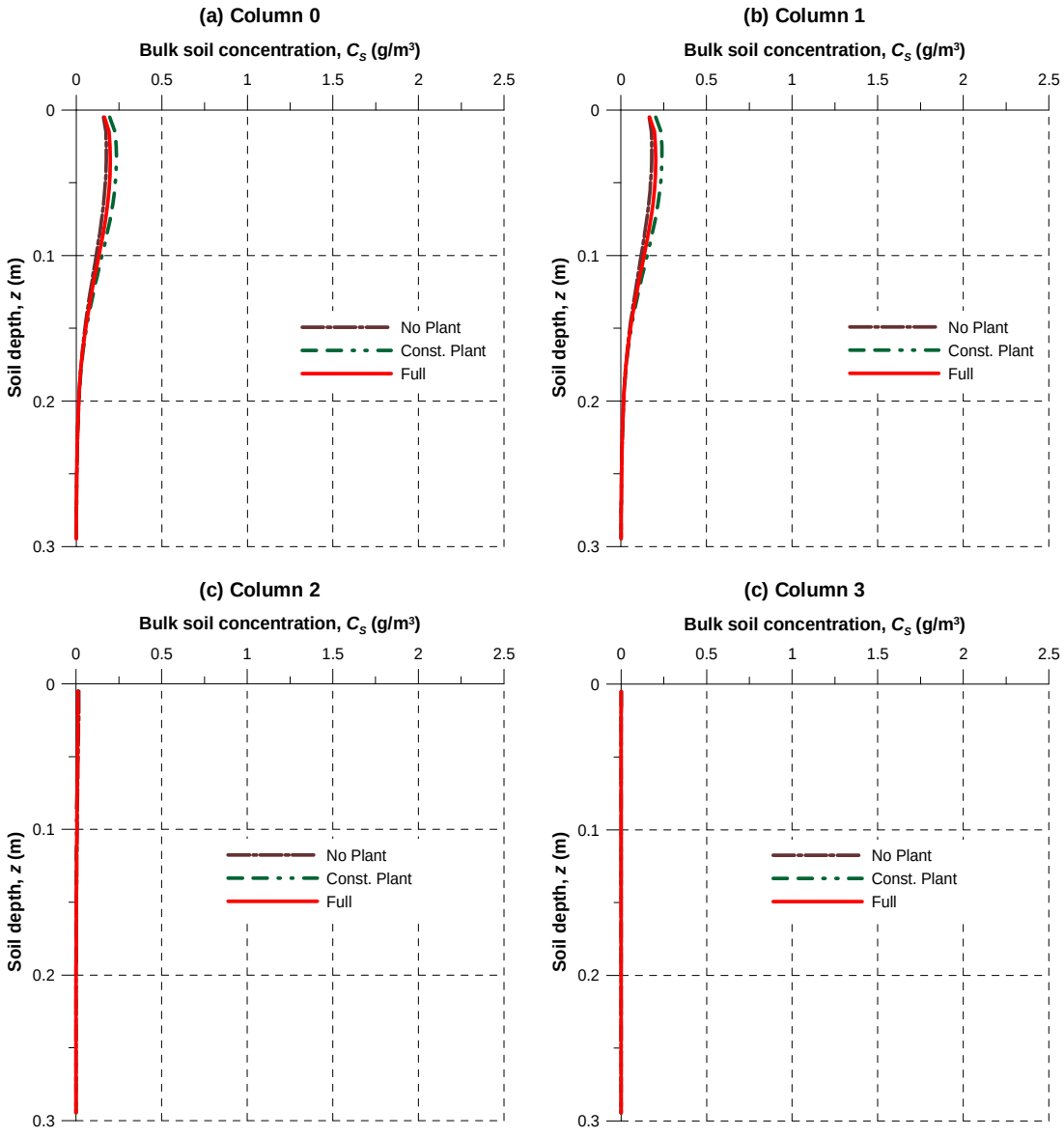

Figure 7.35: Contaminant concentration profiles within the soil columns for the seasonal simulation of sprinkler irrigation. (day = 120)

On the other hand, due to the even distribution of irrigation water, the water stress experienced does not impede plant biomass growth in any of the columns (Figure 7.36). The contaminant concentration variation within the plant is given in Figure 7.37. When compared with the respective in-plant concentrations obtained in the border irrigation simulations (Figure 7.26), it is seen that in columns 0 and 1, plant contamination is slightly higher in sprinkler irrigation simulations. However, in columns 2 and 3, much less contamination is transferred to the plant. This can be explained by the decreased distribution of the contaminant throughout the model domain in sprinkler irrigation simulations due to the avoidance of overland flow generation.

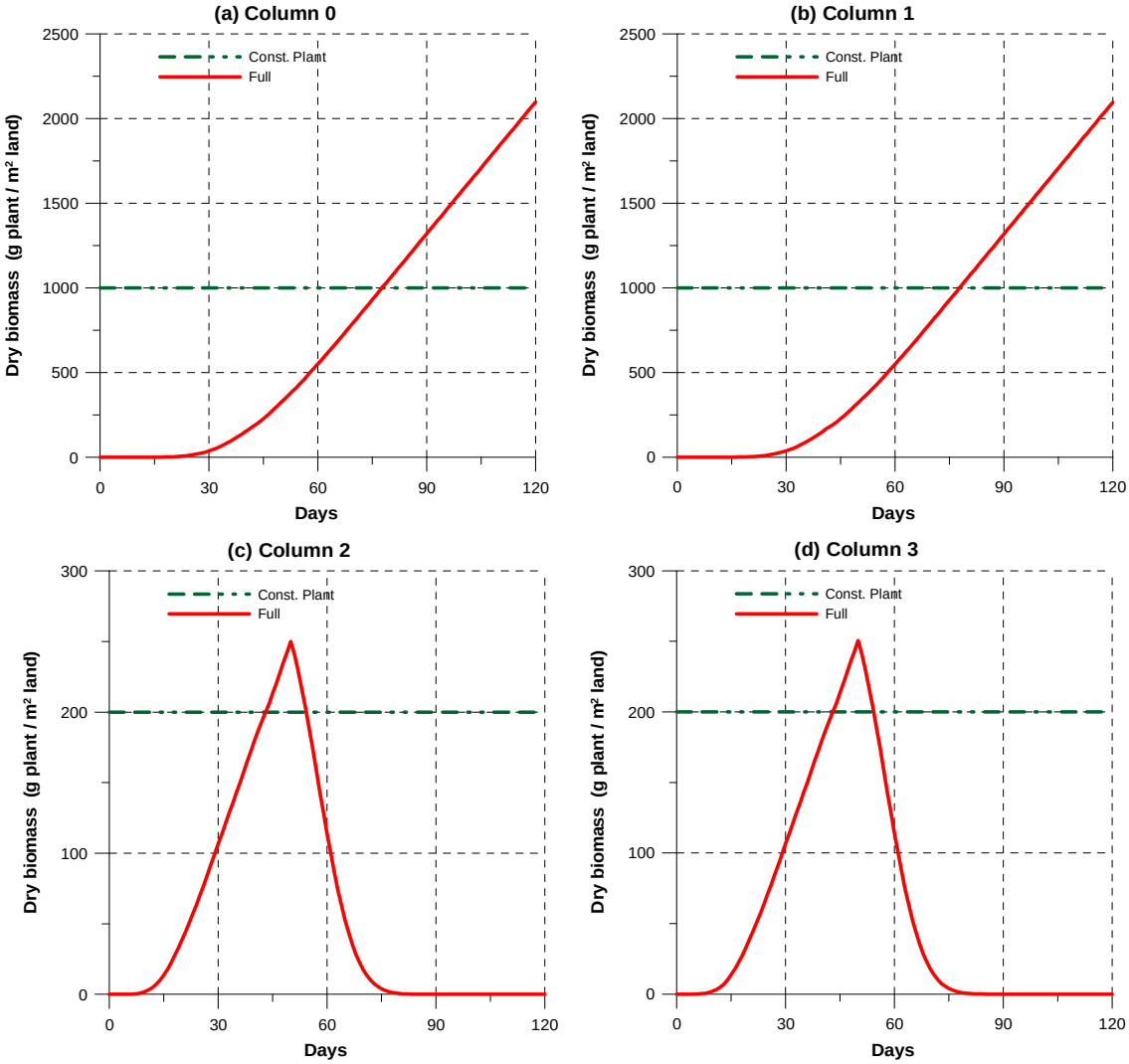

Figure 7.36: Plant biomass simulation results for the seasonal simulation of sprinkler irrigation. (Columns 0 and 1: corn, Columns 2 and 3: hay)

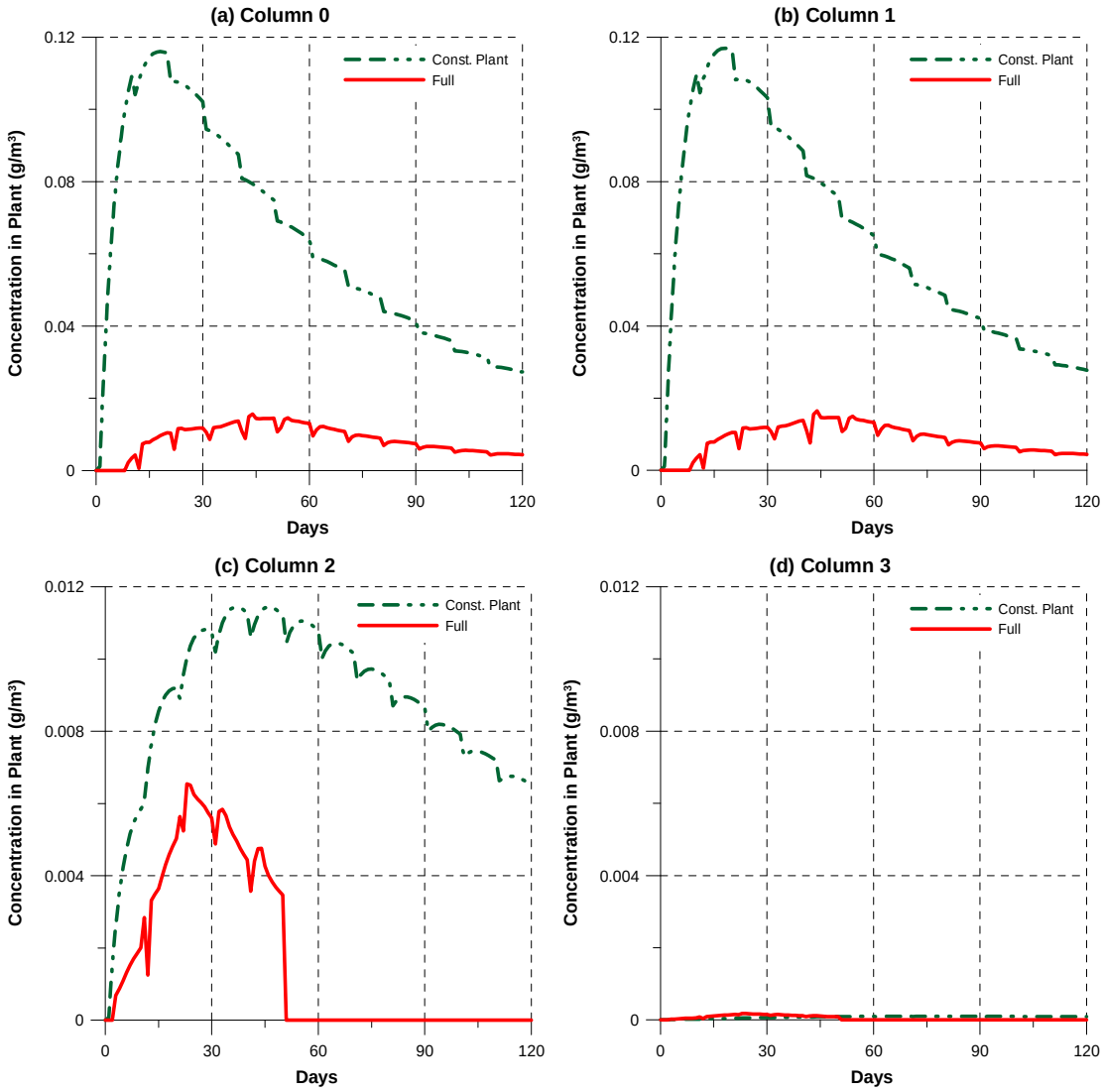

Figure 7.37: Contaminant concentration within the plant for the seasonal simulation of sprinkler irrigation. (Columns 0 and 1: corn, Columns 2 and 3: hay)

7.4 Conclusion

In this chapter, an integrated model of contaminant fate and transport in a terrestrial system has been developed by using the soil-plant system model developed in Chapter 5 as a building block. The integrated transport model uses the water flow dynamics information provided by the integrated flow model developed in Chapter 6. The extensions made to the soil-plant system model in Chapter 6 and here increases the applicability range of the soil-plant system to the fields that have heterogeneous vegetation and soil characteristics.

The applications presented in this chapter demonstrated the ability of the model to describe interactions between the overland and the soil domains. It is seen that overland transport can be a very effective process in distributing the contaminants over large areas within short time periods.

The framework developed in this chapter enables the soil-plant system unit developed in Chapter 5 to interact with other soil-plant system units providing a tool that can be used to analyze the spatial and temporal distribution of contaminants through the soil and plant pathways.

CHAPTER 8

CONCLUSIONS AND RECOMMENDATIONS

8.1 Conclusions

In this study, a holistic view to the environmental contamination problem is adopted. And, it is accepted that the biotic entities are also a part of the environment and represent additional pathways to the contaminant migration besides the abiotic pathways such as soil, air and water. This approach is necessary when studying contaminant fate and transport within soil-plant systems. Soil and plants are in very close interaction and either of them has an impact on the other's conditions. Soil provides contaminants as well as water to the plants and plants interfere with the water and contaminant transport dynamics within the soil. A detailed analysis of these interactions is very critical from an environmental and human health perspective since plants are contamination entry points into the food chain. However, contaminant transport models have not addressed these interactions satisfactorily.

The plant pathway modeling is being studied as a part of multimedia compartmental modeling field and the mathematical definitions of the most important mass transfer processes between the plant and its environment have been developed. However, the multimedia compartmental models of plant pathway tend to ignore the spatial heterogeneity within the soil to various extents. On the other hand, vadose zone transport modeling field has accomplished describing the spatial and temporal distribution of

contaminants within the soil while leaving the plants out of the model domain. In this study, it was aimed to combine the strengths of these two different types of models and to provide an integrated view of the contamination problem within the soil-plant system.

Water flow dynamics in a soil-plant system have to be known in order to be able to carry out a dynamic contamination analysis within the system. So, hydrologic modeling is a prerequisite for contaminant fate and transport modeling in soil-plant systems. And, the presence of plants has to be taken into account when modeling the hydrology of the system. Besides water flow within the system, the various hydrological loss processes (i.e. evaporation, transpiration, interception) are dependent on the characteristics of the plants within the system. In this study, the hydrological processes related with the soil-plant system are modeled as a function of the plant characteristics.

Plants are living organisms and they go through a life-cycle. A holistic approach to the environmental contamination analysis requires that this is taken into account especially when long time periods are being considered in the analysis. Plant life-cycle was modeled in this study taking into account its dependence on the water availability by combining *LAI*, biomass, root growth and root distribution models.

In the first part of the study, an integrated dynamic soil-plant system model was developed focusing on the processes within a single column. The plant life-cycle model was coupled with an unsaturated zone soil-water flow model and also with the hydrological processes of evaporation, transpiration and interception. This was followed

by the coupling of the vadose zone transport and plant pathway models. The coupling of the vadose zone and the plant pathway models is achieved at the numerical time integration phase after the vadose zone model is spatially discretized by using finite volume methods. This methodology proved to be very fruitful as it was also used in coupling the overland flow and soil-water flow models, and then, in coupling the overland transport and vadose zone transport models in the second part of the study where the single column model is extended to multiple columns that are interacting with each other. It also facilitated the incorporation of the subsurface water and contaminant fluxes between the adjacent soil columns.

In this study, by adopting the approaches described above, a modeling framework that incorporates the plant pathway into an integrated water flow and contaminant transport model in terrestrial systems has been developed. The outcome is a tool for analyzing the plant pathway of exposure to contaminants that also provides the spatial and temporal distribution of contaminants within a terrestrial system.

8.2 Recommendations

The research activity performed in this study has led to the identification of several areas that warrants further research to improve upon this study. In this section, these areas are listed for future reference.

The plant pathway model used in this study is a single-compartment model and it can be replaced with a multiple-compartment plant pathway model. This would be a relatively straightforward process since the integrated modeling framework has been established in this study. Similarly, incorporation of non-plant compartments as required by the nature of the analysis can be a further improvement upon the model developed in this study. For example, a litter compartment can be incorporated to model the contaminant introduction to upper soil through litterfall. Also, atmosphere can be included as a separate compartment. Incorporating a lower atmosphere compartment just above the soil will make it possible to include the soil-air-plant pathway in the analysis.

The model developed in this study can be used to test more sophisticated root growth and distribution models. This can be combined with a separate root compartment model and the interaction between the plant roots and the soil can be modeled in more detail.

The plant life-cycle model can be replaced by a more detailed model which can address the effect of nutrient availability on plant growth. For this purpose, the contaminant transport model can be modified to model nutrient transport as well.

It would be a natural extension to the current model to combine it with a risk analysis model and carry out assessments of risk associated with the intake of contaminated food for various contamination and crop growth scenarios. Moreover, a grazing animal model can be integrated to the developed model to describe the contaminant transfer into milk products and meat.

Several areas regarding the numerical solution of the model equations have also been identified. Implementing higher order advective transport schemes (especially for the overland transport model) would increase the accuracy of the results. It is possible to incorporate multiple point and nonlinear schemes into the current modeling framework. Using an efficient ordinary differential equation (ODE) solver that specializes in stiff problems will decrease the run-time requirements for both the integrated flow and integrated transport solutions. Similarly, parallel processing alternatives can be assessed. Decreasing the run-time requirements will make it more feasible to apply the model to large scale problems.

During the development of the modeling framework, certain trends were observed in describing the interactions between different model components in terms of both water flow and contaminant transport. This hints to a possibility of automatizing the integrated model development process for environmental systems. An algorithm can be developed that builds the global matrix equations after being supplied by the partial differential equations and the ODEs that describe the processes within the larger system, and the interactions between the model components are chosen from a set of standardized interaction types.

APPENDIX A

SPATIAL DISCRETIZATION OF THE UNSATURATED FLOW MODEL

The mixed form of the Richard's equation can be written as:

$$\frac{\partial \theta}{\partial t} = \frac{\partial}{\partial z}\left(K_u \left(\frac{\partial h}{\partial z} - 1 \right) \right) - U \tag{A.1}$$

where θ is the volumetric water content [L^3 L^{-3}], t is time [T], K_u is the unsaturated hydraulic conductivity [L T^{-1}], h is the soil-water pressure head [L], z is the soil depth [L] (positively directed downward), and U is the root water uptake rate [T^{-1}].

The soil-water flux, q [L T^{-1}], can be defined as below by using the Darcy's law :

$$q = -K_u \left(\frac{\partial h}{\partial z} - 1 \right) \tag{A.2}$$

Then, Equation (A.1) can be simplified as:

$$\frac{\partial \theta}{\partial t} = -\frac{\partial q}{\partial z} - U \tag{A.3}$$

The mass balance equation (Equation A.3) is integrated over the cell j from $z_{j-1/2}$ to $z_{j+1/2}$ following the spatial discretization of the soil domain as shown in Figure 4.1 as:

$$\int_{z_{j-1/2}}^{z_{j+1/2}} \frac{\partial \theta}{\partial t} dz = -\int_{z_{j-1/2}}^{z_{j+1/2}} \frac{\partial q}{\partial z} dz - \int_{z_{j-1/2}}^{z_{j+1/2}} U dz \tag{A.4}$$

to obtain:

$$\left(\frac{d\theta}{dt}\right)_j \Delta z_j = -q_{j+1/2} + q_{j-1/2} - U_j \Delta z_j \tag{A.5}$$

where $(d\theta/dt)_j$ is the representative mean value of the water content accumulation rate [L^3 L^{-3} T^{-1}] throughout cell j, Δz_j is the thickness [L] of cell j, $q_{j+1/2}$ is the flux [L T^{-1}] at the interface between the cells j and j+1, $q_{j-1/2}$ is the flux [L T^{-1}] at the interface between the cells j and j-1, and U_j is the representative mean value of the root water uptake term [T^{-1}] throughout cell j. $(d\theta/dt)_j$ can be represented as:

$$\left(\frac{d\theta}{dt}\right)_j = \left(\frac{d\theta}{dh}\right)_j \left(\frac{dh}{dt}\right)_j = C_j \left(\frac{dh}{dt}\right)_j \tag{A.6}$$

where $C_j = \left(\frac{d\theta}{dh}\right)_j$ is the specific moisture capacity [L^3 L^{-3} L^{-1}].

The interface fluxes can be approximated as:

$$q_{j+1/2} = -K_{j+1/2}\left(\frac{h_{j+1} - h_j}{0.5\left(\Delta z_{j+1} + \Delta z_j\right)} - 1\right) \tag{A.7}$$

Combining Equations (A.5-A.7) yields:

$$\begin{aligned} C_j \Delta z_j \left(\frac{dh}{dt}\right)_j &- \left(\frac{K_{j-1/2}}{0.5\left(\Delta z_j + \Delta z_{j-1}\right)}\right) h_{j-1} \\ &+ \left(\begin{array}{c} \dfrac{K_{j+1/2}}{0.5\left(\Delta z_{j+1} + \Delta z_j\right)} \\ + \dfrac{K_{j-1/2}}{0.5\left(\Delta z_j + \Delta z_{j-1}\right)} \end{array}\right) h_j \\ &- \left(\frac{K_{j+1/2}}{0.5\left(\Delta z_{j+1} + \Delta z_j\right)}\right) h_{j+1} \qquad = \left[-K_{j+1/2} + K_{j-1/2} + U_j \Delta z_j\right] \end{aligned} \tag{A.8}$$

As a result, the following set of equations is obtained for $j = 1,\ldots,N$ (where N is the total number of soil cells):

$$M_j \left(\frac{dh}{dt}\right)_j + S_j^1 h_{j-1} + S_j^2 h_j + S_j^3 h_{j+1} = F_j \tag{A.9}$$

$$M_j = C_j \Delta z_j \tag{A.9a}$$

$$S_j^1 = -\left(\frac{K_{j-1/2}}{0.5\left(\Delta z_j + \Delta z_{j-1}\right)}\right) \tag{A.9b}$$

$$S_j^2 = \left(\frac{K_{j+1/2}}{0.5\left(\Delta z_{j+1} + \Delta z_j\right)} + \frac{K_{j-1/2}}{0.5\left(\Delta z_j + \Delta z_{j-1}\right)} \right) = -\left(S_j^3 + S_j^1\right) \tag{A.9c}$$

$$S_j^3 = -\left(\frac{K_{j+1/2}}{0.5\left(\Delta z_{j+1} + \Delta z_j\right)} \right) \tag{A.9d}$$

$$F_j = \left[-K_{j+1/2} + K_{j-1/2} - U_j \Delta z_j \right] \tag{A.9e}$$

$$C_j = \frac{\left\{\theta_j\right\}_{t+\Delta t} - \left\{\theta_j\right\}_t}{\left\{h_j\right\}_{t+\Delta t} - \left\{h_j\right\}_t} \tag{A.9f}$$

where Δt is the time step size used in the temporal discretization, and $K_{j\pm1/2}$ are the interblock hydraulic conductivity values [L T^{-1}].

When the solution approaches a steady-state, the denominator of Equation A.9f may be very close to zero. In order to avoid division by zero, Berg (1999) proposes to calculate the specific water capacity as follows:

$$C_j = \left(\frac{d\theta}{dh} \right)_j = \frac{G\left(\left\{h_j\right\}_{t+\Delta t} + \Delta h_j\right) - \left\{\theta_j\right\}_t}{\Delta h_j} \tag{A.10}$$

where Δh_j is determined as:

$$\Delta h_j = \mathrm{SIGN}\left(\left\{h_j\right\}_{t+\Delta t} - \left\{h_j\right\}_t\right) \mathrm{MAX}\left(\left|\left\{h_j\right\}_{t+\Delta t} - \left\{h_j\right\}_t\right|, \Delta h_{\min}\right) \tag{A.11}$$

The function $G(h)=\theta|_h$ is the constitutive relationship between h and θ; SIGN is a function that returns 1 or -1, depending on the sign of the argument; MAX is a function that returns the maximum of the two arguments; and, $\Delta h_{\min}$ is the predefined minimum value of the denominator.

The resultant ODE system can be represented as (Aral 1990; Gunduz and Aral 2005b):

$$\mathbf{M}\left(\frac{\mathbf{dh}}{\mathbf{dt}}\right)+\mathbf{Sh}=\mathbf{F} \tag{A.12}$$

with $\mathbf{M}=\begin{pmatrix} M_1 & & 0 \\ & \ddots & \\ 0 & & M_N \end{pmatrix}$, $\left(\frac{\mathbf{dh}}{\mathbf{dt}}\right)=\begin{pmatrix} \left(\frac{dh}{dt}\right)_1 \\ \vdots \\ \left(\frac{dh}{dt}\right)_N \end{pmatrix}$, $\mathbf{h}=\begin{pmatrix} h_1 \\ \vdots \\ h_N \end{pmatrix}$, $\mathbf{F}=\begin{pmatrix} F_1 \\ \vdots \\ F_N \end{pmatrix}$, and

$$\mathbf{S}=\begin{pmatrix} S_1^2 & S_1^3 & & & & & & \\ S_2^1 & S_2^2 & S_2^3 & & & & & \\ & S_3^1 & S_3^2 & S_3^3 & & & & \\ & & & \ddots & & & & \\ & & & & S_{N-2}^1 & S_{N-2}^2 & S_{N-2}^3 & \\ & & & & & S_{N-1}^1 & S_{N-1}^2 & S_{N-1}^3 \\ & & & & & & S_N^1 & S_N^2 \end{pmatrix}.$$

Handling the Boundary Conditions

Two different approaches are proposed for handling the boundary conditions:

1) Modifying the right-hand-side (RHS) of the boundary cells.
2) Including the boundary conditions as extra equations to the ODE system.

The flux between the uppermost cell (cell 1) and the top boundary (ground surface) can be represented as:

$$q_{1/2} = -K_{1/2}\left(\frac{h_1 - h_0}{0.5(\Delta z_1)} - 1\right) \tag{A.13}$$

where $K_{1/2}$ is the representative hydraulic conductivity value [L T^{-1}] between cell 1 and the ground surface, and h_0 is the water pressure head [L] at the ground surface.

Equation (A.13) can be expanded as:

$$q_{1/2} = -\frac{K_{1/2}}{0.5(\Delta z_1)}h_1 + \frac{K_{1/2}}{0.5(\Delta z_1)}h_0 + K_{1/2} \tag{A.14}$$

In the case of a specified head boundary condition, h_0 is known ($h_0 = h_{top}$), whereas in the case of a specified flux boundary condition, $q_{1/2}$ is known ($q_{1/2} = q_{top}$).

Specified Head Boundary Condition

The mass balance equation for cell 1 is:

$$M_1\left(\frac{dh}{dt}\right)_1 + S_1^1 h_0 + S_1^2 h_1 + S_1^3 h_2 = F_1 \tag{A.15}$$

$$M_1 = C_1 \Delta z_1 \tag{A.15a}$$

$$S_1^1 = -\left(\frac{K_{1/2}}{0.5(\Delta z_1)}\right) \tag{A.15b}$$

$$S_1^2 = \left(\frac{K_{3/2}}{0.5(\Delta z_2 + \Delta z_1)} + \frac{K_{1/2}}{0.5(\Delta z_1)}\right) = -\left(S_j^3 + S_j^1\right) \tag{A.15c}$$

$$S_1^3 = -\left(\frac{K_{3/2}}{0.5(\Delta z_2 + \Delta z_1)}\right) \tag{A.15d}$$

$$F_1 = \left[-K_{3/2} + K_{1/2} - U_1 \Delta z_1\right] \tag{A.15e}$$

Since the value of h_0 is known ($h_0 = h_{top}$), the term associated with it is carried to the RHS:

$$M_1\left(\frac{d\theta}{dt}\right)_1 + S_1^2 h_1 + S_1^3 h_2 = F_1 - S_1^1 h_{top} \tag{A.16}$$

Defining $F_1' = F_1 - S_1^1 h_{top}$ yields:

$$M_1\left(\frac{d\theta}{dt}\right)_1 + S_1^2 h_1 + S_1^3 h_2 = F_1' \tag{A.17}$$

If the specified head boundary condition is desired to be entered as an extra equation to the ODE system, the mass balance equation for cell 1 is left unmodified and the equation $h_0 = h_{top}$ is added to the equation set with the index $j = 0$ referring to the soil surface boundary located just above cell 1:

$$M_0\left(\frac{dh}{dt}\right)_0 + S_0^2 h_0 + S_0^3 h_1 = F_0 \tag{A.18}$$

with $M_0 = 0$, $S_0^2 = 1$, $S_0^3 = 0$, and $F_0 = h_{top}$.

Specified Flux Boundary Condition:

Since the value of $q_{1/2}$ is known ($q_{1/2} = q_{top}$), the term associated with it (Equation A.14) is carried to the RHS of the mass balance equation for cell 1 (Equation A.15):

$$M_1\left(\frac{d\theta}{dt}\right)_1 + S_1^2 h_1 + S_1^3 h_2 = F_1' \tag{A.19}$$

$$M_1 = C_1 \Delta z_1 \tag{A.19a}$$

$$S_1^2 = \left(\frac{K_{3/2}}{0.5\left(\Delta z_2 + \Delta z_1\right)}\right) = -S_1^3 \tag{A.19b}$$

$$S_1^3 = -\left(\frac{K_{3/2}}{0.5\left(\Delta z_2 + \Delta z_1\right)} \right) \tag{A.19c}$$

$$F_1' = \left[-K_{3/2} + q_{top} - U_1 \Delta z_1 \right] \tag{A.19d}$$

If the specified flux boundary condition is desired to be entered as an extra equation to the ODE system, the mass balance equation for cell 1 is left unmodified and the equation $q_{1/2} = q_{top}$ is added to the equation set with the index $j = 0$ referring to the soil surface boundary located just above cell 1:

$$M_0 \left(\frac{dh}{dt} \right)_0 + S_0^2 h_0 + S_0^3 h_1 = F_0 \tag{A.20}$$

$$M_0 = 0 \tag{A.20a}$$

$$S_0^2 = \frac{K_{1/2}}{0.5\left(\Delta z_1\right)} \tag{A.20b}$$

$$S_0^3 = -\frac{K_{1/2}}{0.5\left(\Delta z_1\right)} = -S_0^2 \tag{A.20c}$$

$$F_0 = q_t - K_{1/2} \tag{A.20d}$$

The same approach is used when handling the bottom boundary conditions. They are incorporated either by modifying the mass balance equation for cell N or by adding an extra equation to the set of equations with the index $j = N+1$ referring to the soil surface boundary located just below cell N.

APPENDIX B

SPATIAL DISCRETIZATION OF THE VADOSE ZONE TRANSPORT MODEL

The vadose zone transport equation is given below:

$$\frac{\partial}{\partial t}\left[G_1 C_w\right] = \underbrace{\frac{\partial}{\partial z}\left(G_2 \frac{\partial C_w}{\partial z} - G_3 C_w\right)}_{\text{advection-dispersion}} + \underbrace{G_4 C_w + G_5}_{\text{source/sink/transformation}} \tag{B.1}$$

$$G_1 = \rho_b K_d + \phi s_g K_H + \phi s_w \tag{B.1a}$$

$$G_2 = \phi s_w D_w + \phi s_g D_g K_H \tag{B.1b}$$

$$G_3 = q \tag{B.1c}$$

$$G_4 = -\left(\lambda_s \rho_b K_d + \lambda_g \phi s_g K_H + \lambda_w \phi s_w\right) - r_u \tag{B.1d}$$

$$G_5 = M \tag{B.1e}$$

where G_1 is the bulk coefficient for the partitioning processes [L^3 L^{-3}], C_w is the contaminant concentration in soil-water [M L^{-3}], G_2 is the bulk coefficient for the dispersion processes [L^2 T^{-1}], G_3 is the bulk coefficient for the advection process [L T^{-1}], G_4 is the bulk coefficient for the first-order loss processes [T^{-1}], G_5 is the bulk term for the source/sink processes [M L^{-3} T^{-1}], ρ_b is the soil bulk density [M L^{-3}] , K_d is the partition coefficient between soil-solids and soil-water [L^3 M^{-1}], ϕ is porosity [L^3 L^{-3}], s_g is soil-gas saturation [L^3 L^{-3}], K_H is the dimensionless Henry's Law constant [-], s_w is soil-water saturation [L^3 L^{-3}], D_w is the dispersion coefficient in soil-water [L^2 T^{-1}], D_g is the dispersion coefficient in soil-air [L^2 T^{-1}], λ_s is the first-order transformation rate

coefficient in soil-solids [T^{-1}], λ_g is the first-order transformation rate coefficient in soil-air [T^{-1}], λ_w is the first-order transformation rate coefficient in soil-water [T^{-1}], r_u is the root uptake rate [T^{-1}], and M is the source / sink term [$M\ L^{-3}\ T^{-1}$].

The contaminant transport equation is spatially discretized using the finite volume methods after dividing the soil column into N cells similar to the discretization used in the soil-water flow equation (Figure 4.1). Using the cell centered (CC) finite volume method (FVM), the equation is integrated over a control volume (CV), and then appropriate approximations are made for the fluxes across the boundary of each CV. For a one-dimensional problem, the control volumes reduce to cell thicknesses. The finite volume approximation for each term in the equation is developed separately following the methods used in the finite volume solution software FiPy (Wheeler et al. 2007).

The transient term is approximated as:

$$\int_{z_{j-1/2}}^{z_{j+1/2}} \frac{\partial}{\partial t}\left[G_1 C_w\right] dz \simeq \left(\frac{d\left(G_1 C_w\right)}{dt}\right)_j \Delta z_j \tag{B.2}$$

where Δz_j is the cell thickness for the j^{th} cell.

The advection term is approximated as:

$$\int_{z_{j-1/2}}^{z_{j+1/2}}\left[\frac{\partial}{\partial z}\left(-G_3 C_w\right)\right]dz \simeq \left(-G_3\right)_{j+1/2}\left(C_w\right)_{j+1/2} - \left(-G_3\right)_{j-1/2}\left(C_w\right)_{j-1/2}$$
$$= -\left(G_3\right)_{j+1/2}\left(C_w\right)_{j+1/2} + \left(G_3\right)_{j-1/2}\left(C_w\right)_{j-1/2} \tag{B.3}$$

where $\left(G_3\right)_{j+1/2} = q_{j+1/2}$ and $\left(G_3\right)_{j-1/2} = q_{j-1/2}$, which are known values through the unsaturated flow model outcome.

When using a first order approximation, $\left(C_w\right)_{j\pm1/2}$ values depend on $\left(C_w\right)_j$ and $\left(C_w\right)_{j\pm1}$:

$$\left(C_w\right)_{j+1/2} = \alpha_{j+1/2}\left(C_w\right)_j + \left(1-\alpha_{j+1/2}\right)\left(C_w\right)_{j+1} \tag{B.4a}$$

$$\left(C_w\right)_{j-1/2} = \alpha_{j-1/2}\left(C_w\right)_j + \left(1-\alpha_{j-1/2}\right)\left(C_w\right)_{j-1} \tag{B.4b}$$

So:

$$\int_{z_{j-1/2}}^{z_{j+1/2}}\left[\frac{\partial}{\partial z}\left(-G_3 C_w\right)\right]dz \simeq -\left(G_3\right)_{j+1/2}\left[\alpha_{j+1/2}\left(C_w\right)_j + \left(1-\alpha_{j+1/2}\right)\left(C_w\right)_{j+1}\right]$$
$$+\left(G_3\right)_{j-1/2}\left[\alpha_{j-1/2}\left(C_w\right)_j + \left(1-\alpha_{j-1/2}\right)\left(C_w\right)_{j-1}\right] \tag{B.5}$$

where $\alpha_{j\pm1/2}$ is a weighting factor and is calculated by an appropriate convection scheme.

The dispersion term is approximated as:

$$\int_{z_{j-1/2}}^{z_{j+1/2}} \left[\frac{\partial}{\partial z} \left(G_2 \frac{\partial C_w}{\partial z} \right) \right] dz \simeq \left(G_2 \right)_{j+1/2} \frac{\left(C_w \right)_{j+1} - \left(C_w \right)_j}{\left[\frac{\left(\Delta z \right)_{j+1} + \left(\Delta z \right)_j}{2} \right]} - \left(G_2 \right)_{j-1/2} \frac{\left(C_w \right)_j - \left(C_w \right)_{j-1}}{\left[\frac{\left(\Delta z \right)_j + \left(\Delta z \right)_{j-1}}{2} \right]} \quad \text{(B.6)}$$

where

$$\left(G_2 \right)_{j+1/2} = \frac{\left(G_2 \right)_j + \left(G_2 \right)_{j+1}}{2} \quad \text{(B.7a)}$$

$$\left(G_2 \right)_{j-1/2} = \frac{\left(G_2 \right)_{j-1} + \left(G_2 \right)_j}{2} \quad \text{(B.7b)}$$

The source/sink/transformation term is approximated as:

$$\int_{z_{j-1/2}}^{z_{j+1/2}} \left[G_4 C_w + G_5 \right] dz \simeq \left(G_4 \right)_j \left(C_w \right)_j \Delta z_j + \left(G_5 \right)_j \Delta z_j \quad \text{(B.8)}$$

The “advective strength”, $A_{j\mp1/2}$, is defined as:

$$A_{j-1/2} = \left(G_3 \right)_{j-1/2} \quad \text{(B.9a)}$$

$$A_{j+1/2} = -\left(G_3 \right)_{j+1/2} \quad \text{(B.9b)}$$

The “diffusive conductance”, $D_{j\mp1/2}$, is defined as:

$$D_{j-1/2} = \frac{\left(G_2\right)_{j-1/2}}{\left[\frac{\left(\Delta z\right)_j + \left(\Delta z\right)_{j-1}}{2}\right]} \tag{B.10a}$$

$$D_{j+1/2} = \frac{\left(G_2\right)_{j+1/2}}{\left[\frac{\left(\Delta z\right)_{j+1} + \left(\Delta z\right)_j}{2}\right]} \tag{B.10b}$$

Combining Equations (B.1-10), the complete spatially discretized system is obtained as:

$$\begin{aligned}
&\left(\frac{d\left(G_1 C_w\right)}{dt}\right)_j \Delta z_j \\
&-\left[A_{j-1/2}\left(1-\alpha_{j-1/2}\right) + D_{j-1/2}\right]\left(C_w\right)_{j-1} \\
&-\left[A_{j+1/2}\alpha_{j+1/2} + A_{j-1/2}\alpha_{j-1/2} - D_{j+1/2} - D_{j-1/2} + \left(G_4\right)_j \Delta z_j\right]\left(C_w\right)_j \\
&-\left[A_{j+1/2}\left(1-\alpha_{j+1/2}\right) + D_{j+1/2}\right]\left(C_w\right)_{j+1} \qquad = \left(G_5\right)_j \Delta z_j
\end{aligned} \tag{B.11}$$

As a result, the following set of equations is obtained for $j = 1,\ldots,N$ (where N is the total number of soil cells):

$$\left(\frac{d\left(G_1 C_w\right)}{dt}\right)_j M_j + S_j^1\left(C_w\right)_{j-1} + S_j^2\left(C_w\right)_j + S_j^3\left(C_w\right)_{j+1} = F_j \tag{B.12}$$

$$M_j = \Delta z_j \tag{B.12a}$$

$$S_j^1 = -\left[A_{j-1/2}\left(1-\alpha_{j-1/2}\right) + D_{j-1/2}\right] \tag{B.12b}$$

$$S_j^2 = -\left[A_{j+1/2}\alpha_{j+1/2} + A_{j-1/2}\alpha_{j-1/2} - D_{j+1/2} - D_{j-1/2} + \left(G_4\right)_j \Delta z_j \right] \quad \text{(B.12c)}$$

$$S_j^3 = -\left[A_{j+1/2}\left(1-\alpha_{j+1/2}\right) + D_{j+1/2} \right] \quad \text{(B.12d)}$$

$$F_j = \left(G_5\right)_j \Delta z_j \quad \text{(B.12e)}$$

The values assigned to the weighting factors, $\alpha_{j-1/2}$, determine the specific advection scheme applied. The weighting factors ($\alpha_{j\pm1/2}$) are dependent on the value of the Peclet number:

$$P_{j\pm1/2} = -\frac{A_{j\pm1/2}}{D_{j\pm1/2}} \quad \text{(B.13)}$$

The central differencing scheme is obtained when:

$$\alpha_{j\pm1/2} = \frac{1}{2} \quad \text{(B.14)}$$

The central differencing scheme is numerically stable for $\left|P_{j\pm1/2}\right|$<2.

The upwind scheme is defined with:

$$\alpha_{j\pm1/2} = \begin{cases} 1 & \text{when } P_{j\pm1/2} > 0 \\ 0 & \text{when } P_{j\pm1/2} < 0 \end{cases} \quad \text{(B.15)}$$

The upwind scheme is numerically stable for all Peclet number values but it results in numerical diffusion.

In the exponential scheme:

$$\alpha_{j\pm1/2} = \frac{\left(P_{j\pm1/2} - 1\right)\exp\left(P_{j\pm1/2}\right) + 1}{P_{j\pm1/2}\left(\exp\left(P_{j\pm1/2}\right) - 1\right)} \tag{B.16}$$

The exponential scheme is obtained from the exact solution of the advection/dispersion equation (Berg et al. 2007). It is numerically stable at all Peclet number values and does not result in excessive diffusion.

The resultant ODE system can be represented as (Aral 1990; Gunduz and Aral 2005b):

$$\mathbf{M}\left(\frac{\mathbf{dC_S}}{\mathbf{dt}}\right) + \mathbf{SC_w} = \mathbf{F} \tag{B.17}$$

with $\mathbf{M} = \begin{pmatrix} M_1 & & 0 \\ & \ddots & \\ 0 & & M_N \end{pmatrix}$, $\left(\frac{\mathbf{dC_S}}{\mathbf{dt}}\right) = \begin{pmatrix} \left(\frac{d\left(G_1 C_W\right)}{dt}\right)_1 \\ \vdots \\ \left(\frac{d\left(G_1 C_W\right)}{dt}\right)_N \end{pmatrix}$, $\mathbf{C_w} = \begin{pmatrix} \left(C_w\right)_1 \\ \vdots \\ \left(C_w\right)_N \end{pmatrix}$, $\mathbf{F} = \begin{pmatrix} F_1 \\ \vdots \\ F_N \end{pmatrix}$, and

$$\mathbf{S} = \begin{pmatrix} S_1^2 & S_1^3 & & & & & & & \\ S_2^1 & S_2^2 & S_2^3 & & & & & & \\ & S_3^1 & S_3^2 & S_3^3 & & & & & \\ & & & \ddots & & & & & \\ & & & & S_{N-2}^1 & S_{N-2}^2 & S_{N-2}^3 & & \\ & & & & & S_{N-1}^1 & S_{N-1}^2 & S_{N-1}^3 & \\ & & & & & & S_N^1 & S_N^2 \end{pmatrix}.$$

Handling the Boundary Conditions

The boundary conditions can be incorporated into the ODE system in two different ways: (i) as extra equations; and, (ii) by modifying the right-hand-side (RHS) of the ODE system. The first methodology is described as “adding zero-thickness cells at the boundaries” in the study of Berg et al. (2007). It may be preferred when a detailed description of the transport processes occurring at the soil surface between the atmosphere and the uppermost soil cell (cell 1) is required.

Soil Surface Boundary Condition

Practically, a zero-thickness cell refers to a cell where there is no accumulation. So, when a "zero-thickness" cell is assumed at the soil surface, it leads to a steady state mass balance equation for the inflows to and outflows from the soil surface. The mass fluxes between the soil surface and the atmosphere should be equal to the mass fluxes between the soil surface and the uppermost soil cell. If the water phase concentration at the soil surface is denoted as $(C_w)_0$, the steady state mass balance for the soil surface can be expressed as;

$$-\left[A_{1/2}\alpha_{1/2} - D_{1/2} - D_{Soil-Atm}\right](C_w)_0 = \left[A_{1/2}(1-\alpha_{1/2}) + D_{1/2}\right](C_w)_1 + \left[D_{Atm-Soil}\right]C_A + E_{Atm} + E_0 \quad \text{(B.18)}$$

where $D_{Soil-Atm}$ is the diffusive mass transfer rate coefficient from the soil to the atmosphere (volatilization rate coefficient) [L T^{-1}], $D_{Atm-Soil}$ is the diffusive mass transfer rate coefficient from atmosphere to soil [L T^{-1}] , C_A is the contaminant concentration in the atmosphere [M L^{-3}], $E_{Atm-Soil}$ is the atmospheric deposition rate onto soil [M L^{-2} T^{-1}], and E_0 is the source input rate onto soil surface [M L^{-2} T^{-1}]. The left-hand-side of Equation B.18 defines the mass flux out of the soil surface whereas the right-hand-side terms define the mass flux into the soil surface. Note that no advective outflow from soil surface is assumed and the advective inflows from the atmosphere to the soil surface are

lumped into the atmospheric deposition rate, $E_{Atm-Soil}$. Equation B.18 can be added to the system equation set with the index *j* = 0 after rewriting it as:

$$\left(\frac{d\left(G_1 C_w\right)}{dt}\right)_0 M_0 + S_0^2 \left(C_w\right)_0 + S_0^3 \left(C_w\right)_1 = F_0 \tag{B.19}$$

$$M_0 = \Delta z_0 = 0 \tag{B.19a}$$

$$S_0^2 = -\left[A_{1/2}\alpha_{1/2} - D_{1/2} - D_{Soil-Atm}\right] \tag{B.19b}$$

$$S_0^3 = -\left[A_{1/2}\left(1-\alpha_{1/2}\right) + D_{1/2}\right] \tag{B.19c}$$

$$F_0 = \left[D_{Atm-Soil}\right] C_A + E_{Atm-Soil} + E_0 \tag{B.19d}$$

If a specified concentration boundary condition at the soil surface is desired to be entered as an extra equation to the ODE system, the equation $\left(C_w\right)_0 = \left(C_w\right)_{top}$ is again added to the equation set with the index *j* = 0 referring to the soil surface boundary located just above cell 1:

$$\left(\frac{d\left(G_1 C_w\right)}{dt}\right)_0 M_0 + S_0^0 \left(C_w\right)_0 + S_0^1 \left(C_w\right)_1 = F_0 \tag{B.20}$$

with $M_0 = 0$, $S_0^2 = 1$, $S_0^3 = 0$, and $F_0 = \left(C_w\right)_{top}$.

A specified concentration boundary condition at the soil surface can also be handled by modifying the RHS of the mass balance equation for the uppermost soil cell (cell 1). In

this case the terms associated with the known concentration at the soil surface, $(C_w)_0$ = $(C_w)_{top}$, are moved to the RHS of the equation and the modified equation becomes:

$$\left(\frac{d(G_1 C_w)}{dt}\right)_1 M_1 + S_1^2 (C_w)_1 + S_1^3 (C_w)_2 = F_1 - S_1^1 (C_w)_{top} \quad \text{(B.21)}$$

$$M_1 = \Delta z_1 \quad \text{(B.21a)}$$

$$S_1^1 = -\left[A_{1/2}(1-\alpha_{1/2}) + D_{1/2}\right] \quad \text{(B.21b)}$$

$$S_1^2 = -\left[A_{3/2}\alpha_{3/2} + A_{1/2}\alpha_{1/2} - D_{3/2} - D_{1/2} + (G_4)_1 \Delta z_1\right] \quad \text{(B.21c)}$$

$$S_j^3 = -\left[A_{3/2}(1-\alpha_{3/2}) + D_{3/2}\right] \quad \text{(B.21d)}$$

$$F_1 = (G_5)_1 \Delta z_1 \quad \text{(B.21e)}$$

In case of an atmospheric boundary condition (when instantaneous equilibrium is assumed between the water phase concentration at the soil surface and the atmospheric concentration) the specified concentration at the soil surface is defined as:

$$(C_w)_{top} = \frac{C_A}{K_{aw}} \quad \text{(B.22)}$$

where K_{aw} is the air-water partition coefficient [$L^3\ L^{-3}$].

The same approach can be used for handling the bottom boundary condition as well. In this study, the zero-gradient boundary condition is extensively used to define the

conditions at the bottom boundary of the soil column. If we denote the water-phase contaminant concentration at the bottom boundary as $(C_w)_{N+1} = (C_w)_N$, the zero-gradient boundary condition at the bottom of the soil column can be expressed as:

$$\left(\frac{d(G_1 C_w)}{dt}\right)_N M_N + S_N^1 (C_w)_{N-1} + \left[S_N^2 + S_N^3\right](C_w)_N = F_N \tag{B.23}$$

$$M_N = \Delta z_N \tag{B.23a}$$

$$S_N^1 = -\left[A_{N-1/2}(1-\alpha_{N-1/2}) + D_{N-1/2}\right] \tag{B.23b}$$

$$S_N^2 = -\left[A_{N+1/2}\alpha_{N+1/2} + A_{N-1/2}\alpha_{N-1/2} - D_{N+1/2} - D_{N-1/2} + (G_4)_N \Delta z_N\right] \tag{B.23c}$$

$$S_N^3 = -\left[A_{N+1/2}(1-\alpha_{N+1/2}) + D_{N+1/2}\right] \tag{B.23d}$$

$$S_N^2 + S_N^3 = -\left[A_{N+1/2} + A_{N-1/2}\alpha_{N-1/2} - D_{N-1/2} + (G_4)_N \Delta z_N\right] \tag{B.23e}$$

$$F_N = (G_5)_N \Delta z_N \tag{B.23f}$$

APPENDIX C

SPATIAL DISCRETIZATION OF THE OVERLAND FLOW MODEL

The governing equation for overland flow modeling using the diffusion wave (zero inertia) approximation to the Saint Venant's equations is given as:

$$\frac{\partial H}{\partial t} + \frac{\partial}{\partial x}(q_x) + \frac{\partial}{\partial y}(q_y) = R - I - E \tag{C.1}$$

$$q_x = -\frac{h^{5/3}}{n_x}\frac{1}{\left|\frac{\partial H}{\partial x}\right|^{1/2}}\frac{\partial H}{\partial x} = -D_x\frac{\partial H}{\partial x} \tag{C.1a}$$

$$q_y = -\frac{h^{5/3}}{n_y}\frac{1}{\left|\frac{\partial H}{\partial y}\right|^{1/2}}\frac{\partial H}{\partial y} = -D_y\frac{\partial H}{\partial y} \tag{C.1b}$$

where H is the water surface elevation [L] of overland flow $(H = h + Z)$, h is the flow depth [L], Z is the land surface elevation [L], t is time [T], q_x is the water flux [L^2 T^{-1}] (water flow rate per unit width) in x-direction, q_y is the water flux in y-direction [L^2 T^{-1}] (water flow rate per unit width), R is the rainfall rate [L T^{-1}], I is the infiltration rate [L T^{-1}], and E is the evaporation rate [L T^{-1}], D_x is the diffusion coefficient of flow [L^2 T^{-1}] in x-direction, and D_y is the diffusion coefficient of flow [L^2 T^{-1}] in y-direction, n_x is the Manning's roughness coefficient [T $L^{-1/3}$] in x-direction, and n_y is the Manning's roughness coefficient [T $L^{-1/3}$] in y-direction.

In order to solve Equation (C.1) numerically, the equation is spatially discretized using a finite volume approach. It is assumed that the 2D modeling domain is composed of a finite number of non-overlapping cells and each cell has a grid point at its center (Figure 4.9). It is further assumed that the values of the relevant variables and their variations in space and time within each cell are represented by their values at these grid points. The unit cell *i,j* with its grid point and the representation of water fluxes associated with it are shown in Figure C.1.

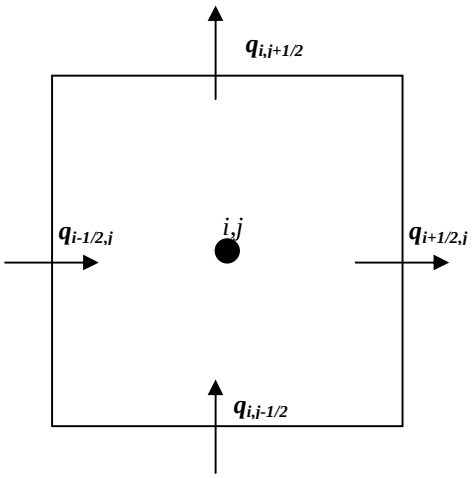

Figure C.1: The inflows and outflows associated with cell *i,j*.

Integrating Equation (C.1) over cell *i,j*:

$$\int_{y_{j-1/2}}^{y_{j+1/2}}\int_{x_{i-1/2}}^{x_{i+1/2}}\frac{\partial H}{\partial t}dxdy+\int_{y_{j-1/2}}^{y_{j+1/2}}\int_{x_{i-1/2}}^{x_{i+1/2}}\frac{\partial}{\partial x}q_x dxdy+\int_{y_{j-1/2}}^{y_{j+1/2}}\int_{x_{i-1/2}}^{x_{i+1/2}}\frac{\partial}{\partial y}q_y dxdy$$
$$=\int_{y_{j-1/2}}^{y_{j+1/2}}\int_{x_{i-1/2}}^{x_{i+1/2}}Rdxdy-\int_{y_{j-1/2}}^{y_{j+1/2}}\int_{x_{i-1/2}}^{x_{i+1/2}}Idxdy-\int_{y_{j-1/2}}^{y_{j+1/2}}\int_{x_{i-1/2}}^{x_{i+1/2}}Edxdy \quad \text{(C.2)}$$

yields:

$$\left(\frac{dH}{dt}\right)_{i,j}\Delta x\Delta y+\left(q_{i+1/2,j}-q_{i-1/2,j}\right)\Delta y+\left(q_{i,j+1/2}-q_{i,j-1/2}\right)\Delta x=R_{i,j}\Delta x\Delta y-I_{i,j}\Delta x\Delta y-E_{i,j}\Delta x\Delta y \quad \text{(C.3)}$$

The discretized form of the flux terms (derived from Equations C.1a-b) using finite differences are:

$$q_{i+1/2,j}=-D_{i+1/2,j}\frac{H_{i+1,j}-H_{i,j}}{\Delta x} \quad \text{(C.4a)}$$

$$q_{i-1/2,j}=-D_{i-1/2,j}\frac{H_{i,j}-H_{i-1,j}}{\Delta x} \quad \text{(C.4b)}$$

$$q_{i,j+1/2}=-D_{i,j+1/2}\frac{H_{i,j+1}-H_{i,j}}{\Delta y} \quad \text{(C.4c)}$$

$$q_{i,j-1/2}=-D_{i,j-1/2}\frac{H_{i,j}-H_{i,j-1}}{\Delta y} \quad \text{(C.4d)}$$

The discretized forms of the diffusion coefficients can be written as (Dutta et al. 2000):

$$D_{i+1/2,j} = \frac{\left(\{H-z\}_{i+1/2,j}\right)^{5/3}}{n_{i+1/2,j}} \frac{1}{\left|\frac{H_{i+1,j}-H_{i,j}}{\Delta x}\right|^{1/2}} \tag{C.5a}$$

$$D_{i-1/2,j} = \frac{\left(\{H-z\}_{i-1/2,j}\right)^{5/3}}{n_{i-1/2,j}} \frac{1}{\left|\frac{H_{i,j}-H_{i-1,j}}{\Delta x}\right|^{1/2}} \tag{C.5b}$$

$$D_{i,j+1/2} = \frac{\left(\{H-z\}_{i,j+1/2}\right)^{5/3}}{n_{i,j+1/2}} \frac{1}{\left|\frac{H_{i,j+1}-H_{i,j}}{\Delta y}\right|^{1/2}} \tag{C.5c}$$

$$D_{i,j-1/2} = \frac{\left(\{H-z\}_{i,j-1/2}\right)^{5/3}}{n_{i,j-1/2}} \frac{1}{\left|\frac{H_{i,j}-H_{i,j-1}}{\Delta y}\right|^{1/2}} \tag{C.5d}$$

In Equation C.5, it is observed that there is a singularity in evaluating the diffusion coefficients when the hydraulic gradient is zero. This is an artifact of ignoring the convective terms in the Saint Venant equations. Feng and Molz (1997) suggest adding a very small positive or negative number to the gradient value in order to handle this singularity. This small number would be standing in for the neglected acceleration terms in the momentum equations (Equation C.1a-b). Another approach is setting the diffusion coefficients to zero when the absolute value of the water heights between adjacent cells is less than a tolerance value (such as 10^{-3} m) following Hromadka and Yen (1986). This latter approach is adopted in this study.

Panday and Huyakorn (2004) uses full upstream weighting between adjacent cells in calculating the flow depth term within the diffusion coefficients. They also propose using the sill elevation at the interface of the two cells as the reference land surface height in calculating the flow depth:

$$\{H-z\}_{i+1/2,j} = \max\left(H_{i+1,j}, H_{i,j}\right) - \max\left(z_{i+1,j}, z_{i,j}\right) \tag{C.6a}$$

$$\{H-z\}_{i-1/2,j} = \max\left(H_{i,j}, H_{i-1,j}\right) - \max\left(z_{i,j}, z_{i-1,j}\right) \tag{C.6b}$$

$$\{H-z\}_{i,j+1/2} = \max\left(H_{i,j+1}, H_{i,j}\right) - \max\left(z_{i,j+1}, z_{i,j}\right) \tag{C.6c}$$

$$\{H-z\}_{i,j-1/2} = \max\left(H_{i,j}, H_{i,j-1}\right) - \max\left(z_{i,j}, z_{i,j-1}\right) \tag{C.6d}$$

As a result of the spatial discretization process, the following ODE system is obtained for i=1,...,K, j=1,…,L (K and L are the number of cells in the x- and y- directions, respectively):

$$\left(\frac{dH}{dt}\right)_{i,j} M_{i,j} + \underbrace{\left[S_{i,j}^{E} + S_{i,j}^{W} + S_{i,j}^{N} + S_{i,j}^{S}\right]}_{S_{i,j}^{0}} H_{i,j} - S_{i,j}^{E} H_{i+1,j} - S_{i,j}^{W} H_{i-1,j} - S_{i,j}^{N} H_{i,j+1} - S_{i,j}^{S} H_{i,j-1} = F_{i,j} \tag{C.7}$$

$$M_{i,j} = \Delta x \Delta y \tag{C.7a}$$

$$S_{i,j}^{E} = D_{i+1/2,j} \frac{\Delta y}{\Delta x} \tag{C.7b}$$

$$S_{i,j}^{W} = D_{i-1/2,j} \frac{\Delta y}{\Delta x} \tag{C.7c}$$

$$S_{i,j}^{N} = D_{i,j+1/2}\frac{\Delta x}{\Delta y} \tag{C.7d}$$

$$S_{i,j}^{S} = D_{i,j-1/2}\frac{\Delta x}{\Delta y} \tag{C.7e}$$

$$F_{i,j} = R\Delta x\Delta y - I\Delta x\Delta y - E\Delta x\Delta y \tag{C.7f}$$

After modifying the two-dimensional spatial index into a one-dimensional index, the system can be written in matrix-vector notation as (Aral 1990; Gunduz and Aral 2005b):

$$\mathbf{M}\left(\frac{\mathbf{dH}}{\mathbf{dt}}\right) + \mathbf{SH} = \mathbf{F} \tag{C.8}$$

The proposed equation to calculate the corresponding 1-D index from the original 2-D index is:

$$p(i,j) = (j-1)K + i \tag{C.9}$$

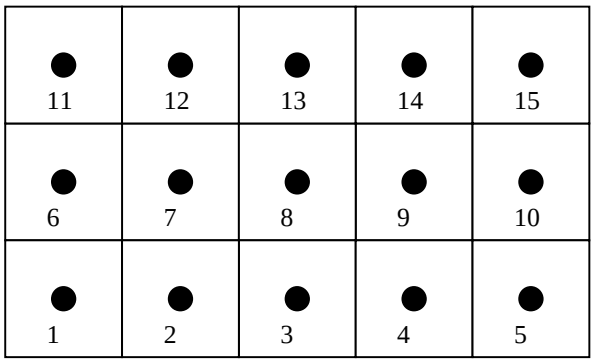

Figure C. 2: Example indexing to be used in overland flow model discretization (for *K*=5 and *L*=3).

Using the modified index *p* yields:

$$\left(\frac{dH}{dt}\right)_p M_p + \underbrace{\left[S_p^E + S_p^W + S_p^N + S_p^S\right]}_{S_p^0} H_p - S_p^E H_{p+1} - S_p^W H_{p-1} - S_p^N H_{p+K} - S_p^S H_{p-K} = F_p \tag{C.10}$$

Using the above indexing (Equations C.9-10) results in a banded **S** matrix with a semi-bandwidth of 4.

For the model domain shown in Figure C.2, the matrix **S** is:

$$\mathbf{S} = \begin{pmatrix}
S_1^0 & -S_1^E & & & & -S_1^N & & & & & & & & & \\
-S_2^W & S_2^0 & -S_2^E & & & & -S_2^N & & & & & & & & \\
 & -S_3^W & S_3^0 & -S_3^E & & & & -S_3^N & & & & & & & \\
 & & -S_4^W & S_4^0 & -S_4^E & & & & -S_4^N & & & & & & \\
 & & & -S_5^W & S_5^0 & & & & & -S_5^N & & & & & \\
-S_6^S & & & & & S_6^0 & -S_6^E & & & & -S_6^N & & & & \\
 & -S_7^S & & & & -S_7^W & S_7^0 & -S_7^E & & & & -S_7^N & & & \\
 & & -S_8^S & & & & -S_8^W & S_8^0 & -S_8^E & & & & -S_8^N & & \\
 & & & -S_9^S & & & & -S_9^W & S_9^0 & -S_9^E & & & & -S_9^N & \\
 & & & & -S_{10}^S & & & & -S_{10}^W & S_{10}^0 & & & & & -S_{10}^N \\
 & & & & & -S_{11}^S & & & & & S_{11}^0 & -S_{11}^E & & & \\
 & & & & & & -S_{12}^S & & & & -S_{12}^W & S_{12}^0 & -S_{12}^E & & \\
 & & & & & & & -S_{13}^S & & & & -S_{13}^W & S_{13}^0 & -S_{13}^E & \\
 & & & & & & & & -S_{14}^S & & & & -S_{14}^W & S_{14}^0 & -S_{14}^E \\
 & & & & & & & & & -S_{15}^S & & & & -S_{15}^W & S_{15}^0
\end{pmatrix}$$

with the other components of the ODE system being:

$$\mathbf{M} = \begin{pmatrix} M_1 & & 0 \\ & \ddots & \\ 0 & & M_{15} \end{pmatrix}, \left(\frac{\mathbf{dH}}{\mathbf{dt}}\right) = \begin{pmatrix} \left(\frac{dH}{dt}\right)_1 \\ \vdots \\ \left(\frac{dH}{dt}\right)_{15} \end{pmatrix}, \mathbf{H} = \begin{pmatrix} H_1 \\ \vdots \\ H_{15} \end{pmatrix}, \text{ and } \mathbf{F} = \begin{pmatrix} F_1 \\ \vdots \\ F_{15} \end{pmatrix}.$$

Handling the Boundary Conditions

All the cells for which *i* is equal to 1 or *K*, or *j* is equal to 1 or *L* are boundary cells. The boundary condition can be a specified head value or a specified flux value at the outer cell boundary.

Specified Head Boundary Condition:

This is the case when the *H* value is known at the outer boundary of the cell.

Below is an example where cell *q* is at the west boundary of the modeling domain. Then, the mass balance equation for cell *q* is:

$$\left(\frac{dH}{dt}\right)_q M_q + \underbrace{\left[S_q^E + \left(S_q^{W,b}\right) + S_q^N + S_q^S\right]}_{S_q^0} H_q - S_q^E H_{q+1} - \left(S_q^{W,b} H_q^{W,b}\right) - S_q^N H_{q+K} - S_q^S H_{q-K} = F_q \quad \text{(C.11)}$$

where the superscript *b* denotes that that particular term is calculated at the boundary.

In this case, the value of $H_q^{W,b}$ is known and the value of $S_q^{W,b}$ can be calculated as it is shown in Equation C.13. So, the known term in the left hand side (LHS) of the equation can be moved to the right hand side (RHS) to be a part of the RHS vector.

$$\left(\frac{dH}{dt}\right)_q M_q + \underbrace{\left[S_q^E + \left(S_q^{W,b}\right) + S_q^N + S_q^S\right]}_{S_q^0} H_q - S_q^E H_{q+1} - S_q^N H_{q+K} - S_q^S H_{q-K} = F_q + \left(S_q^{W,b} H_q^{W,b}\right) \quad \text{(C.12)}$$

The value of $S_q^{W,b}$ is calculated following the same procedure for the calculation of the other *S* terms while taking into account that it is a coefficient calculated at the boundary.

$$S_q^{W,b} = D_q^{W,b} \frac{\Delta y}{\Delta x / 2} \quad \text{(C.14)}$$

$$D_q^{W,b} = \frac{\left(\left\{H - z\right\}_q^{W,b}\right)^{5/3}}{n_q} \frac{1}{\left|\frac{H_q - H_q^{W.b}}{\Delta x / 2}\right|^{1/2}} \quad \text{(C.15)}$$

$$\left\{H - z\right\}_q^{W,b} = H_q^{W.b} - z_q \quad \text{(C.16)}$$

In Equation (C.13) and (C.14), Δx is divided by 2 because the distance between the cell center and the cell boundary is $\Delta x / 2$.

Specified Flux Boundary Condition

This is the case when the flux at the outer boundary of the cell is known.

If the flux at the west boundary of cell q is known, this means that the value $S_q^{W,b}\left(H_q - H_q^{W,b}\right) = Q_q^W$ (in m^3/s) is known. So, this term can be moved to the right-hand-side to modify the mass balance equation for cell q as:

$$\left(\frac{dH}{dt}\right)_q M_q + \underbrace{\left[S_q^E + S_q^N + S_q^S\right]}_{S_q^0} H_q - S_q^E H_{q+1} - S_q^N H_{q+K} - S_q^S H_{q-K} = F_q - Q_q^W \qquad \text{(C.17)}$$

For a zero depth gradient boundary, the discharge per unit width normal to the flow direction ise given by (Panday and Huyakorn 2004):

$$Q'_{zdb} = \frac{1}{n} h^{5/3} \sqrt{S_0} \qquad \text{(C.18)}$$

where Q'_{zdb} is discharge per unit width [$L^2\ T^{-1}$] at the zero depth gradient boundary, and S_0 is the bed slope at the zero depth gradient boundary [$L\ L^{-1}$].

For a critical depth boundary, the discharge per unit width normal to the flow direction would be given by (Panday and Huyakorn 2004):

$$Q'_{cdb} = \sqrt{gh^3} \qquad \text{(C.19)}$$

where g is the gravitational acceleration [$L^2\ T^{-1}$].

APPENDIX D

SPATIAL DISCRETIZATION OF THE OVERLAND TRANSPORT MODEL

The governing equation for overland transport is given below:

$$\frac{\partial (hC_o)}{\partial t} = \underbrace{-\frac{\partial (G_{3x}C_o)}{\partial x} - \frac{\partial (G_{3y}C_o)}{\partial y}}_{\text{Advection}} + \underbrace{\frac{\partial}{\partial x}\left(G_{2x}\frac{\partial C_o}{\partial x}\right) + \frac{\partial}{\partial y}\left(G_{2y}\frac{\partial C_o}{\partial y}\right)}_{\text{Dispersion}} + \underbrace{G_4 C_o}_{\text{Reaction}} + \underbrace{G_5}_{\text{Source}} \tag{D.1}$$

$$G_{2x} = hD_x \tag{D.1a}$$

$$G_{2y} = hD_y \tag{D.1b}$$

$$G_{3x} = hv_x \tag{D.1c}$$

$$G_{3y} = hv_y \tag{D.1d}$$

$$G_4 = -\lambda h \tag{D.1e}$$

$$G_5 = M \tag{D.1f}$$

where C_o is the vertically averaged contaminant concentration [M L^{-3}] in the overland flow, h is the overland flow depth [L], t is time [T], v_x is the overland flow velocity in the x-direction. [L T^{-1}], v_y is the overland flow velocity in the y-direction [L T^{-1}], x is the horizontal spatial direction [L], y is the vertical spatial direction [L], D_x is the dispersion coefficient in the x-direction [L^2 T^{-1}], D_y is the dispersion coefficient in the y-direction

[L^2 T^{-1}], λ is the first order decay rate coefficient [T^{-1}], M is the contaminant source input rate [M L^{-2} T^{-1}].

The overland transport model uses the same domain, cell and grid structure as the overland flow model (Figure 4.9). The spatial discretization of the overland transport equation is achieved by applying the two-dimensional counterpart of the procedure used for the vadose zone transport model details of which are given in Appendix B.

The outcome of the spatial discretization is the following set of equations for i = 1,...,K, and j = 1,…,L (K and L are the number of cells in the x- and y- directions, respectively):

$$\left(\frac{d\left[hC_o\right]}{dt}\right)_{i,j} M_{i,j} + S^W_{i,j}\left(C_o\right)_{i-1,j} + S^S_{i,j}\left(C_o\right)_{i,j-1} + S^0_{i,j}\left(C_o\right)_{i,j} + S^E_{i,j}\left(C_o\right)_{i+1,j} + S^N_{i,j}\left(C_o\right)_{i,j+1} = F_{i,j} \quad \text{(D.2)}$$

$$M_{i,j} = \Delta x_{i,j}\Delta y_{i,j} \quad \text{(D.2a)}$$

$$S^W_{i,j} = -\left\{\left[A^W_{i,j}\left(1-\alpha^W_{i,j}\right) + D^W_{i,j}\right]\Delta y_{i,j}\right\} \quad \text{(D.2b)}$$

$$S^S_{i,j} = -\left\{\left[A^S_{i,j}\left(1-\alpha^S_{i,j}\right) + D^S_{i,j}\right]\Delta x_{i,j}\right\} \quad \text{(D.2c)}$$

$$S^0_{i,j} = -\left\{\begin{array}{l}\left[A^E_{i,j}\alpha^E_{i,j} + A^W_{i,j}\alpha^W_{i,j} - D^E_{i,j} - D^W_{i,j}\right]\Delta y_{i,j} \\ +\left[A^N_{i,j}\alpha^N_{i,j} + A^S_{i,j}\alpha^S_{i,j} - D^N_{i,j} - D^S_{i,j}\right]\Delta x_{i,j} + \left(G_4\right)_{i,j}\Delta x_{i,j}\Delta y_{i,j}\end{array}\right\} \quad \text{(D.2d)}$$

$$S^E_{i,j} = -\left\{\left[A^E_{i,j}\left(1-\alpha^E_{i,j}\right) + D^E_{i,j}\right]\Delta y_{i,j}\right\} \quad \text{(D.2e)}$$

$$S^N_{i,j} = -\left\{\left[A^N_{i,j}\left(1-\alpha^N_{i,j}\right) + D^N_{i,j}\right]\Delta x_{i,j}\right\} \quad \text{(D.2f)}$$

$$F_{i,j} = \left(G_5\right)_{i,j}\Delta x_{i,j}\Delta y_{i,j} \quad \text{(D.2g)}$$

with

$$A_{i,j}^{S} = A_{i,j-1/2} = \left(G_{3y}\right)_{i,j-1/2} \tag{D.3a}$$

$$A_{i,j}^{N} = A_{i,j+1/2} = -\left(G_{3y}\right)_{i,j+1/2} \tag{D.3b}$$

$$A_{i,j}^{W} = A_{i-1/2,j} = \left(G_{3x}\right)_{i-1/2,j} \tag{D.3c}$$

$$A_{i,j}^{E} = A_{i+1/2,j} = -\left(G_{3x}\right)_{i+1/2,j} \tag{D.3d}$$

and

$$D_{i,j}^{S} = D_{i,j-1/2} = \frac{\left(G_{2y}\right)_{i,j-1/2}}{\left[\frac{\left(\Delta y\right)_{i,j} + \left(\Delta y\right)_{i,j-1}}{2}\right]} \tag{D.4a}$$

$$D_{i,j}^{N} = D_{i,j+1/2} = \frac{\left(G_{2y}\right)_{i,j+1/2}}{\left[\frac{\left(\Delta y\right)_{i,j+1} + \left(\Delta y\right)_{i,j}}{2}\right]} \tag{D.4b}$$

$$D_{i,j}^{W} = D_{i-1/2,j} = \frac{\left(G_{2x}\right)_{i-1/2,j}}{\left[\frac{\left(\Delta x\right)_{i,j} + \left(\Delta x\right)_{i-1,j}}{2}\right]} \tag{D.4c}$$

$$D_{i,j}^{E} = D_{i+1/2,j} = \frac{\left(G_{2x}\right)_{i+1/2,j}}{\left[\frac{\left(\Delta x\right)_{i+1,j} + \left(\Delta x\right)_{i,j}}{2}\right]} \tag{D.4d}$$

The terms $A_{i,j}^{E}$, $A_{i,j}^{W}$, $A_{i,j}^{N}$, $A_{i,j}^{S}$ represent the "advective strength" at the east, west, north and south interfaces of cell *i,j*, respectively. The terms $\alpha_{i,j}^{E}$, $\alpha_{i,j}^{W}$, $\alpha_{i,j}^{N}$, $\alpha_{i,j}^{S}$ are the

weighting factors used in the discretization of the advection term at the east, west, north and south interfaces of cell *i*,*j*, respectively. And the terms $D_{i,j}^{E}$, $D_{i,j}^{W}$, $D_{i,j}^{N}$, $D_{i,j}^{S}$ represent the "diffusive conductance" at the east, west, north and south interfaces of cell *i*,*j*, respectively (Wheeler et al. 2007).

Since the absolute value of the Peclet numbers (Equation B.13) associated with the overland transport processes are expected to be higher high due to the relative dominance of the advection process, the exponential scheme (Equation B.16) is used to determine the weighting factors in the overland transport model.

After modifying the two-dimensional spatial index into a one-dimensional index using the same indexing method as the one used in the overland flow model (Equation C.9), the system can be written in matrix-vector notation as (Aral 1990; Gunduz and Aral 2005b):

$$\mathbf{M}\left(\frac{\mathbf{d}\left[\mathbf{hC_o}\right]}{\mathbf{dt}}\right) + \mathbf{SC_o} = \mathbf{F} \tag{D.5}$$

with the matrices: $\mathbf{M} = \left[\mathbf{M}\right]_{(K\times L)\times(K\times L)}$, $\mathbf{h} = \left[\mathbf{h}\right]_{(K\times L)\times(K\times L)}$, $\mathbf{S} = \left[\mathbf{S}\right]_{(K\times L)\times(K\times L)}$; and, the vectors: $\mathbf{C_o} = \left\{\mathbf{C_o}\right\}_{K\times L}$, $\mathbf{F} = \left\{\mathbf{F}\right\}_{K\times L}$

Handling the Boundary Conditions

All the cells for which *i* is equal to 1 or *K*, or *j* is equal to 1 or *L* are boundary cells.

Wherever the overland flow model has no flow boundary conditions, the boundary conditions for the transport model will be automatically handled as the advective strengths and the diffusive conductances at that boundary are assigned the value of 0.

The overland transport model uses zero-gradient boundary conditions at the overland flow outlets. This type of boundary condition is conveniently handled by assigning a concentration value equal to the boundary cell's concentration value to the imaginary cell on the other side of the boundary. For instance, the no-gradient boundary condition at the east of the cell *p* is assigned by modifying the mass balance equation for cell p:

$$\left(\frac{d\left[G_1 C_o\right]}{dt}\right)_p M_p + S_p^W \left(C_o\right)_{p-1} + S_p^S \left(C_o\right)_{p-K} + S_p^0 \left(C_o\right)_p + S_p^E \left(C_o\right)^E + S_p^N \left(C_o\right)_{p+K} = F_p \quad \text{(D.6)}$$

where $\left(C_o\right)^E$ is the contaminant concentration at the imaginary cell on the east of cell *p*.

Inserting $\left(C_o\right)_p = \left(C_o\right)^E$ to Equation (D.6) yields:

$$\left(\frac{d\left[G_1 C_o\right]}{dt}\right)_p M_p + S_p^W \left(C_o\right)_{p-1} + S_p^S \left(C_o\right)_{p-K} + \left[S_p^0 + S_p^E\right]\left(C_o\right)_p + S_p^N \left(C_o\right)_{p+K} = F_p \quad \text{(D.7)}$$

APPENDIX E

TIME INTEGRATION

The time integration of the spatially discretized equations of vadose zone transport (Section 4.2, Appendix B) and overland transport (Section 4.4, Appendix D) models are implemented through an implicit scheme

The general ODE system obtained after spatial discretization is:

$$\mathbf{M}\left(\frac{\mathbf{d}[\mathbf{G_1C}]}{\mathbf{dt}}\right) + \mathbf{SC} = \mathbf{F} \tag{E.1}$$

The ODE system can be rewritten as:

$$\left(\frac{\mathbf{d}[\mathbf{G_1C}]}{\mathbf{dt}}\right) = -\mathbf{M}^{-1}\mathbf{SC} + \mathbf{M}^{-1}\mathbf{F} \tag{E.2}$$

The implicit time integration scheme yields

$$[\mathbf{G_1C}]_{t+\Delta t} = [\mathbf{G_1C}]_t + \Delta t\left(\frac{\mathbf{d}[\mathbf{G_1C}]}{\mathbf{dt}}\right)\Bigg|_{t+\Delta t} \tag{E.3}$$

Equations E.2 and E.3 are combined to have:

$$\left[\mathbf{G_1C}\right]_{t+\Delta t} = \left[\mathbf{G_1C}\right]_t + \Delta t\left(-\mathbf{M}^{-1}\mathbf{SC} + \mathbf{M}^{-1}\mathbf{F}\right)\Big|_{t+\Delta t} \tag{E.4}$$

which can be rewritten as:

$$\left[\mathbf{G_1C}\right]_{t+\Delta t} = \left[\mathbf{G_1C}\right]_t + \Delta t\left(-\left[\mathbf{M}\right]^{-1}\left[\mathbf{S}\right]_{t+\Delta t}\left(\mathbf{C}\right)_{t+\Delta t} + \left[\mathbf{M}\right]^{-1}\left(\mathbf{F}\right)_{t+\Delta t}\right) \tag{E.5}$$

We know that:

$$\left[\mathbf{G_1}\right]_{t+\Delta t} = \begin{pmatrix} \left(G_1\right)_{1,t+\Delta t} & & 0 \\ & \ddots & \\ 0 & & \left(G_1\right)_{N,t+\Delta t} \end{pmatrix} \tag{E.6}$$

So,

$$\left[\mathbf{G_1}\right]_{t+\Delta t}\left(\mathbf{C}\right)_{t+\Delta t} = \left[\mathbf{G_1C}\right]_t + \Delta t\left\{-\left[\mathbf{M}\right]^{-1}\left[\mathbf{S}\right]_{t+\Delta t}\left(\mathbf{C}\right)_{t+\Delta t} + \left[\mathbf{M}\right]^{-1}\left(\mathbf{F}\right)_{t+\Delta t}\right\} \tag{E.7}$$

Multiplying each side of Equation (E.7) by $\left[\mathbf{M}\right]$ yields

$$\left[\mathbf{M}\right]\left[\mathbf{G_1}\right]_{t+\Delta t}\left(\mathbf{C}\right)_{t+\Delta t} = \left[\mathbf{M}\right]\left[\mathbf{G_1C}\right]_t + \Delta t\left\{-\left[\mathbf{S}\right]_{t+\Delta t}\left(\mathbf{C}\right)_{t+\Delta t} + \left(\mathbf{F}\right)_{t+\Delta t}\right\} \tag{E.8}$$

Then, the linear system to be solved to obtain $\left(\mathbf{C}\right)_{t+\Delta t}$ is

$$\left\{[\mathbf{M}][\mathbf{G_1}]_{t+\Delta t} + \Delta t[\mathbf{S}]_{t+\Delta t}\right\}(\mathbf{C})_{t+\Delta t} = [\mathbf{M}][\mathbf{G_1 C}]_t + \Delta t(\mathbf{F})_{t+\Delta t} \tag{E.9}$$

Introducing the superscript *n* to denote the time step yields:

$$\left([\mathbf{M}][\mathbf{G_1}]^{n+1} + \Delta t[\mathbf{S}]^{n+1}\right)\mathbf{C}^{n+1} = [\mathbf{M}][\mathbf{G_1 C}]^n + \Delta t\mathbf{F}^{n+1} \tag{E.10}$$

Note that this analysis is valid when $[\mathbf{M}]$ is independent of time and $[\mathbf{G_1}]^{n+1}$ is known.

APPENDIX F

TIME INTEGRATION WITH PICARD ITERATION

The time integration of the spatially discretized equations of unsaturated zone transport (Section 4.1, Appendix A) and overland flow (Section 4.3, Appendix C) models are implemented through an implicit scheme combined with Picard iteration since the ODE systems are nonlinear for these models.

$$\mathbf{M}\left(\frac{\mathbf{d}\boldsymbol{\varphi}}{\mathbf{dt}}\right) + \mathbf{S}\boldsymbol{\varphi} = \mathbf{F} \tag{F.1}$$

The ODE system can be rewritten as:

$$\left(\frac{\mathbf{d}\boldsymbol{\varphi}}{\mathbf{dt}}\right) = -\mathbf{M}^{-1}\mathbf{S}\boldsymbol{\varphi} + \mathbf{M}^{-1}\mathbf{F} \tag{F.2}$$

The implicit time integration scheme implies the following approximation:

$$\{\boldsymbol{\varphi}\}_{t+\Delta t} = \{\boldsymbol{\varphi}\}_{t} + \Delta t \left\{\frac{\mathbf{d}\boldsymbol{\varphi}}{\mathbf{dt}}\right\}_{t+\Delta t} \tag{F.3}$$

Equations F.2 and F.3 are combined to have:

$$[\boldsymbol{\varphi}]_{t+\Delta t} = [\boldsymbol{\varphi}]_{t} + \Delta t \left(-\mathbf{M}^{-1}\mathbf{S}\boldsymbol{\varphi} + \mathbf{M}^{-1}\mathbf{F}\right)\Big|_{t+\Delta t} \tag{F.4}$$

Introducing the subscript *n* to denote the time step yields:

$$\boldsymbol{\varphi}^{n+1} = \boldsymbol{\varphi}^{n} + \Delta t\left(-[\mathbf{M}]^{-1}\left[\mathbf{S}\right]^{n+1}\boldsymbol{\varphi}^{n+1} + [\mathbf{M}]^{-1}\mathbf{F}^{n+1}\right) \tag{F.5}$$

Introducing the subscript *m* to denote the iteration gives:

$$\boldsymbol{\varphi}^{n+1,m+1} = \boldsymbol{\varphi}^{n} + \Delta t\left(-[\mathbf{M}]^{-1}\left[\mathbf{S}\right]^{n+1,m}\boldsymbol{\varphi}^{n+1,m+1} + [\mathbf{M}]^{-1}\mathbf{F}^{n+1,m}\right) \tag{F.6}$$

Rearranging Equation (F.6) yields:

$$\left(\left[\mathbf{M}\right]^{n+1,m} + \Delta t\left[\mathbf{S}\right]^{n+1,m}\right)\left\{\boldsymbol{\varphi}\right\}^{n+1,m+1} = \left[\mathbf{M}\right]^{n+1,m}\left\{\boldsymbol{\varphi}\right\}^{n} + \Delta t\left\{\mathbf{F}\right\}^{n+1,m} \tag{F.7}$$

In Equation (F.7), for any iteration step, the right hand side is known. And, the solution of Equation (F.7) gives the vector $\boldsymbol{\varphi}$ for the next iteration step. The values of $\boldsymbol{\varphi}$ for the next time step are obtained when the iteration converges.

An Euclidian norm is used to determine convergence (Aral 1990):

$$\left[\frac{\sum_{j=1}^{N}\left(h_i^{m+1} - h_i^{m}\right)^2}{\sum_{j=1}^{N}\left(h_i^{m}\right)^2}\right] < \varepsilon \tag{F.8}$$

where ε is the error tolerance.

REFERENCES

Abbasi, F., Simunek, J., van Genuchten, M. T., Feyen, J., Adamsen, F. J., Hunsaker, D. J., Strelkoff, T. S., and Shouse, P. (2003). "Overland water flow and solute transport: Model development and field-data analysis." *Journal of Irrigation and Drainage Engineering-Asce*, 129(2), 71-81.

Abrahamsen, P., and Hansen, S. (2000). "Daisy: an open soil-crop-atmosphere system model." *Environmental Modelling & Software*, 15(3), 313-330.

Ajayi, A. E., van de Giesen, N., and Vlek, P. (2008). "A numerical model for simulating Hortonian overland flow on tropical hillslopes with vegetation elements." *Hydrological Processes*, 22(8), 1107-1118.

Akan, A. O. (1987). "Pollutant Washoff by Overland-Flow." *Journal of Environmental Engineering-Asce*, 113(4), 811-823.

Allen, R. G., and Pereira, L. S. (2009). "Estimating crop coefficients from fraction of ground cover and height." *Irrigation Science*, 28(1), 17-34.

Allen, R. G., Pereira, L. S., Raes, D., and Smith, M. (1998). "Crop evapotranspiration - Guidelines for computing crop water requirements." *56*, FAO, Rome.

Aral, M. M. (1990). "Ground water modeling in multilayer aquifers: unsteady flow." Lewis Publishers, 143.

Aral, M. M. (2010). *Environmental Modeling and Health Risk Analysis (Acts/Risk)*, Springer, 470p.

Asaeda, T., Rajapakse, L., and Fujino, T. (2008). "Applications of organ-specific growth models; modelling of resource translocation and the role of emergent aquatic plants in element cycles." *Ecological Modelling*, 215(1-3), 170-179.

Batiha, M. A., Kadhum, A. A. H., Mohamad, A. B., Takriff, M. S., Fisal, Z., Daud, W. R. W., and Batiha, M. M. (2009). "Modeling the fate and transport of non-volatile organic chemicals in the agro-ecosystem: A case study of Cameron Highlands, Malaysia." *Process Safety and Environmental Protection*, 87(2), 121-134.

Belmans, C., Wesseling, J. G., and Feddes, R. A. (1983). "Simulation-Model of the Water-Balance of a Cropped Soil - Swatre." *Journal of Hydrology*, 63(3-4), 271-286.

Bennett, D. H., Margni, M. D., McKone, T. E., and Jolliet, O. (2002). "Intake fraction for multimedia pollutants: A tool for life cycle analysis and comparative risk assessment." *Risk Analysis*, 22(5), 905-918.

Berg, P. (1999). "Long-term simulation of water movement in soils using mass-conserving procedures." *Advances in Water Resources*, 22(5), 419-430.

Berg, P., Swaney, D., Rysgaard, S., Thamdrup, B., and Fossing, H. (2007). "A fast numerical solution to the general mass-conservation equation for solutes and solids in aquatic sediments." *Journal of Marine Research*, 65(3), 317-343.

Bixio, A. C., Gambolati, G., Paniconi, C., Putti, M., Shestopalov, V. M., Bublias, V. N., Bohuslavsky, A. S., Kasteltseva, N. B., and Rudenko, Y. F. (2002). "Modeling groundwater-surface water interactions including effects of morphogenetic depressions in the Chernobyl exclusion zone." *Environmental Geology*, 42(2-3), 162-177.

Boegh, E., Thorsen, M., Butts, M. B., Hansen, S., Christiansen, J. S., Abrahamsen, P., Hasager, C. B., Jensen, N. O., van der Keur, P., Refsgaard, J. C., Schelde, K., Soegaard, H., and Thomsen, A. (2004). "Incorporating remote sensing data in physically based distributed agro-hydrological modelling." *Journal of Hydrology*, 287(1-4), 279-299.

Bonfante, A., Basile, A., Acutis, M., De Mascellis, R., Manna, P., Perego, A., and Terribile, F. (2010). "SWAP, CropSyst and MACRO comparison in two contrasting soils cropped with maize in Northern Italy." *Agricultural Water Management*, 97(7), 1051-1062.

Braud, I., Dantasantonino, A. C., Vauclin, M., Thony, J. L., and Ruelle, P. "A Simple Soil-Plant-Atmosphere Transfer Model (SISPAT) Development and Field Verification." 213-250.

Braud, I., Varado, N., and Olioso, A. (2005). "Comparison of root water uptake modules using either the surface energy balance or potential transpiration." *Journal of Hydrology*, 301(1-4), 267-286.

Briggs, G. G., Bromilow, R. H., and Evans, A. A. (1982). "RELATIONSHIPS BETWEEN LIPOPHILICITY AND ROOT UPTAKE AND TRANSLOCATION OF NON-IONIZED CHEMICALS BY BARLEY." *Pesticide Science*, 13(5), 495-504.

Brisson, N., Mary, B., Ripoche, D., Jeuffroy, M. H., Ruget, F., Nicoullaud, B., Gate, P., Devienne-Barret, F., Antonioletti, R., Durr, C., Richard, G., Beaudoin, N., Recous, S., Tayot, X., Plenet, D., Cellier, P., Machet, J. M., Meynard, J. M., and Delecolle, R. (1998). "STICS: a generic model for the simulation of crops and their water and nitrogen balances. I. Theory and parameterization applied to wheat and corn." *Agronomie*, 18(5-6), 311-346.

Brouwer, C., Prins, K., Kay, M., and Heibloem, M. (1988). "Irrigation Water Management: Irrigation methods." FAO.

Burken, J. G., and Schnoor, J. L. (1996). "Phytoremediation: Plant Uptake of Atrazine and Role of Root Exudates." *Journal of Environmental Engineering*, 122(11), 958-963.

Calamari, D., Vighi, M., and Bacci, E. (1987). "The Use of Terrestrial Plant Biomass as a Parameter in the Fugacity Model." *Chemosphere*, 16(10-12), 2359-2364.

Carsel, R. F., and Parrish, R. S. (1988). "Developing Joint Probability-Distributions of Soil-Water Retention Characteristics." *Water Resources Research*, 24(5), 755-769.

Celia, M. A., Bouloutas, E. T., and Zarba, R. L. (1990). "A General Mass-Conservative Numerical-Solution for the Unsaturated Flow Equation." *Water Resources Research*, 26(7), 1483-1496.

Chapman, S. C., Hammer, G. L., and Meinke, H. (1993). "A SUNFLOWER SIMULATION-MODEL .1. MODEL DEVELOPMENT." *Agronomy Journal*, 85(3), 725-735.

Charbeneau, R. J. (2000). *Groundwater hydraulics and pollutant transport*, Prentice Hall, Upper Saddle River, NJ :,

Chiou, C. T., Sheng, G. Y., and Manes, M. (2001). "A partition-limited model for the plant uptake of organic contaminants from soil and water." *Environmental Science & Technology*, 35(7), 1437-1444.

Chow, V. T. (1959). *Open-channel hydraulics*, McGraw-Hill civil engineering series, McGraw-Hill, New York,

Chu, X., and Mariño, M. A. (2006). "Improved Compartmental Modeling and Application to Three-Phase Contaminant Transport in Unsaturated Porous Media." *J. Envir. Engrg.*, 132(2), 211-219.

Chu, X. F., and Marino, M. A. (2004). "Semidiscrete pesticide transport modeling and application." *Journal of Hydrology*, 285(1-4), 19-40.

Clemmens, A. J. (2009). "Errors in Surface Irrigation Evaluation from Incorrect Model Assumptions." *Journal of Irrigation and Drainage Engineering-Asce*, 135(5), 556-565.

Clemmens, A. J., Eisenhauer, D. E., and Maheswari, B. L. "Infiltration and Roughness Equations for Surface Irrigation: How Form Influences Estimation." *ASAE Annual International Meeting Paper No: 01-2255*, Sacramento, California, USA.

Collins, C., Fryer, M., and Grosso, A. (2006). "Plant uptake of non-ionic organic chemicals." *Environmental Science & Technology*, 40(1), 45-52.

Collins, C. D., and Fryer, M. E. (2003). "Model intercomparison for the uptake of organic chemicals by plants." *Environmental Science & Technology*, 37(8), 1617-1624.

Cooley, R. L. (1983). "Some New Procedures for Numerical-Solution of Variably Saturated Flow Problems." *Water Resources Research*, 19(5), 1271-1285.

Coulibaly, L., Labib, M. E., and Hazen, R. (2004a). "A GIS-based multimedia watershed model: development and application." *Chemosphere*, 55(7), 1067-1080.

Coulibaly, L., Labib, M. E., and Meegoda, J. N. (2004b). "Multimedia Model for Analysis of Contaminant Releases in Passaic River Watershed." *Practice Periodical of Hazardous, Toxic, and Radioactive Waste Management*, 8(4), 220-227.

Cousins, I. T., and Mackay, D. (2000). "Transport Parameters and Mass Balance Equations for Vegetation in a Level III Fugacity Model." Internal report published on the website of the Canadian Environmental Modelling Centre (http://www.trentu.ca/academic/aminss/envmodel/CEMC200001.pdf) (Accessed: November 16, 2010).

Cousins, I. T., and Mackay, D. (2001). "Strategies for including vegetation compartments in multimedia models." *Chemosphere*, 44(4), 643-654.

Cox, W. J., and Jolliff, G. D. (1986). "GROWTH AND YIELD OF SUNFLOWER AND SOYBEAN UNDER SOIL-WATER DEFICITS." *Agronomy Journal*, 78(2), 226-230.

Currado, G. M., and Harrad, S. (2001). "Transfer of POPs into Vegetation: Implications and Mechanisms." Persistent Organic Pollutants: Environmental Behaviour and Pathways for Human Exposure, S. Harrad, ed., Kluwer Academic Publishers, Boston, 53-77.

Dawson, C. (2008). "A continuous/discontinuous Galerkin framework for modeling coupled subsurface and surface water flow." *Computational Geosciences*, 12(4), 451-472.

Dettenmaier, E. M., Doucette, W. J., and Bugbee, B. (2009). "Chemical Hydrophobicity and Uptake by Plant Roots." *Environmental Science & Technology*, 43(2), 324-329.

Di Vittorio, A. V., Anderson, R. S., White, J. D., Miller, N. L., and Running, S. W. (2010). "Development and optimization of an Agro-BGC ecosystem model for C4 perennial grasses." *Ecological Modelling*, 221(17), 2038-2053.

DiGiammarco, P., Todini, E., and Lamberti, P. (1996). "A conservative finite elements approach to overland flow: The control volume finite element formulation." *Journal of Hydrology*, 175(1-4), 267-291.

Drouet, J. L., and Pages, L. (2003). "GRAAL: a model of GRowth, Architecture and carbon ALlocation during the vegetative phase of the whole maize plant - Model description and parameterisation." *Ecological Modelling*, 165(2-3), 147-173.

Dutta, D., Herath, S., and Musiake, K. (2000). "Flood inundation simulation in a river basin using a physically based distributed hydrologic model." *Hydrological Processes*, 14(3), 497-519.

Dwyer, L. M., and Stewart, D. W. (1986). "LEAF-AREA DEVELOPMENT IN FIELD-GROWN MAIZE." *Agronomy Journal*, 78(2), 334-343.

Ebel, B. A., Mirus, B. B., Heppner, C. S., VanderKwaak, J. E., and Loague, K. (2009). "First-order exchange coefficient coupling for simulating surface water-groundwater interactions: parameter sensitivity and consistency with a physics-based approach." *Hydrological Processes*, 23(13), 1949-1959.

Eitzinger, J., Trnka, M., Hosch, J., Zalud, Z., and Dubrovsky, M. (2004). "Comparison of CERES, WOFOST and SWAP models in simulating soil water content during growing season under different soil conditions." *Ecological Modelling*, 171(3), 223-246.

Esfandiari, M., and Maheshwari, B. L. (1998). "Suitability of selected flow equations and variation of Manning's n in furrow irrigation." *Journal of Irrigation and Drainage Engineering-Asce*, 124(2), 89-95.

Farahani, H. J., Howell, T. A., Shuttleworth, W. J., and Bausch, W. C. (2007). "Evapotranspiration: Progress in measurement and modeling in agriculture." *Transactions of the Asabe*, 50(5), 1627-1638.

Fasinmirin, J. T., Olufayo, A. A., and Oguntunde, P. G. (2008). "Calibration and validation of a soil water simulation model (WaSim) for field grown Amaranthus cruentus." *International Journal of Plant Production*, 2(3), 269-277.

Feddes, R. A., Bresler, E., and Neuman, S. P. (1974). "FIELD-TEST OF A MODIFIED NUMERICAL-MODEL FOR WATER UPTAKE BY ROOT SYSTEMS." *Water Resources Research*, 10(6), 1199-1206.

Feddes, R. A., Hoff, H., Bruen, M., Dawson, T., de Rosnay, P., Dirmeyer, O., Jackson, R. B., Kabat, P., Kleidon, A., Lilly, A., and Pitman, A. J. (2001). "Modeling root water uptake in hydrological and climate models." *Bulletin of the American Meteorological Society*, 82(12), 2797-2809.

Feddes, R. A., Kowalik, P., Kolinskamalinka, K., and Zaradny, H. (1976). "SIMULATION OF FIELD WATER-UPTAKE BY PLANTS USING A SOIL-WATER DEPENDENT ROOT EXTRACTION FUNCTION." *Journal of Hydrology*, 31(1-2), 13-26.

Feddes, R. A., Kowalik, P. J., and Zaradny, H. (1978). *Simulation of Field Water Use and Crop Yield*, John Wiley & Sons, New York, 188p.

Feng, K., and Molz, F. J. (1997). "A 2-D, diffusion-based, wetland flow model." *Journal of Hydrology*, 196(1-4), 230-250.

Fetter, C. W. (1999). *Contaminant Hydrogeology*, Prentice Hall, 500p.

Feyen, J., Jacques, D., Timmerman, A., and Vanderborght, J. (1998). "Modelling water flow and solute transport in heterogeneous soils: A review of recent approaches." *Journal of Agricultural Engineering Research*, 70(3), 231-256.

Fournier, C., and Andrieu, B. (1998). "A 3D architectural and process-based model of maize development." *Annals of Botany*, 81(2), 233-250.

Fournier, C., and Andrieu, B. (1999). "ADEL-maize: an L-system based model for the integration of growth processes from the organ to the canopy. Application to regulation of morphogenesis by light availability." *Agronomie*, 19(3-4), 313-327.

Furman, A. (2008). "Modeling coupled surface-subsurface flow processes: A review." *Vadose Zone Journal*, 7(2), 741-756.

Furman, A., Warrick, A. W., Zerihun, D., and Sanchez, C. A. (2006). "Modified Kostiakov infiltration function: Accounting for initial and boundary conditions." *Journal of Irrigation and Drainage Engineering-Asce*, 132(6), 587-596.

Gandolfi, C., and Savi, F. (2000). "A mathematical model for the coupled simulation of surface runoff and infiltration." *Journal of Agricultural Engineering Research*, 75(1), 49-55.

Garcia-Navarro, P., Playan, E., and Zapata, N. (2000). "Solute transport modeling in overland flow applied to fertigation." *Journal of Irrigation and Drainage Engineering-Asce*, 126(1), 33-40.

Gillies, M., and Smith, R. (2005). "Infiltration parameters from surface irrigation advance and run-off data." *Irrigation Science*, 24(1), 25-35.

Gokgoz-Kilic, S., and Aral, M. M. (2008). "Probabilistic fugacity analysis of Lake Pontchartrain pollution after Hurricane Katrina." *Journal of Environmental Management*, 88(3), 448-457.

Gokgoz Kilic, S. (2008). "Dynamic fugacity modeling in environmental systems," Ph.D. Thesis, Georgia Institute of Technology, Atlanta, Ga. :.

Gottardi, G., and Venutelli, M. (1993). "A control-volume finite-element model for two-dimensional overland flow." *Advances in Water Resources*, 16(5), 277-284.

Green, S. R., Kirkham, M. B., and Clothier, B. E. (2006). "Root uptake and transpiration: From measurements and models to sustainable irrigation." *Agricultural Water Management*, 86(1-2), 165-176.

Green, W. H., and Ampt, G. A. (1911). "Studies on soil physics Part I - The flow of air and water through soils." *Journal of Agricultural Science*, 4, 1-24.

Groenendijk, P., Kroes, J. G., and Van Dam, J. C. (2006). "Comments on "A set of analytical benchmarks to test numerical models of flow and transport in soils"." *Vadose Zone Journal*, 5(1), 126-127.

Gunduz, O. (2004a). "Coupled Flow and Contaminant Transport Modeling in Large Watersheds," Thesis, Georgia Institute of Technology, Atlanta.

Gunduz, O. (2004b). "Coupled Flow and Contaminant Transport Modeling in Large Watersheds," Ph.D. Thesis, Georgia Institute of Technology, Atlanta.

Gunduz, O., and Aral, M. M. (2005a). "A Dirac-delta function notation for source/sink terms in groundwater flow." *Journal of Hydrologic Engineering*, 10(5), 420-427.

Gunduz, O., and Aral, M. M. (2005b). "River networks and groundwater flow: a simultaneous solution of a coupled system." *Journal of Hydrology*, 301(1-4), 216-234.

Hansen, S. (2002). "Daisy, a flexible Soil-Plant-Atmosphere system Model."

Haverkamp, R., and Vauclin, M. (1979). "NOTE ON ESTIMATING FINITE-DIFFERENCE INTERBLOCK HYDRAULIC CONDUCTIVITY VALUES FOR TRANSIENT UNSATURATED FLOW PROBLEMS." *Water Resources Research*, 15(1), 181-187.

He, Z. G., Wu, W. M., and Wang, S. S. Y. (2008). "Coupled finite-volume model for 2D surface and 3D subsurface flows." *Journal of Hydrologic Engineering*, 13(9), 835-845.

He, Z. G., Wu, W. M., and Wang, S. S. Y. (2009). "Integrated Two-Dimensional Surface and Three-Dimensional Subsurface Contaminant Transport Model Considering Soil Erosion and Sorption." *Journal of Hydraulic Engineering-Asce*, 135(12), 1028-1040.

Hollander, A., Huijbregts, M. A. J., Ragas, A. M. J., and van de Meent, D. (2006). "BasinBox: a generic multimedia fate model for predicting the fate of chemicals in river catchments." *Hydrobiologia*, 565, 21-38.

Hopmans, J. W., and Bristow, K. L. (2002). "Current capabilities and future needs of root water and nutrient uptake modeling." Advances in Agronomy, Academic Press, 103-183.

Hromadka, T. V., McCuen, R. H., and Yen, C. C. (1987). "COMPARISON OF OVERLAND-FLOW HYDROGRAPH MODELS." *Journal of Hydraulic Engineering-Asce*, 113(11), 1422-1440.

Hromadka, T. V., and Yen, C. C. (1986). "A Diffusion Hydrodynamic Model (Dhm)." *Advances in Water Resources*, 9(3), 118-170.

Huang, G. B., and Yeh, G. T. (2009). "Comparative Study of Coupling Approaches for Surface Water and Subsurface Interactions." *Journal of Hydrologic Engineering*, 14(5), 453-462.

Hung, H., and Mackay, D. (1997). "A novel and simple model of the uptake of organic chemicals by vegetation from air and soil." *Chemosphere*, 35(5), 959-977.

Hunter, N. M., Bates, P. D., Horritt, M. S., and Wilson, M. D. (2007). "Simple spatially-distributed models for predicting flood inundation: A review." *Geomorphology*, 90(3-4), 208-225.

Jain, M. K., and Singh, V. P. (2005). "DEM-based modelling of surface runoff using diffusion wave equation." *Journal of Hydrology*, 302(1-4), 107-126.

Jara, J., and Stockle, C. O. (1999). "Simulation of water uptake in maize, using different levels of process detail." *Agronomy Journal*, 91(2), 256-265.

Joshi, M. B., Murthy, J. S. R., and Shah, M. M. (1995). "CROSOWAT - A DECISION TOOL FOR IRRIGATION SCHEDULE." *Agricultural Water Management*, 27(3-4), 203-223.

Juraske, R., Anton, A., and Castells, F. (2008). "Estimating half-lives of pesticides in/on vegetation for use in multimedia fate and exposure models." *Chemosphere*, 70(10), 1748-1755.

Juraske, R., Castells, F., Vijay, A., Munoz, P., and Anton, A. (2009). "Uptake and persistence of pesticides in plants: Measurements and model estimates for imidacloprid after foliar and soil application." *Journal of Hazardous Materials*, 165(1-3), 683-689.

Jury, W. A., and Fluhler, H. (1992). "TRANSPORT OF CHEMICALS THROUGH SOIL - MECHANISMS, MODELS, AND FIELD APPLICATIONS." *Advances in Agronomy*, 47, 141-201.

Kolditz, O., Delfs, J. O., Burger, C., Beinhorn, M., and Park, C. H. (2008). "Numerical analysis of coupled hydrosystems based on an object-oriented compartment approach." *Journal of Hydroinformatics*, 10(3), 227-244.

Kollet, S. J., and Maxwell, R. M. (2006). "Integrated surface-groundwater flow modeling: A free-surface overland flow boundary condition in a parallel groundwater flow model." *Advances in Water Resources*, 29(7), 945-958.

Komprda, J., Kubosova, K., Dvorska, A., Scheringer, M., Klanova, J., and Holoubek, I. (2009). "Application of an unsteady state environmental distribution model to a decadal time series of PAH concentrations in Central Europe." *Journal of Environmental Monitoring*, 11(2), 269-276.

Kouznetsov, M. Y., Roodsari, R., Pachepsky, Y. A., Sheltonc, D. R., Sadeghi, A. M., Shirmohammadi, A., and Starr, J. L. (2007). "Modeling manure-borne bromide and fecal coliform transport with runoff and infiltration at a hillslope." *Journal of Environmental Management*, 84(3), 336-346.

Kroes, J. G., Van Dam, J. C., Groenendijk, P., Hendriks, R. F. A., and Jacobs, C. M. J. (2008). "SWAP version 3.2. Theory description and user manual." *Alterra Report1649*, Weganingen, Alterra.

Kroes, J. G., Wesseling, J. C., and Van Dam, J. C. (2000). "Integrated modelling of the soil-water-atmosphere-plant system using the model SWAP 2.0 an overview of theory and an application." *Hydrological Processes*, 14(11-12), 1993-2002.

Kumar, M., Duffy, C. J., and Salvage, K. M. (2009). "A Second-Order Accurate, Finite Volume-Based, Integrated Hydrologic Modeling (FIHM) Framework for Simulation of Surface and Subsurface Flow." *Vadose Zone Journal*, 8(4), 873-890.

Lagos, L. O., Martin, D. L., Verma, S. B., Suyker, A., and Irmak, S. (2009). "Surface energy balance model of transpiration from variable canopy cover and evaporation from residue-covered or bare-soil systems." *Irrigation Science*, 28(1), 51-64.

Lai, C. T., and Katul, G. (2000). "The dynamic role of root-water uptake in coupling potential to actual transpiration." *Advances in Water Resources*, 23(4), 427-439.

Lauenroth, W., and Bradford, J. (2006). "Ecohydrology and the Partitioning AET Between Transpiration and Evaporation in a Semiarid Steppe." *Ecosystems*, 9(5), 756-767.

Lecina, S., and Playan, E. (2006a). "Model for the simulation of water flows in irrigation districts. I: Description." *Journal of Irrigation and Drainage Engineering-Asce*, 132(4), 310-321.

Lecina, S., and Playan, E. (2006b). "Model for the simulation of water flows in irrigation districts. II: Application." *Journal of Irrigation and Drainage Engineering-Asce*, 132(4), 322-331.

Lehmann, F., and Ackerer, P. (1998). "Comparison of Iterative Methods for Improved Solutions of the Fluid Flow Equation in Partially Saturated Porous Media." *Transport in Porous Media*, 31(3), 275-292.

Li, K. Y., Boisvert, J. B., and De Jong, R. (1999). "An exponential root-water-uptake model." *Canadian Journal of Soil Science*, 79(2), 333-343.

Li, K. Y., De Jong, R., and Boisvert, J. B. (2001). "An exponential root-water-uptake model with water stress compensation." *Journal of Hydrology*, 252(1-4), 189-204.

Li, K. Y., De Jong, R., Coe, M. T., and Ramankutty, N. (2006a). "Root-water-uptake based upon a new water stress reduction and an asymptotic root distribution function." *Earth Interactions*, 10, 22.

Li, Q. L., Zhu, T., Qiu, X. H., Hu, H. X., and Vighi, M. (2006b). "Evaluating the fate of p,p '-DDT in Tianjin, China using a non-steady-state multimedia fugacity model." *Ecotoxicology and Environmental Safety*, 63(2), 196-203.

Liang, D. F., Falconer, R. A., and Lin, B. L. (2007). "Coupling surface and subsurface flows in a depth averaged flood wave model." *Journal of Hydrology*, 337(1-2), 147-158.

Liong, S. Y., Selvalingam, S., and Brady, D. K. (1989). "ROUGHNESS VALUES FOR OVERLAND-FLOW IN SUBCATCHMENTS." *Journal of Irrigation and Drainage Engineering-Asce*, 115(2), 203-214.

Luo, Y., He, C. S., Sophocleous, M., Yin, Z. F., Ren, H. R., and Zhu, O. Y. (2008). "Assessment of crop growth and soil water modules in SWAT2000 using extensive field experiment data in an irrigation district of the Yellow River Basin." *Journal of Hydrology*, 352(1-2), 139-156.

Luo, Y., and Yang, X. (2004). "A High-Resolution Multimedia Model for Chemical Transport Using GIS." ASAE/CSAE Annual International Meeting, ASAE/CSAE, Ottawa, Ontario, Canada.

Luo, Y. Z., Gao, Q., and Yang, X. S. (2007). "Dynamic modeling of chemical fate and transport in multimedia environments at watershed scale - I: Theoretical considerations and model implementation." *Journal of Environmental Management*, 83(1), 44-55.

Luo, Y. Z., and Yang, X. S. (2007). "A multimedia environmental model of chemical distribution: Fate, transport, and uncertainty analysis." *Chemosphere*, 66(8), 1396-1407.

Mackay, D. (2001). *Multimedia environmental models : the fugacity approach*, Boca Raton : Lewis Publishers, 261p.

Mackay, D., Webster, E., Woodfine, D., Cahill, T. M., Doyle, P., Couillard, Y., and Gutzman, D. (2003). "Towards consistent evaluation of the persistence of organic, inorganic and metallic substances." *Human and Ecological Risk Assessment*, 9(6), 1445-1474.

MacLeod, M., and Mackay, D. (2004). "Modeling transport and deposition of contaminants to ecosystems of concern: a case study for the Laurentian Great Lakes." *Environmental Pollution*, 128(1-2), 241-250.

Macleod, M., McKone, T. E., and Mackay, D. (2005). "Mass balance for mercury in the San Francisco Bay Area." *Environmental Science & Technology*, 39(17), 6721-6729.

MacLeod, M., Woodfine, D., Brimacombe, J., Toose, L., and Mackay, D. (2002). "A dynamic mass budget for toxaphene in North America." *Environmental Toxicology and Chemistry*, 21(8), 1628-1637.

MacLeod, M., Woodfine, D. G., Mackay, D., McKone, T., Bennett, D., and Maddalena, R. (2001). "BETR North America: A regionally segmented multimedia contaminant fate model for North America." *Environmental Science and Pollution Research*, 8(3), 156-163.

Maheshwari, B. L. (1992). "SUITABILITY OF DIFFERENT FLOW EQUATIONS AND HYDRAULIC RESISTANCE PARAMETERS FOR FLOWS IN SURFACE IRRIGATION - A REVIEW." *Water Resources Research*, 28(8), 2059-2066.

Maheshwari, B. L., and McMahon, T. A. (1993a). "PERFORMANCE EVALUATION OF BORDER IRRIGATION MODELS FOR SOUTH-EAST AUSTRALIA .1. ADVANCE AND RECESSION CHARACTERISTICS." *Journal of Agricultural Engineering Research*, 54(1), 67-87.

Maheshwari, B. L., and McMahon, T. A. (1993b). "PERFORMANCE EVALUATION OF BORDER IRRIGATION MODELS FOR SOUTH-EAST AUSTRALIA .2. OVERALL SUITABILITY FOR FIELD APPLICATIONS." *Journal of Agricultural Engineering Research*, 54(2), 127-139.

Mailhol, J., and Merot, A. (2008). "SPFC: a tool to improve water management and hay production in the Crau region." *Irrigation Science*, 26(4), 289-302.

Mailhol, J. C., Olufayo, A. A., and Ruelle, P. (1997). "Sorghum and sunflower evapotranspiration and yield from simulated leaf area index." *Agricultural Water Management*, 35(1-2), 167-182.

Maneta, M., Schnabel, S., and Jetten, V. (2008). "Continuous spatially distributed simulation of surface and subsurface hydrological processes in a small semiarid catchment." *Hydrological Processes*, 22(13), 2196-2214.

Manzini, G., and Ferraris, S. (2004). "Mass-conservative finite volume methods on 2-D unstructured grids for the Richards' equation." *Advances in Water Resources*, 27(12), 1199-1215.

Matthies, M., and Behrendt, H. (1995). "Dynamics of Leaching, Uptake, and Translocation: The Simulation Model Network Atmosphere-Plant-Soil (SNAPS)." Plant Contamination: Modeling and Simulation of Organic Chemical Processes, S. Trapp and J. C. Mc Farlane, eds., Lewis Publishers, Boca Raton, FL, 215-243.

Milly, P. C. D. (1985). "A Mass-Conservative Procedure for Time-Stepping in Models of Unsaturated Flow." *Advances in Water Resources*, 8(1), 32-36.

Molz, F. J., and Remson, I. (1970). "EXTRACTION TERM MODELS OF SOIL MOISTURE USE BY TRANSPIRING PLANTS." *Water Resources Research*, 6(5), 1346-&.

Morita, M., and Yen, B. C. (2002). "Modeling of conjunctive two-dimensional surface-three-dimensional subsurface flows." *Journal of Hydraulic Engineering-Asce*, 128(2), 184-200.

Muller, J. F., Hawker, D. W., and Connell, D. W. (1994). "CALCULATION OF BIOCONCENTRATION FACTORS OF PERSISTENT HYDROPHOBIC COMPOUNDS IN THE AIR/VEGETATION SYSTEM." *Chemosphere*, 29(4), 623-640.

Nielsen, D. R., Vangenuchten, M. T., and Biggar, J. W. (1986). "Water-Flow and Solute Transport Processes in the Unsaturated Zone." *Water Resources Research*, 22(9), S89-S108.

Nimah, M. N., and Hanks, R. J. (1973). "MODEL FOR ESTIMATING SOIL-WATER, PLANT, AND ATMOSPHERIC INTERRELATIONS .1. DESCRIPTION AND SENSITIVITY." *Soil Science Society of America Journal*, 37(4), 522-527.

Novak, V. (1987). "Estimation of Soil-Water Extraction Patterns by Roots." *Agricultural Water Management*, 12(4), 271-278.

NRCS/USDA. (2008). "National Engineering Handbook, Section 15, Irrigation, Chapter 4: Border Irrigation."

Ojha, C. S. P., Prasad, K. S. H., Shankar, V., and Madramootoo, C. A. (2009). "Evaluation of a Nonlinear Root-Water Uptake Model." *Journal of Irrigation and Drainage Engineering-Asce*, 135(3), 303-312.

Panday, S., and Huyakorn, P. S. (2004). "A fully coupled physically-based spatially-distributed model for evaluating surface/subsurface flow." *Advances in Water Resources*, 27(4), 361-382.

Paterson, S., Mackay, D., and McFarlane, C. (1994). "A MODEL OF ORGANIC-CHEMICAL UPTAKE BY PLANTS FROM SOIL AND THE ATMOSPHERE." *Environmental Science & Technology*, 28(13), 2259-2266.

Pengelly, B. C., Muchow, R. C., and Blamey, F. P. C. (1999). "Predicting leaf area development in response to temperature in three tropical annual forage legumes." *Australian Journal of Agricultural Research*, 50(2), 253-259.

Pennington, D. W., Margni, M., Ammann, C., and Jolliet, O. (2005). "Multimedia fate and human intake modeling: Spatial versus nonspatial insights for chemical emissions in Western Europe." *Environmental Science & Technology*, 39(4), 1119-1128.

Perrochet, P. (1987). "WATER-UPTAKE BY PLANT-ROOTS - A SIMULATION-MODEL .1. CONCEPTUAL-MODEL." *Journal of Hydrology*, 95(1-2), 55-61.

Personne, E., Perrier, A., and Tuzet, A. (2003). "Simulating water uptake in the root zone with a microscopic-scale model of root extraction." *Agronomie*, 23(2), 153-168.

Philip, J. R. (1957). "The theory of infiltration: 1. The infiltration equation and its solution." *Soil Science*, 83, 435-448.

Powell, R. L. (1997). "The use of vascular plants as "field" biomonitors." Plants for Environmental Studies, W. Wang, J. W. Gorsuch, and J. S. Hughes, eds., Lewis Publishers, Boca Raton, 335-365.

Prasad, R. (1988). "A LINEAR ROOT WATER-UPTAKE MODEL." *Journal of Hydrology*, 99(3-4), 297-306.

Prevedouros, K., MacLeod, M., Jones, K. C., and Sweetman, A. J. (2004). "Modelling the fate of persistent organic pollutants in Europe: parameterisation of a gridded distribution model." *Environmental Pollution*, 128(1-2), 251-261.

Ramaswami, A., Milford, J. B., and Small, M. J. (2005). *Integrated environmental modeling : pollutant transport, fate, and risk in the environment*, J. Wiley, Hoboken, N.J. :, 678p.

Richards, L. A. (1931). "Capillary conduction of liquids through porous mediums." *Physics*, 1(5), 318-333.

Riederer, M. (1995). "Partitioning and Transport of Organic Chemicals between the Atmospheric Environment and Leaves." Plant Contamination: Modeling and Simulation of Organic Chemical Processes, S. Trapp and J. C. Mc Farlane, eds., Lewis Publishers, Boca Raton, FL, 153-190.

Robertson, D., Wood, M., and Wang, Q. J. (2004). "Estimating hydraulic parameters for a surface irrigation model from field conditions." *Australian Journal of Experimental Agriculture*, 44(2), 173-179.

Schnabel, R. R., and Richie, E. B. (1984). "CALCULATION OF INTERNODAL CONDUCTANCES FOR UNSATURATED FLOW SIMULATIONS - A COMPARISON." *Soil Science Society of America Journal*, 48(5), 1006-1010.

Schymanski, S. J., Sivapalan, M., Roderick, M. L., Beringer, J., and Hutley, L. B. (2008). "An optimality-based model of the coupled soil moisture and root dynamics." *Hydrology and Earth System Sciences*, 12(3), 913-932.

Setiyono, T. D., Weiss, A., Specht, J. E., Cassman, K. G., and Dobermann, A. (2008). "Leaf area index simulation in soybean grown under near-optimal conditions." *Field Crops Research*, 108(1), 82-92.

Severinsen, M., and Jager, T. (1998). "Modelling the influence of terrestrial vegetation on the environmental fate of xenobiotics." *Chemosphere*, 37(1), 41-62.

Simunek, J., and Bradford, S. A. (2008). "Vadose zone modeling: Introduction and importance." *Vadose Zone Journal*, 7(2), 581-586.

Simunek, J., and Hopmans, J. W. (2009). "Modeling compensated root water and nutrient uptake." *Ecological Modelling*, 220(4), 505-521.

Simunek, J., Sejna, M., Saito, H., Sakai, M., and van Genuchten, M. T. (2008). "The HYDRUS-1D Software Package for Simulating the Movement of Water, Heat, and Multiple Solutes in Variably-Saturated Media, Version 4.08." Department of Environmental Sciences, University of Clifornia Riverside, Riverside, California, USA.

Simunek, J., van Genuchten, M. T., and Sejna, M. (2006). "The HYDRUS Software Package for Simulating Two- and Three Dimensional Movement of Water, Heat, and Multiple Solutes in Variably-Saturated Media, Version 1.0." PC Progress, Prague, Czech Republic.

Singh, V., and Bhallamudi, S. M. (1998). "Conjunctive surface-subsurface modeling of overland flow." *Advances in Water Resources*, 21(7), 567-579.

Smith, P. C., De Noblet-Ducoudré, N., Ciais, P., Peylin, P., Viovy, N., Meurdesoif, Y., and Bondeau, A. (2010). "European-wide simulations of croplands using an improved terrestrial biosphere model: Phenology and productivity." *J. Geophys. Res.*, 115(G1), G01014.

Smith, R. E., and Woolhiser, D. A. (1971). "OVERLAND FLOW ON AN INFILTRATING SURFACE." *Water Resources Research*, 7(4), 899-&.

Spellman, F. R. (2008). *The science of water : concepts and applications*, CRC Press, Boca Raton :,

Stephenson, D., and Meadows, M. E. (1986). *Kinematic Hydrology and Modeling*, Developments in Water Science, Vol.26, 250p.

Stewart, D. W., and Dwyer, L. M. (1994). "A MODEL OF EXPANSION AND SENESCENCE OF INDIVIDUAL LEAVES OF FIELD-GROWN MAIZE (ZEA-MAYS L)." *Canadian Journal of Plant Science*, 74(1), 37-42.

Stöckle, C. O., Donatelli, M., and Nelson, R. (2003). "CropSyst, a cropping systems simulation model." *European Journal of Agronomy*, 18(3-4), 289-307.

Stockle, C. O., Martin, S. A., and Campbell, G. S. (1994). "CropSyst, a cropping systems simulation model: Water/nitrogen budgets and crop yield." *Agricultural Systems*, 46(3), 335-359.

Strelkoff, T. S., Clemmens, A. J., and Bautista, E. (2009). "Field Properties in Surface Irrigation Management and Design." *Journal of Irrigation and Drainage Engineering-Asce*, 135(5), 525-536.

Sweetman, A. J., Cousins, I. T., Seth, R., Jones, K. C., and Mackay, D. (2002). "A dynamic level IV multimedia environmental model: Application to the fate of polychlorinated biphenyls in the United Kingdom over a 60-year period." *Environmental Toxicology and Chemistry*, 21(5), 930-940.

Tao, S., Cao, H. Y., Liu, W. X., Li, B. G., Cao, J., Xu, F. L., Wang, X. J., Coveney, R. M., Shen, W. R., Qin, B. P., and Sun, R. (2003). "Fate modeling of phenanthrene with regional variation in Tianjin, China." *Environmental Science & Technology*, 37(11), 2453-2459.

Toose, L., Woodfine, D. G., MacLeod, M., Mackay, D., and Gouin, J. (2004). "BETR-World: a geographically explicit model of chemical fate: application to transport of alpha-HCH to the Arctic." *Environmental Pollution*, 128(1-2), 223-240.

Topp, E., Scheunert, I., Attar, A., and Korte, F. (1986). "FACTORS AFFECTING THE UPTAKE OF C-14-LABELED ORGANIC-CHEMICALS BY PLANTS FROM SOIL." *Ecotoxicology and Environmental Safety*, 11(2), 219-228.

Trapp, S. (1995). "Model for Uptake of Xenobiotics into Plants." Plant Contamination: Modeling and Simulation of Organic Chemical Processes, S. Trapp and J. C. Mc Farlane, eds., Lewis Publishers, Boca Raton, FL, 107-151.

Trapp, S. (2002). "Dynamic root uptake model for neutral lipophilic organics." *Environmental Toxicology and Chemistry*, 21(1), 203-206.

Trapp, S. (2004). "Plant uptake and transport models for neutral and ionic chemicals." *Environmental Science and Pollution Research*, 11(1), 33-39.

Trapp, S. (2007). "Fruit Tree model for uptake of organic compounds from soil and air." *Sar and Qsar in Environmental Research*, 18(3-4), 367-387.

Trapp, S., and Matthies, M. (1995). "GENERIC ONE-COMPARTMENT MODEL FOR UPTAKE OF ORGANIC-CHEMICALS BY FOLIAR VEGETATION." *Environmental Science & Technology*, 29(9), 2333-2338.

Trapp, S., and McFarlane, C. (1995). "Plant contamination : modeling and simulation of organic chemical processes." S. Trapp and C. McFarlane, eds., Lewis Publishers, Boca Raton :.

Travis, C. C., and Arms, A. D. (1988). "BIOCONCENTRATION OF ORGANICS IN BEEF, MILK, AND VEGETATION." *Environmental Science & Technology*, 22(3), 271-274.

Turner, A. K., and Chanmeesri, N. (1984). "SHALLOW FLOW OF WATER THROUGH NON-SUBMERGED VEGETATION." *Agricultural Water Management*, 8(4), 375-385.

Undeman, E., Czub, G., and McLachlan, M. S. (2009). "Addressing Temporal Variability When Modeling Bioaccumulation in Plants." *Environmental Science & Technology*, 43(10), 3751-3756.

van Dam, J. C., and Feddes, R. A. (2000). "Numerical simulation of infiltration, evaporation and shallow groundwater levels with the Richards equation." *Journal of Hydrology*, 233(1-4), 72-85.

van Dam, J. C., Groenendijk, P., Hendriks, R. F. A., and Kroes, J. G. (2008). "Advances of modeling water flow in variably saturated soils with SWAP." *Vadose Zone Journal*, 7(2), 640-653.

van den Honert, T. H. (1948). "Water Transport in Plants as a Catenary Process." *Discussions of the Faraday Society*, 3, 146-153.

van Dijk, A., and Bruijnzeel, L. A. (2001a). "Modelling rainfall interception by vegetation of variable density using an adapted analytical model. Part 1. Model description." *Journal of Hydrology*, 247(3-4), 230-238.

van Dijk, A., and Bruijnzeel, L. A. (2001b). "Modelling rainfall interception by vegetation of variable density using an adapted analytical model. Part 2. Model validation for a tropical upland mixed cropping system." *Journal of Hydrology*, 247(3-4), 239-262.

Van Genuchten, M. T. (1980). "A closed form equation for predicting the hydraulic conductivity of unsaturated soils." *Soil Science Society of America Journal*, 44, 892-898.

van Genuchten, M. T., and Alves, W. J. (1982). *Analytical solutions of the one-dimensional convective-dispersive solute transport equation*, Technical Bulletin No. 1661, U.S. Department of Agriculture, Washington, D.C., 151p.

van Ittersum, M. K., Leffelaar, P. A., van Keulen, H., Kropff, M. J., Bastiaans, L., and Goudriaan, J. (2003). "On approaches and applications of the Wageningen crop models." *European Journal of Agronomy*, 201-234.

van Leer, B. (1974). "Towards the ultimate conservative difference scheme. II. Monotonicity and conservation combined in a second-order scheme." *Journal of Computational Physics*, 14(4), 361-370.

Vanderborght, J., Kasteel, R., Herbst, M., Javaux, M., Thiery, D., Vanclooster, M., Mouvet, C., and Vereecken, H. (2005). "A set of analytical benchmarks to test numerical models of flow and transport in soils." *Vadose Zone Journal*, 4(1), 206-221.

Vanderborght, J., Kasteel, R., Vereecken, H., Javaux, M., Vanclooster, M., Thiery, D., and Mouvet, C. (2006). "Response to "Comments on 'A set of analytical benchmarks to test numerical models of flow and transport in soils'"." *Vadose Zone Journal*, 5(1), 128-128.

VanderKwaak, J. E. (1999). "Numerical simulation of flow and chemical transport in integrated surface-subsurface hydrologic systems," Thesis (Ph.D.)-University of Waterloo, 1999. Thesis.

Varado, N., Braud, I., and Ross, P. J. (2006). "Development and assessment of an efficient vadose zone module solving the 1D Richards' equation and including root extraction by plants." *Journal of Hydrology*, 323(1-4), 258-275.

Villalobos, F. J., Hall, A. J., Ritchie, J. T., and Orgaz, F. (1996). "OILCROP-SUN: A development, growth, and yield model of the sunflower crop." *Agronomy Journal*, 88(3), 403-415.

Vogel, T., van Genuchten, M. T., and Cislerova, M. (2001). "Effect of the shape of the soil hydraulic functions near saturation on variably-saturated flow predictions." *Advances in Water Resources*, 24(2), 133-144.

Wallach, R., Grigorin, G., and Rivlin, J. (2001). "A comprehensive mathematical model for transport of soil-dissolved chemicals by overland flow." *Journal of Hydrology*, 247(1-2), 85-99.

Wang, E. L., and Smith, C. J. (2004). "Modelling the growth and water uptake function of plant root systems: a review." *Australian Journal of Agricultural Research*, 55(5), 501-523.

Wania, F., Breivik, K., Persson, N. J., and McLachlan, M. S. (2006). "CoZMo-POP 2 - A fugacity-based dynamic multi-compartmental mass balance model of the fate of persistent organic pollutants." *Environmental Modelling & Software*, 21(6), 868-884.

Warren, C. S., Mackay, D., Webster, E., and Arnot, J. A. (2009). "A CAUTIONARY NOTE ON IMPLICATIONS OF THE WELL-MIXED COMPARTMENT ASSUMPTION AS APPLIED TO MASS BALANCE MODELS OF CHEMICAL FATE IN FLOWING SYSTEMS." *Environmental Toxicology and Chemistry*, 28(9), 1858-1865.

Wei, Y. F., Nishimori, M., Kobara, Y., and Akiyama, T. (2008). "Development of global scale multimedia contaminant fate model: Incorporating paddy field compartment." *Science of the Total Environment*, 406(1-2), 219-226.

Wheeler, D., Guyer, J. E., and Warren, J. A. (2007). "FiPy User's Guide, version 1.2." National Institute of Standards and Technology, Technology Administration, U.S. Department of Commerce.

Wohling, T., and Mailhol, J. C. (2007). "Physically based coupled model for simulating 1D surface-2D subsurface flow and plant water uptake in irrigation furrows. II: Model test and evaluation." *Journal of Irrigation and Drainage Engineering-ASCE*, 133(6), 548-558.

Wohling, T., and Schmitz, G. H. (2007). "Physically based coupled model for simulating 1D surface-2D subsurface flow and plant water uptake in irrigation furrows. I: Model development." *Journal of Irrigation and Drainage Engineering-ASCE*, 133(6), 538-547.

Woodfine, D., MacLeod, M., and Mackay, D. (2002). "A regionally segmented national scale multimedia contaminant fate model for Canada with GIS data input and display." *Environmental Pollution*, 119(3), 341-355.

Woodfine, D. G., MacLeod, M., Mackay, D., and Brimacombe, J. R. (2001). "Development of continental scale multimedia contaminant fate models: Integrating GIS." *Environmental Science and Pollution Research*, 8(3), 164-172.

Wu, J. Q., Zhang, R. D., and Gui, S. X. (1999). "Modeling soil water movement with water uptake by roots." *Plant and Soil*, 215(1), 7-17.

Xanthopoulos, T., and Koutitas, C. (1976). "Numerical-Simulation of a 2 Dimensional Flood Wave-Propagation Due to Dam Failure." *Journal of Hydraulic Research*, 14(4), 321-331.

Yadav, B. K., and Mathur, S. (2008). "Modeling soil water uptake by plants using nonlinear dynamic root density distribution function." *Journal of Irrigation and Drainage Engineering-Asce*, 134(4), 430-436.

Yadav, B. K., Mathur, S., and Siebel, M. A. (2009a). "Soil Moisture Dynamics Modeling Considering the Root Compensation Mechanism for Water Uptake by Plants." *Journal of Hydrologic Engineering*, 14(9), 913-922.

Yadav, B. K., Mathur, S., and Siebel, M. A. (2009b). "Soil Moisture Flow Modeling with Water Uptake by Plants (Wheat) under Varying Soil and Moisture Conditions." *Journal of Irrigation and Drainage Engineering-Asce*, 135(3), 375-381.

Yan, M., and Kahawita, R. (2000). "Modelling the fate of pollutant in overland flow." *Water Research*, 34(13), 3335-3344.

Zerihun, D., Furman, A., Warrick, A. W., and Sanchez, C. A. (2005a). "Coupled surface-subsurface flow model for improved basin irrigation management." *Journal of Irrigation and Drainage Engineering-Asce*, 131(2), 111-128.

Zerihun, D., Furman, A., Warrick, A. W., and Sanchez, C. A. (2005b). "Coupled surface-subsurface solute transport model for irrigation borders and basins. I. Model development." *Journal of Irrigation and Drainage Engineering-Asce*, 131(5), 396-406.

Zerihun, D., Sanchez, C. A., Furman, A., and Warrick, A. W. (2005c). "Coupled surface-subsurface solute transport model for irrigation borders and basins. II. Model evaluation." *Journal of Irrigation and Drainage Engineering-Asce*, 131(5), 407-419.

Zhang, H. H., and Brandle, J. R. (1996). "Windbreak effect on biomass and grain mass accumulation of corn: A modeling approach." *Agronomy Journal*, 88(4), 607-613.

Zhang, Q. O., Crittenden, J. C., Shonnard, D., and Mihelcic, J. R. (2003). "Development and evaluation of an environmental multimedia fate model CHEMGL for the Great Lakes region." *Chemosphere*, 50(10), 1377-1397.